



University of
Nottingham

UK | CHINA | MALAYSIA

Industrial Exploitation of
Supercritical Carbon Dioxide
as a Solvent

Alice Haddleton

Thesis submitted to the University of Nottingham for the degree of Doctor of
Philosophy, September 2019

Disclaimer

All of the work presented in this thesis is the original work of the author, with the exception of results referenced to other sources. It has not been submitted as part of any other degree or professional qualification.

Signed:

A handwritten signature in black ink on a light green rectangular background. The signature reads "A Haddleton" in a cursive script.

Date: 13/09/19

Alice Jane Haddleton

Acknowledgements

Firstly, I would like to thank Professor Steve Howdle for giving me the chance to complete my PhD in his group and for his continued support and guidance throughout. I have thoroughly enjoyed my time in Nottingham. Thanks must also go to my industrial funders Kaneka, in particular Dr Harald Braun for his guidance and Dr Sofie Sannen for her scientific knowledge and the testing of the materials carried out in Chapter 5. It has been a pleasure to work with you both and I was also grateful to be able to visit you at Kaneka Belgium during my first year.

The smooth running of the high-pressure equipment during my time in the lab would not have been possible without our workshop. Help from the following people has been greatly appreciated; Rich Wilson, Pete Fields, Mark Guyler, Matt McAdam, Martin Dellar, James Warren and Dave Litchfield - all of whom helped to fix the numerous issues that arose, virtually daily, with the autoclaves.

I could not have completed the scale-up work presented in Chapter 4 without the help of Dr Simon Bassett, who was instrumental in the initial investigations into the possibility of carrying out the reactions at larger scale, which brought in the funding for this project. He also helped in assembling the 1 L equipment and spent countless hours being my “lab- buddy” in the bomb-proof room on the roof of the department, where the 1 L autoclave was located.

I would like to thank my B10 family, in particular; Sam Irving who has been with me since day one of my PhD and together we have experienced many of the ups and downs associated with working with high-pressure and George Hargreaves for naming the 1 L autoclave Juanita, although it was initially a joke it seems to have stuck! I am indebted to the postdocs from the group including; Oliva Monaghan, Tom Bennett, Andrea Hufendiek and Vincenzo Taresco for their endless scientific advice and patience when reading the drafts of my thesis. Many thanks also to Marianna Gameiro, Rachel Atkinson, Katie Reynolds, Katie Pepper, Amy Stimpson and Rabea Loczenski whose friendships and support over the past 4 years have really meant a lot to me. I am also very grateful to all past and present members of B10 for not only

making the lab an enjoyable place to work but also for putting up with me over the last 4 years!

Finally, I would not have reached the end of my PhD without the support of my family and friends outside of the lab. Special thanks go to my Dad who has helped develop my love of chemistry over the years and is always happy to have a discussion about polymers even over the dinner table (sorry Mom!). You could say polymers are in my blood!

Overview

The work described in this thesis can be divided into two main topic areas; the synthesis of polymer particles via dispersion polymerisation using supercritical carbon dioxide (scCO₂) as the reaction medium and the scale-up of these reactions. The fundamental concepts used to achieve these aims are detailed in Chapter 1.

As high pressures and temperatures are involved, utilising scCO₂ as a reaction medium requires specialised equipment. The high-pressure equipment used throughout this thesis is summarised in Chapter 2. This includes the details of a 1 L high-pressure autoclave, previously only used for extraction, which has been used for the scale-up of polymer synthesis. The techniques used to analyse the polymers produced are also outlined.

The first main topic area of this thesis is the synthesis of polymer particles via dispersion polymerisation, which is discussed in Chapter 3. The first structure investigated is a poly(methyl methacrylate) (PMMA) particle incorporating a crosslinking component. The loading of the crosslinking component was varied to establish the effect this had on the particle structure, as well as the glass transition temperature (T_g). These parameters were probed using scanning electron microscopy (SEM) and dynamic mechanical analysis (DMA) respectively. A second particle of interest contained a core-shell internal morphology. Two monomer compositions were investigated, both containing a PMMA shell encasing either a poly(butyl acrylate) (PBA) or poly(benzyl acrylate) (PBzA) core. The loading of the core material (BA or BzA) was gradually increased and once again the changes in the particle morphology and T_g were probed. The ability to preferentially stain the PBzA allowed for probing of the internal morphology of the PBzA containing particles using transmission electron microscopy (TEM).

Utilising scCO₂ as the reaction medium removes the need for high-energy post polymerisation drying steps usually associated with dispersion polymerisations carried out in traditional solvents. However, despite numerous advantages, scale remains a hurdle which has thus far limited the applicability of scCO₂ for the commercial production of polymer particles. As this thesis was industrially funded,

the second topic area of investigation was the feasibility of increasing the scale of the high-pressure reactions, which is discussed in Chapter 4. The dispersion polymerisation of methyl methacrylate (MMA) was chosen as a model system as it has been well-studied in the literature. In this Chapter, comparisons are made between the particles produced on a small (60 mL) scale and those produced on a larger (1 L) scale using analogous reaction conditions. SEM was used to analyse the morphology of the particles produced. Control of the particle size, by variation of the concentration of the poly(dimethyl siloxane) stabiliser (PDMS) is demonstrated, with similar size particles being produced on both scales.

The desired application for these particles is as impact modifiers. With this in mind, the synthesised particles were combined with various PVC formulations and tested at Kaneka Belgium. Several industrially standard tests were performed, including Brabender torque rheometry, transparency and Izod impact tests. The results of these tests are summarised in Chapter 5. Comparisons are made between the particles synthesised in Nottingham and those produced commercially by Kaneka, intended for the same application. These tests allowed for conclusions to be drawn about the composition of the particles as well as the internal morphology present. The data collected complimented the analysis carried out in Nottingham. It also provided an opportunity to assess areas that could be improved upon in the future production of particles.

Abbreviations and Symbols

A	Pre-exponential Factor
AA	Acrylic Acid
ABS	Acrylonitrile-butadiene-styrene
Acetone-D ₆	Deuterated Acetone
AFM	Atomic Force Microscopy
AIBN	2,2'-Azobis(isobutyronitrile)
AIM	Acrylic Impact Modifier
AMA	Allyl Methacrylate
ATRP	Atom-transfer Radical Polymerisation
BA	Butyl Acrylate
BD	Butadiene
BIC	Bicontinuous
BzA	Benzyl Acrylate
BzMA	Benzyl Methacrylate
CBr ₄	Tetrabromoethane
CCTP	Catalytic Chain Transfer Polymerisation
CDCl ₃	Deuterated Chloroform
CL	Crosslinked
CO ₂	Carbon Dioxide
CPE	Chlorinated Polyethylene
CTA	Chain Transfer Agent

CYL	Cylindrical
\bar{D}	Dispersity
D	Diameter
DDSA	Dodecyl Succinic Anhydride
DEGDMA	Diethylene Glycol Dimethacrylate
DIS	Disordered
DMA	Dynamic Mechanical Analysis
DMAEMA	<i>N,N</i> -Dimethylaminoethyl Methacrylate
DRI	Differential Refractometer
DSC	Differential Scanning Calorimetry
DVB	Divinylbenzene
E_a	Activation Energy
EGDMA	Ethylene Glycol Dimethacrylate
EPDM	Ethylene Propylene Diene Monomer
EPR	Electron Paramagnetic Resonance
EVA	Ethylene-vinyl Acetate
EVB	Ethylvinylbenzene
FRP	Free Radical Polymerisation
G' (E')	Storage Modulus
G'' (E'')	Loss Modulus
GMA	Glycidyl Methacrylate
GPC	Gel Permeation Chromatography

HiP	High Pressure Equipment
HPLC	High Pressure Liquid Chromatography
<i>hPSt</i>	Polystyrene Homopolymer
I	Transmitted Light
I_0	Incident Light
II	Initiator Injection
J_{crit}	Critical Molecular Weight
k_d	Rate of Decomposition
$K_2SO_2O_8$	Potassium Persulfate
L_0	Feature Spacing
LAM	Lamella
MA	Methyl Acrylate
MALS	Multi Angle Light Scatter
MBS	Methacrylate-butadiene-styrene
MCR	Mid Chain Radical
MMA	Methyl Methacrylate
MNA	Methyl Nadic Anhydride
M_n	Number Average Molecular Weight
M_p	Peak Molecular Weight
MPTMS	Methacryloxypropyltrimethoxysilane
M_v	Viscosity Average Molecular Weight
M_w	Weight Average Molecular Weight

$N_{(0)}$	Initial Population
$N_{(t)}$	Population at Time t
NBR	Nitrile Rubber
NMP	Nitroxide Mediated Polymerisation
NMR	Nuclear Magnetic Resonance
NRV	Non-return Valve
O_2	Oxygen
PAA	Poly(acrylic acid)
PBA	Poly(butyl acrylate)
PBD	Polybutadiene
P(BD/St)	Poly(butadiene/styrene)
PBD-b-PEO	Polybutadiene-block-poly(ethylene oxide)
PBMBA	Poly(butadiene-methyl methacrylate-butylacrylate)
PBT	Poly(butylene terephthalate)
PBzA	Poly(benzyl acrylate)
PBzMA	Poly(benzyl methacrylate)
P_c	Critical Pressure
PC	Polycarbonate
PCL	Polycaprolactone
PDEGDMA	Poly(diethylene glycol dimethacrylate)
PDMAEA	Poly(2-(dimethylamino) ethyl methacrylate)
PDMAEMA	Poly(2-(dimethyl amino)ethyl methacrylate)

PDMS	Poly(dimethyl siloxane)
PDMS-MA	Monomethyl Methacrylate Terminated Poly(dimethyl siloxane)
PDMS-OH	Hydroxy Terminated Poly(dimethyl siloxane)
PE	Polyethylene
PEO	Polyethylene Oxide
PFOA	Poly(1,1-dihydroperfluorooctyl acrylate)
PFOMA	Poly(1,1-dihydroperfluorooctyl methacrylate)
PHEMA	Poly(2-hydroxyethyl methacrylate)
phr	Parts Per Hundred Rubber
P <i>i</i> BMA	Poly(<i>i</i> -butyl methacrylate)
P <i>i</i> BMA- <i>b</i> -PSt	Poly(<i>i</i> -butyl methacrylate)-block-polystyrene
PLGA	Poly(D,L-lactide-co-glycolide)
PMMA	Poly(methyl methacrylate)
P(MMA/St)	Poly(methyl methacrylate/styrene)
PLA	Poly(lactic acid)
PP	Polypropylene
ppm	Parts Per Million
PSD	Particle Size Distribution
PSt	Polystyrene
PSt- <i>b</i> -PnBA- <i>b</i> -PSt	Polystyrene-block-poly(<i>n</i> -butyl acrylate)-block-polystyrene
PSt- <i>b</i> -PEO	Polystyrene-block-poly(ethylene oxide)
PSt- <i>b</i> -PBD	Polystyrene-block-polybutadiene

P(St- <i>co</i> -BD)	Poly(styrene- <i>co</i> -butadiene)
PVC	Poly(vinyl chloride)
PVP	Poly(vinyl pyrrolidone)
R	Universal Gas Constant
RAFT	Reversible Addition-fragmentation Chain-transfer
RI	Refractive Index
ROP	Ring Opening Polymerisation
rpm	Revolutions Per Minute
RuO ₄	Ruthenium Tetroxide
scCO ₂	Supercritical Carbon Dioxide
SCF	Supercritical Fluids
SEC	Size Exclusion Chromatography
SEM	Scanning Electron Microscopy
SOP	Standard Operating Procedure
SPH	Spherical
SPR	Secondary Propagating Radical
SR	Standard Reaction
St	Styrene
T	Absolute Temperature
Tan δ	Loss/Storage Modulus
T _c	Critical Temperature
T _{cry}	Crystallisation Temperature

TEM	Tunneling Electron Microscopy
T _g	Glass Transition Temperature
THF	Tetrahydrofuran
T _m	Melting Temperature
TMS	Tetramethylsilane
TOF-SIM	Time-of-flight Secondary Ion Mass Spectrometry
TPR	Tertiary Propagating Radical
T _r	Total Transmittance
Tween	Polyoxyethylene Sorbitan Monooleate
UV	Ultraviolet
v/v	Volume by Volume
VA	Vinyl Acetate
VC	Vinyl Chloride
VOCs	Volatile Organic Compounds
w/v	Weight by Volume
wrt	With Respect To
wt%	Weight Percent
W _x	Weight Fraction of x
X _{CIE}	X Tristimulus Value
Y _{CIE}	Y Tristimulus Value
Y _i	Yellowness Index
Z _{CIE}	Z Tristimulus Value

ZrO ₂	Zirconium Dioxide
H	Viscosity (Intrinsic)
λ	Decay Constant
$\tau_{1/2}$	Half-life
Φ or f_s	Volume Fraction

Table of Contents

Disclaimer.....	I
Acknowledgements.....	III
Overview	V
Abbreviations and Symbols.....	VII
Table of Contents	XV
Chapter 1: Introduction	21
1.1. Overview	21
1.2. Polymers.....	21
1.3. Free Radical Polymerisation.....	25
1.3.1. Initiation	25
1.3.2. Propagation	26
1.3.3. Termination	27
1.4. Polymer Synthesis	29
1.4.1. Bulk Polymerisation.....	29
1.4.2. Solution Polymerisation	29
1.5. Polymer Particle Synthesis.....	30
1.5.1. Emulsion Polymerisation	30
1.5.2. Dispersion Polymerisation.....	32
1.5.3. Structured Polymer Particles.....	35
1.5.3.1. Block Copolymers	35
1.5.3.2. Core-shell Particles	38
1.6. Impact Modifiers	40
1.7. Supercritical Fluids	43
1.7.1. Supercritical Carbon Dioxide	43
1.8. Polymer Synthesis in scCO_2	44
1.9. Particle Synthesis in scCO_2	46

1.9.1. Emulsion and Suspension Polymerisation in scCO ₂	46
1.9.2. Precipitation and Dispersion Polymerisations in scCO ₂	47
1.9.3. Structured Particle Synthesis in scCO ₂	51
1.9.4. Core-shell Particle Synthesis in scCO ₂	52
1.10. Summary and Thesis Aims	55
1.11. References.....	57
Chapter 2: Experimental Equipment and Analytical Methods	62
2.1. Overview.....	62
2.2. High-pressure Equipment	62
2.2.1. High-pressure Pump	62
2.2.2. 60 mL Autoclave	63
2.2.2.1. Equipment Overview	63
2.2.2.2. Standard Operating Procedure.....	65
2.2.3. 1 L Autoclave.....	67
2.2.3.1. Equipment Overview	67
2.2.3.2. Standard Operating Procedure.....	71
2.3. Analytical Methods.....	73
2.3.1. Scanning Electron Microscopy.....	73
2.3.2. Transmission Electron Microscopy.....	73
2.3.3. Gel Permeation Chromatography	74
2.3.4. UV Spectrometry	75
2.3.5. Nuclear Magnetic Resonance	75
2.3.6. Differential Scanning Calorimetry	76
2.3.7. Dynamic Mechanical Analysis.....	76
2.4. References.....	78

Chapter 3: Core-Shell Particle Synthesis	79
3.1. Overview	79
3.2. Introduction	79
3.2.1. Impact Modifiers	80
3.2.2. PVC Modification	81
3.2.3. Core-shell Impact Modifiers	82
3.2.3.1. Methacrylate-butadiene-styrene	83
3.2.3.2. Acrylic Impact Modifiers	84
3.2.3.3. Acrylonitrile-butadiene-styrene	85
3.2.3.4. Poly(butyl acrylate) Impact Modifiers	85
3.2.4. Crosslinking in Core-shell Particles	88
3.2.5. Core-shell Particle Synthesis in scCO ₂	89
3.2.6. Crosslinked Particles in scCO ₂	89
3.3. Aims and Objectives	91
3.4. Experimental	92
3.4.1. Materials	92
3.4.2. BA/PMMA Particle Synthesis in 60 mL Autoclave	92
3.4.2.1. One-stage Batch Reactions	92
3.4.2.2. Multi-stage Reactions	94
3.4.3. BzA/PMMA Particle Synthesis in 60 mL Autoclave	95
3.4.3.1. Multi-stage Reactions	95
3.4.4. Crosslinked Particle Synthesis in 60 mL Autoclave	99
3.4.4.1. One-stage Batch Reactions	99
3.4.4.2. Multi-stage Reactions	99
3.4.5. Combination of Crosslinking and PBzA	100

3.4.5.1. Incorporation of Crosslinker with PBzA	100
3.4.5.2. Incorporation of Crosslinked Shell	100
3.4.5.3. Self-Crosslinking of PBzA.....	101
3.4.6. Homopolymer Synthesis.....	101
3.4.6.1. BA Synthesis	102
3.4.6.2. BzA Synthesis	102
3.5. Results and Discussion	103
3.5.1. BA/PMMA Particle Synthesis in 60 mL Autoclave	103
3.5.2. BzA/PMMA Particle Synthesis in 60 mL Autoclave	119
3.5.3. Crosslinked Particle Synthesis in 60 mL Autoclave.....	138
3.5.4. Combination of Crosslinking and PBzA.....	143
3.6. Conclusions.....	156
3.7. References.....	158
Chapter 4: Scale up and Particle Size Control.....	163
4.1. Overview	163
4.2. Introduction.....	164
4.2.1. Particle Size Control.....	164
4.2.2. Stabiliser	167
4.2.3. Scale Up	171
4.3. Aims and Objectives	172
4.4. Experimental	173
4.4.1. Materials.....	173
4.4.2. PMMA Particle Synthesis in 60 mL Autoclave	173
4.4.2.1. One-stage Reaction.....	173
4.4.2.2. Two-stage Reaction	174

4.4.2.3. Initiator Injection Reactions	175
4.4.3. PMMA Particle Synthesis in 1 L Autoclave	176
4.4.3.1. One-stage Reaction	176
4.4.3.2. Two-stage Reaction	176
4.4.3.3. Initiator Injection Reactions	177
4.4.4. Core-shell Particles Synthesis in 1 L Autoclave	177
4.4.4.1. BA/PMMA Particle Synthesis.....	177
4.5. Results and Discussion	179
4.5.1. PMMA Particle Synthesis in 60 mL Autoclave.....	179
4.5.1.1. One-stage Reactions	179
4.5.1.2. Two-stage Reactions.....	181
4.5.1.3. Initiator Injection Reactions	183
4.5.2. PMMA Particle Synthesis in 1 L Autoclave.....	185
4.5.2.1. Equipment Test.....	185
4.5.2.2. One-stage Reactions	188
4.5.2.3. Initiator Injection Reactions	195
4.5.2.4. Two-stage Reactions.....	198
4.5.3. BA/PMMA Particle Synthesis in 1 L Autoclave	211
4.6. Conclusions	215
4.7. References.....	217
Chapter 5: Conclusions and Future Work	221
6.1. Overview	221
6.2. Conclusions	221
6.3. Future Work.....	223
6.4. References.....	226

Appendix.....	228
Analysis and Testing of Core-shell Particles.....	228
¹ H NMR Data.....	257

Chapter 1: Introduction

1.1. Overview

The aim of this chapter is to provide a general background to the fundamental concepts used throughout this thesis. The focus of the work presented can be split into two main topic areas; the scale-up of the well-understood dispersion polymerisation of methyl methacrylate (MMA) and the synthesis of well-defined polymer particles for use as impact modifiers. Both areas have made the use of supercritical carbon dioxide (scCO₂) as an alternative reaction medium to traditionally used organic solvents. The main drive for utilising scCO₂ is the ability to produce dry polymer particles, essential for the end application. This removes the need for energy intensive drying steps, associated with the removal of solvent in conventional dispersion polymerisations. A general discussion of polymerisation techniques in both scCO₂ and traditional solvents is given, with a particular focus on dispersion polymerisation. The synthesis of structured particles is also discussed, as this is a key characteristic needed for particles to be used as impact modifiers. Finally, an introduction to impact modifiers is included. This chapter provides a broad overview of the key concepts in this work and has been kept relatively brief. A more detailed discussion of relevant topics is given at the start of each results chapter.

1.2. Polymers

Polymers are long chains of monomers connected by covalent bonds, forming macromolecules. There are many naturally occurring polymers, such as silk, polyisoprene (naturally occurring rubber) and polynucleotides, which make up DNA. Polymers are synthesised using two main mechanisms; step growth and chain growth. The step growth mechanism proceeds by a series of individual reactions to form dimers, followed by trimers and higher order oligomers (Figure 1-1, solid red line). These species then combine to give long polymer chains. This type of reaction

usually involves the elimination of a smaller molecule so is often known as condensation polymerisation. Step-growth polymerisation forms low molecular weight polymer at low conversion, and only at high conversion are high molecular weight polymers formed (Figure 1-1), as described by the Carothers equation shown in Equation 1-1.

$$\overline{X}_n = \frac{1}{1 - p} \quad \text{Equation 1-1}$$

Here, \overline{X}_n is the number average degree of polymerisation and p is extent of the reaction (conversion to polymer) which is calculated using Equation 1-2.

$$p = \frac{N_0 - N}{N} \quad \text{Equation 1-2}$$

In Equation 1-2, N_0 is the number of molecules present initially as monomer and N is the number of molecules present after time t , including all degrees of polymerisation (dimer, trimer, oligomer etc.)

Examples of polymers synthesised by this method include polyesters and nylons (polyamides).¹ Due to the multifunctional nature of the monomers, polymers produced by this mechanism are much more likely to exhibit a wider range of structures, from linear to heavily crosslinked.^{2, 3}

In chain growth polymerisation, monomer units are added to the growing chain one at a time hence, it is also known as addition polymerisation and there is usually no by-product. The reaction method involves an active centre such as a radical or ion. This commercially important polymerisation technique usually occurs through addition to a vinyl group, producing a polymer chain with a carbon-carbon backbone. High molecular weight polymers are formed at low conversion and then a plateau in the molecular weight is observed (Figure 1-1, solid blue line). Usually only linear or

lightly branched polymers are formed by the chain growth method.^{2,3} Examples of polymers synthesised using this method include polyethylene (PE), polypropylene (PP) and poly(vinylchloride) (PVC).^{4,5}

A further type of chain growth polymerisation is living polymerisation. In this polymerisation the ability of a growing polymer to chain transfer, or terminate, has been removed. A narrow molecular weight distribution is achieved by living polymerisation, with the molecular weight increasing linearly with conversion (Figure 1-1, dashed green line). Living polymerisation can follow anionic, cationic and radical polymerisation mechanisms.

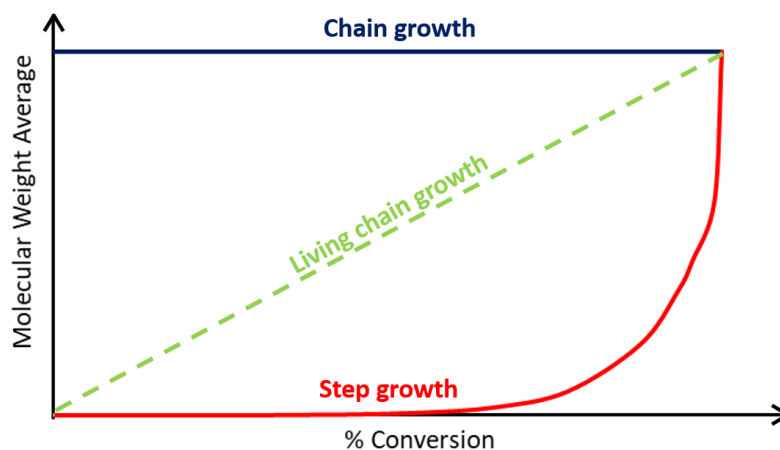


Figure 1-1: Relationship between molecular weight and conversion for chain growth polymerisation (solid blue), step growth polymerisation (solid red) and living chain growth (dashed green).⁶For step growth % conversion is measured as functional group depletion.

Synthetic polymers can be grouped based on their structure as either a homopolymer, in which the repeating monomer unit is the same, or a copolymer in which there are two or more different monomer units. These differing structures can occur in several arrangements (Figure 1-2).

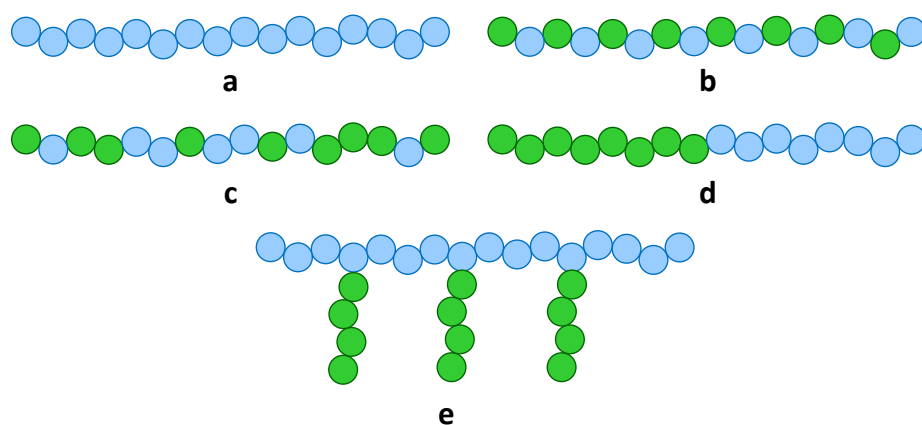


Figure 1-2: Schematic representing the differing polymer structures that can be synthesised; homopolymer (a), alternating copolymer (b), statistical copolymer (c), block copolymer (d) and grafted copolymer (e). Coloured circles represent different monomer units.

The amount of branching and the type of monomer present dictates the way the polymer chains pack together, which impacts the properties of the polymer and in turn, the applications for which it can be used. The structures formed from packing of polymer chains can be categorised in three ways; crystalline, semi-crystalline or amorphous. Crystalline polymers exhibit regular, ordered chain packing, amorphous polymers have no order in chain packing and semi-crystalline polymers contain both regions.² The polymers studied in this thesis were amorphous.

An important parameter associated with amorphous polymers is the glass transition temperature (T_g). It corresponds to the temperature at which the polymer changes from a glass-like state to a rubber-like state. At temperatures above the T_g , the individual polymer chains have enough energy to move and partially untangle, causing the polymer to become soft, a rubber elastomer. Below the T_g , the polymer chains are packed together with little energy, forming a hard, brittle, glass-like state, a plastic. The T_g of a polymer is a very important property as it dictates the applications for which it can be used with regards to temperature. For example, where a flexible rubber is required, the polymer has to have a low T_g and where a hard non-flexible material is required, it must have a higher T_g than the temperature it will be used at. The T_g of a polymer is often measured by differential scanning calorimetry (DSC) or dynamic mechanical analysis (DMA).^{7,8}

There are several mechanisms used to synthesise polymers, including cationic, anionic, Ziegler-Natta catalyst (polyolefins), olefin metathesis and ring-opening. The work presented has used a radical polymerisation method.

1.3. Free Radical Polymerisation

Free radical polymerisation (FRP) is a widely used polymerisation technique. It is a type of chain growth polymerisation, which is utilised for a variety of different monomer types, mainly vinyl monomers. It is used extensively on the laboratory scale as well as in industry due to its relative simplicity. FRP consists of four key steps; initiator decomposition (radical generation), initiation (radical addition), propagation (further radical addition and chain growth) and finally termination by either combination or disproportionation (radical re-combination).^{6,9}

1.3.1. Initiation

Initiation of the reaction requires a radical centre to start chain growth, which is typically supplied by the decomposition of an initiator molecule. Common initiators used in FRP are peroxide or azo compounds. These can decompose by several mechanisms, including thermal decomposition. The initiator used in this work was 2,2'-Azobis(isobutyronitrile) (AIBN), which is commonly used in a range of organic solvents, and decomposes thermally over a useful timeframe at 50-70 °C.⁶ AIBN is also soluble in scCO₂, the solvent used in this thesis, under the reaction conditions employed (65 °C, 207 bar).¹⁰ The driving force of the decomposition is the formation of two 2-cyano-2-propyl radicals which are stabilised by the electron withdrawing CN group and release of N₂ gas (Figure 1-3).

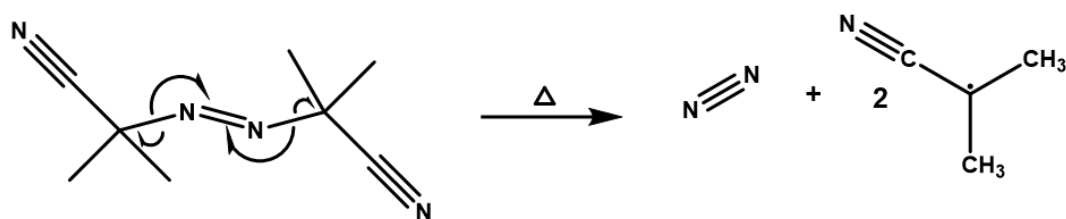


Figure 1-3: Schematic of AIBN thermal decomposition, producing N_2 and two active 2-cyano-2-propyl radicals.

After initiator decomposition, the initiator radical generated reacts with the double bond present in the vinyl monomer unit to start growth of a polymer chain. This is facilitated in MMA by the electron withdrawing ester group (Figure 1-4).

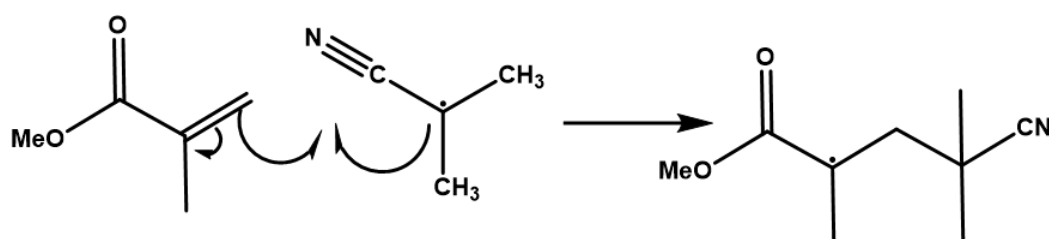


Figure 1-4: Schematic showing the initiation of a MMA monomer unit by an AIBN radical.

1.3.2. Propagation

Once initiated, the radical, which is now located on the terminal monomer unit, will react further with more monomer units to propagate a polymer chain. This addition occurs in a head-to-tail fashion, thus maintaining stabilisation by the electron withdrawing ester group. Asymmetric monomers are described as having a head and a tail, where the carbon atom carrying the pendent substituent is usually called the head. Whether head-to-head or tail-to-head addition occurs will affect the properties of the polymer produced. With vinyl polymers, the head-to-tail addition is favoured.⁶ An example of propagation using MMA (Figure 1-5) shows at each addition the radical centre is transferred to the end of the chain. High activity of the radical is maintained throughout the reaction and a relatively high molecular weight polymer is formed.

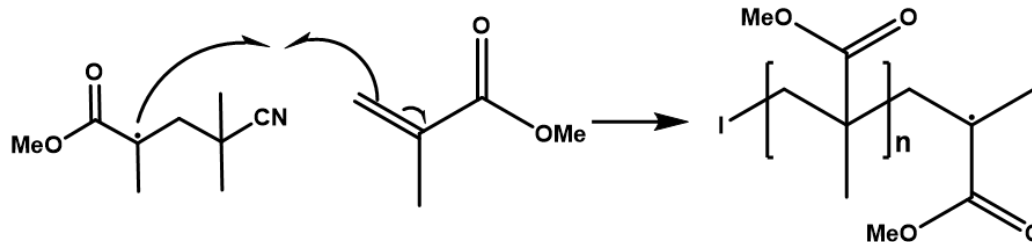


Figure 1-5: Schematic showing propagation of a growing MMA polymer chain, where the initiating molecule has been abbreviated to I. The degree of polymerisation is given by n.

1.3.3. Termination

After some time, termination of the reaction occurs, and the growth of the polymer chain ceases. Termination happens when two active species (radicals) react together. This can take place via two different mechanisms: combination, the addition of two growing polymer radical chains; or disproportionation, abstraction of a hydrogen from a second growing polymer chain.⁶ Termination by combination proceeds via head-to-head addition of two growing polymer chains, resulting in the formation of high molecular weight polymer. Abstraction of a hydrogen from the end of another growing polymer chain, leads to disproportionation. The result is the formation of two separate polymer chains; one with a terminal hydrogen and the other with a double bond at the end of the chain. Both processes are kinetically equivalent and are shown with a PMMA chain (Figure 1-6).

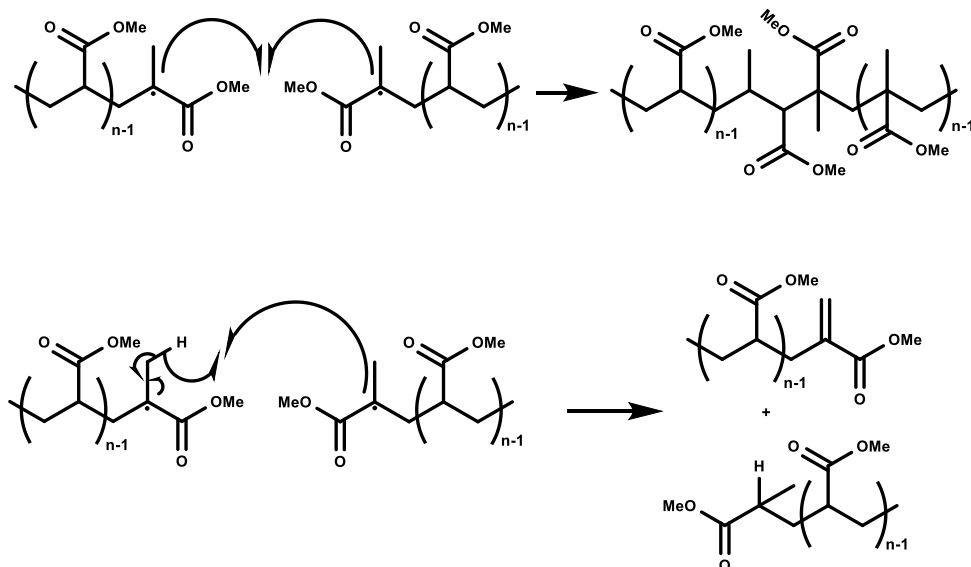


Figure 1-6: Schematic showing chain termination of PMMA via combination (top) and disproportionation (bottom).

FRPs high tolerance of trace impurities allows for the synthesis of high molecular weight polymers from commercially available monomers without the requirement for the removal of the stabilisers and in the presence of trace amounts of oxygen or in solvents that have not been rigorously dried or purified.⁶ However, a limitation with FRP is that it exhibits relatively low control over the molecular weight of the polymer produced, reducing the capacity to produce complex polymer architectures when compared to living polymerisation. Relatively broad dispersities (\mathcal{D}) are often observed ($\mathcal{D} > 2.0$) and chains are irreversibly terminated, preventing the formation of block copolymers. To overcome this there are several controlled polymerisation techniques such as reversible addition-fragmentation chain-transfer (RAFT) polymerisations, atom transfer radical polymerisation (ATRP) and nitroxide mediated polymerisation (NMP).⁶ All these techniques use a reversible-deactivation radical polymerisation mechanism. They exhibit many of the characteristics of living polymerisation but can undergo chain transfer and termination. The reactions contain species that limit the radical present in the reaction and control the kinetics. This control gives the ability to form polymers with narrow molecular weight distribution with low dispersities ($\mathcal{D} > 1.2$). The reaction mechanisms also terminate

the polymer chains with end groups capable of re-initiation, allowing for the synthesis of block copolymers.^{6, 11}

1.4. Polymer Synthesis

FRP can be employed in a variety of different polymer synthesis methods that will now be described further.

1.4.1. Bulk Polymerisation

Bulk polymerisation is the simplest form of a polymerisation reaction and involves the addition of an initiating species to pure monomer, in the absence of a solvent. This method can produce high molecular weight polymers but has some significant disadvantages. As the reaction proceeds, the medium becomes more viscous and heat dissipation decreases. This leads to an increased rate of polymerisation, which in turn, increases viscosity leading to an uncontrolled reaction. As the viscosity increases, the rate of diffusion of polymers is reduced and in turn the rate of termination decreases. Diffusion of monomer is not affected. This results in a decrease in the rate of termination with little change in the rate of propagation. As the reaction is exothermic, more heat is produced which accelerates the rate further, generating more heat and further increasing the temperature. This is known as the Trommsdorff effect (or gel effect) and can have dangerous consequences.^{2, 3}

1.4.2. Solution Polymerisation

Addition of a solvent can reduce the risk of the Trommsdorff effect occurring. The solvent reduces the viscosity of the reaction and aids heat dissipation. However, the addition of solvent has disadvantages of its own. It introduces the complication of isolating the products at the end of the reaction, along with having to select the right solvent for the polymerisation. A further disadvantage is the reduced polymerisation

rate, leading to longer reaction times and lower molecular weight polymers being formed. Solvent based polymerisations can be heterogeneous or homogeneous.^{2, 3}

1.5. Polymer Particle Synthesis

The synthesis of well-defined polymer particles has attracted a large amount of research interest. This is as a result of their diverse range of applications, for example as fillers in paints, chromatography column packing and spacers in liquid crystal display screens.¹² Polymer particles can be synthesised via various solution based radical polymerisation methods such as emulsion or dispersion.¹³ The choice of synthesis method depends on numerous factors such as desired particle size, area of application and monomers used, to name a few. Synthesis techniques will be discussed further in the following section, with particular focus on polystyrene (PSt) and PMMA particles, as production of these via the various techniques is well-studied.

1.5.1. Emulsion Polymerisation

Emulsion polymerisation is a heterogeneous, solvent based, FRP process. It involves emulsification of a relatively hydrophobic monomer in water by a surfactant, forming large monomer droplets. Once the surfactant is above a critical concentration, micelles are formed. Initially, monomer is held mostly in a separate droplet phase, with a limited amount dissolved in the continuous phase and in the micelles. The initiator present is soluble in the continuous phase. Initiation occurs in the continuous phase before monomer diffuses out of the droplet and into the micelle where the reaction continues and polymer precipitates. The reaction proceeds until the monomer is depleted and then the reaction ends. The final product is a suspension of polymer particles in water, which is often referred to as a latex (Figure 1-7).¹⁴

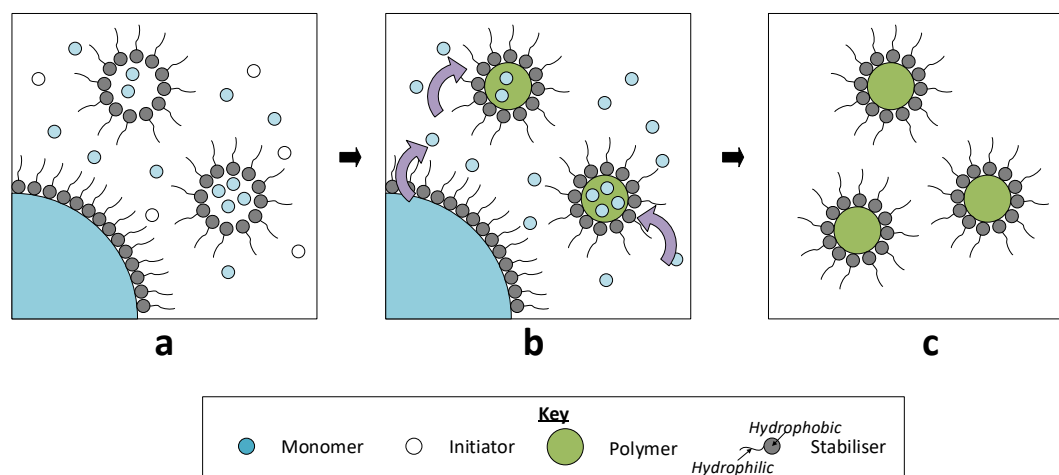


Figure 1-7: Schematic representing the mechanism of emulsion polymerisation. Initially monomer is held mostly in a separate droplet phase, with a limited amount dissolved in the continuous phase and in micelles, (a). The initiator present is soluble in the continuous phase. Monomer diffuses out of the droplet and into the micelle where the reaction occurs and polymer precipitates, (b). The reaction proceeds until the monomer is depleted. The resulting product is particles suspended in the continuous phase, (c).

Emulsion polymerisation usually produces particles with diameters of approximately 0.05-1 μm .¹⁴⁻¹⁶ Typical monomers polymerised using this technique include butyl acrylate (BA), styrene (St), vinyl acetate (VA) and vinyl chloride (VC), all of which are frequently reported in literature.^{14, 16-18}

In 1959, Zimmt *et al.* reported the comparison of the emulsion polymerisation of MMA to St.¹⁹ The polymerisation reactions were performed at 60 °C, on a 600 g scale using Tergitol “7” as surfactant and potassium persulfate ($\text{K}_2\text{S}_2\text{O}_8$) as initiator. The kinetics of the polymerisations were studied along with the effect of stirring rate on particle size. The most significant difference was reported as the strong acceleration observed during the polymerisation of MMA in comparison to St. This was attributed to the fact that the polymerisation of MMA is subject to a strong gel effect, whereas this is not observed with St. The stirring speed had negligible effect on the size of the MMA and St particles produced.

More recently, in 2010, Arora *et al.* described the synthesis of PMMA particles by batch emulsion polymerisation.¹⁵ Here, $\text{K}_2\text{S}_2\text{O}_8$ and sodium stearate were used as initiator and surfactant respectively. The kinetics of the FRP was studied by

measurement of conversion and rate of polymerisation with respect to time. The reaction system was also modelled. The authors found evidence for the Trommsdoff effect from the degree of polymerisation and conversion measured.¹⁵

This shows that even though FRP of MMA has existed for a long time, there is still a large amount research being carried out to better understand the system.

1.5.2. Dispersion Polymerisation

Dispersion is another type of polymerisation that is used to prepare micron sized particles (Figure 1-8). The reaction is initially homogeneous with the initiator, monomer and surfactant being soluble in the continuous phase (or solvent).

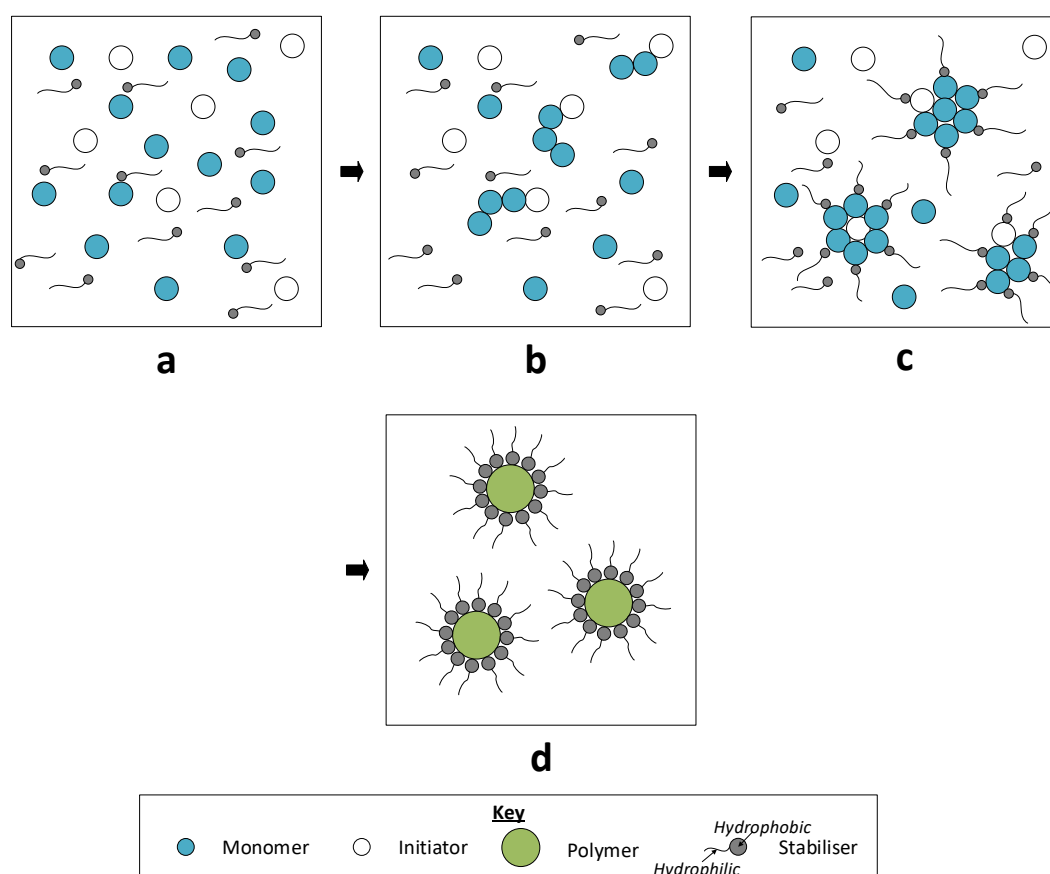


Figure 1-8: Schematic representation of steric stabilisation in dispersion polymerisation. Polymerisation begins (a), polymer chains begin to propagate (b), polymer chains reach critical molecular weight and precipitate before being stabilised (c), particles with a “hairy” layer of stabiliser are formed (d).

As the polymerisation proceeds, chains reach a critical molecular weight (J_{crit}) and become insoluble in the solvent. This causes phase separation to occur. At this point the growing polymer is stabilised by the surfactant via the steric stabilisation mechanism; either by absorption or chemical bonding to the surface. This prevents aggregation and promotes growth of discrete particles. Polymer propagation continues in the growing particles and initiation occurs in the continuous phase.^{20, 21} Dispersion polymerisation produces spherical polymer particles with the final particle size and distribution largely determined by amount of monomer and the type of surfactant present. The typical size ranges from 100 nm to 10 μm .^{22, 23}

Several monomers have been polymerised by this method. Okubo *et al.* reported the synthesis of micron-sized monodisperse polymer particles of PSt by seeded dispersion polymerisation (Figure 1-9).²⁴ Seeded polymerisation involves the addition of preformed seed particles at the start of the reaction which provides a nucleation site for further polymerisation. These polymer seeds help to remove the variability in the nucleation stage that arises from the sensitive production of radicals. Particles of 6.1 μm were synthesised using a method the authors named the “dynamic swelling method”. In this method monodisperse PSt seed particles were prepared in an ethanol-water medium in the presence of a poly(acrylic acid) (PAA) stabiliser and AIBN. These seed particles were then swollen with monomer before further polymerisation took place.²⁴

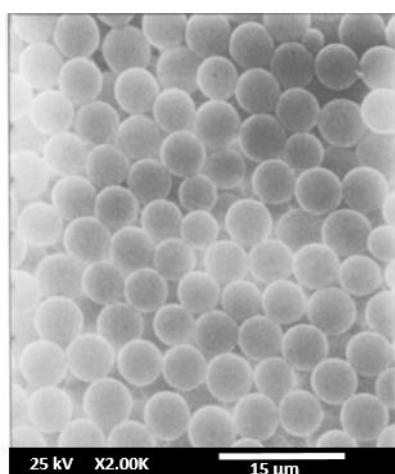


Figure 1-9: SEM image of PSt particles synthesised using the dynamic swelling method.²⁴

Shen *et al.* reported the dispersion polymerisation of MMA to form particles ranging in diameter from 2 to 10 μm .²⁵ Several parameters were varied individually and in combination to investigate what effect they had on particle size. Increasing the polymerisation temperature, concentration and decomposition rate of the initiator and solvency of the dispersion medium caused an increase in particle size. Decreasing the concentration and molecular weight of the polymeric stabiliser poly(vinyl pyrrolidone) (PVP) also increased the size of the particles produced. The smallest particles were afforded with a monomer concentration of 10 wt%, the reasons for which are discussed further in Chapter 3.

The effect of temperature and initiator levels was also investigated by Ober *et al.* in the dispersion polymerisation of St.²⁶ It was reported that as the initiator concentration or temperature was increased, the particle size increased (Figure 1-10). This was said to be related to the molecular weight of the polymer formed during the nucleation stage. In order to produce monodisperse particles, a specific initiator concentration was required for each reaction temperature.

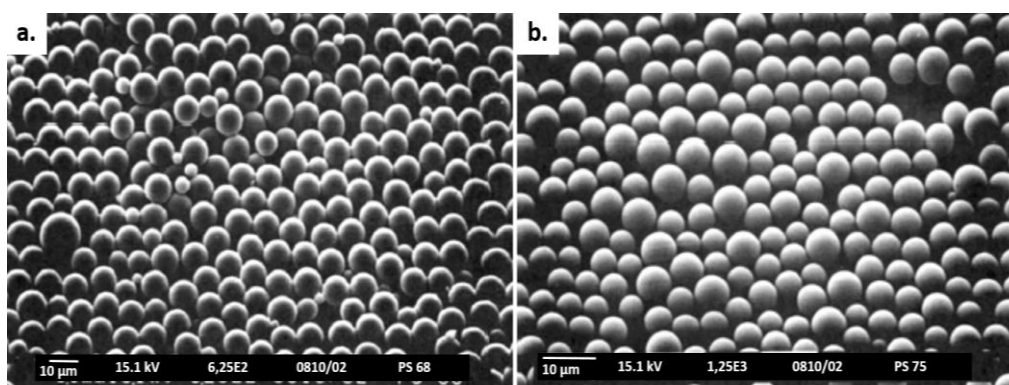


Figure 1-10: SEM images of PSt particles synthesised at 68 °C (a) and 75 °C (b). Particles produced at 68 °C were larger than those produced at 75 °C.²⁶

Sáenz *et al.* also investigated the effect of several parameters such as type of agitation, monomer purification and nitrogen purge had on the particle size distribution of PSt synthesised by dispersion polymerisation in ethanol.²⁷ The same parameters were also varied with the copolymerisation of St and BA in a water-

ethanol mix. It was found that monomer purification along with purging with nitrogen were most important in achieving monodispersity in size for both reaction systems.

1.5.3. Structured Polymer Particles

Structured particles have potential uses in many applications including drug delivery,²⁸ optical electronics²⁹ and coatings.³⁰ The structures present can take many different forms such as core-shell (Figure 1-11, images a), or one polymer dispersed within another (Figure 1-11, images c and d). They can even be porous.³¹ Two main topic areas will be discussed in the following sections including the formation of structured particles by block copolymers and the formation of core-shell particles from non-covalently linked polymers.

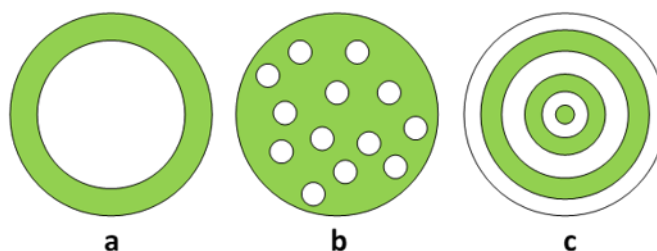


Figure 1-11: Images showing different structured particles; core-shell (a) and spherical and lamellar domains of polymer 1 in polymer 2 (b,c).

1.5.3.1. Block Copolymers

The most common method for forming structured particles is through the synthesis of block copolymers. The use of controlled polymerisation techniques such as RAFT allow for the formation of polymer chains with end groups capable of re-initiation, a vital property for the synthesis of block copolymers. A block copolymer consists of two or more chemically different polymers that are covalently bound.³² Under the right conditions, if the two polymer blocks are immiscible, these materials will undergo micro phase separation and self-assemble.³³ Traditionally, the structure

that forms is dependent on the volume fraction of the two blocks along with the miscibility of the two polymers. Common structures that block copolymers form are spheres, gyroid, cylindrical and lamellar (Figure 1-12).³²

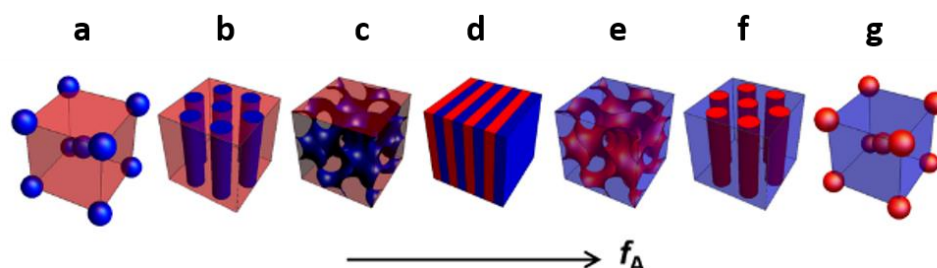


Figure 1-12: Schematic showing how the morphology of a block copolymer changes as the volume fraction of monomer A (shown in blue) increases from left to right. The following morphology are formed; spherical (a), cylindrical (b), gyroid (c), lamellar (d), inverse gyroid (e), inverse cylindrical (f) and inverse spherical (g).³²

Kagawa *et al.* synthesised submicron-sized poly(*i*-butyl methacrylate)-block-polystyrene (PiBMA-*b*-PSt) particles by two-step ATRP in aqueous medium.³⁴ PiBMA particles were prepared by miniemulsion-ATRP with polyoxyethylene sorbitan monooleate (Tween) as emulsifier. These particles were then used as seeds in the seeded-ATRP of St. Transmission electron microscopy (TEM) images of cross sections of the particles showed an ‘onion-like’ structure (lamellar), had been formed (Figure 1-13).

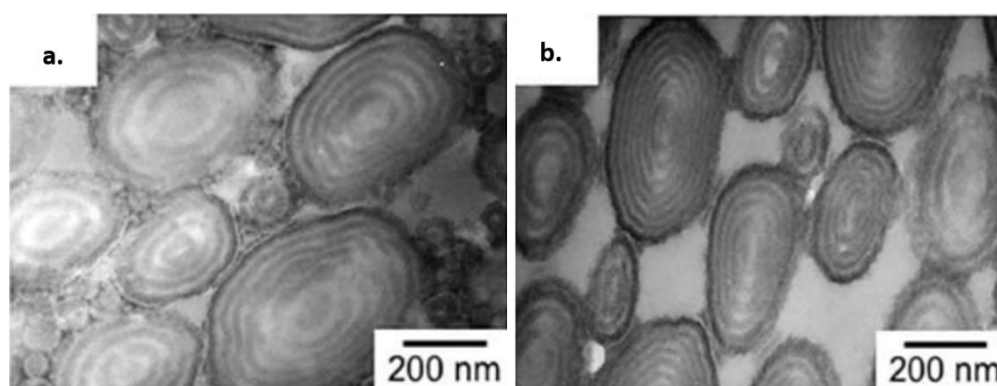


Figure 1-13: TEM images of PiBMA-*b*-PSt particles stained with RuO₄, prepared by seeded-ATRP with PiBMA particles prepared by the miniemulsion-ATRP at Tween 80 concentrations of 3 wt% (a) and 6 wt% (b) based on iBMA. An ‘onion-like’ structure was observed.³⁴

PSt is frequently used in block copolymers and Jeon *et al.* reported the synthesis of symmetric diblock copolymers of polystyrene-block-polybutadiene (PSt-*b*-PBD) via anionic polymerisation.^{35, 36} The authors investigated the interface-driven morphological development of this block copolymer when confined in oil-in-water emulsion droplets. Addition of an amphiphilic stabilising copolymer of either polystyrene-block-poly(ethylene oxide) (PSt-*b*-PEO) or polybutadiene-block-poly(ethylene oxide) (PBD-*b*-PEO), controlled the surface preferences of the PSt and PBD blocks at the emulsion interface. Inclusion of PSt homopolymer (hPSt) also contributed to the self-assembled morphology formed. Several parameters were found to influence the internal morphology, including the volume fraction (Φ) of hPSt out of the total volume of hPSt and PSt-*b*-PBD, and the volume fraction (f_s) of PSt blocks out of the total volume of PSt in the PSt-*b*-PEO and PB-*b*-PEO surfactant. These parameters coupled with the ratio of the diameter (D) of the emulsion drop to the feature spacing (L_0) of the phase-separated periodic domains. The emulsion drops were solidified by evaporating the solvent, yielding particles of PSt-*b*-PBD and hPSt with unique external shapes and internal morphologies that were examined by scanning electron microscopy (SEM) and TEM respectively (Figure 1-14).

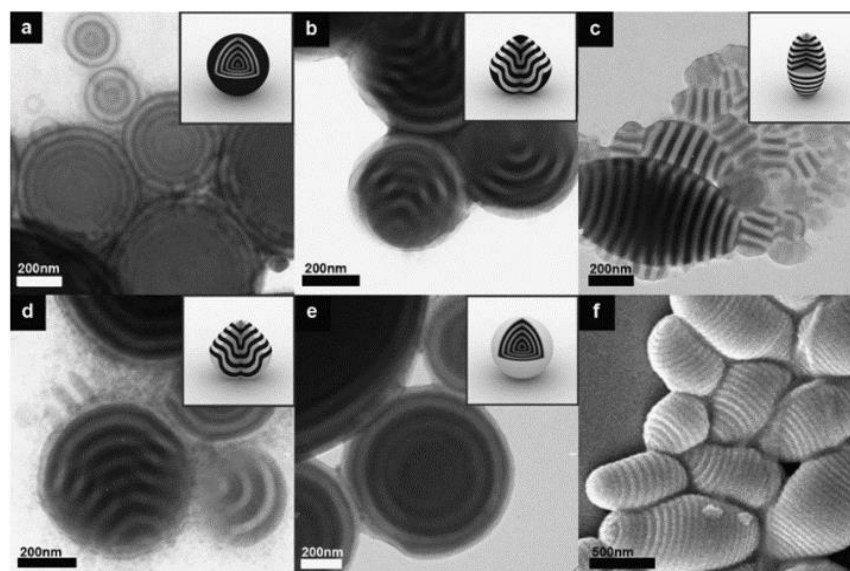


Figure 1-14: TEM images of particles containing different internal morphologies; “onion-like” particles for $f_s=0$ (a), “tulip-bulb” particles for $f_s=0.36$ (b), prolate particles for $f_s=0.46$ (c), inverted “tulip-bulb” particles for $f_s=0.77$ (d), inverted “onion-like” particles for $f_s=1$ (e) and an SEM image of the prolate particles for $f_s=0.46$ (f).³⁵

Particles of this type have various applications such as catalytic supports, and optochemical sensing.³⁵

More recently, Luo *et al.* described the controlled synthesis of polystyrene-block-poly(butyl acrylate)-block-polystyrene (PSt-*b*-PnBA-*b*-PSt) triblock copolymers.³⁷ Emulsion polymerisation using specifically designed macro-RAFT agents afforded particles with high conversion and low dead chain content. A lamellar internal structure was observed in TEM analysis of samples containing PSt-PnBA-PSt with the molecular weights 45K-90K-45K respectively. DSC analysis confirmed two T_g transition, indicating the presence of both a PSt and a PnBA phase.

Structure can also be formed in a method known as polymerisation-induced self-assembly (PISA). This technique exploits the increasing insolubility of a propagating polymer chain to induce the self-assembly process during polymerisation. The strategy typically utilises a soluble homopolymer that is extended by the addition of another monomer. As more monomer is added, the growing block gradually becomes insoluble, and the resulting polymer self-assembles to minimise the unfavourable solvent interactions. The most common polymerisation method used in PISA is RAFT.³⁸⁻⁴⁰

1.5.3.2. Core-shell Particles

A further internal morphology observed in particles is the core-shell structure. The definition of a core-shell particle given by IUPAC is “*polymer particle comprising at least two phase domains, one of which (the core) lies within the other(s) that form the polymeric outer layer(s) (the shell(s))*” (Figure 1-15).^{13,41} Particles with a core-shell structure can be used in a wide range of applications including coatings,³⁰ catalysts, adhesives⁴² and drug delivery systems.^{13, 43}

Previously discussed block copolymers can self-assemble to give structures classed, by the above definition, as core-shell. However, block copolymers are most likely to form spherical structures (Figure 1-15 images c and d). It is unlikely that desired structures such as images a and b will be formed (Figure 1-15). Here, the main

notable difference between the two is the internal domain size. Structures similar to images a and b are more likely to be formed with non-covalently bonded polymers (Figure 1-15).

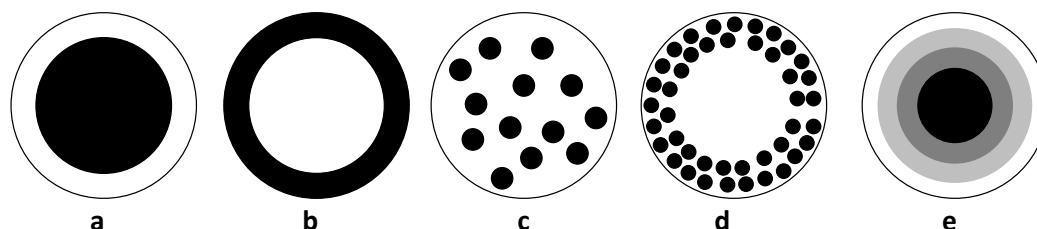


Figure 1-15: Schematic showing structures categorized as core-shell; core-shell (a), inverse core-shell (b), domains of polymer 1 in polymer 2 (c,d) and gradient composition change of particle shell (e).¹³

Particles with the core-shell structure containing a large internal domain can be synthesised in various ways. Methods are usually divided into one-, two- or higher-step syntheses. A one-step process involves the direct copolymerisation of two polymers that self-assemble to give internal structure. This is similar to block copolymer formation, but as mentioned is rarely observed with block copolymers. Synthesis of a core followed by the formation of a shell is known as the two-step method. The shell can be generated by various means when using a two-stage process. The most common method is swelling of a polymer seed with a comonomer, which is subsequently polymerised. A grafting from method can be utilised if there are reactive sites present on the polymer core. Alternatively, various macromolecules may be bound to these active sites on the polymer seed, this is known as the grafting-to method.¹³

A large area of interest for core-shell particles is their use as additives. Improving the properties of thermoplastic products is of great importance due to their uses in a variety of applications. Many materials have limitations, such as brittleness, which restricts the function for which they can be used. One way of overcoming this is the addition of polymer particles to modify the properties of a material. Many properties can be modified such as colour, viscosity and transparency.⁴⁴ The class of additives

used to enhance mechanical property is known as an impact modifier.⁴⁵ Particles used as impact modifiers usually utilise a core-shell structure. The particles consist of a soft/low T_g core which can absorb energy from an impact. This is usually encased in a hard/high T_g shell which helps the particle maintain its morphology during processing. The shell also aids compatibilisation and the dispersion of the particles in the polymer matrix to which they are being added. In general, the internal structure parameters of the particles which impact their toughening efficiency include; particle size, shell thickness and degree of crosslinking.⁴⁶⁻⁴⁸ The composition and synthesis of core-shell particles specifically used to increase impact resistance are discussed further in Chapter 4.

1.6. Impact Modifiers

Impact resistance is defined as *“the ability of a material or structure therefrom to withstand the application of a sudden load without failure”*.⁴⁹ Factors such as the structure of the thermoplastic, the type of the stress state it experiences during the impact event, the rate at which the impact load is applied, and the temperature of the material all contribute to the impact resistance of a material.⁵⁰ Polymer particles with a core-shell internal morphology can be used to improve impact resistance. These particles are incorporated into the compounded material prior to moulding or extrusion. Impact modifiers are added to a wide range of polymer matrices including PVC, PSt and PP.^{51, 52} When incorporated into a polymer matrix, well-dispersed core-shell particles can induce several different toughening mechanisms such as crazing, shear yielding and rubber particle cavitation. These locally diffuse microscopic mechanisms of deformation can occur individually or in combination. They make the matrix in which the particles are incorporated capable of dissipating large impact energies, thus avoid catastrophic failure.⁵²

Shear yielding and crazing are the two main localised deformation mechanisms inherent to amorphous glassy polymers. Shear is a strain produced by the application of pressure. Shear yielding is thermoplastic deformation in the form of shear bands, which are areas of intense strain that distort the body shape without significant

volume distortion.⁵² Further deformation by this mechanism leads to material hardening, which in turn results in multiplication and propagation of shear bands through the material. This process is often preceded by particle cavitation; the formation of small voids within the particle.⁵³ This ability of the rubber modifier to deform by elongation and/or cavitation also aids in altering impact resistance.⁵⁰

Crazing is the nucleation of microvoids in regions of stress concentration such as a crack. The microvoids form a network through the material (Figure 1-16, image b). These voids are stabilised by highly stretched molecular chains (also known as fibrils) preventing the propagation of the crack and instead forming crazes (Figure 1-16).⁵⁴ Crazes propagate through a material perpendicular to the direction of the applied stress. Collision with a neighbouring core-shell particle causes termination of these crazes (Figure 1-16, image c).⁵²

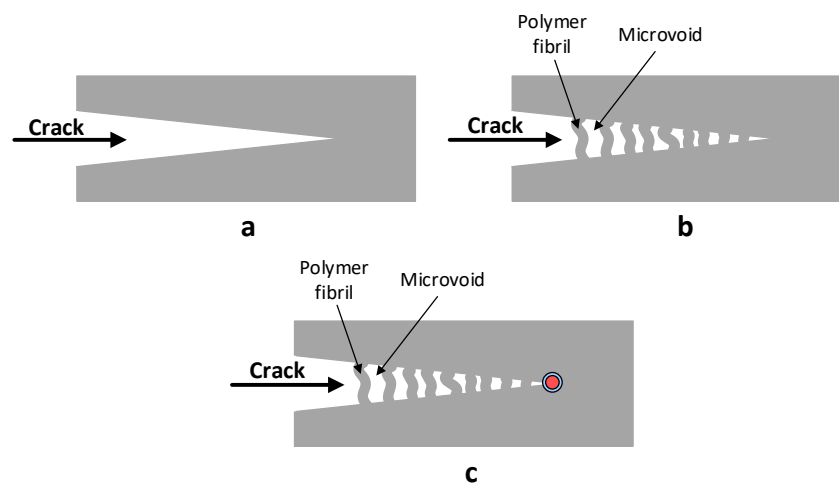


Figure 1-16: Schematic show a section of crack (a), a stabilised crack known as a craze (b) and termination of a craze by a core-shell particle (c).⁵²

When dispersed within the matrix, the core-shell particles act as stress concentrators that provide multiple sites at which shear yielding and/or crazing can be initiated.⁵⁰ In the region surrounding the equator of the modifier particle, the tensile stress is amplified. Moving away from the modifier particle, the amplified stress decays relatively quickly to the level of the applied stress (Figure 1-17).⁵⁰

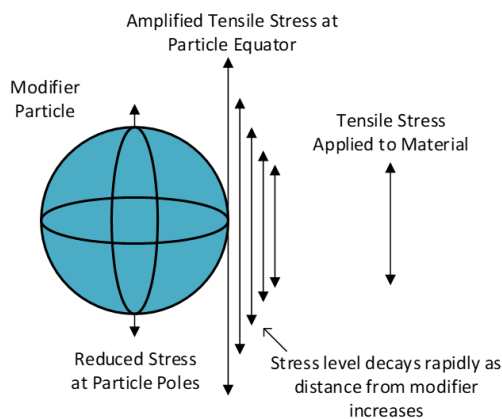


Figure 1-17: Schematic depicting stress concentration that occur in the polymer matrix around an impact modifier upon application of a tensile stress to the material.⁵⁰

Incorporation of core-shell particles within a material creates multiple sites at which the discussed toughening mechanisms can occur; shear yielding and/or crazing. Impact on a material containing core-shell particles results in a structure with a large number of small crazes and/or shear bands (Figure 1-18). This is a more stable structure and which is less prone to failure than a material with a small number of large crazes or shear bands which would be created in the absence of the core-shell particles.^{50, 52}

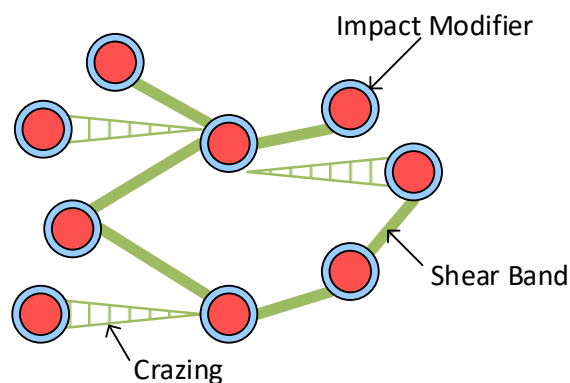


Figure 1-18: Schematic depicting a material containing a large number of small crazes and shear bands facilitated by the incorporation of core-shell impact modifier particles.⁵²

Core-shell particles synthesised by traditional solvent based techniques yield a latex as the end product. For applications such as impact modifiers, a dry polymer powder

is needed. Hence, removal of the solvent is required which can be achieved in various ways such as filtration or spray drying, both of which are energy intensive. One possible alternative is the use of supercritical fluids (SCFs) as a reaction medium, which upon release of the pressure post polymerisation affords free-flowing, solvent-free polymer powder.

1.7. Supercritical Fluids

Many polymerisations are carried out using volatile organic compounds (VOCs), chlorofluorocarbons and water as solvents.²² However, as we become more concerned with the environmental impact of our work, there has been an increased interest in alternative, greener solvents.⁵⁵ In recent years attention has turned to using SCFs as a reaction medium. SCFs have unique physical properties, exhibiting diffusion coefficients similar to a gas whilst having liquid like densities allowing for solvation of many compounds.⁵⁶ A substance exists in its supercritical state when it is above its critical temperature (T_c) and critical pressure (p_c), this is known as its critical point.

1.7.1. Supercritical Carbon Dioxide

More specifically, supercritical carbon dioxide ($scCO_2$) has been investigated as a reaction medium. $scCO_2$ is a promising alternative to conventional solvents because of its tuneable properties and high natural abundance. It has an easily accessible critical point; $T_c = 31.1\text{ }^\circ\text{C}$ and $p_c = 73.8\text{ bar}$.^{22,56} This transition can be visualised using a view cell as shown in images a, b and c in Figure 1-19.

Initially, two phases can be observed; liquid (bottom) and gas (top) (image c, Figure 1-19). As the temperature of the sealed system is increased the liquid begins to boil and expand as its density decreases (image b, Figure 1-19). At the same time the density of the gas phase is increasing. When the densities become equal the critical point is reached and a single phase is observed (image a, Figure 1-19).

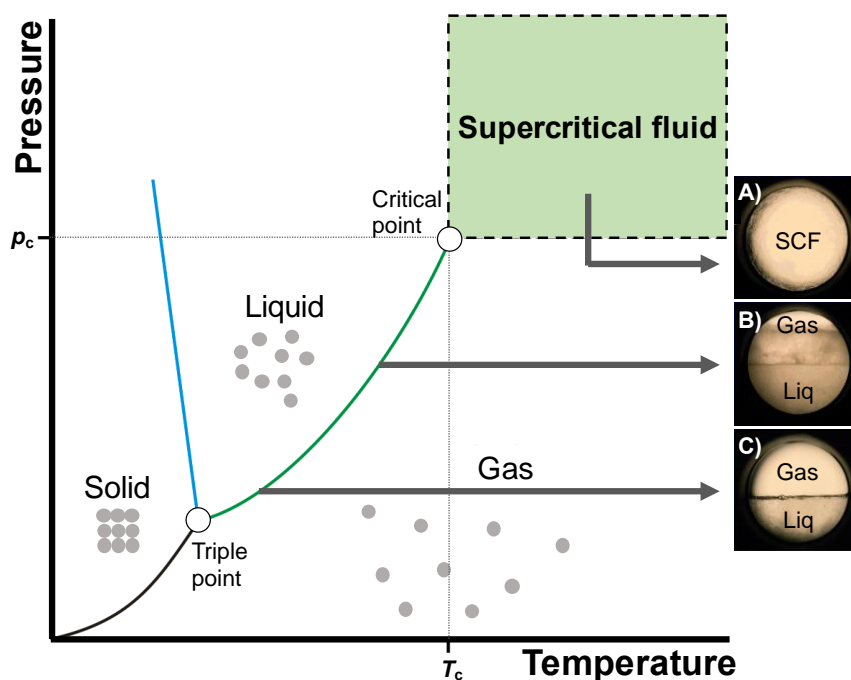


Figure 1-19: Pressure-temperature phase diagram for a pure component CO₂ system, showing the supercritical fluid (SCF) region. The critical pressure (P_c) and critical temperature (T_c) are indicated.^{57, 58} Photos on the right show the different stages in a view cell.

CO₂ can be recovered as a by-product from other processes including fermentation, combustion and ammonia synthesis, therefore producing no net contribution to the greenhouse effect making it a green solvent.⁵⁹ scCO₂ has been used in polymer processing, such as extraction of low molecular weight contaminants or fractionation of polymers or copolymers by molecular weight and/or composition. Recent research that has looked into using scCO₂ as a solvent for polymer synthesis will be reviewed in the following section.^{56, 58, 60}

1.8. Polymer Synthesis in scCO₂

CO₂ is inexpensive, non-toxic, non-flammable and is readily available in high purity. These properties coupled with the fact that it reverts to its gaseous state upon depressurisation, eliminating energy intensive drying steps, make it a desirable solvent for carrying out polymerisations. Several different polymerisation reactions including free radical chain growth, cationic chain growth, oxidative coupling,

Other fluorinated acrylates, methacrylates and fluoroalkyl-derivatised St monomers have also been polymerised or copolymerised in scCO₂ via homogeneous methods.^{56, 58, 68} Beuermann *et al.* reported homogeneous FRP of St in scCO₂.⁶⁹ For this, harsher conditions were needed (80 °C, 200-1,500 bar) and a tetrabromomethane (CBr₄) chain transfer agent (CTA) was required to reduce the molecular weight. The high-pressure conditions and low conversion caused the reaction to remain homogeneous and only low molecular weight polymer was synthesised (11,000 g mol⁻¹). Other successful homogeneous polymerisations in scCO₂ include cationic polymerisation of vinyl and cyclic ethers.^{62, 63}

1.9. Particle Synthesis in scCO₂

The lack of solubility of most common high molecular weight polymers in CO₂, under practical conditions, is often regarded as a disadvantage in its use as a polymerisation medium. However, for heterogeneous polymerisation processes such as precipitation, emulsion, suspension and dispersion, this insolubility is a prerequisite for the reaction.⁵⁶

1.9.1. Emulsion and Suspension Polymerisation in scCO₂

Emulsion and suspension polymerisations have also been reported in scCO₂. Beckman *et al.* investigated the water-in-oil or “inverse” emulsion polymerisation of acrylamide in scCO₂ (AIBN, 65 °C, 352 bar, 1 hour). Addition of a surfactant gave a more stable latex, although high molecular weight and good monomer conversion was achieved in the absence of surfactant.⁷⁰

Synthesis of biodegradable polyesters using scCO₂ by emulsion polymerisation in scCO₂ has also been reported. Hile *et al.* discuss the copolymerisation of D,L-lactide and glycolide giving poly(D,L-lactide-*co*-glycolide) (PLGA). The reaction proceeds via a Sn catalysed ring-opening polymerisation (ROP). Inclusion of the fluoropolymer surfactant PFOA allowed for delayed precipitation of the polymer, leading to an

increase in conversion. Conversion of 99% and 65% for glycolide and D,L-lactide respectively were reached after 72 hours at 200 bar and 70 °C.⁶⁶

Bratton *et al.* also reported the suspension polymerisation of L-lactide in scCO₂.^{71, 72} The authors reported the use of a poly(caprolactone)-telechelic dihydroxyl terminated perfluoropolyether-poly(caprolactone) (PCL-*b*-PFPE-*b*-PCL) triblock copolymer as stabiliser.⁷¹ The PCL segments were “polymer-philic” and the PFPE central block was CO₂ soluble (“CO₂-philic”). Ring opening polymerisation (ROP) performed utilising this stabiliser gave acceptable yields and molecular weights. It was reported that the stirring rate was important in controlling the formation of a fine, powdered product. At a PCL-*b*-PFPE-*b*-PCL loading of 10 wt% and a stirring speed of 300 rpm particles of 5–10 µm were synthesised. In contrast, the same loading of PCL-*b*-PFPE-*b*-PCL and a stirring speed of 50 rpm yielded particles in the range of 40-60 µm.⁷¹

1.9.2. Precipitation and Dispersion Polymerisations in scCO₂

Precipitation polymerisation methods have been used to successfully synthesise a range of polymers, including the heavily researched area of vinyl monomers because of their industrial importance.⁵⁸ Common vinyl monomers exhibit high solubility in CO₂, with the corresponding polymers exhibiting very poor solubility.^{56, 73}

Romack *et al.* reported the successful precipitation polymerisation of acrylic acid (AA) in scCO₂ at pressures ranging from 125 to 365 bar, with AIBN as the initiator. It was shown that pressure had no effect on the molecular weight, molecular weight distribution, or particle structure. Addition of a CTA allowed for molecular weight control.⁷⁴ Similarly, precipitation polymerisations of MMA and AA have been successful with molecular weight being controlled by CTAs.⁵⁸

Dispersion polymerisation has also been successful in scCO₂ and in the last 25 years many monomers have been polymerised utilising this reaction technique (Figure 1-21).^{56, 60}

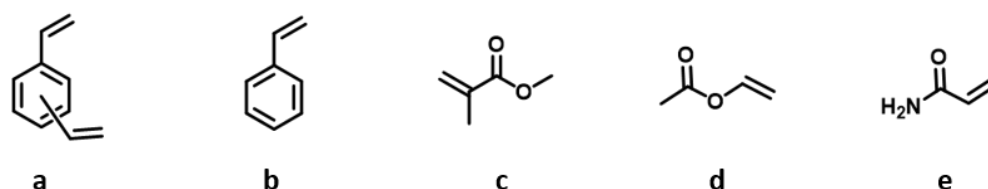


Figure 1-21: Structures of monomers synthesis via dispersion polymerisation utilising CO_2 as a reaction medium; divinyl benzene (a), styrene (b), methyl methacrylate (c), vinyl acetate (d) and acrylamide (e).⁵⁶

However, there is not one defined system that works for all types of monomer. Factors such as polymerisation rate, polymer plasticisation and solubility of the polymer in its monomer, coupled with experimental conditions such as temperature and pressure play a crucial role in primary particle nucleation. Hence, each monomer has different optimum conditions for polymerisation.⁵⁸

The first example of free radical dispersion polymerisation utilising scCO_2 as the reaction medium was reported in 1994 by DeSimone.²² Relatively low molecular weight PMMA ($77\text{-}149 \text{ kg mol}^{-1}$) and low monomer conversion (10-40%) was achieved with the absence of any stabiliser. Addition of a CO_2 soluble surfactant, PFOA, increased conversion (>90%) and molecular weight ($190\text{-}325 \times 10^3 \text{ kg mol}^{-1}$) of the PMMA formed under mild conditions (65 °C, 204 bar). SEM analysis showed uniform spherical particles with an average diameter in the range 1.2 to 2.5 μm were produced (Figure 1-22).⁷⁵

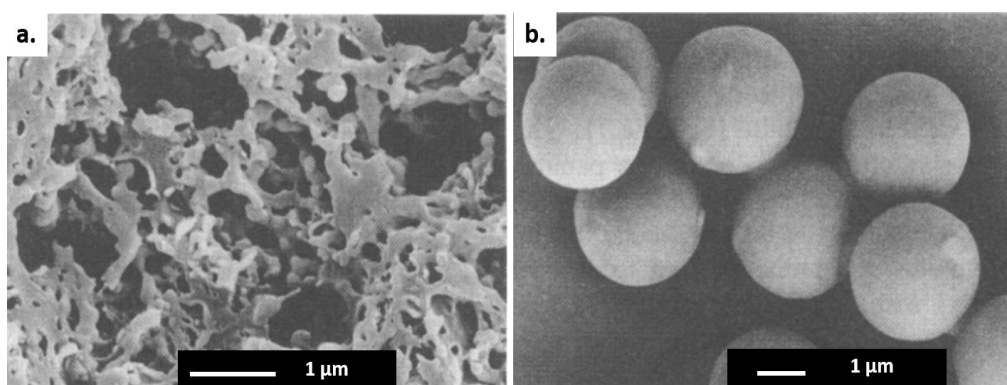


Figure 1-22: SEM images showing PMMA synthesis by dispersion polymerisation; in the absence of stabiliser (a) and with 2% (w/v) PFOA stabiliser.⁷⁵ In the absence of stabiliser no particles are formed.

DeSimone and other groups went on to investigate free radical dispersion polymerisation of not only MMA but also VA and St using a variety of stabilisers.^{22, 56, 58, 76}

Synthesis of PSt particles in scCO₂ was also reported by Shiho *et al.* via dispersion polymerisation. High yields were reported (> 85%) under mild conditions (40 hours, 370 bar, 65 °C). PFOA as well as poly(1,1-dihydroperfluorooctyl methacrylate) PFOMA were used as stabilisers to yield uniform PSt particles ranging from 2.9 to 9.6 µm in diameter (Figure 1-23).^{77, 78}

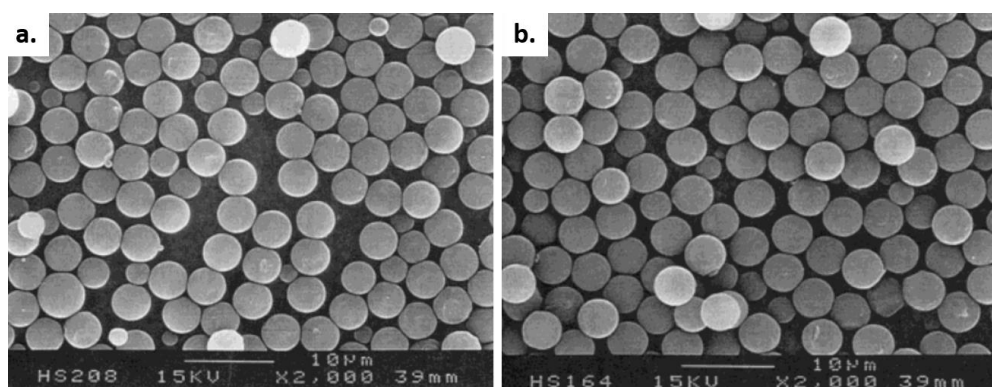


Figure 1-23: SEM images of PSt particles synthesised by dispersion polymerisation using; PFOA (a) and PFOMA (b) as stabiliser.⁷⁷ Both stabilisers formed monodisperse particles. Scale bars are 10 µm.

Moving away from fluorinated stabilisers, research into dispersion polymerisations using siloxane-based surfactants, such as poly(dimethyl siloxane) (PDMS) has increased. Silicon based stabilisers are generally cheaper, more environmentally friendly and the solubility of silicone polymers aids characterisation. In 1996 Shaffer *et al.* reported synthesis of high molecular weight PMMA via dispersion polymerisation in scCO₂ using methacrylate terminated PDMS (PDMS-MA) and AIBN (65 °C, 340 bar, 4 hours).⁷⁶ Particles with diameters between 1.1 and 2.8 µm were formed, with a trend of decreasing particle size as concentration of PDMS-MA increased.

O'Neill *et al.* also investigated the dispersion polymerisation of MMA in scCO₂ using a similar PDMS macromonomer which reacts *in situ* to form a stabiliser species. Polymerisations were carried out using this stabiliser in both liquid and supercritical CO₂, giving particles ranging from 1.1-5.8 µm. *In situ* turbidimetry was used to study the particle formation and growth. A linear increase in average particle diameter was observed after 15 minutes.^{79, 80}

The same type of PDMS-MA macromolecule stabilisers were used for dispersion polymerisation in scCO₂ by Giles *et al.*^{81, 82} The authors varied both the molecular weight and concentration of the PDMS-MA. It was found that at least 2 wt% of 10,000 molar mass PDMS-MA was needed to stabilise the dispersion. At this concentration high yields and high conversion were reported. At a concentration of 5 wt% and above, spherical particles of 2-3 µm were produced. Similarly, when 5,000 molar mass PDMS-MA was employed, at least 5 wt% was needed to stabilise the reaction. In contrast, when employing a 2,000 molar mass PDMS-MA only 2 wt% was needed to form particles.⁸¹

In recent years, increasingly more sophisticated chemistry has been reported using scCO₂ as a reaction medium for polymer synthesis. Three of the most widely used controlled/living radical polymerisation techniques: NMP, ATRP and RAFT, have been used in the synthesis of many novel particle-based polymer materials. All three mechanisms have been successful in synthesising well-defined particles with narrow size distributions.⁸³⁻⁸⁷

1.9.3. Structured Particle Synthesis in scCO₂

As with traditional solvent based polymerisation, the controlled techniques mentioned give access to more complex structures. These methods have also been employed in scCO₂ to produce particles including crosslinked,⁸⁸ inorganic nanoparticles⁸⁹ and more recently block copolymer particles with internal phase separation.^{90, 91}

Jennings *et al.* reported the synthesis of block copolymers using a range of monomers including methacrylates, acrylamides and styrenics via a one-pot RAFT polymerisation in scCO_2 .⁹¹ The resulting block copolymers self-assembled to form nanostructures within the polymer particles. The structure formed was dependent on the chemical nature of the blocks as shown in Figure 1-24 with block copolymers consisting of PMMA and poly(benzyl methacrylate) (PBzMA).

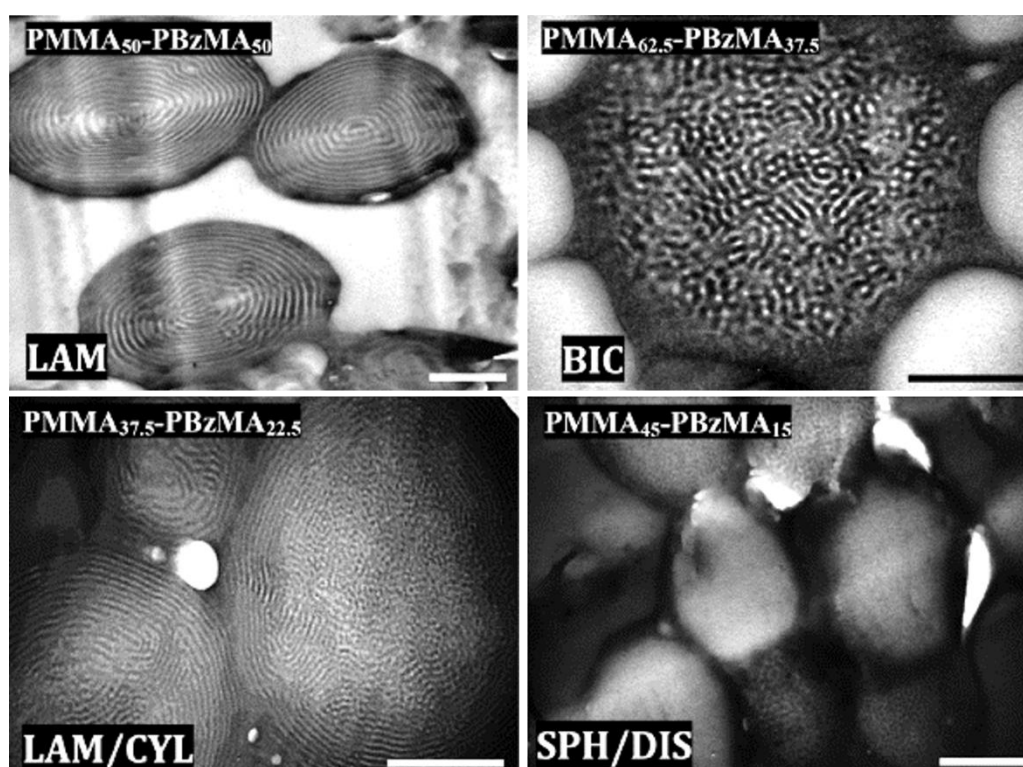


Figure 1-24: TEM images of cross-sectioned PMMA-*b*-PBzMA particles prepared in different experiments and targeting a range of different final volume fraction and molecular weights. A variety of morphologies were observed; lamellar (LAM), bicontinuous (BIC), lamellar/cylindrical coexistence (LAM/CYL) and spherical/disorder coexistence (SPH/DIS). The scale bar in all images is 500 nm.⁹¹

Nanostructures including multilayer, curved cylindrical and spherical domains were observed. This work was built upon with an analysis of the blocking efficiency of the RAFT technique via gel permeation chromatography (GPC) and investigation into the phase behaviour of a collection of structurally varied block copolymers. Interestingly, the authors report that the relative CO_2 -philicity of the two blocks can influence the

observed volume fraction, thus the phase separation, leading to non-equilibrium morphologies.^{90, 92}

Polymerisations in scCO₂ have also produced well-defined crosslinked polymer particles. Cooper *et al.* reported the polymerisation of divinyl benzene (DVB) at 65 °C and 310 ± 15 bar using AIBN. Particle size was found to be influenced by the amount of stabiliser present (1.5-5 µm). High yields were obtained both with and without stabiliser.⁸⁸

1.9.4. Core-shell Particle Synthesis in scCO₂

Synthesis of core-shell structures has also been reported using scCO₂ as the reaction medium. Haldorai *et al.* reported the encapsulation of Zirconium dioxide (ZrO₂) by PMMA via *in situ* radical dispersion of ZrO₂ particles (200 nm) with MMA.⁹³ The commercially available stabiliser poly(dimethylsiloxane)-*g*-pyrrolidone carboxylic acid was used (Monosil PCA, Uniquema). The ZrO₂ particles were first synthesised by a sol-gel method before being surface modified by a methacryloxypropyltrimethoxysilane (MPTMS) coupling agent. The surface modified particles were dispersed in MMA before being placed in a high-pressure vessel, to which AIBN and stabiliser were added. The polymerisation of MMA was performed at 65 °C and 345 bar for 12 hours. TEM confirmed the successful encapsulation of the ZrO₂ (Figure 1-25).

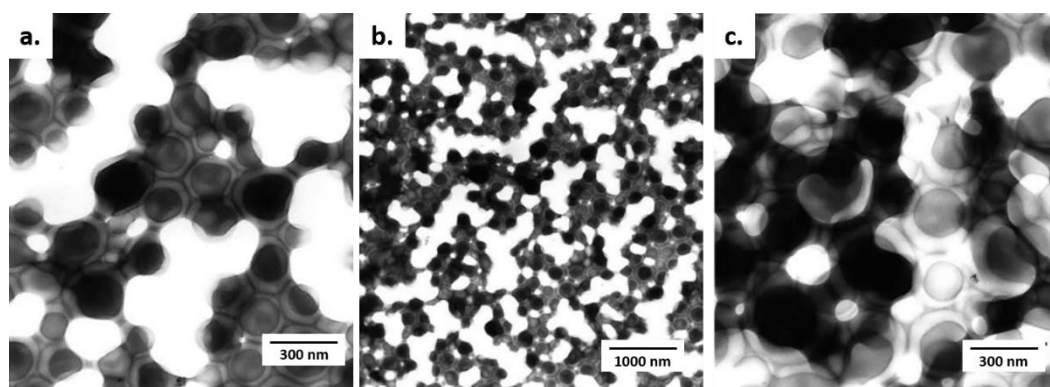


Figure 1-25: TEM images of PMMA/ZrO₂-2.5% (a), PMMA/ZrO₂-5% (b) and PMMA/ZrO₂-10% (c) composites. Images show the presence of a core-shell structure for all loadings. The PMMA core is light and the ZrO₂ is dark.

Core-shell polyurethane-PDMS particles ($\approx 1 \mu\text{m}$), with applications in the biomedical field have also been synthesised via step growth polymerisation in scCO_2 .⁹⁴ Chambon *et al.* reported the use of the CO_2 soluble hydroxyl terminated PDMS (PDMS-OH) stabiliser in the polymerisation of isocyanate in scCO_2 . The hydroxyl functional group present in the stabiliser reacted with the isocyanate to form core-shell type structure; PDMS outer shell, polyurethane core. Procedures were carried out at 60°C and 200-250 bar. TEM analysis confirmed the presence of a core-shell structure.

The latter example shows the synthesis of core-shell particle in CO_2 utilising a one-step polymerisation, in which a block copolymer structure self-assembles to form a core-shell type morphology. McAllister *et al.* reported the development a two-stage synthesis method for the dispersion polymerisation of MMA in scCO_2 .¹² This method allowed for the addition of a second monomer whilst the reaction was still under pressure. In this example, an extra charge of MMA was used to reduce particle size distribution. In theory, this same method could be used for addition of a different second monomer, opening up the possibility to form core-shell particles. This method would mimic the common two-stage injection method used in the synthesis of core-shell particles in tradition solvent based systems.⁹⁵⁻⁹⁷

McAllister *et al.* have recently expanded on this method of the injection of a second monomer part way through the dispersion polymerisation reaction.⁹⁸ The authors synthesised PMMA particles before the addition of various second monomer species including dimethylaminoethyl methacrylate (DMAEMA). Comparisons were made between reactions carried out in scCO_2 and an analogous procedure carried out in dodecane. DMA confirmed the presence of two polymer phases, exhibiting two T_g transitions similar to the homopolymers. TEM analysis supported this, indicating particles synthesised in CO_2 produced a core-shell structure, with domains of DMAEMA within PMMA. Particles synthesised in traditional solvents produced the inverse of this, with a core of PMMA surrounded by a shell of DMAEMA (Figure 1-26). A DMAEMA feed of 67 wt% gave incorporation of 49 wt% poly(dimethylaminoethyl acrylate) (PDMAEMA), which was confirmed by ^1H NMR. The difference in morphology between the particles synthesised in scCO_2 vs. dodecane (core-shell vs.

inverse core-shell respectively) was attributed to the plasticisation ability of $scCO_2$. Under the conditions used the PMMA particle, synthesised first, would be plasticised allowing for penetration of the second monomer. This plasticisation would not be as exaggerated in dodecane and hence polymer formed in the second stage would remain on the surface of the particle. Use of this method to include a diacrylate dye species and an EGDMA crosslinking species was also reported.⁹⁸

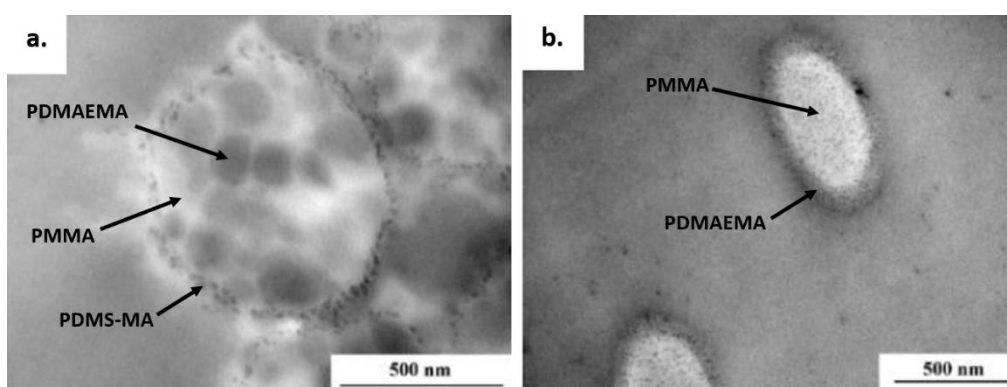


Figure 1-26: TEM images showing the internal morphology observed in particles synthesised using a multi-stage dispersion polymerisation method using, $scCO_2$ (a) and dodecane (b) as the reaction medium. Different polymer phases are indicated.⁹⁸ Scale bars are 500 nm.

1.10. Summary and Thesis Aims

The fundamentals behind radical polymerisation, along with the synthesis of polymer particles via dispersion polymerisation using scCO_2 as a reaction medium, have been introduced in this chapter. This has been expanded on to introduce the concept and synthesis of particles containing internal morphology. This is a key feature needed in the aim of synthesising particles for use as impact modifiers.

Chapter 2 outlines the specialist high-pressure equipment needed to carry out reactions in scCO_2 . A focus of this thesis is the industrial application of scCO_2 as a reaction medium. Therefore, reactions at an increased scale were performed. The design, assembly and safety testing of the equipment required for these large-scale 1 L reactions is also outlined. Further to this, the analytical techniques used to assess the products synthesised are also described in Chapter 2.

The aim of Chapter 3 is to detail the synthesis of core-shell particles for the application of impact modifying. Three structures of interest will be investigated;

- A poly(methyl methacrylate) (PMMA) core with a crosslinked outer PMMA shell (Figure 1-27, image a).
- A poly(butyl acrylate) (PBA) core with a PMMA shell (Figure 1-27, image b).
- A poly(benzyl acrylate) (PBzA) core with a PMMA shell (Figure 1-27, image c).

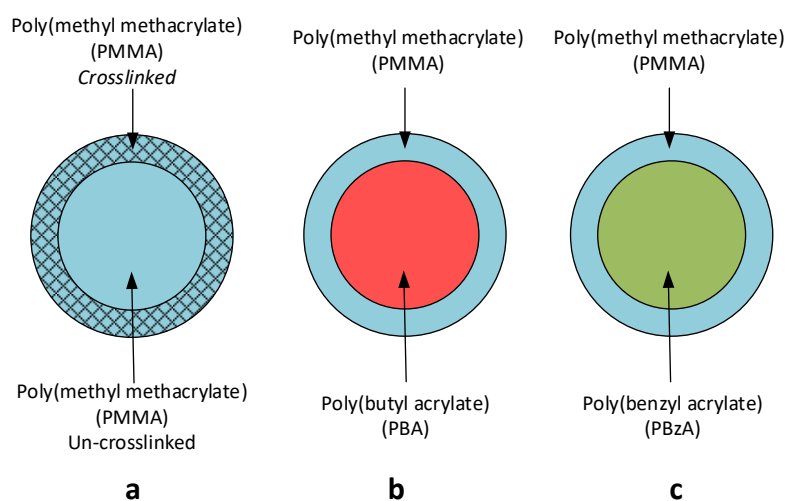


Figure 1-27: Schematic showing the different proposed core-shell structure that were investigated.

The reasons for these structures and choices of monomer will be discussed further. One- and two-stage reaction methods will be tested for synthesis and the internal structure formed was probed with a variety of techniques including DMA, GPC and TEM.

Current industrial polymerisations are performed using emulsion methods. With water as the solvent, which requires highly energy intensive drying steps to yield a powder. Therefore, alternative greener synthesis routes are of interest. With the aim of assessing whether scCO₂ is a viable solvent at the industrial scale, Chapter 4 will look at taking the well-known synthesis of PMMA particles on 60 mL scale to the 1 L scale and assessing whether comparable polymers can be synthesised. Ways of controlling the particle size will also be investigated.

1.11. References

1. S. N. Vouyiouka, E. K. Karakatsani and C. D. Papaspyrides, *Progress in Polymer Science*, 2005, **30**, 10-37.
2. J. W. Nicholson, *The Chemistry of Polymers*, The Royal Society of Chemistry, 2006.
3. D. Walton and P. Lorimer, *Polymers*, Oxford University Press.
4. D. Braun, *Journal of Vinyl and Additive Technology*, 2005, **11**, 86-90.
5. M. van Meurs, G. J. P. Britovsek, V. C. Gibson and S. A. Cohen, *Journal of the American Chemical Society*, 2005, **127**, 9913-9923.
6. G. Odian, *Principles of Polymerisation*, John Wiley & Sons, Inc., 4th edn., 2004.
7. R. Faria, J. C. Duncan and R. G. Brereton, *Polymer Testing*, 2007, **26**, 402-412.
8. M. Reading, A. Luget and R. Wilson, *Thermochimica Acta*, 1994, **238**, 295-307.
9. K. Matyjaszewski and T. P. Davis, *Handbook of Radical Polymerization*, John Wiley & Sons, 2003.
10. Z. Guan, J. R. Combes, Y. Z. Menciloglu and J. M. DeSimone, *Macromolecules*, 1993, **26**, 2663-2669.
11. G. Moad, E. Rizzardo and S. H. Thang, *Australian Journal of Chemistry*, 2005, **58**, 379-410.
12. T. D. McAllister, L. D. Farrand and S. M. Howdle, *Macromolecular Chemistry and Physics*, 2016, **217**, 2294-2301.
13. M. Gosecka and M. Gosecki, *Colloid and Polymer Science*, 2015, **293**, 2719-2740.
14. C. S. Chern, *Progress in Polymer Science*, 2006, **31**, 443-486.
15. P. Arora, R. Jain, K. Mathur, A. Sharma and A. Gupta, *African Journal of Pure and Applied Chemistry*, 2010, **4**, 152-157.
16. J. Ugelstad, M. S. El-Aasser and J. W. Vanderhoff, *Journal of Polymer Science: Polymer Letters Edition*, 1973, **11**, 503-513.
17. S. Okamura and T. Motoyama, *Journal of Polymer Science*, 1962, **58**, 221-228.
18. J. Ugelstad, P. C. Mork, P. Dahl and P. Rangnes, *Journal of Polymer Science Part C*, 1969, **27**, 49-68.
19. W. S. Zimmt, *Journal of Applied Polymer Science*, 1959, **1**, 323-328.
20. P. A. Mueller, G. Storti and M. Morbidelli, *Chemical Engineering Science*, 2005, **60**, 377-397.
21. P. A. Mueller, G. Storti and M. Morbidelli, *Chemical Engineering Science*, 2005, **60**, 1911-1925.

22. J. M. DeSimone, E. E. Maury, Y. Z. Menceloglu, J. B. McClain, T. J. Romack and J. R. Combes, *Science*, 1994, **265**, 356-359.
23. K. P. Lok and C. K. Ober, *Canadian Journal of Chemistry*, 1985, **63**, 209-216.
24. M. Okubo, M. Shiozaki, M. Tsujihiro and Y. Tsukuda, *Colloid and Polymer science*, 1991, **269**, 222-226.
25. S. Shen, E. D. Sudol and M. S. El-Aasser, *Journal of Polymer Science Part A: Polymer Chemistry*, 1993, **31**, 1393-1402.
26. C. K. Ober and M. L. Hair, *Journal of Polymer Science Part A: Polymer Chemistry*, 1987, **25**, 1395-1407.
27. J. M. Sáenz and J. M. Asua, *Journal of Polymer Science Part A: Polymer Chemistry*, 1995, **33**, 1511-1521.
28. J. C. Sung, B. L. Pulliam and D. A. Edwards, *Trends in Biotechnology*, 2007, **25**, 563-570.
29. A. P. Richez, L. Farrand, M. Goulding, J. H. Wilson, S. Lawson, S. Biggs and O. J. Cayre, *Langmuir*, 2014, **30**, 1220-1228.
30. K. R. Christopher, A. Pal, G. Mirchandani and T. Dhar, *Progress in Organic Coatings*, 2014, **77**, 1063-1068.
31. M. T. Gokmen and F. E. Du Prez, *Progress in Polymer Science*, 2012, **37**, 365-405.
32. N. A. Lynd, A. J. Meuler and M. A. Hillmyer, *Progress in Polymer Science*, 2008, **33**, 875-893.
33. J.-T. Sun, C.-Y. Hong and C.-Y. Pan, *Polymer Chemistry*, 2013, **4**, 873-881.
34. Y. Kagawa, H. Minami, M. Okubo and J. Zhou, *Polymer*, 2005, **46**, 1045-1049.
35. S. J. Jeon, G. R. Yi and S. M. Yang, *Advanced Materials*, 2008, **20**, 4103-4108.
36. S. J. Jeon, G. R. Yi, C. M. Koo and S. M. Yang, *Macromolecules*, 2007, **40**, 8430-8439.
37. Y. Luo, X. Wang, Y. Zhu, B.-G. Li and S. Zhu, *Macromolecules*, 2010, **43**, 7472-7481.
38. B. Charleux, G. Delaittre, J. Rieger and F. D'Agosto, *Macromolecules*, 2012, **45**, 6753-6765.
39. M. J. Derry, L. A. Fielding and S. P. Armes, *Progress in Polymer Science*, 2016, **52**, 1-18.
40. N. J. Warren and S. P. Armes, *Journal of the American Chemical Society*, 2014, **136**, 10174-10185.
41. S. Slomkowski, J. V. Alemán, R. G. Gilbert, M. Hess, K. Horie, R. G. Jones, P. Kubisa, I. Meisel, W. Mormann and S. Penczek, *Pure and Applied Chemistry*, 2011, **83**, 2229-2259.

42. C. Zhou, R. Che, L. Zhong, W. Xu, D. Guo and J. Lei, *Journal of Applied Polymer Science*, 2011, **119**, 2857-2865.
43. C. F. Lee, M. L. Hsu, C. H. Chu and T. Y. Wu, *Journal of Polymer Science Part A: Polymer Chemistry*, 2014, **52**, 3441-3451.
44. British Plastic Fedaration, Plastics Additives, <https://www.bpf.co.uk/plastipedia/additives/default.aspx>, (accessed 02 May, 2019).
45. G. F. Wu, J. F. Zhao, H. T. Shi and H. X. Zhang, *European Polymer Journal*, 2004, **40**, 2451-2456.
46. M. Chen, C. Zhou, Z. Liu, C. Cao, Z. Liu, H. Yang and H. Zhang, *Polymer International*, 2010, **59**, 980-985.
47. J. S. Lee and F. C. Chang, *Polymer Engineering and Science*, 2004, **44**, 1885-1889.
48. Q. B. Si, C. Zhou, H. D. Yang and H. X. Zhang, *European Polymer Journal*, 2007, **43**, 3060-3067.
49. A. F. Yee, *Encyclopedia of Polymer Science and Engineering*, John Wiley and Sons Inc., New York, 1987.
50. J. C. Stevenson, *Journal of Vinyl and Additive Technology*, 1995, **1**, 41-45.
51. L. J. Effler and M. T. Berard, *Journal of Vinyl and Additive Technology*, 2003, **9**, 19-25.
52. R. Greco, in *Plastics Additives*, Springer, 1998, pp. 375-385.
53. C. Bucknall, V. Soares, H. Yang and X. Zhang, *Macromolecular Symposia*, 1996, **101**, 265-271.
54. R. Estevez, M. G. A. Tijssens and E. Van der Giessen, *Journal of the Mechanics and Physics of Solids*, 2000, **48**, 2585-2617.
55. E. J. Beckman, *The Journal of Supercritical Fluids*, 2004, **28**, 121-191.
56. J. L. Kendall, D. A. Canelas, J. L. Young and J. M. DeSimone, *Chemical Reviews*, 1999, **99**, 543-564.
57. F. Cansell, B. Chevalier, A. Demourgues, J. Etourneau, C. Even, V. Pessey, S. Petit, A. Tressaud and F. Weill, *Journal of Materials Chemistry*, 1999, **9**, 67-75.
58. A. I. Cooper, *Journal of Materials Chemistry*, 2000, **10**, 207-234.
59. S. G. Kazarian, *Polymer Science Series*, 2000, **42**, 78-101.
60. C. Boyère, C. Jérôme and A. Debuigne, *European Polymer Journal*, 2014, **61**, 45-63.
61. D. A. Canelas and J. M. DeSimone, *Metal Complex Catalysts Supercritical Fluid Polymerization Supramolecular Architecture*, 1997, **133**, 103-140.
62. M. Clark and J. M. DeSimone, *Macromolecules*, 1995, **28**, 3002-3004.

63. M. Clark, J. Kendall and J. DeSimone, *Macromolecules*, 1997, **30**, 6011-6014.
64. S. Curia and S. M. Howdle, *Polymer Chemistry*, 2016, **7**, 2130-2142.
65. D. D. Hile and M. V. Pishko, *Macromolecular Rapid Communications*, 1999, **20**, 511-514.
66. D. D. Hile and M. V. Pishko, *Journal of Polymer Science Part A: Polymer Chemistry*, 2001, **39**, 562-570.
67. J. M. DeSimone, Z. Guan and C. Elsbernd, *Science*, 1992, **257**, 945-947.
68. C. D. Wood, A. I. Cooper and J. M. DeSimone, *Current Opinion in Solid State and Materials Science*, 2004, **8**, 325-331.
69. S. Beuermann, M. Buback, C. Isemer and A. Wahl, *Macromolecular Rapid Communications*, 1999, **20**, 26-32.
70. F. A. Adamsky and E. J. Beckman, *Macromolecules*, 1994, **27**, 312-314.
71. D. Bratton, M. Brown and S. M. Howdle, *Macromolecules*, 2003, **36**, 5908-5911.
72. D. Bratton, M. Brown and S. M. Howdle, *Journal of Polymer Science Part A: Polymer Chemistry*, 2005, **43**, 6573-6585.
73. K. Cho, J. Yang and C. E. Park, *Polymer*, 1998, **39**, 3073-3081.
74. T. J. Romack, E. E. Maury and J. M. DeSimone, *Macromolecules*, 1995, **28**, 912-915.
75. Y.-L. Hsiao, E. E. Maury, J. M. DeSimone, S. Mawson and K. P. Johnston, *Macromolecules*, 1995, **28**, 8159-8166.
76. K. A. Shaffer, T. A. Jones, D. A. Canelas, J. M. DeSimone and S. P. Wilkinson, *Macromolecules*, 1996, **29**, 2704-2706.
77. H. Shiho and J. M. DeSimone, *Journal of Polymer Science Part A: Polymer Chemistry*, 1999, **37**, 2429-2437.
78. H. Shiho and J. M. DeSimone, *Journal of Polymer Science Part A: Polymer Chemistry*, 2000, **38**, 1146-1153.
79. M. L. O'Neill, M. Z. Yates, K. P. Johnston, C. D. Smith and S. P. Wilkinson, *Macromolecules*, 1998, **31**, 2838-2847.
80. M. L. O'Neill, M. Z. Yates, K. P. Johnston, C. D. Smith and S. P. Wilkinson, *Macromolecules*, 1998, **31**, 2848-2856.
81. M. R. Giles, J. N. Hay, S. M. Howdle and R. J. Winder, *Polymer*, 2000, **41**, 6715-6721.
82. M. R. Giles and S. M. Howdle, *European Polymer Journal*, 2001, **37**, 1347-1351.
83. A. M. Gregory, K. J. Thurecht and S. M. Howdle, *Macromolecules*, 2008, **41**, 1215-1222.

84. G. Hawkins, P. B. Zetterlund and F. Aldabbagh, *Journal of Polymer Science Part A: Polymer Chemistry*, 2015.
85. K. J. Thurecht and S. M. Howdle, *Australian Journal of Chemistry*, 2009, **62**, 786-789.
86. J. Xia, T. Johnson, S. G. Gaynor, K. Matyjaszewski and J. M. DeSimone, *Macromolecules*, 1999, **32**, 4802-4805.
87. P. B. Zetterlund, F. Aldabbagh and M. Okubo, *Journal of Polymer Science Part A: Polymer Chemistry*, 2009, **47**, 3711-3728.
88. A. I. Cooper, W. P. Hems and A. B. Holmes, *Macromolecular Rapid Communications*, 1998, **19**, 353-357.
89. T. Hasell, K. J. Thurecht, R. D. W. Jones, P. D. Brown and S. M. Howdle, *Chemical Communications*, 2007, 3933-3935.
90. J. Jennings, M. Beija, J. T. Kennon, H. Willcock, R. K. O'Reilly, S. Rimmer and S. M. Howdle, *Macromolecules*, 2013, **46**, 6843-6851.
91. J. Jennings, M. Beija, A. P. Richez, S. D. Cooper, P. E. Mignot, K. J. Thurecht, K. S. Jack and S. M. Howdle, *Journal of the American Chemical Society*, 2012, **134**, 4772-4781.
92. J. Jennings, S. P. Bassett, D. Hermida-Merino, G. Portale, W. Bras, L. Knight, J. J. Titman, T. Higuchi, H. Jinnai and S. M. Howdle, *Polymer Chemistry*, 2016, **7**, 905-916.
93. Y. Haldorai, T. Zong and J.-J. Shim, *Journal of Applied Polymer Science*, 2012, **123**, 1176-1183.
94. P. Chambon, E. Cloutet and H. Cramail, *Macromolecules*, 2004, **37**, 5856-5859.
95. A. P. Richez, H. N. Yow, S. Biggs and O. J. Cayre, *Progress in Polymer Science*, 2013, **38**, 897-931.
96. J.-S. Song, F. Tronc and M. A. Winnik, *Journal of the American Chemical Society*, 2004, **126**, 6562-6563.
97. J.-S. Song and M. A. Winnik, *Macromolecules*, 2005, **38**, 8300-8307.
98. T. D. McAllister, Expanding the Scope of Free-Radical Dispersion Polymerisation in Supercritical Carbon Dioxide, Doctor of Philosophy, The University of Nottingham, 2017, (*PhD Thesis*).

Chapter 2: Experimental Equipment and Analytical Methods

2.1. Overview

The high-pressure work performed in this thesis was completed in two high-pressure vessels both of fixed volume; a 60 mL and a 1 L autoclave. Both reactors were designed and built in-house and will be discussed further in this chapter. This chapter also covers the analytical techniques used to analyse the synthesised materials.

2.2. High-pressure Equipment

2.2.1. High-pressure Pump

CO₂ was delivered to the system by a PM-101 high-pressure pump (New Ways of Analytics, Germany) (Figure 2-1). Gaseous CO₂ from a cylinder (at a pressure of approximately 55 bar) is drawn by the pump and condensed into liquid form by the pump refrigerator.

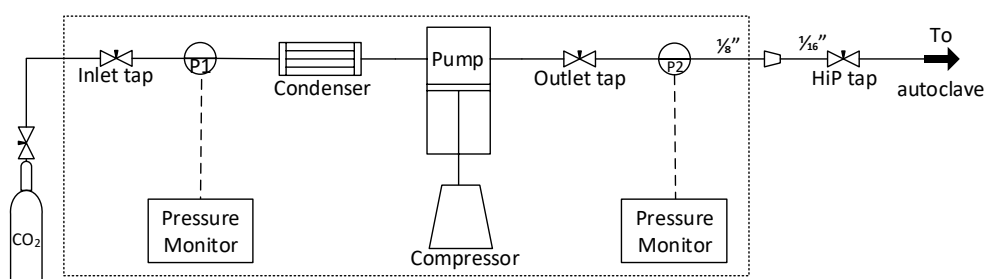


Figure 2-1: Schematic of high-pressure pump used to deliver CO₂.

Compressed air at 3-5 bar (supplied by an external compressor) was used to compress the liquefied CO₂ to give the desired output pressure (200-300 bar) which can be set via an external input on the pump.

2.2.2. 60 mL Autoclave

2.2.2.1. Equipment Overview

The reaction set-up consisted of a pump (described in section 2.2.1), an autoclave, the related pipework, a high-pressure liquid chromatography (HPLC) pump (Jasco PU980) and the associated electronics used to control and monitor the system (Figure 2-2).

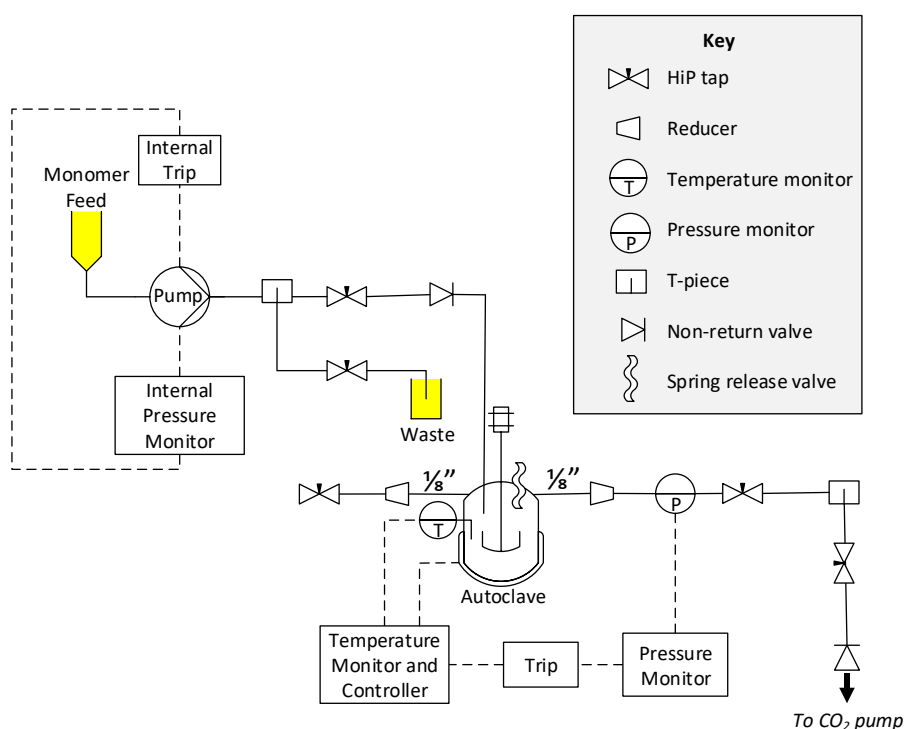


Figure 2-2: Rig diagram of the 60 mL high-pressure autoclave. All pipe work had a diameter of 1/16" unless otherwise labelled.

All pipework used was Swagelok SS316, HiP taps (High Pressure Equipment) were used to control the flow of CO₂ into and out of the autoclave. Non-return valves (NRV) prevented the back flow of reagents into the CO₂ cylinder and HPLC pump.

High-pressure autoclaves, developed and built at The University of Nottingham, were used for polymerisation in supercritical carbon dioxide (scCO₂) (Figure 2-3). The autoclave is constructed from 316 stainless steel and consists of two main parts; a head and a base. The head incorporates a stirring motor, thermocouple, spring-loaded relief valve, safety key, HPLC inlet, CO₂ inlet and outlet. A removable stirrer is used to agitate the system. The head and base are sealed together by placing an ethylene propylene diene monomer (EPDM) O-ring in the ridge of the base and the clamp is fastened around the joint. A unique safety key is used to both lock the clamp and seal the vessel (Figure 2-3, label f). The key acts as a safety barrier, as each key is unique to each clamp, the pressure has to be released by removing the key before the clamp can then be removed and the autoclave opened.

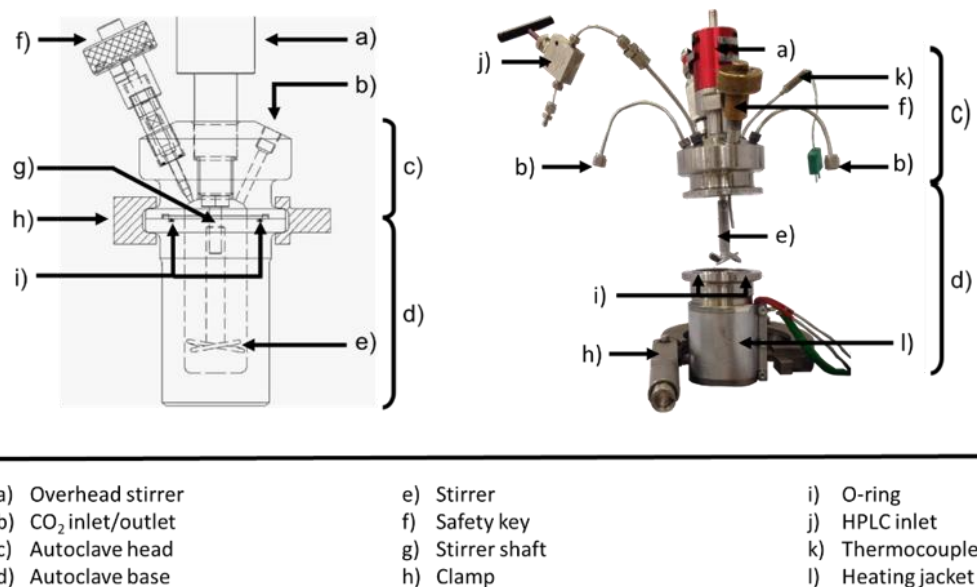


Figure 2-3: Images showing the 60 mL high-pressure autoclave.

A further safety device incorporated in the head is a spring-loaded pressure release valve. If the pressure in the autoclave exceeds 345 bar this release valve opens and

the pressure will reduce preventing any pressure build-up. Once the pressure decreases below 345 bar the valve reseals. The vessel is heated to temperature via a heating jacket attached around the outside of the base. A thermocouple is used to monitor the internal temperature of the system and this feeds back to the control box so the temperature can be kept constant. The pressure of the system is monitored by a piezoelectric transducer located on the CO₂ inlet. As an extra safety precaution, the system is designed to trip, if the pressure exceeds a set limit (approximately 241 bar), where the control box will automatically shut down the power to the heater. A HPLC inlet allows the addition of liquid reagents whilst the autoclave is under pressure via a Jasco PU980 HPLC pump (label J, Figure 2-3). The pump also incorporates a pressure transducer and the power will cut out in the event of a pressure build-up in the pump.

2.2.2.2. Standard Operating Procedure

To ensure safety the following standard operating procedure (SOP) was rigorously followed when performing high-pressure polymerisations:

1: The autoclave is assembled by placing an EPDM O-ring between the autoclave body and head before clamping them together. The clamp is tightened using the safety key, which is then screwed into the head of the autoclave. All fittings to the CO₂ inlet and outlet are secured and all valves are closed. The heating jacket is fitted tight around the autoclave base, but not connected to the heating box at this stage. The thermocouple is plugged in.

2: The system is leak tested by filling the autoclave with CO₂ (approximately 55 bar). Each joint is checked for leaks using Swagelok Snoop[®] leak detector fluid (bubbles will be seen if the joint is leaking). In the event of a leak, the system is depressurised to ambient pressure and any leaking fittings tightened. It is noted that for safety reasons the joints must not be tightened whilst the autoclave is under pressure. The autoclave is refilled with CO₂ (approximately 55 bar) and retested for leaks. In the satisfactory absence of leaks the system is vented to ambient pressure.

3: The safety key is removed revealing a small hole and the autoclave is purged with a flow of CO₂ (2 bar) for 30 minutes in order to remove residual oxygen. After this time, and still under a positive flow of CO₂ the autoclave can be charged with reagents via a syringe through the safety keyhole and re-insert the safety key. Connect the overhead stirrer and switch on.

4: The autoclave is filled with CO₂ (48 bar) before connecting the heating jacket and ensuring that the thermocouple is in place. The temperature is set to 55 °C and allowed to stabilise before gradually increasing the pressure to 138 bar, ensuring that the temperature is stable. Finally, the temperature is set to 65 °C and the temperature and pressure are monitored throughout heating. Once the desired temperature had been reached, if required, increase the pressure to reaction conditions (usually 207 bar).

4a: *(At the required addition time for reaction using the HPLC pump only)*. The HPLC pump and associated pipework is flushed with acetone (approximately 20 mL). The pump is charged with required reagents and the HPLC pipework is filled with the solution. The HPLC pipework is connected to the HPLC inlet located in the autoclave head. When the HPLC inlet tap is closed, the pump is used to build up a pressure that is equal to or just above the pressure inside the autoclave. The HPLC inlet tap is opened and the desired amount of reagents were injected into the autoclave. At the end of the injection procedure the HPLC pipework is disconnected from the autoclave and flushed with acetone.

5: After the desired reaction time, the heating box is set to 0 °C and the heating jacket unplugged from the control box. The autoclave is allowed to cool to room temperature, monitoring the temperature by means of the internal thermocouple.

6: After allowing the autoclave to cool to ambient temperature the remaining CO₂ is slowly vented into the fume hood.

7: Once at ambient temperature and pressure, the key is removed creating a hole and ensuring all residual gas pressure is released, only then is the clamp removed.

The Swagelok fittings of the inlet and outlet are undone. The product is collected for analysis.

2.2.3. 1 L Autoclave

2.2.3.1. Equipment Overview

All “large scale” high-pressure reactions were carried out in a 1 L autoclave analogous to the 60 mL autoclave described in section 2.2.2. As this 1 L equipment had only previously been used for extraction, and not for synthesis, the operating procedure for polymerisations was developed throughout the project. The vessel itself was built by the in-house workshop from 316 stainless steel and consists of a head and base pot (Figure 2-4). Owing to the size, it is housed on a custom build stand in its own room. This room is the high pressure “bomb-proof” room located in the roof of the department.

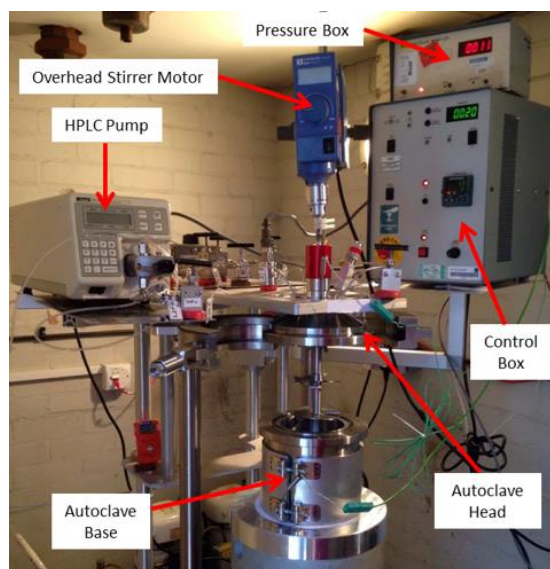


Figure 2-4: Image showing the 1 L high pressure autoclave set-up.

Monitoring of the system, throughout reaction process, was possible by a window in the room as well as from a web camera (Figure 2-5). The system could be controlled

from a computer located outside the room. This also allowed for emergency shutdown of the equipment without the need to enter the room.

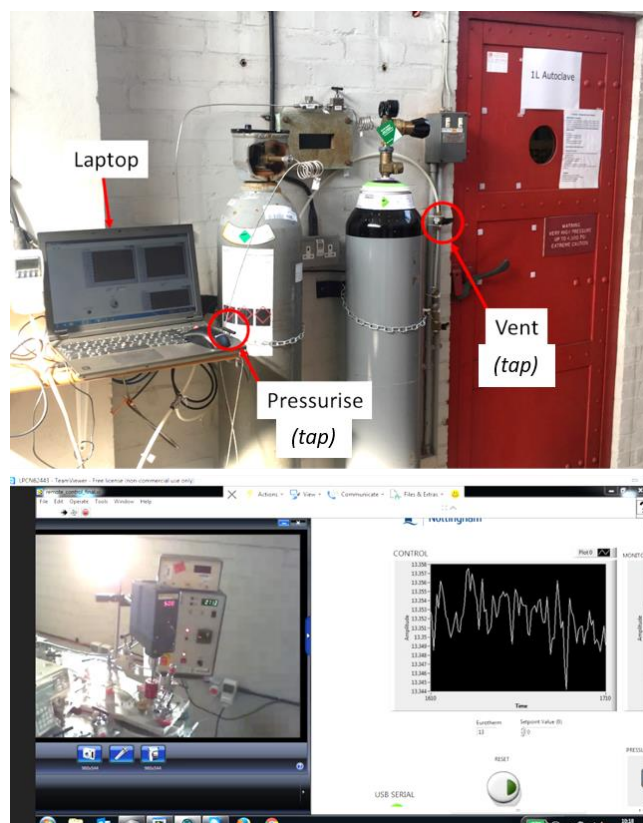
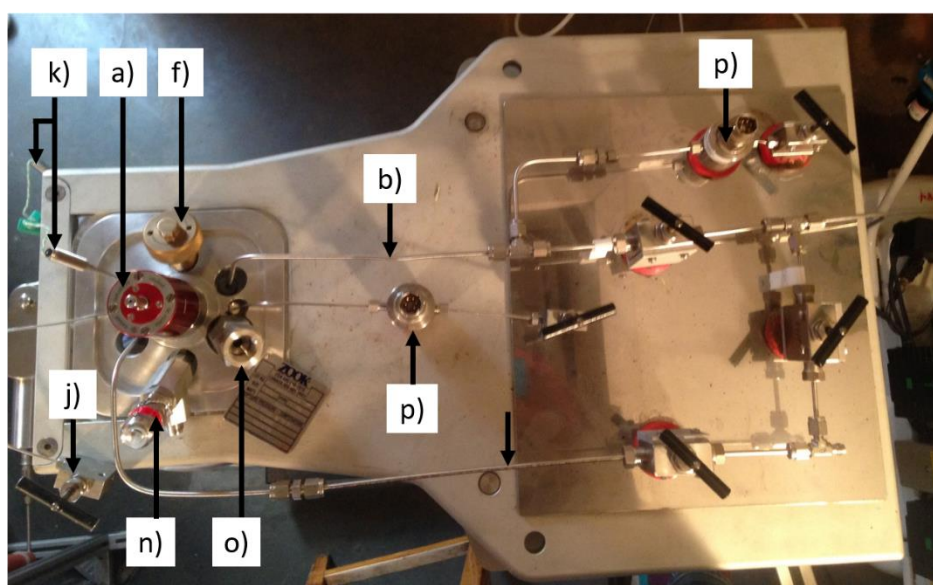
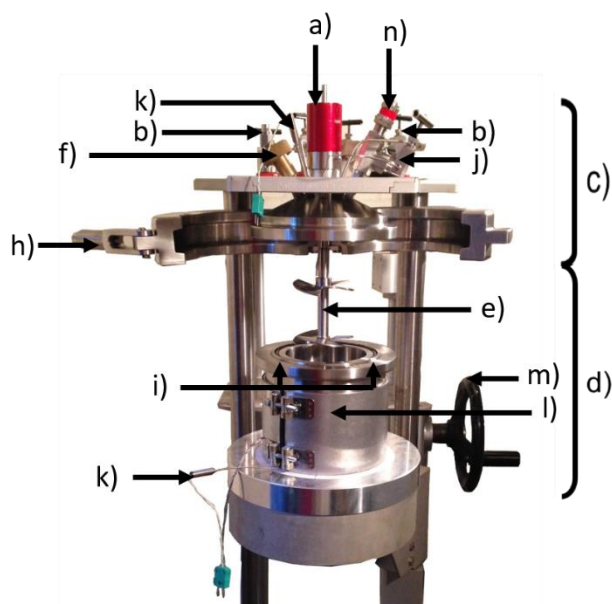


Figure 2-5: Images showing the computer used to control the system and the ability to remotely access the computer enabling monitoring via web-camera and the control box software of both the pressure and temperature throughout reactions.

As with the 60 mL autoclave the head incorporates a stirring motor, spring-loaded relief valve, safety key, HPLC inlet, thermocouple, pressure transducer, CO₂ inlet and outlet (Figure 2-6). As a result of the scale of the autoclave, an additional rupture disc is required as an extra safety feature. A rupture disc is designed to burst at a set temperature and immediately release the content of the autoclave. The system contains a removable stirrer with adjustable height blades. The vessel is heated to reaction temperature via a heating jacket attached around the outside of the base.



- | | | |
|---------------------------------|-------------------|-------------------------------|
| a) Overhead stirrer | g) Stirrer shaft | m) Wheel |
| b) CO ₂ inlet/outlet | h) Clamp | n) Spring loaded relief valve |
| c) Autoclave head | i) O-ring | o) Rupture disc |
| d) Autoclave base | j) HPLC inlet | p) Pressure transducer |
| e) Stirrer | k) Thermocouple | |
| f) Safety key | l) Heating jacket | |

Figure 2-6: Images showing the 1 L high pressure autoclave and pipe work set-up (top down view).

An external thermocouple is used to monitor the temperature of the jacket and an internal thermocouple is used to monitor the temperature of the reaction. Monitoring of the internal temperature is essential on 1 L scale due to the thickness of the autoclave walls. This creates a lag between the external temperature of the

autoclave and the internal temperature so monitoring of them both is crucial to ensure the system is operating safely.

Alongside the pressure valves, the system itself is designed to trip and the control box will automatically shut down the power to the heater if pressure exceeds 241 bar. The vessel is pressurised to the desired pressure via a CO₂ inlet tap (tap-a, Figure 2-7).

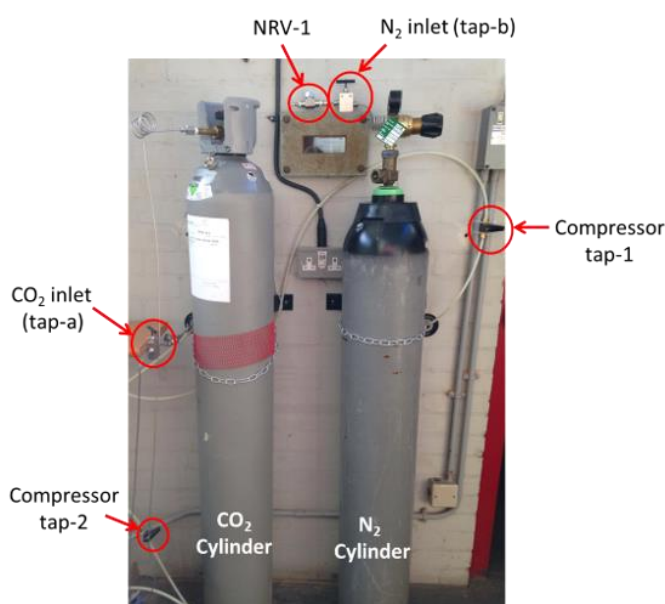


Figure 2-7: Image showing the outside of the 1 L autoclave room where the cylinders are housed and the pipework needed to pressurise and depressurise the reactor is located.

An actuated ball valve system is used for venting once depressurisation is required. Exposing the actuator to pressure (approximately 2 bar) via the compressor causes the ball valve to open. Once this pressure is removed the valve closes. As with the 60 mL autoclave the head incorporates a HPLC inlet, which allows the addition of liquid reagents once the system is under pressure via a HPLC pump. The rig diagram for the set-up is shown in Figure 2-8. A control box, made by the in-house electronics workshop, is used to control the heating of the system, whilst also logging the temperature and pressure of the vessel.

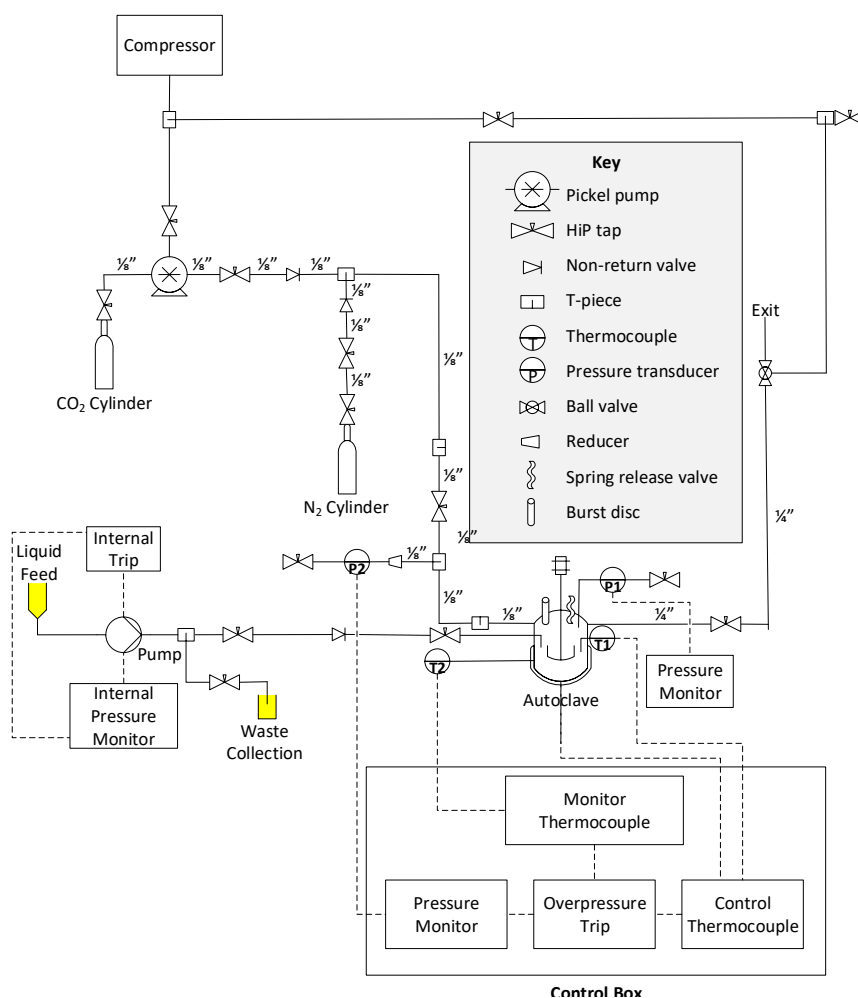


Figure 2-8: Schematic showing the rig diagram for the 1 L high pressure autoclave. All pipework was $\frac{1}{16}$ " unless otherwise labelled.

2.2.3.2. Standard Operating Procedure

In order to ensure safety, the following SOP was developed throughout the project and was rigorously followed when performing high pressure polymerisation.

1: The autoclave is assembled by placing an EPDM O-ring between the autoclave body and head before clamping together. The clamp is tightened using the safety key, which is then screwed into the head of the autoclave. All fittings to the CO₂ inlet and outlet are secured and all valves are closed. The heating jacket is fitted around the autoclave base and the internal and external thermocouple are plugged in.

2: The autoclave is filled with N₂ (approximately 55 bar, used for leak testing, as opposed to CO₂, due to costs). Each joint is checked for leaks using Swagelok Snoop®

leak detector fluid (bubbles will be seen if the joint is leaking). In the event of a leak the system is depressurised, by exposing the actuator to 2 bar pressure, to ambient pressure and any leaking fittings are tightened. It is noted that for safety reasons the joints must not be tightened whilst the autoclave is under pressure. The autoclave is refilled with N₂ (approximately 103 bar) and the fittings are retested for leaks. Once satisfied the system is not leaking the autoclave is vented to ambient pressure.

3: The safety key is removed, revealing a small hole and the autoclave is purged with N₂ (approximately 2 bar) for 30 minutes to remove residual oxygen. Make sure the extractor is turned on during this process.

4: The autoclave is charged with the deoxygenated reagents via the keyhole under a positive flow of nitrogen. The flow of N₂ is stopped before quickly sealing the autoclave with the key.

5: The vessel is filled with 55 bar of CO₂ before the heating jacket is set to 55 °C. The pressure is monitored throughout the heating process. The pressure is gradually increased to 207 bar and the temperature to 65 °C. The system is allowed to stabilise at these conditions.

5a: *(At the required addition time for reactions using the HPLC pump only)*. The HPLC pump and associated pipe work is flushed with acetone (approximately 20 mL). The pump is charged with remainder of reagents and the HPLC pipe work is filled with the solution. The HPLC pipework is connected to the HPLC inlet located in the autoclave head. Ensuring the HPLC inlet tap is closed, use the pump to build up a pressure that is equal to or just above the pressure of the autoclave. The HPLC inlet tap is opened and the desired amount of reagents is injected into the autoclave. Once finished the HPLC pipework is disconnected from the autoclave and flush with acetone.

7: After the desired reaction time set the heating to 0 °C on the control box and disconnect the heating jacket. The vessel is allowed to cool to room temperature. The autoclave was vented by exposing the actuator to the compressor line causing the CO₂ outlet to open and the CO₂ to be released. Once the autoclave has reached

atmospheric pressure the compressor line to the actuator is closed causing the CO₂ outlet to seal.

8: Swagelok fittings of the inlet and outlet are undone, followed by the clamp and the autoclave base is lowered using the wheel. The product is collected for analysis.

2.3. Analytical Methods

2.3.1. Scanning Electron Microscopy

The microparticles produced were analysed using scanning electron microscopy (SEM) in order to determine the morphology and to check whether uniform, spherical particles had been produced. An electron beam is focused and fired at the sample in an ultra-high vacuum chamber. Back-scattered electrons are emitted from the sample and a detector converts them into an electrical signal. This signal is then amplified and converted into the final images as presented. Prior to analysis the dry particles were mounted on SEM stubs via carbon tape. A platinum coating was applied by a platinum coater (120 seconds, 2.2 V, Polaron SC7640), this provided a conductive surface and prevented charge build up. The particles were then imaged using a Phillips XL30 SEM at varying magnification. If stated, particles were washed by centrifuging in dodecane three times (10 minutes, 4000 rpm) before being dispersed on to a glass slide and dried prior to coating and imaging. Average particle sizes for each sample were calculated from analysing the diameter of 100 particles using an image-J plugin software.^{1, 2}

2.3.2. Transmission Electron Microscopy

Transmission electron spectroscopy (TEM) allowed analysis of the internal structure of the particles. An electron beam is transmitted through a specimen and an image is formed from the interactions of the beam with the sample. The analysis was performed using a FEI Technai Bio Twin-12 electron microscope with an accelerating voltage of 2.2 kV. Prior to imaging the samples were set in an epoxy resin. The resin

consisted of Agar 100 resin, dodecanyl succinic anhydride (DDSA), methyl nadic anhydride (MNA) and benzyl dimethyl amine (BDMA) in the ratios 2.5: 4.5: 6.0: 0.6 by volume. The resin was sectioned using an RMC Powertome XL ultramicrotome and a diamond knife. The resulting sections (< 100 nm thick) were placed on a copper TEM grid. Where stated, the grids were stained for the indicated period of time with RuO₄, which was made *in situ* by combining RuCl₃ (12.4 mg) with a solution of NaIO₄ (4.2 mg) in H₂O (1 mL), shown in Scheme 2-1^{3,4}



2.3.3. Gel Permeation Chromatography

The molecular weight and dispersity of the materials produced were analysed using gel permeation chromatography (GPC). GPC separates analytes based on hydrodynamic volume which is related to the macromolecular size in solution. The separation occurs via a column packed with porous beads; smaller analytes enter the pores and hence spend longer time in the column so elute slower, larger analytes spend less time in the column and are hence elute quicker.⁵ The two most common ways to report molecular weight are the number average molecular weight (M_n) and the weight average molecular weight (M_w). These are defined by Equation 2-1 and Equation 2-2, where M_i is the molecular weight and N_i is the number, of polymer chains with chain length i .

$$M_n = \frac{\sum N_i M_i}{\sum N_i} \quad \text{Equation 2-1}$$

$$M_w = \frac{\sum N_i M_i^2}{\sum N_i M_i} \quad \text{Equation 2-2}$$

The molecular weight distribution of a polymer sample is referred to as its dispersity (\mathcal{D}) and can be found from the relationship between M_n and M_w (Equation 2-3). A monodisperse sample would give a \mathcal{D} equal to one, as $M_n = M_w$, but due to the nature of polymerisation processes this is impossible to achieve.

$$\mathcal{D} = \frac{M_w}{M_n} \quad \text{Equation 2-3}$$

Two GPC systems were used, with both using tetrahydrofuran (THF, HPLC grade, Fisher Scientific) as the eluent at 40 °C and a flow rate of 1 mL min⁻¹. For lower molecular weight samples System A was used, which consisted of two Agilent PL-gel mixed-D columns connected in series, whereas for high molecular weight samples system B was used which contained two Agilent PL-gel mixed-C columns connected in series. Both systems used a multi angle light scattering detector (MALS, Wyatt, Optilab Dawn 8+), along with a Viscometer (Wyatt, ViscoStar-2) and a differential refractometer (DRI, Agilent 1260) for sample detection. System A also included an ultraviolet light (UV, 260 nm, Agilent, 1260) to aid with for sample detection. A standard column calibration (12 x PMMA standards across a range of M_p s from 1,000 to 400,000 g mol⁻¹) was used to calculate the molecular weights of the synthesised materials from both systems. Which system was used is noted with the presented GPC data.

2.3.4. UV Spectrometry

Solutions of PMMA and PBzA (2 mg mL⁻¹) were made in THF and the UV spectrum was recorded on a Lambda 25 UV/Vis spectrometer (PerkinElmer). A full wavelength scan (190–900 nm) was performed and data was analysed using UV WinLab (PerkinElmer).

2.3.5. Nuclear Magnetic Resonance

The percentage conversion, of monomers into polymers, of each reaction was determined using proton nuclear magnetic resonance (^1H NMR) by comparing the vinyl proton peaks present in the monomer to the broad polymer proton peak adjacent to the ester group. Samples (1-2 mg) were dissolved in deuterated chloroform (CDCl_3) and analysed using a Bruker DPX 300 MHz spectrometer. As the benzene group in the samples containing PBzA overlap with the chloroform signals tetramethylsilane (TMS) was used as a reference. Alternatively, where stated analysis of samples containing PBzA were recorded in deuterated acetone (acetone- D_6). Data were analysed using the MNova software (Mestrelab). Full spectra for the synthesised polymers are shown in the appendix.

2.3.6. Differential Scanning Calorimetry

Differential Scanning Calorimetry (DSC) is a thermo analytical technique that enables the measurement of the thermal transitions of polymers. Thermal properties of the amorphous polymers prepared, namely the glass transition temperature (T_g) were studied. As the polymer goes through a transition, the amount of energy required to maintain the temperature of the pan containing the sample relative to an empty reference pan, is measured during heating and cooling cycles. The difference in heat flow between the sample and the reference is measured while they are subjected to a controlled temperature profile. The difference is indicative of thermal transitions in the material.⁶ The analysis was performed on a TA-Q2000 (TA instruments), which was calibrated with an indium standard under N_2 flow. The sample (1-3 mg) was weighed into a T-zero sample pan (TA instruments) with a reference T-zero pan remaining empty. The pans were heated at a rate of $10\text{ }^\circ\text{C min}^{-1}$, from $-90\text{ }^\circ\text{C}$ to $200\text{ }^\circ\text{C}$ for all samples. To remove any thermal history of the individual samples, two heating cycles were recorded with the T_g being measured from the second cycle. Data were analysed with Universal Analysis software.

2.3.7. Dynamic Mechanical Analysis

Dynamic mechanical analysis (DMA) was also used to determine the T_g of the synthesised polymers. This technique is used to characterise the properties of a material as a function of temperature, time frequency, stress or a combination of these parameters. Similar to DSC, DMA can be used to measure T_g . An oscillatory force at a set frequency is applied to a sample and changes in the stress are recorded. These changes are reported as modulus and $\tan \delta$ ($\tan \delta$). The viscous component of the sample is referred to as the loss modulus (E'') and the elastic component is referred to as the storage modulus (E'). The ratio of E''/E' is known as the loss tangent or $\tan \delta$. A peak in the $\tan \delta$ corresponds to a T_g . Measurements were performed on a Triton Technologies DMA (now Mettler Toledo DMA1) using the powder pocket accessory. The use of this attachment allowed for direct measurement of the synthesised powder with no further sample preparation required.^{7, 8} The sample (40 ± 5 mg) was weighed into a powder pocket. Samples were measured at 1 and 10 Hz in single cantilever bending geometry between 25 to 250 °C or -100 to 250 °C depending on the region of interest. The two frequencies were used to confirm the nature of the T_g transition. A T_g transition is frequency dependent and thus should result in offset peak maxima for the two frequencies. By contrast, melting (T_m) and crystallisation (T_{cry}) are frequency independent and hence the peak maxima will occur at the same place for both frequencies. The value of the T_g was taken as the peak of the $\tan \delta$ curve at a frequency of 1 Hz.

2.4. References

1. T. D. McAllister, L. D. Farrand and S. M. Howdle, *Macromolecular Chemistry and Physics*, 2016, **217**, 2294-2301.
2. A. P. Richez, L. Farrand, M. Goulding, J. H. Wilson, S. Lawson, S. Biggs and O. J. Cayre, *Langmuir*, 2014, **30**, 1220-1228.
3. G. Brauer, *Handbook of preparative inorganic chemistry*, Elsevier, 2012.
4. J. S. Trent, J. I. Scheinbeim and P. R. Couchman, *Macromolecules*, 1983, **16**, 589-598.
5. Agilent, *A Guide to Multi-detector Gel Permeation Chromatography*, 2012.
6. G. Höhne, W. F. Hemminger and H.-J. Flammersheim, *Differential Scanning Calorimetry*, Springer Science & Business Media, 2013.
7. M. G. Abiad, O. H. Campanella and M. T. Carvajal, *Pharmaceutics*, 2010, **2**, 78-90.
8. D. Mahlin, J. Wood, N. Hawkins, J. Mahey and P. G. Royall, *International Journal of Pharmaceutics*, 2009, **371**, 120-125.

Chapter 3: Core-Shell Particle Synthesis

3.1. Overview

Core-shell polymer particles are widely used as additives for impact modification of thermoplastics such as poly(vinyl chloride) (PVC). Synthesis of polymer particles, with a core-shell internal morphology, from traditional solvent and emulsion based techniques is well established. Relatively small particles are produced using this technique, usually between 100-200 nm. However, the products formed are often a latex and the removal of water to afford a dry powder, needed for the application, is energy intensive. Utilising supercritical carbon dioxide (scCO₂) as a reaction medium for dispersion polymerisation allows for the production of dry, free-flowing powders upon release of the CO₂ post polymerisation. Employing dispersion polymerisation also allows for synthesis of particles between 0.5-5 µm, relatively large in comparison to those produced by emulsion polymerisation. Although there is a cost associated in the compression of the CO₂ used in the supercritical reactions, this is an order of magnitude lower than the cost associated with the removal of water.

This work demonstrates the ability to produce three different types of polymer particles with varying compositions; firstly, a particle containing a PBA core with a PMMA shell, secondly a particle containing a PBzA core with a PMMA shell and thirdly a particle containing a MMA core with a crosslinked MMA shell. Finally, combination of crosslinking with the formation of a core-shell structure is also demonstrated.

3.2. Introduction

Polymerisation utilising scCO₂ as a reaction medium was first reported in 1992 by DeSimone *et al.* who published the synthesis of fluoropolymers in scCO₂.¹ ScCO₂ has been shown to be a versatile medium for free radical polymerisation and in particular

for dispersion polymerisation. Dispersion polymerisation can be facilitated by the use of amphiphilic surfactants including fluoro polymers and polysiloxanes.² Recently, increasingly more sophisticated chemistries have been reported using scCO₂ as a reaction medium. The three most widely used controlled/living radical polymerisation techniques; nitroxide-mediated radical polymerisation (NMP), atom transfer radical polymerisation (ATRP) and reversible addition-fragmentation chain transfer polymerisation (RAFT) have all been used to synthesise many novel particle-based polymeric materials with well-defined particles with narrow size distributions.³⁻⁷

These techniques can give access to more complex structures including crosslinking,^{8,} ⁹ metal nanoparticles,¹⁰ and more recently block copolymer particles with internal phase separation.^{11, 12}

3.2.1. Impact Modifiers

A thermoplastic is an organic material that becomes pliable or mouldable at a certain elevated temperature and solidifies upon cooling. Many modern-day activities are influenced by, and sometimes entirely dependent on thermoplastic products. Several synthetic thermoplastics require additives to alter and improve their properties, make them safer, give them colour and improve their processability.¹³⁻¹⁵ Thus, most modern-day thermoplastic products are made from polymers mixed with a complex blend of additives. One area of high importance with many thermoplastics is their ability to withstand impact.¹⁶ Additives specifically designed to improve impact resistance are known as impact modifiers.

Impact modifiers help protect materials that often encounter collisions, such as cars, construction materials, wire cables and materials used outdoors.¹⁷⁻¹⁹ Impact modifiers are incorporated in compounded materials to help improve durability and toughness of thermoplastic resins. Addition of impact modifiers can not only improve the impact performance of a thermoplastic, but they can also improve several other characteristics of the material such as optical and tensile properties, weatherability,

processability, flammability, heat distortion and cost.^{16, 20} Impact modifiers can also be added to recycled polymers. During the regrind process, materials can lose some of their chemical and physical properties,^{21, 22} and impact modifiers can be added to help prevent cracking and splitting while increasing a products ductility.²³

3.2.2. PVC Modification

Poly(vinyl chloride) (PVC) is the third most widely produced thermoplastic in the world, however for many application it requires impact modification due to its brittle nature.²⁴⁻²⁶ There are several impact modifiers used with PVC which fall into two basic categories; traditional rubber-particle type including acrylic impact modifiers (AIM),¹⁹ methacrylate-butadiene-styrene modifiers (MBS),²³ acrylonitrile-butadiene-styrene modifiers (ABS)²⁷ and plasticising polymers that are semi-compatible with the PVC including chlorinated polyethylene (CPE),^{28, 29} nitrile rubbers (NBR)³⁰ and ethylene/vinyl acetate copolymers (EVA).³¹ Traditional rubber-particle modifiers are added to the PVC matrix, whereas semi-compatible plasticising polymers are grafted within the PVC chains (Figure 3-1).

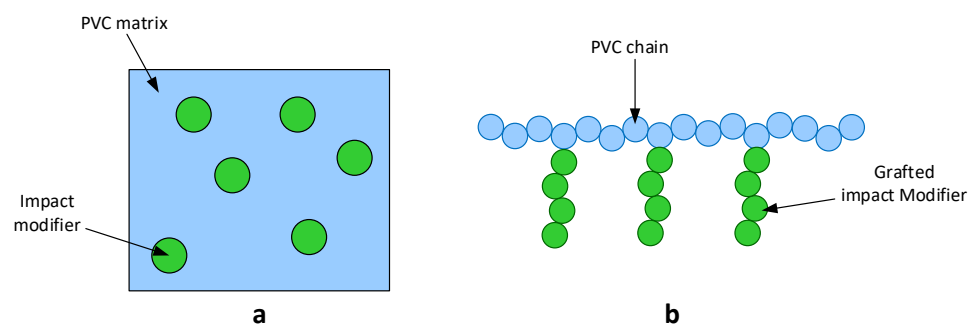


Figure 3-1: Schematic representing the two types of impact modification; traditional rubber particles (a) and semi-compatible plasticising polymer (b).

The mechanism of impact modification differs between the two categories. Semi-compatible polymers disperse into small discrete domains in the PVC matrix and serve as impact modifiers.³² EVA and CPE modifiers envelope the primary particles

of PVC creating a network that can dissipate forces without cracking.¹⁹ Conversely, MBS, AIM and ABS type modifiers create a distinct dispersed phase throughout the PVC matrix.²⁵ The end application of the material often dictates which impact modifier is most suitable.

3.2.3. Core-shell Impact Modifiers

Common impact modifiers use a core-shell particle structure for reasons that will be discussed. Typical core-shell particles used for impact modification contain a rubbery core that induces the toughening and absorbs the impact. This is then surrounded by a glassy outer shell which is important in enhancing the adhesion of the particles with the polymer matrix in which it is dispersed, as well as ensuring the particles remain discrete and uniform during processing (Figure 3-2). The most common core-shell structures used to improve the impact strength of PVC are; MBS and ABS based particles.^{15, 23, 25, 33, 34}

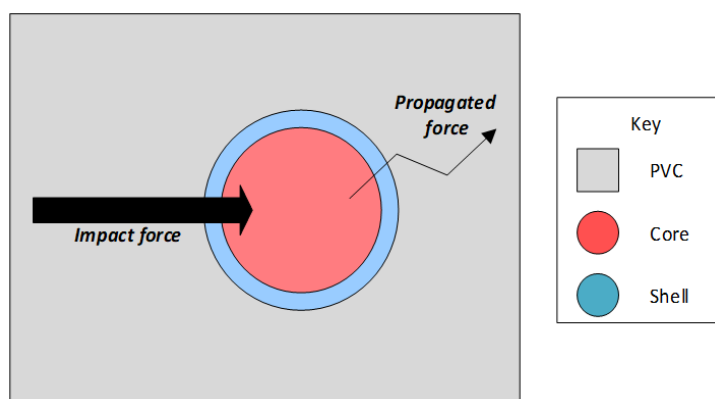


Figure 3-2: Schematic showing the action of an impact modifier particle. The bold black arrow represents the incoming force to the PVC and the smaller black arrow represents the force leaving the impact modifier that has not been absorbed.

Synthetic methods to give core-shell particles vary and can be divided into one-, two- or higher-step syntheses. The direct copolymerisation of two monomers is known as a one-step process. The two-step method consists of the synthesis of a core followed by the formation of a shell. The shell can be generated by various means when using

a two-stage process. Usually, a polymer seed is swollen with a comonomer, which is subsequently polymerised. If there are reactive sites present on the polymer core these may be used for further polymerisation, which is known as the grafting-from method.³⁵ Alternatively, various macromolecules may be bound to these active sites on the polymer seed, this is known as the grafting-to method.³⁶ The following sections will summarise the synthesis of various impact modifiers.

3.2.3.1. Methacrylate-butadiene-styrene

Emulsion polymerisation is frequently used to synthesise core-shell particles as it produces defined structures. Methacrylate-butadiene-styrene (MBS) is a common type of impact modifier and it consists of a poly(butadiene/styrene) (P(BD/St)) core encased in a poly(methyl methacrylate/St) (P(MMA/St)) shell. Si *et al.* investigated how the monomer feed process could be coupled with the initiating system to affect the internal morphology of the MBS particles.³⁷ The authors produced three different internal morphologies by using a semi-continuous monomer feed, compared to pre-swelling of the polybutadiene (PBD) seeds and varying the initiator used. The synthesised particles were blended with PVC and the mechanical properties of the materials produced were tested. It was found that the size of the inclusions of PSt within the PBD core impacted the grafting abilities of the particles (Figure 3-3).

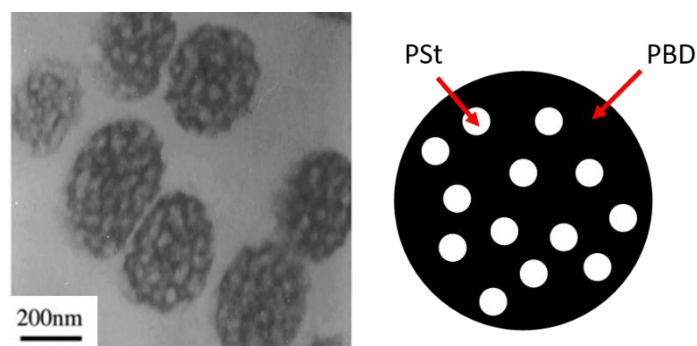


Figure 3-3: TEM image showing sub-inclusion of PSt within a PBD core where the dark region corresponds to the PBD and the lighter regions corresponding to PSt.³⁷ This is represented schematically (right).

This, in turn, impacted the ability of the particles to be dispersed within the PVC matrix and the impact strength of the resulting material. Transparency of the material, which can be an important property depending on the end application of the material, was also altered with the addition of the particles.

Wu *et al.* built on this work by similarly altering the internal morphology of MBS core-shell particles.³⁴ Three different internal morphologies were produced; “salami”, core-shell and multi-layer (Figure 3-4). The authors found that when blended with a PVC matrix the particles with the multi-layer internal morphology performed best in impact testing.³⁴

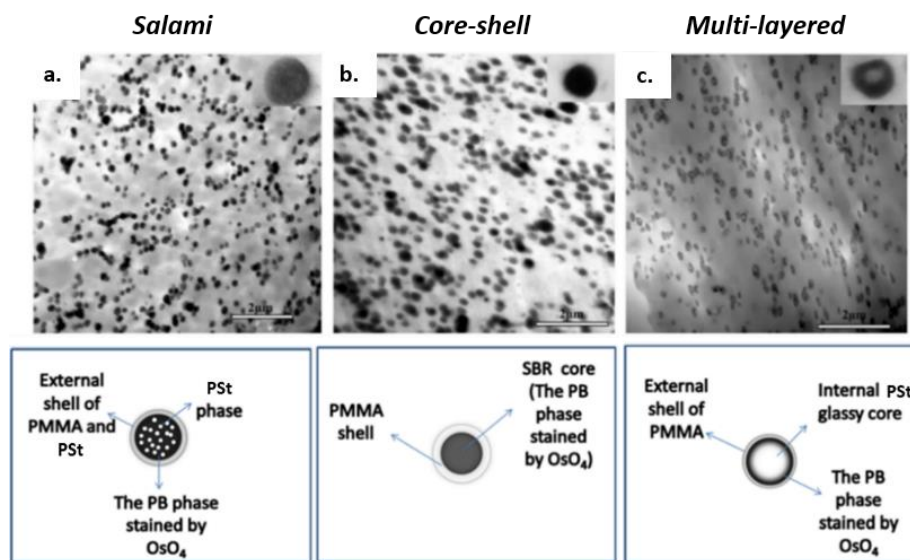


Figure 3-4: TEM analysis and schematic representation showing the different internal morphologies formed by Wu *et al.*: salami (a), core-shell (b) and multi-layered (c).³⁴

3.2.3.2. Acrylic Impact Modifiers

A second type of modifier consists only of a copolymer of acrylic monomers. Rabinovic *et al.* compared the use of an all acrylic impact modifier to the use of chlorinated polyethylene (CPE) and ethylene-vinyl acetates (EVAs) as modifiers for PVC. It was found that acrylic impact modifiers (AIMs) had many advantages over CPEs and EVAs such as good impact strength efficiency, high tensile properties as

well as excellent weather performance. By implementing EVA and CPE systems the impact resistance had a greater dependency on the processing conditions compared to AIM.¹⁹ AIMS are of great commercial interest as shown by a number of patents from companies including DuPont.^{16, 38, 39}

3.2.3.3. Acrylonitrile-butadiene-styrene

Acrylonitrile-butadiene-styrene (ABS) copolymer particles are also often used as impact modifiers. They consist of a butadiene rich core with a styrene-acrylonitrile copolymer shell, which is miscible in the PVC matrix. Matiti *et al.* blended different ratios of ABS particles with PVC and analysed both the composition and mechanical properties of the materials produced. The authors found that the mechanical strength of the PVC increased significantly with the incorporation of the impact modifiers. The higher rubber content ABS particles showed the greatest increase in impact resistance.²⁷

Zhou *et al.* compared the influence of ABS modifiers to CPE impact modifiers on the mechanical properties of PVC. They found that both modifiers greatly enhanced the impact resistance of the PVC, with CPE exhibiting the greatest toughening effect. SEM analysis showed that the ABS modifiers formed discrete phases, whereas the CPE modifiers formed a network structure within the PVC matrix.⁴⁰

3.2.3.4. Poly(butyl acrylate) Impact Modifiers

Core-shell particles containing a PBA component, synthesised by traditional emulsion polymerisations, have been extensively researched.⁴¹⁻⁴⁴ The low T_g of PBA (-45 °C) and its partial miscibility with PVC are attractive properties for its application as an impact modifier.^{33, 45} Particles containing a crosslinked poly(styrene-co-butadiene) (P(St-co-BD)) core with a grafted PSt and PBA shell were synthesised via emulsion polymerisation by Chen *et al.*. The authors found that increasing the PBA

content increased the impact strength of the PVC matrix as well as aided dispersion of the particles.³³

Pérez-Carrillo *et al.* studied the effect of the particle size on the mechanical properties of particles containing a PBA core encased in a PSt shell, synthesised by a two-stage emulsion polymerisation. Particles ranging from 30-200 nm were produced. TEM confirmed the presence of a PSt shell with a PBA core, which was expected as the PBA was synthesised as a seed before the addition of St (Figure 3-5). The core-shell structure was inverted when St was polymerised prior to the addition of BA. High conversion and good control over particle size were achieved for both structures.

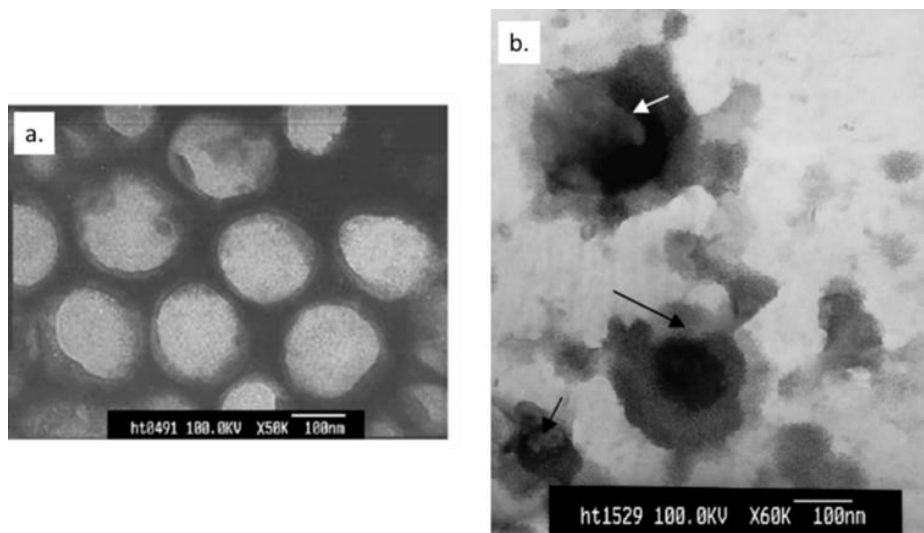


Figure 3-5: TEM images showing core-shell particles formed using a PBA seed (a) and a PSt seed (b). Samples were stained with 1 % phosphotungstic acid. Dark regions correspond to PSt and light regions correspond to PBA. Arrows indicate areas of phase inversion.⁴⁶

It was found that the mechanical properties of the PVC/core-shell particle blends were strongly influenced by the particle size coupled with the location and ratio of the two polymers.⁴⁶ Similar core-shell particles with a slightly crosslinked PBA rubbery core encased in a PMMA shell were synthesised by Cho *et al.*. The authors found that there was an optimum diameter for the PBA core of 0.25 μm and suggested that core diameters less than this are unable to undergo cavitation, a key

mechanism needed for impact modification.⁴⁷ Cavitation of the rubber particle is a crucial process for the enhancement of toughness and is a phenomenon in which small voids are formed within the particle core. Cavitation of the rubber particles relieves the hydrostatic tension present in the material. This relief originates from the stress state in the fibrils of matrix material between the voids being converted from triaxial to a more uniaxial tensile stress. This new stress state is favourable for the initiation of shear bands, a key toughening mechanism as described in section 1.6 of Chapter 1.⁴⁸

Zhu *et al.* used reversible addition-fragmentation chain transfer (RAFT) emulsion polymerisation to synthesis PMMA-*b*-PBA polymers that self-assembled to formed core-shell particles. The composition of the diblock copolymer and its effect on the morphology and mechanical properties when blended with polycarbonate (PC) was investigated. The MMA was polymerised first, forming the shell and the BA was subsequently polymerised forming the core. DSC analysis confirmed the presence of two separate phases of PMMA and PBA. The resulting particles were effective in increasing the impact resistance of PC. It was found that the composition of the particles had the biggest influence on their ability as impact modifiers with PMMA₂₅₀-*b*-PnBA₅₅ performing the best.⁴⁹

A further system containing PBA was reported by Gharieh *et al.*. The authors synthesised a series of particles based on butadiene-methyl methacrylate-butyl acrylate with core-shell morphology. The core consisted of polybutadiene (PBD) and the shell was based on a copolymer of MMA and BA. Shells with a range of T_g 's were prepared by variation of the P(MMA-*co*-BA) composition and the effect this had on the ability of the particles as impact modifiers was investigated. TEM confirmed the presence of a core-shell structure. It was found that as the T_g of the shell decreased the impact strength increased.⁵⁰

Hassan *et al.* studied the impact properties of acrylate rubber modified PVC and the influence of temperature. They added three different core-shell particles consisting of different sizes of PBA rubber cores (0.2, 0.3 and 0.4 μm) encased in a PMMA shell. These particles were blended with PVC and it was found that the smaller the rubber

core the more efficient the particles were at shifting the brittle-ductile transition to lower temperatures. Hence, the authors concluded that rubber particle size is an important factor in the efficiency of the particles to act as impact modifiers.⁴⁸ The process of rubber cavitation with various impact modifiers and the related matrix shear yielding has been reported in the literature for PVC.^{51, 52}

3.2.4. Crosslinking in Core-shell Particles

An important component in core-shell particles used for impact modifying is crosslinking as this helps maintain the particle structure during processing.²⁵ However, a major toughening mechanism for a semi-ductile matrix is cavitation of the rubber particles.⁵³ The crosslinking density of the core determines the cavitation resistance of the particles and in turn their ability as impact modifiers.⁴⁷ Takaki *et al.* studied the effect of rubber particle size on the fracture behaviour of PVC/MBS blends, finding particles of 200 nm gave the highest impact strength. The crosslinking degree of MBS on the impact strength of blends was also studied. The authors reported that as crosslinking density decreased, cavitation was more likely to occur, and the impact strength of the blend was improved.^{54, 55}

Fu *et al.* investigated the influence of crosslinking density of the rubber phase, among other parameters, on the toughening of poly(butylene terephthalate) (PBT) by glycidyl methacrylate (GMA) functionalised ABS core-shell particles. It was found that divinylbenzene (DVB), a common crosslinking reagent, improved the crosslinking degree of the PBT core but decreased the cavitation ability of the particles and in turn their ability as impact modifiers.⁵³

These two examples show that there is an optimum level of crosslinking in core-shell particles. Enough is needed to help the particle maintain its structure but too much can have a negative influence on the ability of the particles as an impact modifier.

3.2.5. Core-shell Particle Synthesis in scCO₂

There are few examples of particles synthesised in scCO₂ exhibiting a core-shell internal morphology intended for the application of impact modifying. However, there are a few examples of the synthesis of core-shell particles for different applications. Cao *et al.* prepared polymeric nanoparticles consisting of a temperature-sensitive core encased in a pH-sensitive shell from a one-step seed polymerisation. The polymers obtained were fine, free-flowing powders with monodispersed nano-sized particles being formed.⁵⁶

McAllister *et al.* recently reported the synthesis of core-shell particles consisting of poly(2-(dimethyl amino)ethyl methacrylate) (PDMAEMA) and PMMA via a multi-stage dispersion polymerisation.⁵⁷ Particles synthesised in scCO₂ produced a core-shell structure with domains of PDMAEMA within PMMA. In contrast, particles synthesised in traditional solvents produced the inverse of this, with a core of PMMA surrounded by a shell of PDMAEMA.

There are several examples of block copolymers synthesised in scCO₂ exhibiting micro phase separation to give varying internal particle morphology. To the best of my knowledge, investigations into utilising these as impact modifiers have not yet been reported.^{11, 12}

3.2.6. Crosslinked Particles in scCO₂

As previously mentioned, the incorporation of a crosslinking component is essential for helping the particles maintain their structure during processing. Cooper *et al.* synthesised well-defined crosslinked polymer particles in scCO₂. DVB and ethylvinylbenzene (EVB) were copolymerised at 65 °C and 310 ± 15 bar using AIBN as the initiator. Particle size was found to be influenced by the amount of stabiliser present (1.5-5 µm).⁵⁷

Highly crosslinked, discrete poly(diethylene glycol dimethacrylate) (PDEGDMA) particles were synthesised by free radical heterogeneous polymerisation in scCO₂. Casimiro *et al.* investigated how the initial concentration of stabiliser, monomer and

initiator affected the yield and structure of the resulting particles. Free-flowing powders with a narrow particle size distribution (1.28-2.08 μm) were achieved in high yields (> 85%) and short reaction times (180 minutes).⁸

Shin *et al.* used dispersion polymerisation to synthesise crosslinked PMMA particles in scCO_2 using a variety of different crosslinkers (Figure 3-6). The authors investigated the effects chemical structure, concentration of the crosslinking agent, reaction pressure and CO_2 density had upon the structure, polydispersity and crosslinking density of the particles produced. It was found that as the concentration of the crosslinking component was increased, the tendency of the particles to agglomerate also increased. This trend was also observed with decreasing reaction pressure. The T_g of the particles increased as the crosslinker content increased, with particles crosslinked with ethylene glycol dimethacrylate (EGDMA) giving the highest T_g .⁹

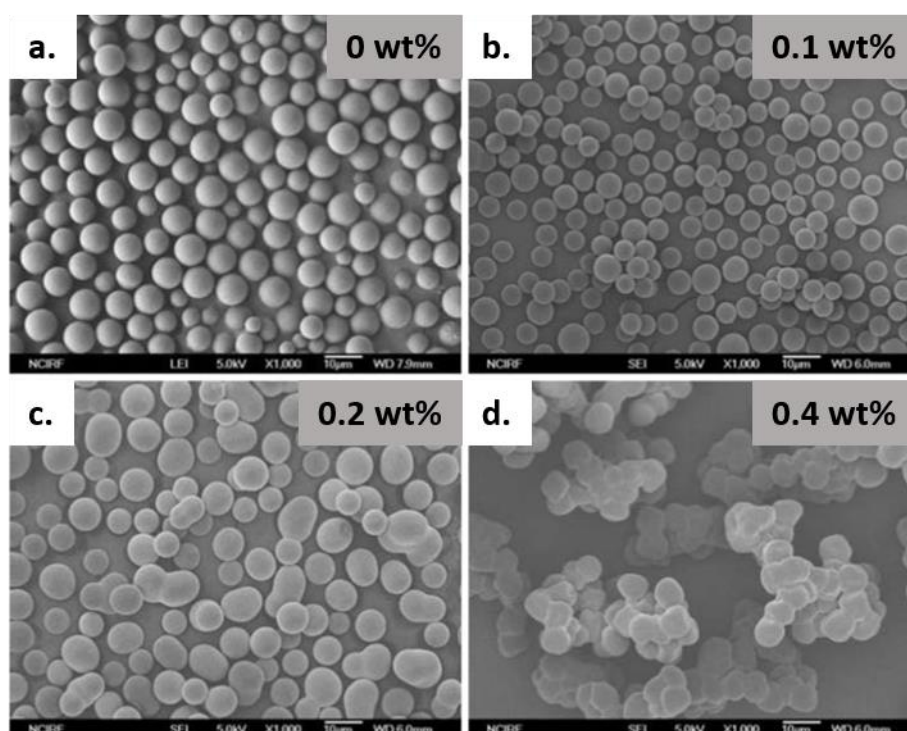


Figure 3-6: SEM images of PMMA particles incorporation a. 0, b. 0.1, c. 0.2 and d. 0.4 wt% EGDMA.⁹ All scale bars are 10 μm . The images show that as EGDMA content increases particle quality decreases.

3.3. Aims and Objectives

The synthesis of core-shell particles for use as impact modifiers using traditional solvent-based techniques has been widely reported. These studies aim to create a core-shell particle synthesised by dispersion polymerisation in $scCO_2$. The use of $scCO_2$ allows for the formation of internal morphologies that may not be accessible using traditional solvents. It also enables the synthesis of dry powders, removing the need for an energy intensive drying step post polymerisation, which is required with solvent-based polymerisations. This is beneficial as polymer additives are usually added as dry powders to the polymer matrix. This work investigates the use of $scCO_2$ as a reaction medium in the synthesis of three polymer particle systems; an MMA core with a crosslinked MMA shell (Figure 3-7, images a), a PBA core with a PMMA shell (Figure 3-7, image b) and a PBzA core with a PMMA shell (Figure 3-7, image c). Finally, combination of crosslinking with the formation of a core-shell structure is also examined, as this is an essential component for particles used as impact modifiers.

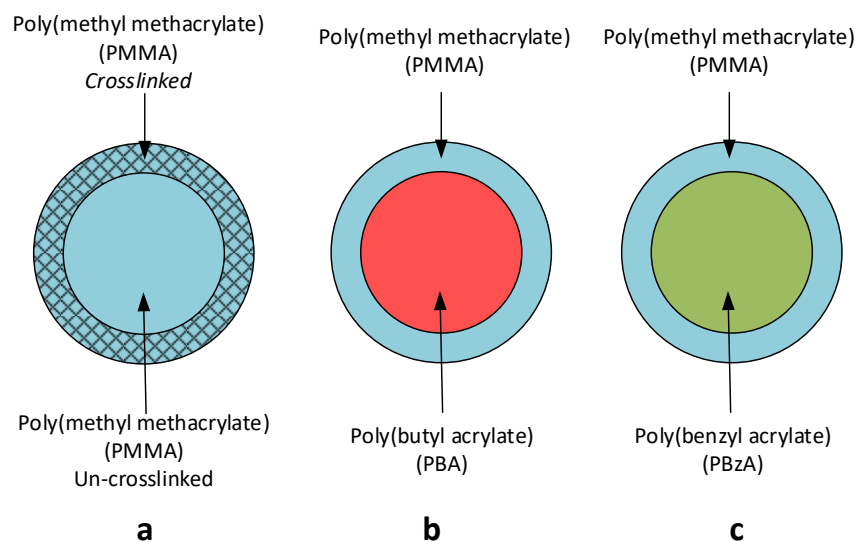


Figure 3-7: Schematic showing proposed core-shell particle to be synthesised in $scCO_2$.

3.4. Experimental

All high-pressure reactions were performed in a 60 mL high pressure autoclave built in-house, as described in Chapter 2. The autoclave was set up as described in section 2.2.2.. Two reaction methods were used; a one-stage batch synthesis and a multi-stage reaction which are outlined in the following sections.

3.4.1. Materials

Polymerisations were carried out using methyl methacrylate (MMA, ProSciTech, 99%), benzyl acrylate (BzA, Alfa Aesar, 98%), and butyl acrylate (BA, BASF) as monomers. 2,2'-Azobis(isobutyronitrile) (AIBN, Sigma Aldrich, 98%) was used as an initiator and methacrylate terminated polydimethylsiloxane (PDMS-MA, $M_n \sim 10$ KDa) (ABCR GmbH & Co.) as a stabiliser. Divinylbenzene (DVB, Aldrich, 55 %) and ethylene glycol dimethacrylate (EGDMA, Merck, 97.5%) were used as crosslinkers. All reactions were carried out in SCF grade 4.0 CO₂ ($\geq 99.99\%$), BOC Special Gases). To simulate industrial conditions all chemicals were used as received.

3.4.2. BA/PMMA Particle Synthesis in 60 mL Autoclave

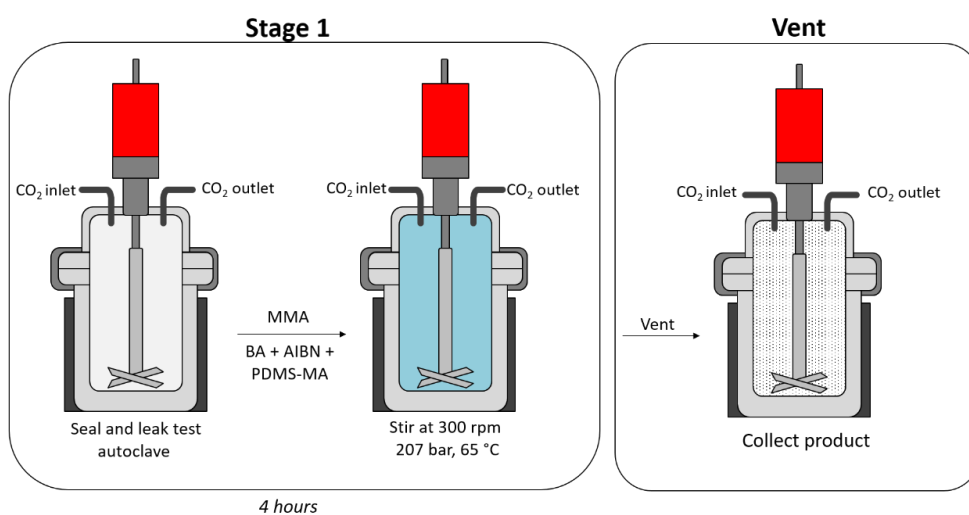
3.4.2.1. One-stage Batch Reactions

A typical synthesis was as follows: MMA (amounts shown in Table 3-1) was deoxygenated under argon for 30 minutes. BA (amounts shown in Table 3-1) and a mixture of PDMS-MA stabiliser (5 wt% wrt total monomer content, 0.468 g, 0.85 mmol) and AIBN (1 wt% wrt total monomer content, 0.094 g, 0.57 mmol) were separately flushed with argon for 30 minutes.

Table 3-1: Amount of MMA and BA used for each loading. wt% wrt total amount of monomer.

Entry	MMA (mL)	MMA (mmol)	BA Loading (wt%)	BA (mL)	BA (mmol)
1	9.0	84	9	0.94	6.53
2	7.2	67	27	2.82	19.58

The autoclave was deoxygenated by purging with CO₂ for 30 minutes at 1-2 bar. The MMA and BA were combined with the AIBN/PDMS-MA and injected into the autoclave via a syringe under a positive pressure of CO₂. The autoclave was sealed, pressurised to 48 bar, and heated to 65 °C before the addition of further CO₂ to reach reaction pressure (207 bar). The beginning of the reaction was recorded as the moment at which the temperature reached 65 °C, after which the reaction was left stirring (300 rpm) for 4 hours (Figure 3-8). After this time heating was removed, and the autoclave was allowed to cool naturally to room temperature before being depressurised. Figure 3-8 The resulting products were typically collected as free-flowing white powders.

**Figure 3-8: Schematic showing the batch reaction of MMA and BA (9 wt%) in the 60 mL autoclave.**

3.4.2.2. Multi-stage Reactions

The total monomer content of the reaction was kept approximately constant (9.31 g) as the loading of BA was varied. A typical multi-stage synthesis was as follows; MMA (amounts shown in Table 3-2) was deoxygenated under argon for 30 minutes. A mixture of AIBN (1 wt% wrt total monomer content, 0.094 g, 0.57 mmol) and PDMS-MA (5 wt% wrt total monomer content, 0.47 g, 0.047 mmol) was separately flushed with argon for 30 minutes. The autoclave was deoxygenated by purging with CO₂ for 30 minutes at 1-2 bar. The MMA was combined with the AIBN/PDMS-MA and injected into the autoclave via a syringe under a positive pressure of CO₂. The autoclave was sealed, pressurised to 48 bar, and heated to 65 °C before the addition of further CO₂ to reach reaction pressure (207 bar). The beginning of the reaction was recorded as the moment at which the temperature reached 65 °C, after which the reaction was left stirring (300 rpm) for 1 hour. A charge of BA (amounts shown in Table 3-2) was added via a HPLC pump at 0.2 mL min⁻¹, inducing a pressure increase.

Table 3-2: Amount of MMA and BA used for each loading. wt% wrt total monomer.

Entry	MMA (mL)	MMA (mmol)	BA Loading (wt%)	BA (mL)	BA (mmol)
1	9.0	84	9	0.94	6.53
2	8.1	75	18	1.88	13.05
3	7.2	67	27	2.82	19.58
4	6.3	59	36	3.77	29.41

The reaction was left for a further 4 hours. After this time, the heating was removed, and the autoclave was allowed to naturally cool to room temperature before being depressurised (Figure 3-9). The resulting products were typically collected as free-flowing white powders.

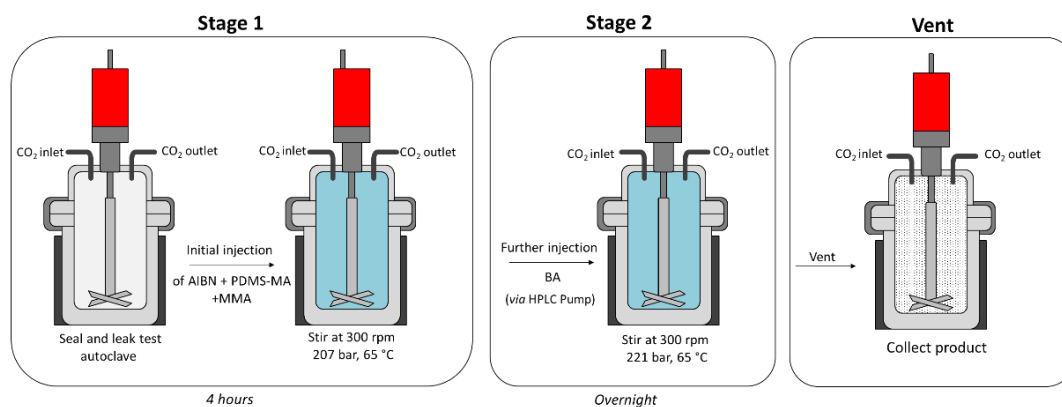


Figure 3-9: Schematic showing a multi-stage reaction where PMMA particles were synthesised first, followed by addition of BA in a 60 mL autoclave.

3.4.3. BzA/PMMA Particle Synthesis in 60 mL Autoclave

3.4.3.1. Multi-stage Reactions

One-stage Addition of BzA

The total monomer content (mass) of the reaction was kept approximately constant (9.31 g) as the loading of BzA was varied. A standard reaction followed the same procedure as detailed in section 3.4.2.2 with the following differences; for stage 1 the following quantities were used: MMA (amounts shown in Table 3-3), AIBN (1 wt% wrt total monomer content, 0.094 g, 0.57 mmol) and PDMS-MA (5 wt% wrt total monomer content, 0.47 g, 0.047 mmol). For stage 2, a charge of BzA (amounts shown in Table 3-3) was added via a HPLC pump at 0.2 mL min^{-1} , inducing a pressure increase.

Table 3-3: Amount of MMA and BzA used for each loading. Loading wt% wrt total monomer.

Entry	MMA (mL)	MMA (mmol)	BzA Loading (wt%)	BzA (mL)	BzA (mmol)
1	9	84	9	0.79	5.16
2	8.1	75	27	1.58	10.34
3	7.2	67	36	3.16	20.65

Two-stage Addition of BzA

As the BzA content was increased above 36 wt% the quality of the particles produced using a one-stage addition of BzA was reduced, with SEM analysis showing high levels of aggregation. In an attempt to improve this the BzA was added over two-stages (Figure 3-10).

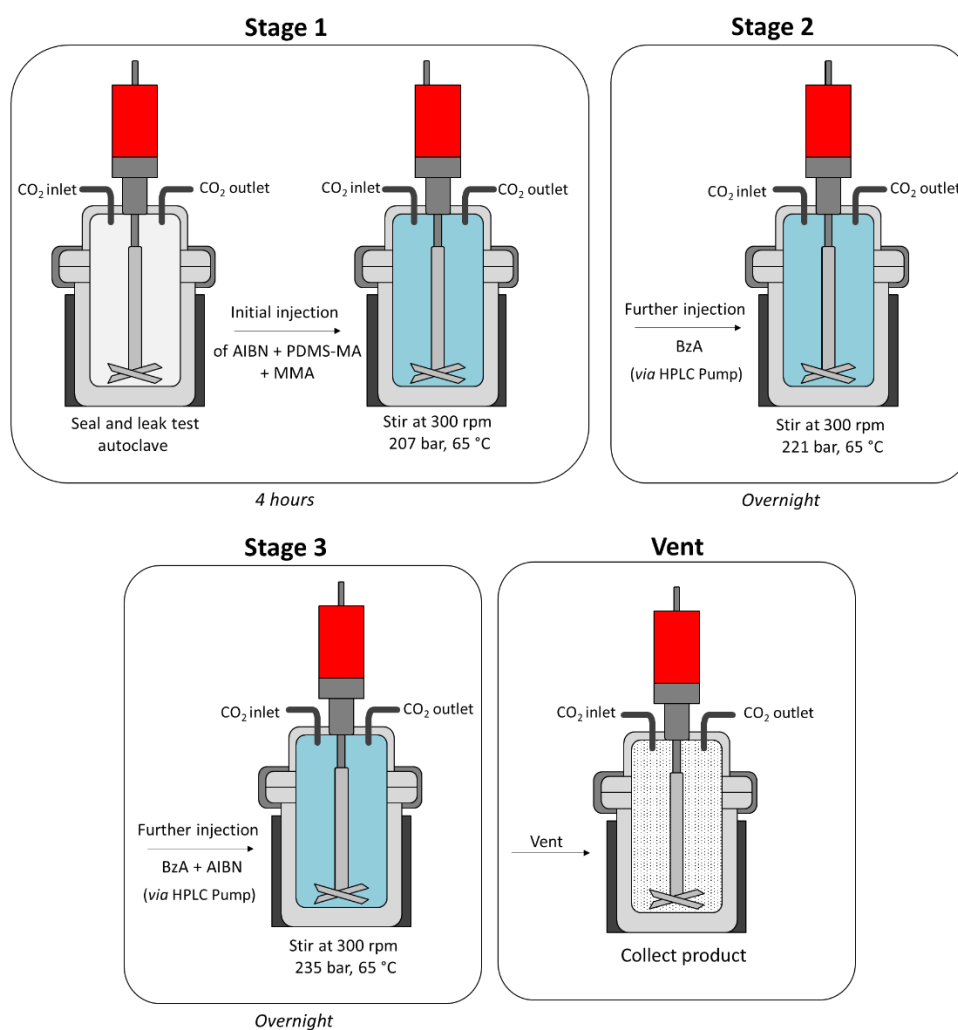


Figure 3-10: Schematic showing a multi-stage reaction where PMMA particles were synthesised first, followed by addition of BzA in two steps in a 60 mL autoclave.

The initial stage of the reaction remained the same as described in section 3.4.3.1. The total amount of monomer was increased to 12 mL to allow for sufficient amounts of MMA needed for nucleation in the primary loading (amounts shown in Table 3-8).

The PDMS-MA concentration was kept constant (5 wt% wrt total monomer content, 0.6 g, 0.06 mmol), as was the AIBN concentration (1 wt% wrt total monomer content, 0.12 g, 0.73 mmol).

Table 3-4: Amount of MMA in the initial charge for BzA loadings 50 and 60 wt%. Loading wt% wrt total monomer (12 mL).

Entry	BzA Loading (wt%)	MMA (mL)	MMA (mmol)
1	50	6.38	59.3
2	60	5.11	47.5

After 4 hours the first charge of BzA (amounts shown in Table 3-5) was added via a HPLC pump at 0.2 mL min⁻¹. The injection induced a pressure increase. The reaction was left overnight (18 hours). Subsequently, a second charge of BzA (amounts shown in Table 3-5) was added via a HPLC pump again at 0.2 mL min⁻¹. As before, the injection induced a pressure increase.

Table 3-5: Amounts of BzA added for different loadings of the two-stage addition. Loading wt% wrt total amount of monomer.

Entry	BzA Loading (wt%)	Charge 1		Charge 2	
		BzA (mL)	BzA (mmol)	BzA (mL)	BzA (mmol)
1	50	2.83	18.50	2.83	18.50
2	60	3.40	22.22	3.40	22.22

The half-life of radical initiator in scCO₂ can be calculated if certain parameters are known. Guan *et al.* published values for AIBN. The rate constant for decomposition (k_d) can be found using the Arrhenius equation (Equation 3-1):

$$k_d = Ae^{\frac{-E_a}{RT}} \quad \text{Equation 3-1}$$

Where A is known as the pre-exponential factor, E_a is the activation energy of decomposition, R is the universal gas constant and T is the absolute temperature.

For AIBN in scCO₂ at 338.15 K (65 °C) and 207 bar, k_d was calculated to be $7.84 \times 10^{-6} \text{ s}^{-1}$. This is then converted into a half-life, $\tau_{1/2}$ (Equation 3-2):

$$\tau_{1/2} = \frac{0.693}{k_d} \quad \text{Equation 3-2}$$

The half-life for AIBN under the reaction condition is 24 hours.⁵⁷ As the reaction had been carried out for approximately 24 hours, additional AIBN (0.059 g, 0.33 mmol) was included in the second charge. This increased the AIBN concentration back to the original concentration used at the start of the reaction. The AIBN quantity required was calculated using Equation 3-3:

$$N(t) = N_{(0)} e^{-\lambda t} \quad \text{Equation 3-3}$$

Where $N(t)$ is the population at time t , $N_{(0)}$ is the initial population and λ is the decay constant (k_d).

The reaction was left overnight (18 hours). After this time the heating was removed, and the autoclave was allowed to naturally cool to room temperature before being depressurised. The resulting products were collected for analysis.

Synthesis of PBzA Seeds

The synthesis of a PBzA seed used the same procedure as described in section 3.4.2.2 (two-stage addition) with the following differences; the initial charge used in stage 1 consisted of BzA (5.66 mL, 36 mmol), AIBN (1 wt% wrt total monomer content, 0.12 g, 0.73 mmol) and PDMS-MA (5 wt% wrt total monomer content, 0.6 g, 0.06 mmol). For stage 2, a charge of MMA (3.19 mL, 3.0 g, 29.65 mmol) was added via a HPLC pump at 0.2 mL min^{-1} .

3.4.4. Crosslinked Particle Synthesis in 60 mL Autoclave

3.4.4.1. One-stage Batch Reactions

The same procedure was followed as detailed in section 3.4.2.1 with the following quantities; MMA (10 mL, 93 mmol), EGDMA (amounts shown in Table 3-6), PDMS-MA (5 wt% wrt total amount MMA, 0.468 g, 0.05 mmol) and AIBN (1 wt% wrt total amount MMA, 0.094 g, 0.57 mmol).

Table 3-6: Amounts of EGDMA used for each loading. Loading wt% wrt total amount of MMA.

Entry	EGDMA Loading (wt%)	EGDMA (mL)	EGDMA (mmol)
1	1	0.1	0.53
2	2	0.2	1.06

3.4.4.2. Multi-stage Reactions

A typical synthesis followed the same procedure as described in 3.4.2.2 with the following quantities; MMA (8 mL, 74.4 mmol), AIBN (1 wt% wrt total MMA, 0.0705 g, 0.43 mmol) and PDMS-MA (5 wt% wrt total MMA, 0.468 g, 0.05 mmol) for stage 1. In stage 2, a second charge of MMA (2 mL, 19 mmol) and EGDMA (amounts shown in Table 3-7) was added via a HPLC pump at 0.2 mL min⁻¹. Products were typically collected as a free-flowing powder.

Table 3-7: Amounts for each loading of EGDMA. Loading wt% wrt shell MMA (2 mL).

Entry	EGDMA Loading (wt%)	EGDMA (mL)	EGDMA (mmol)
1	1	0.018	0.095
2	9	0.090	0.477
3	4.8	0.179	0.948
4	33	0.895	4.74

3.4.5. Combination of Crosslinking and PBzA

For the application of impact modification, it is essential that the particles contain some degree of crosslinking, as this ensures the particle maintains its structure throughout the high temperature processing. For this reason, particles were synthesised that contained a low T_g component (PBzA) with crosslinking.

3.4.5.1. Incorporation of Crosslinker with PBzA

A standard synthesis followed the same procedure as discussed in section 3.4.3.1 (two-stage addition forming particles with a 50 wt % BzA loading) with the following differences; for stage 3 of the reaction BzA (2.83 mL, 18.50 mmol), AIBN (1 wt% wrt total monomer, 0.12 g, 0.73 mmol) and DVB (1 wt% wrt stage 3 BzA, 0.0259 mL, 0.15 mmol) or EGDMA (1 wt% wrt stage 3 BzA, 0.0297 mL, 0.19 mmol) was added.

3.4.5.2. Incorporation of Crosslinked Shell

A typical synthesis followed the same initial procedure as described in section 3.4.3.1 (two-stage addition of BzA) to form particles containing PBzA (50 wt%). An additional stage was included (stage 4, Figure 3-11) to create a crosslinked shell in which MMA (3 mL, 28 mmol) and DVB (1 wt% wrt MMA shell, 0.027 mL, 19 mmol) were added via a HPLC pump at 0.2 mL min^{-1} , which induced a pressure increase.

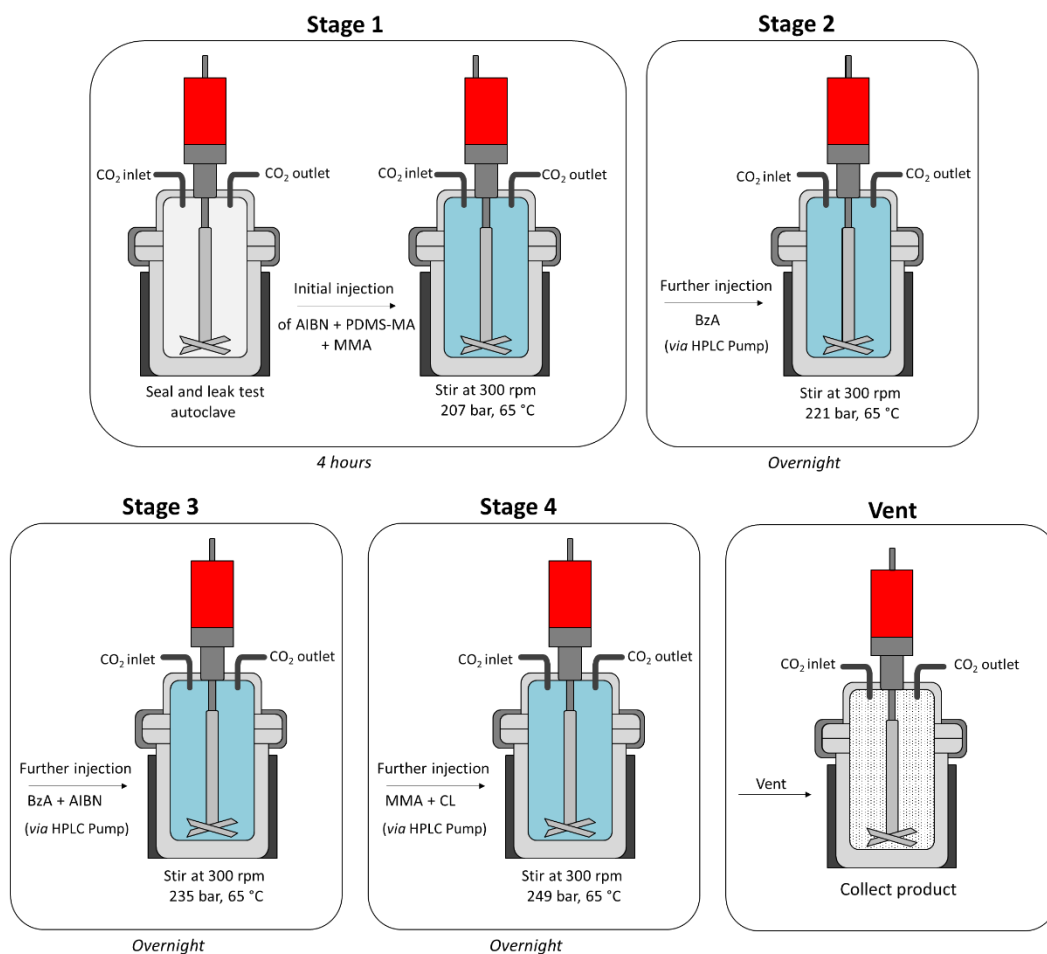


Figure 3-11: Schematic showing synthesis procedure to form a crosslinked MMA shell on a PMMA/PBzA (50 wt%) particles.

3.4.5.3. Self-Crosslinking of PBzA

Reactions were set-up as described in section 3.4.3.1. The length of the final stage was varied for 24, 36 and 72 hours.

3.4.6. Homopolymer Synthesis

For analysis comparison, samples of homopolymer were produced.

3.4.6.1. PBA Synthesis

The synthesis followed the same procedure as outlined in 3.4.2.1 with the following differences; BA (10 mL, 8.9 g, 69.4 mmol) and AIBN (1 wt% wrt BA, 0.089 g, 0.54 mmol) were separately deoxygenated by flushing with argon for 30 minutes. Due to poor solubility in BA, the PDMS-MA (5 wt% wrt BA, 0.445 g, 0.04 mmol) was deoxygenated in the autoclave by purging through the keyhole with CO₂ (1-2 bar).

3.4.6.2. PBzA Synthesis

The synthesis followed the same procedure as detailed in 3.4.2.1 with the following differences; BzA (6 mL, 6.36 g, 39 mmol) and AIBN (1 wt% wrt BzA, 0.064 g, 0.39 mmol) were separately deoxygenated by flushing with argon for 30 minutes. Due to poor solubility in BzA, the PDMS-MA (5 wt% wrt BzA, 0.327 g, 0.03 mmol) was deoxygenated in the autoclave by purging through the keyhole with CO₂ (1-2 bar).

3.5. Results and Discussion

3.5.1. BA/PMMA Particle Synthesis in 60 mL Autoclave

The first proposed core-shell system that was investigated, was composed of a poly(butyl acrylate) (PBA) core encased in a PMMA shell, with T_g s measured by DMA of $-45\text{ }^\circ\text{C}$ and $144\text{ }^\circ\text{C}$ respectively (Figure 3-12). These monomers were chosen as they are currently used by the supporting company in products that are designed for impact modification. They also fulfil the criteria of having a lower T_g , “soft core” and a higher T_g , “hard shell”. The soft core of the particle absorbs the energy of an impact. This is an essential characteristic of a particle used for impact modification. The hard shell allows the particle to maintain its structure during processing and must be compatible with the matrix into which it is being mixed. In this case, the shell is PMMA which is compatible with the PVC matrix.⁵⁰

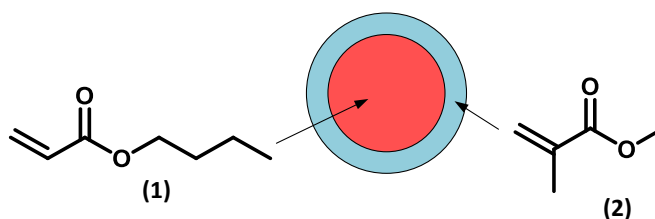


Figure 3-12: Chemical structures of BA (1) and MMA (2) monomers used to form the core and shell respectively.

The method used to synthesise this structure would traditionally follow a two-stage emulsion polymerisation, in which the PBA core was synthesised before the addition of MMA. However, it is known that the dispersion polymerisation of low T_g monomers in scCO_2 does not readily produce particles. The main reason for this is the fact that the CO_2 readily plasticises the polymer particles, lowering their T_g and causing agglomeration. Wang *et al.* observed aggregated solids in homopolymerisation of poly(2-(dimethylamino) ethyl) (PDMAEA) at $16\text{ }^\circ\text{C}$. Addition of MMA produced a copolymer with a higher T_g that was therefore able to form stable particles.⁵⁸ Aggregation attributed to low T_g was also observed in the synthesis

of poly(ethyl methacrylate).⁵⁹ For these reasons, dispersion polymerisation of higher T_g MMA was performed prior to addition of the lower T_g BA, in attempt to create the desired PBA/PMMA core-shell morphology. Synthesis of PMMA first will create a stable seed particle. This seed particle will be plasticised under the condition used, in theory allowing for penetration of a second monomer/polymer creating the desired core-shell structure.

Muller *et al.* carried out detailed simulations of dispersion polymerisation of MMA in scCO₂.⁶⁰ The authors reported that after precipitation of the growing polymer chain, polymerisation occurs almost exclusively in the continuous (scCO₂) phase to form oligomers. These oligomers precipitate onto the surface of the already formed core particles and growth of these chains proceeds near the surface of the particles before termination. The lifetime of the propagating radicals is very short, and the viscosity of the particle is relatively high, meaning that the radicals are unlikely to diffuse into the particles before termination occurs. New polymer formed later in the reaction should therefore accumulate around the particle, forming a shell.⁶⁰⁻⁶² However, DeSimone *et al.* showed that under the conditions used in this work (65 °C, 207 bar) the PMMA particles would be plasticised by the CO₂, reducing the particle viscosity. This potentially allows for the penetration of flexible oligomers of a second monomer (Figure 3-13).^{2, 57} A further driving force for migration of the growing polymer chain inside the particle is polarity. In the case of emulsion polymerisation, if a polymer is more polar it will be more thermodynamically favourable for it to migrate to the interior of the particle.⁶³

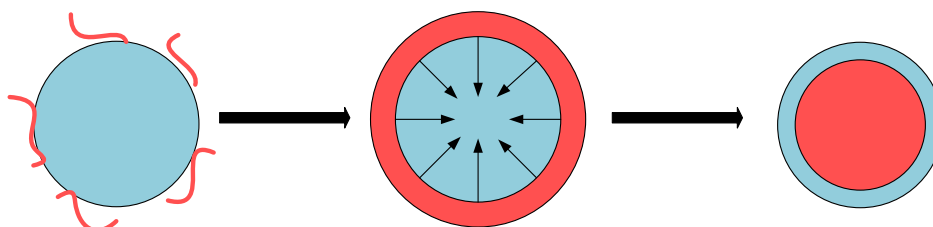


Figure 3-13: Proposed mechanism for the formation of an internal PBA core. Oligomers of PBA will initially deposit on the surface of the already formed PMMA particles. As the PMMA particle is plasticised under the conditions used, these PBA oligomers will be able to migrate into the middle of the particle giving, in theory, a core-shell structure.⁵⁷

An alternative mechanism for the formation of the internal morphology is that with reduced viscosity, the reaction could occur within the PMMA particles as plasticised PMMA may be a better solvent for the BA than the CO₂.⁶⁴ It is therefore proposed, that once the initial PMMA particles have been formed, the BA should polymerise within or migrate into these particles producing a core shell particle, where the core is soft PBA and the shell is hard PMMA. If it is possible to produce these particles, they could see potential use as impact modifiers. The initial synthesis used a two-stage technique as previously described in the experimental section 3.4.2.2. The first stage was the synthesis of PMMA particles, followed by injection and polymerisation of BA. The ability to add a second monomer has been well studied in the group previously, using several different monomers.⁵⁷ The ratio of BA to MMA was varied to investigate the effect this had on the particle structure as well as the T_g. Loadings of 9, 18 and 27 wt% BA were tested (Table 3-8).

Table 3-8: Summary of 60 mL two-stage HPLC reactions with various loadings of BA. All reactions were completed in a triplicate to check batch-to-batch variability.

Entry	BA Loading (wt%)	Time (hours)	PBA Content ^a (%)	BA Conversion ^a (%)	Particle Size ^c (nm)
1	0	18	0	0	1640 ± 220
2	9	18	7	71	1700 ± 220
3	18	18	14	68	1450 ± 200
4	27	18	22	68	900 ± 150

^a- measured by ¹H NMR, ^b- measured by DMA, ^c - measured from SEM images (including standard deviation).

BA conversion was calculated from ¹H NMR by comparison of the unreacted monomer signal (chemical shift 6.12 ppm, c) to polymer signal (chemical shift 4.04 ppm, c') (Figure 3-14).

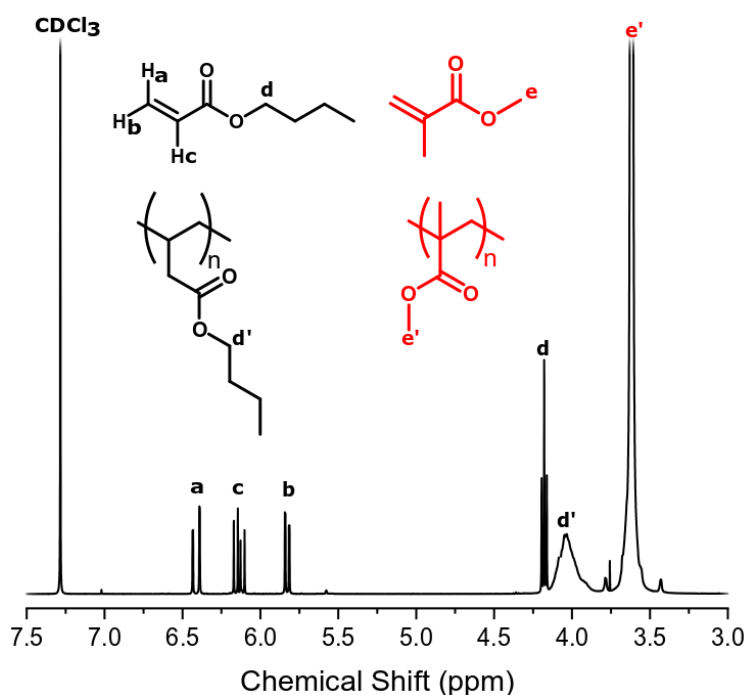


Figure 3-14: ^1H NMR spectrum of PMMA particles with a feed of BA (27 wt%); chemical shifts labelled c and c' were used to calculate the PBA content.

The presence of unreacted BA (chemical shifts labelled a, b and c) could affect the T_g of the material. If required for the end application this could be easily removed by flushing with CO_2 post polymerisation. PBA content was calculated by comparison of the PMMA signal (chemical shift 3.60 ppm, d') to the PBA signal (chemical shift 4.04 ppm, c'). At all loadings, BA conversion reached > 68%, increasing reaction time did not lead to any further increase in conversion. This is likely a result of O_2 present in the BA; a known inhibitor of polymerisation reactions.⁶⁵ The procedure using the HPLC pump to inject the BA unavoidably introduces O_2 into the system, as the BA was kept in an open reservoir throughout pumping. The PBA content of the particles was slightly lower than the feed for all loadings, but this probably reflects the BA conversion of < 70%. However, as the feed loading is increased, an increase in PBA content was observed. McAllister *et al.* observed this same trend, where the content of a second monomer in the particles, in this case 2-(dimethyl amino) ethyl methacrylate (DMAEMA), was lower than the monomer feed, suggesting that use of the HPLC pump and introduction of O_2 is the reason for lower conversion.^{57, 66}

SEM analysis showed that discrete, well-defined particles were produced for all loadings of BA (Figure 3-15, images b, c, d). By comparison to the pure PMMA particles (Figure 3-15, image a) there was no significant reduction in particle quality.

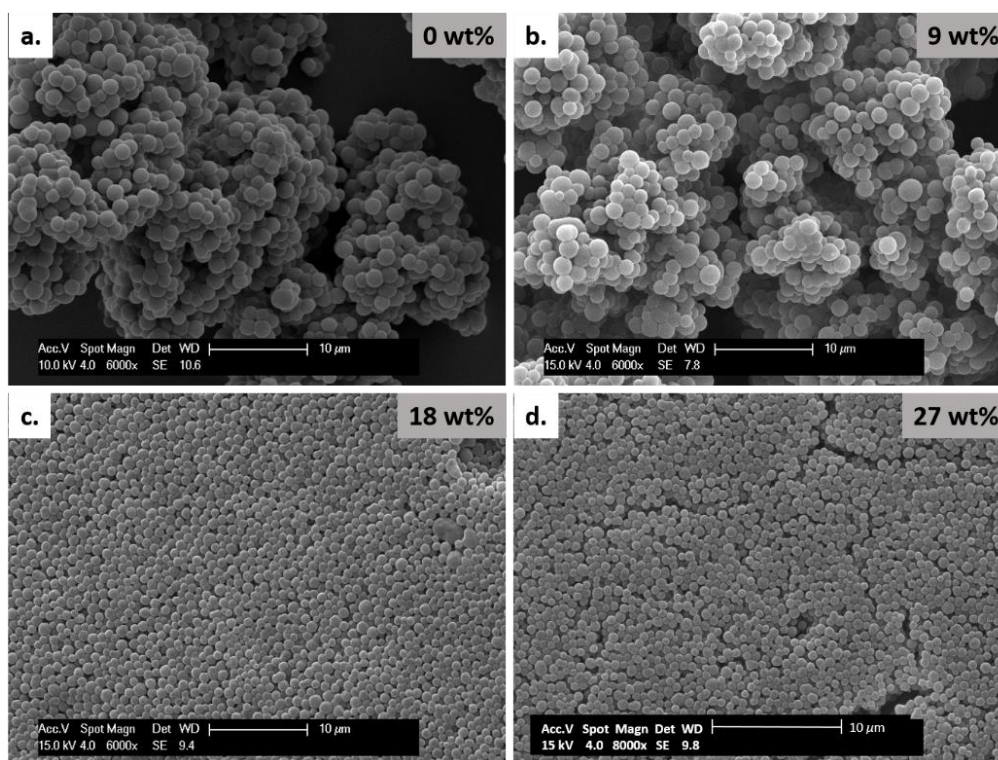


Figure 3-15: SEM images of PMMA particles formed using a two-stage reaction method incorporating; 0 wt% (a, Table 3-8, entry 1), 9 wt% (b, Table 3-8, entry 2), 18 wt% (c, Table 3-8, entry 3) and 27 wt% (d, Table 3-8, entry 4) BA. Particle structure was maintained as BA content increased. Samples were washed and dried prior to imaging. All scale bars are 10 μm.

Particles synthesised with a loading of 9 wt% were similar in size to the pure PMMA particles. A trend of decreasing average particle size as PBA content increased was observed (Table 3-8). This can be explained by the total amount of monomer remaining the same for all loadings of BA therefore, as BA loading increases the amount of MMA in the initial stage of the reaction is reduced. This initial period of the reaction is when nucleation of the particles occurs and the ratio of MMA to PDMS-MA dictates the size of the particles produced. As the amount of PDMS-MA remains the same and the amount of MMA reduces, the PMMA particles formed will

be smaller. SEM, however, cannot determine if the desired core-shell internal morphology was obtained. Therefore, further analysis was required.

Dynamic Mechanical Analysis (DMA) was used to establish whether phase separation had occurred within the particles by measuring the glass transition temperature (T_g). It is well known that core-shell particles show two $\tan \delta$ peaks, with the lower temperature peak corresponding to the soft, rubbery phase and the higher temperature peak corresponding to the hard, glassy phase.³³ The trace for pure PMMA shows two clear peaks (Figure 3-16, black trace).

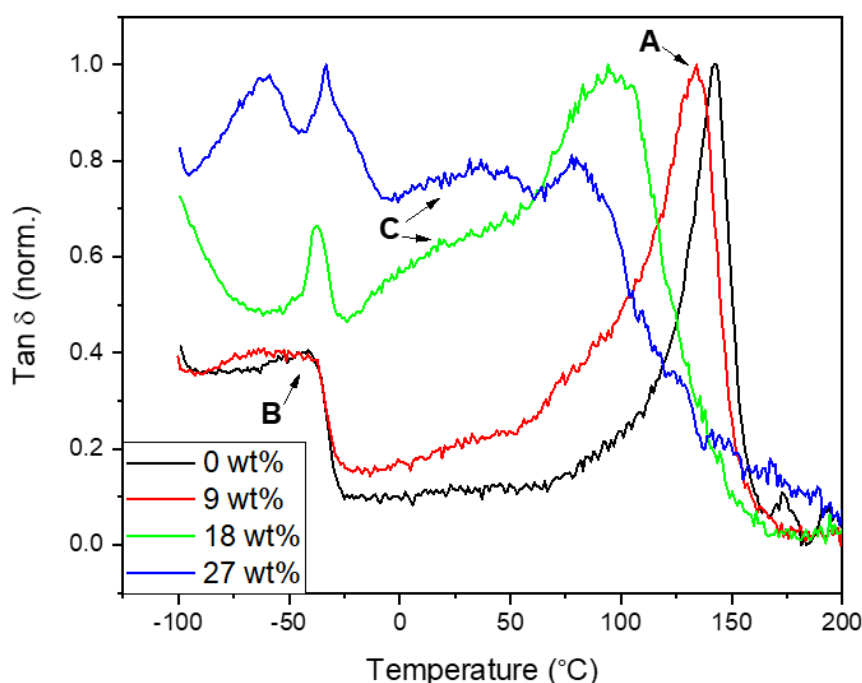


Figure 3-16: DMA traces for PMMA particles synthesis to which 0 wt% (black), 9 wt% (red), 18 wt% (green) and 27 wt% (blue) BA was added. A shift to lower T_g and peak broadening is observed as BA loading increases. Data has been normalised.

A peak at approximately 144 °C (A) corresponds to the T_g of the PMMA phase; and a second at -50 °C (B), corresponding to the melting transition (T_m) of the stabiliser used (PDMS-MA). A small amount of PDMS-MA is incorporated into the particles via the stabilisation mechanism present in dispersion polymerisation. Residual surfactant can be removed by washing or extraction of the particles with CO_2 ,⁶⁷ if the

final application warrants it. The T_g peak is also seen to broaden as BA content is increased. This is attributed to the presence of a range of different particle compositions that arise from the difference in reactivity ratios of BA and MMA.⁶⁸

Concentrating on the “PMMA type” peak, the addition of 9 wt% of BA caused a shift to a lower temperature of 128 °C (Figure 3-16, black to red trace). This was expected as the amount of soft component in the particle, with a lower T_g , has increased. This trend was shown to continue as BA loading was increased further (Table 3-9).

Table 3-9: Summary of T_g data collected for the “PMMA type” peak collected from DMA for different loadings of BA.

Entry	BA Loading (wt%)	“PMMA Type” T_g (°C)
1	0	143
2	9	128
3	18	97
4	27	77

The fact that the entire peak is shifting suggests that a homogeneous blend is being formed as opposed to discrete domains. However, potential phase separation may be occurring in the 18 and 27 wt% samples as indicated by a shoulder peak forming to the left of the PMMA peak (Figure 3-16, (C)). DSC analysis exhibited transitions only for PDMS-MA and PMMA. Here, a shift of the PMMA transition was not observed. This is not surprising as DSC is known to be a less sensitive technique than DMA.^{69, 70}

As previously discussed, if a core-shell structure was present, then a T_g peak for both the “soft” PBA phase and the “hard” PMMA phase of the particles would be observed. However, in our system, the crystal melt for the PDMS-MA stabiliser, occurs at -50 °C, which is very close to the T_g of PBA at -45 °C (Figure 3-17). Hence, it is very difficult to determine if a homogeneous PBA peak was present.

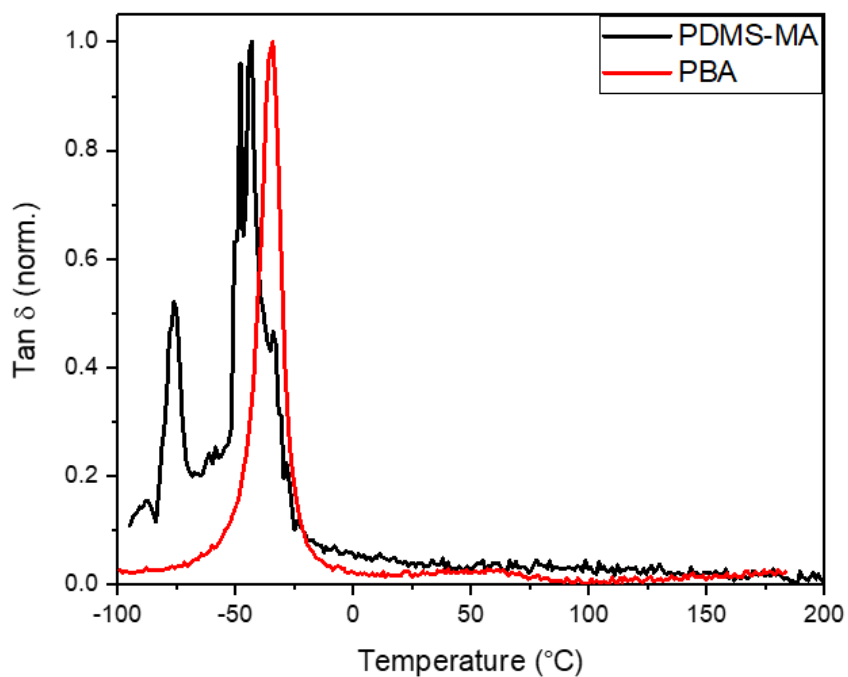


Figure 3-17: DMA traces for pure PDMS-MA (black) and pure PBA (red) demonstrating the overlap of the two species. Data has been normalised.

Focusing on the peak around -45 °C, it can be seen that for loadings above 18 wt% the appearance of this peak changes in comparison to the pure PMMA sample (Figure 3-18). This could possibly indicate the presence of a pure PBA phase. Indeed, the shape of the peak looks like a combination of the PDMS-MA signal in the pure PMMA sample and T_g of pure PBA (Figure 3-18).

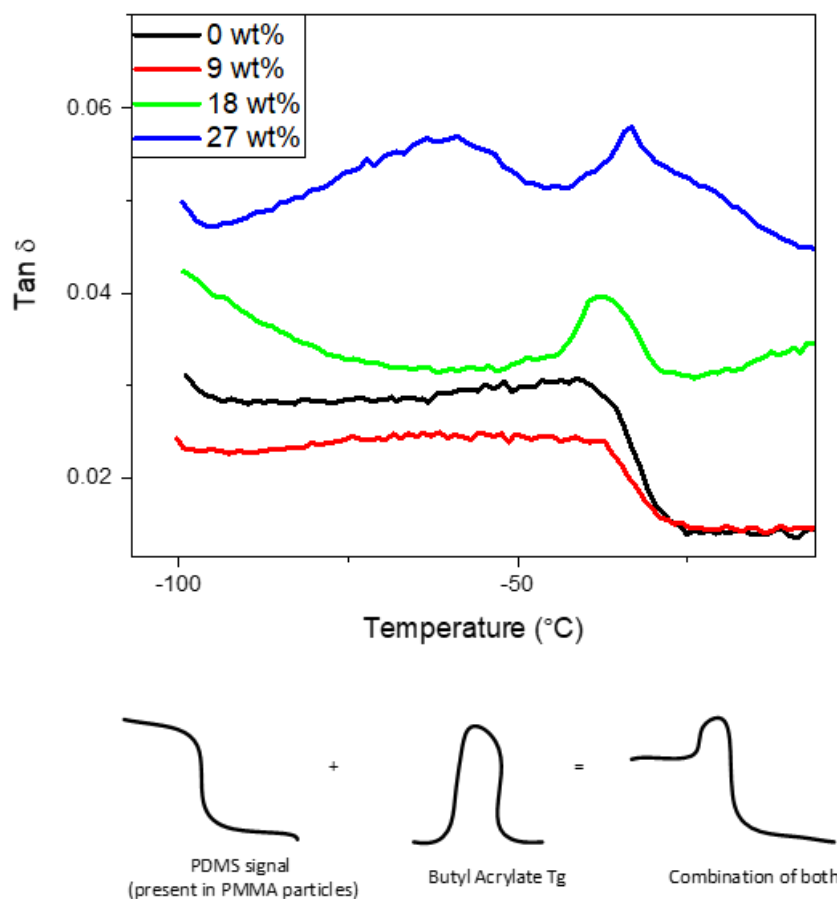


Figure 3-18: DMA traces for PMMA particles (black) to which 9 wt% (red), 18 wt% (green) and 27 wt% (blue) BA was added showing the lower temperature region. Data has been not normalised. At loadings above 18 wt% the appearance of the peak changes. Below the graph is a schematic representation of the shape of the trace achieved through combination of DMA signals for PDMS-MA (present in the PMMA samples) and pure BA.

As previously mentioned, the shift in the “PMMA-type” transition indicated the possibility of a blend being formed. The effect upon the overall T_g of adding a second monomer or plasticiser to a system can be predicted using the Flory-Fox Equation, Equation 3-4, where W_1 is the weight fraction of monomer 1, W_2 is the weight fraction of monomer 2, $T_{g,1}$ is the T_g of monomer 1 and $T_{g,2}$ is the T_g of monomer 2.⁷¹

$$\frac{1}{T_g} = \frac{w_1}{T_{g,1}} + \frac{w_2}{T_{g,2}} \quad \text{Equation 3-4}$$

The particles synthesised gave T_g values close to what was predicted from the Flory-Fox Equation for the different loadings of BA (Figure 3-19). This supports the evidence that the particles formed are a homogeneous blend of PMMA and PBA, with the PBA effectively acting as a plasticiser. This is unusual as PMMA is normally considered to be immiscible with PBA.⁷²

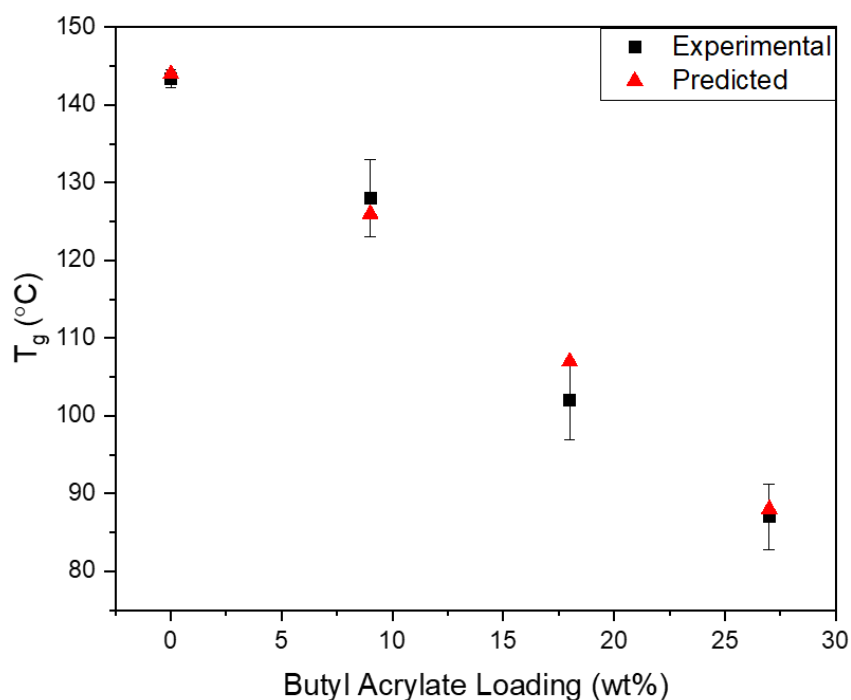


Figure 3-19: Graph showing that the measured T_g of the particles decreased as BA loading was increased (black series, ■). The trend observed agrees with values calculated using the Fox equation (red series, ▲).

The conversion of MMA was > 95% at the point when the BA was added. Hence any new polymer formed would consist almost entirely of BA. This suggested that the PBA forming was becoming entangled with the already present PMMA to give blended, homogeneous particles, as opposed to a core-shell structure (Figure 3-20).

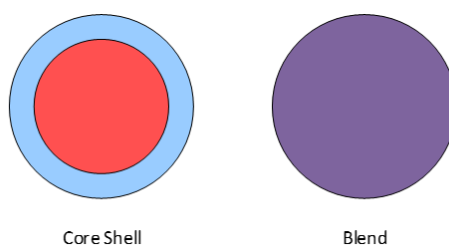


Figure 3-20: Illustration representing the internal particle morphology; desired core-shell morphology (left) and blended (right).

GPC analysis offered further insight into the species that were present for each loading of BA (Figure 3-21). The trace for a BA loading of 9 wt% showed a monomodal peak that was shifted in comparison to pure PMMA, but not significantly. It also showed a slight, high molecular weight shoulder peak, which suggested that the sample contained two species. In comparison, multimodal peaks were observed for higher loadings of BA. For example, at 18 wt% a clear bimodal peak is observed, again with a slightly high molecular weight shoulder, whereas a loading of 27 wt% gave a trimodal peak. This suggested the presence of more than one species; there might be pure PMMA, pure PBA and/or a copolymer of the two.

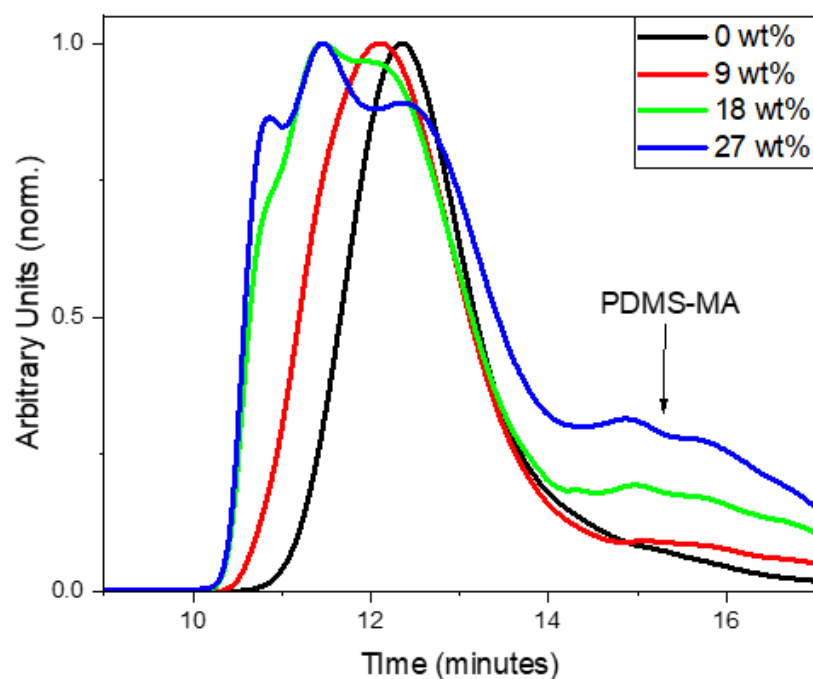


Figure 3-21: GPC traces (DRI) for PMMA particles to which; 0 wt% (black), 9 wt% (red), 18 wt% (green) and 27 wt% (blue) BA has been added using a two-stage reaction method. Low molecular weight shoulder peak labelled is caused by PDMS-MA. Data was collected using GPC system B and has been normalised. Multiple species are present for loadings of 18 and 25 wt%.

The peak at approximately 15 minutes in all the traces was due to the presence of PDMS-MA in the sample. An overlay of the GPC traces of PDMS-MA and that of the synthesised PMMA particles is shown in Figure 3-22. Residual PDMS-MA is left in the sample post synthesis, which can be removed by extraction with scCO_2 .⁷³

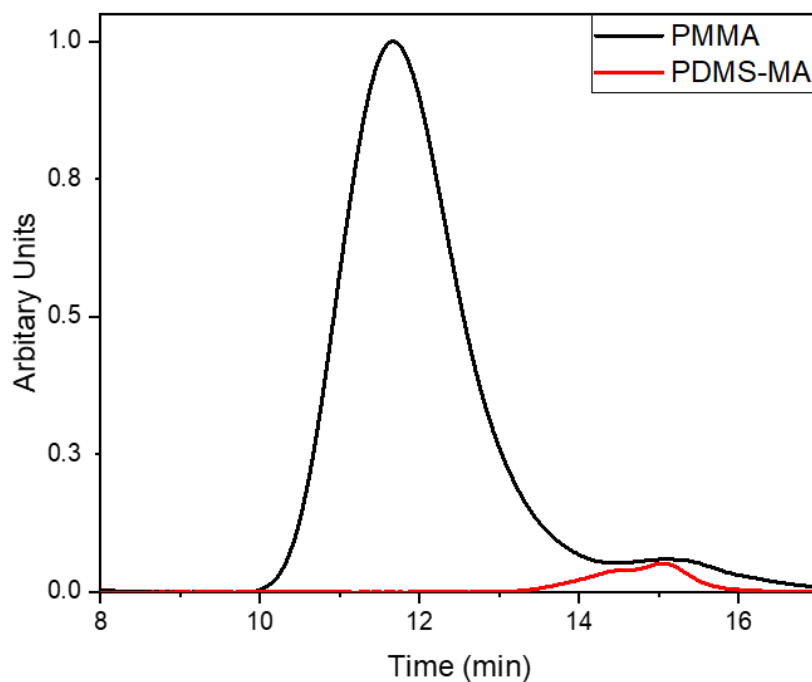


Figure 3-22: GPC traces for synthesised PMMA (black) and PDMS-MA (red). The shoulder peak present in the synthesised PMMA is caused by residual PDMS-MA present in the sample. Data was collected using GPC system A.

To probe the internal morphology of the particles, transmission electron microscopy (TEM) coupled with preferential staining of one phase is required. This is a common technique used to distinguish the structure of two component particles.^{36, 74} However, as a result of the similarities in functional groups between the two monomers used (MMA and BA), preferential staining of one phase is not possible. To overcome this, additional analysis that could help characterise the internal morphology would be atomic force microscopy (AFM). This utilises the tapping mode and the different T_g values of the soft and hard polymers. Insight into where the BA is polymerising could be obtained through use of this technique. Sommer *et al.* used AFM to investigate the surface morphology of PBA/PMMA core-shell latexes

synthesised by a two-stage seeded emulsion polymerisation.⁷⁵ Access to this analysis technique was not available and hence it was not used.

In an attempt to further understand the system, this sample was then compared to a sample produced in a one-stage reaction in which BA was incorporated at the beginning of the reaction (Table 3-10). BA conversion was higher in the one-stage reaction compared to using the two-stage reaction; likely a result of the lower amount of O₂ present, as when using the one-stage batch conditions, both monomers are deoxygenated prior to addition to the autoclave. The PBA content of the particles produced using this one-stage method was slightly lower than the feed, because the conversion was only 90%. Overall, the PBA content is higher than the two-stage reaction, again this is expected as the one-stage reaction shows higher conversion.

Table 3-10: Comparison of 60 mL reactions utilising both the one- and two-stage reaction methods.

Entry	BA Loading (wt%)	Conditions	PBA Content ^a (%)	BA Conversion ^a (%)	T _g ^b (°C)	Particle Size ^c (nm)
1	9	Two-stage	7	71	128	1700 ± 220
2	9	One-stage	8	90	110	High aggregation
3	27	Two-stage	22	68	77	900 ± 150
4	27	One-stage	21	83	41	High aggregation

^a – measured by ¹H NMR, ^b – measured by DMA, ^c – measured from SEM images (including standard deviation).

All reactions were recorded as a duplicate.

SEM analysis of the samples prepared using the batch one-stage method with a loading of 9 wt% BA, showed poor particle structure and high aggregation (Figure 3-23).

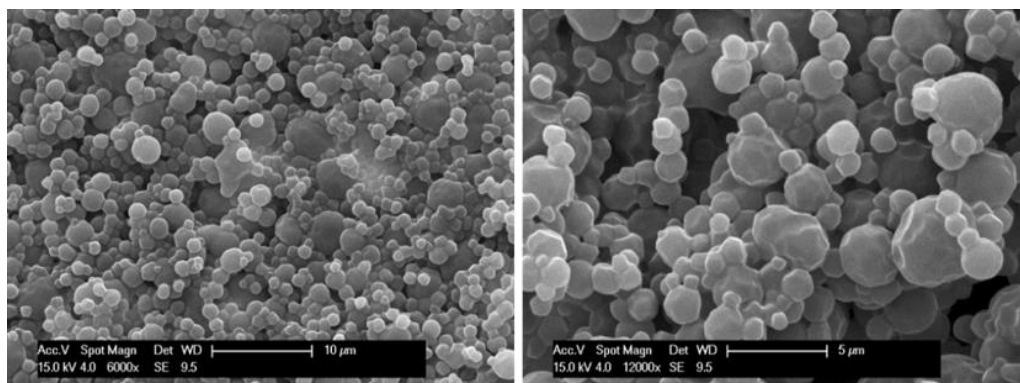


Figure 3-23: SEM images of the products from the one-stage batch reaction with 9 wt% loading of BA. Samples were imaged directly from the autoclave. Although particles were obtained, they were not well-defined.

A copolymer of PBA and PMMA is formed using the one-stage batch reaction conditions. The particles were less defined, which could indicate that the particle surface is PBA rich and hence “softer”. Jiang *et al.* also observed this when synthesising particles using conventional dispersion copolymerisation of MMA and BA.⁷⁶ Increasing the BA loading to 27 wt% also led to poor morphology control and agglomeration (Figure 3-24). This suggested the particle nucleation, and thus particle formation, had been disrupted because of the low T_g of PBA.^{58, 59}

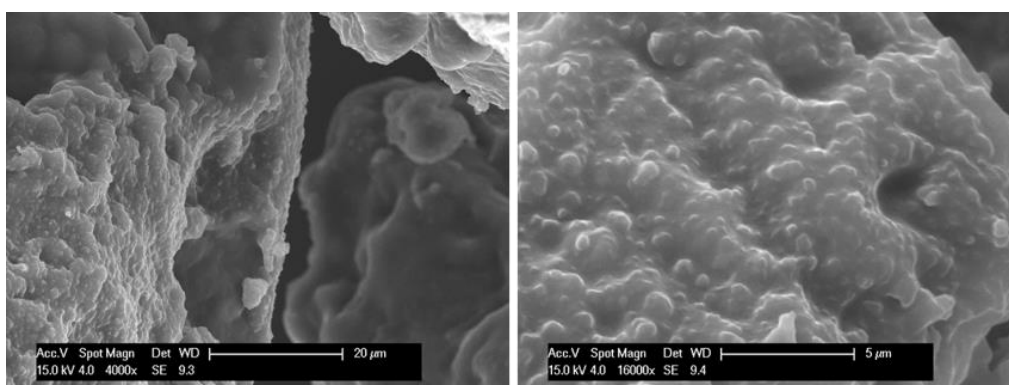


Figure 3-24: SEM images of the products formed in a one-stage batch reaction with 27 wt% loading of BA, poor control of particle structure was observed. Samples were imaged straight from the autoclave.

The DMA traces for both the one- and two-stage reactions showed the presence of two clear peaks, a “PMMA type” and a PDMS-MA peak (Figure 3-25). In DMA, the

presence of pure polymer phases is indicated by separate T_g peaks, occurring at the same temperature as the homopolymer. By contrast, if a blend is being formed the T_g peak will shift away from the T_g temperature of the homopolymer. The magnitude of the shift indicates the amount of blending that is present. Focusing on the one-stage reaction, a shift of 34 °C in the “PMMA type” peak was observed, in comparison to particles containing no BA (Figure 3-25, green trace to black trace). This shift of the “PMMA type” peak is larger than the 11 °C shift observed with the particles synthesised using the two-stage method (Figure 3-25, green trace to red trace). From this difference in shift, two conclusions can be drawn. Firstly, in the one-stage reaction a copolymer of MMA and BA is forming and hence phase separation does not readily occur. The larger shift of the T_g peak suggested the presence of a blended phase of PBA and PMMA is being formed. Secondly, in the two-stage method the polymer formed is most likely to be two homopolymers and hence partial phase separation is more likely to occur. This is evident by a smaller shift.

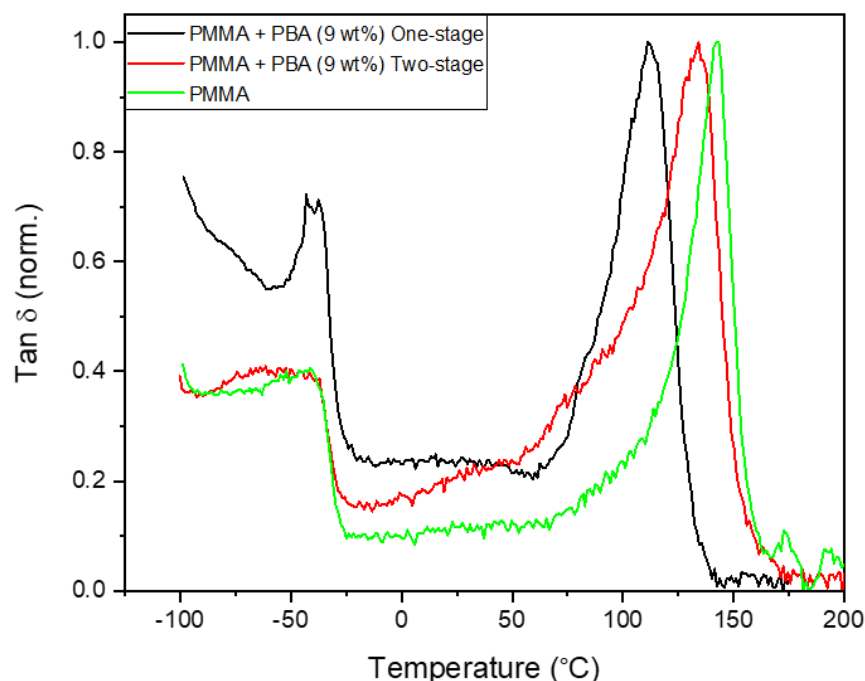


Figure 3-25: DMA traces for PMMA particles (green trace) to which 9 wt% BA has been added at the start of the reaction using the one-stage batch method (black trace) and as a second step using HPLC method (red trace). A shift of the “PMMA type” peak is observed with both methods. Traces have been normalised.

The peak present at approximately $-45\text{ }^{\circ}\text{C}$ in the one-stage batch reaction (Figure 3-25, black trace) is more defined in comparison to the particles produced using the two-stage method at the same loading of BA (Figure 3-25, red trace). As before, the shape of the trace appears to be a combination of the PDMS-MA and PBA signals. This could indicate a pure PBA phase being present in the one-stage batch reaction, however further analysis is needed to confirm this. The DMA trace for the sample synthesised with a 27 wt% loading of BA under one-stage batch conditions showed similar trends.

GPC traces of the one-stage process showed the evolution of a unimodal system with a small low molecular weight shoulder peak as the BA loading was increased (Figure 3-26). It is believed that this lower molecular weight shoulder peak is caused by the presence of PDMS-MA in the sample. It appears larger in the 27 wt% sample (Figure 3-26, red trace) because the data has been normalised. The presence of a single peak for the main distribution is consistent with the formation of one species as opposed to two separate polymers chains which would give two peaks.

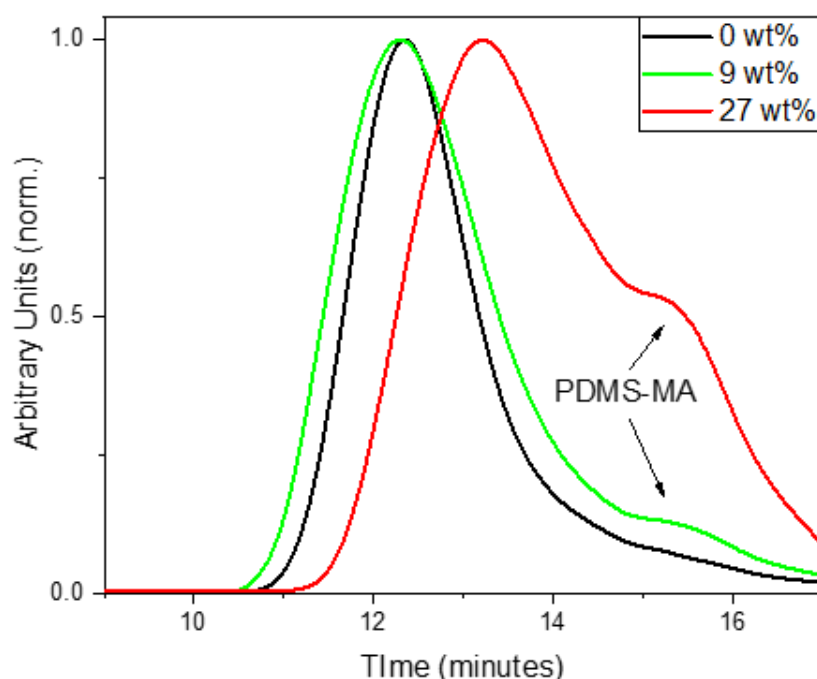


Figure 3-26: GPC traces obtained from the products formed in a one-stage batch reactions incorporating 0 wt% (black), 9 wt% (green) and 27 wt% (red) BA. All reaction show one peak indicating the presence of one species. Shoulder peak labelled is caused by PDMS-MA. Data has been normalised and was collected using GPC system A.

Because TEM staining is not possible, there is no clear route to analyse the internal morphology. Conflicting conclusions could be from the DMA data. Samples with lower loadings of BA appeared to form a blend, whereas with high loadings it could be inferred that a PBA phase is present. In addition, the GPC data shows similar trends, with the traces obtained from the lower loadings of BA, suggesting only one species is present, but at higher loading multiple species may be present. For these reasons we set out to develop an alternative polymer combination to allow TEM analysis.

3.5.2. BzA/PMMA Particle Synthesis in 60 mL Autoclave

Owing to the difficulties in confirming the internal morphology of the PMMA/PBA system, a second monomer system was investigated. The proposed structure kept the PMMA shell but used a poly(benzyl acrylate) (PBzA) core (Figure 3-27). PBzA has a T_g measured by DMA of 2 °C, which is higher than that of PBA, but lower than PMMA meaning that it can still be considered “soft”. The presence of the benzyl pendent group allows for the preferential staining of the PBzA phase.⁷⁷

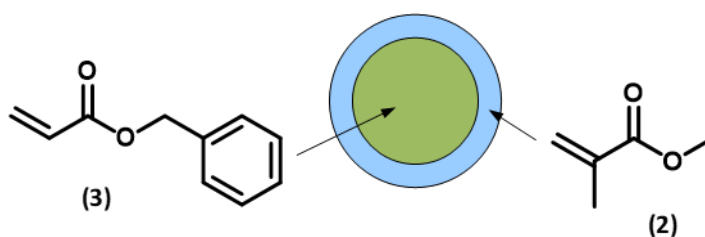


Figure 3-27: Schematic showing the second proposed core-shell structure formed from a MMA (2) and BzA (3) monomers.

Initial experiments followed the same two-stage procedure used with the BA reactions. A PMMA particle was synthesised first before addition of BzA (at varying loading wt%) in the second stage. Reactions were completed in duplicate in order to assess the reproducibility, with the exception of 50 wt% BzA loading. The results from these experiments are summarised in Table 3-11.

Table 3-11: Summary of 60 mL reactions with various loadings of BzA. All reactions were completed in a duplicate to check batch-to-batch variability (with the exception of the 50 wt% reaction).

Entry	BzA Loading (wt%)	PBzA Content ^a (%)	BzA Conversion ^a (%)	Particle Size ^b (nm)
1	9	12	100	1400 ± 212
2	9	13	100	1540 ± 279
3	27	20	100	1080 ± 201
4	27	19	97	1200 ± 251
5	36	27	97	940 ± 207
6	36	27	97	1310 ± 236
7	50	31-38	97	Highly aggregated

^a- measured by ¹H NMR, ^b - measured from SEM images (including standard deviation).

The conversion of BzA was calculated from the ¹H NMR spectrum by comparing the integral of the unreacted vinyl signals in the monomer (Figure 3-28, chemical shift 6.20 ppm, c) to the polymer signals (Figure 3-28, chemical shift 5.00 ppm, c'). Similar to the PBA system, the unreacted BzA (chemical shifts labelled a, b and c) could impact the T_g but, if necessary, could be removed by flushing with CO₂ post reaction. The PBzA content was calculated from ¹H NMR by comparing the integral of the PMMA peak (Figure 3-28, chemical shift 3.63 ppm, e') to the PBzA peak (Figure 3-28, chemical shift 5.00 ppm, c').

The PBzA content was lower in the final product than the feed ratio at all loadings of BzA. This was unexpected, because of the high conversion of BzA (> 97%) (Table 3-11), but could be a result of the conversion being artificially high because of the loss of residual monomer during venting of the autoclave. As with the particles containing PBA, a trend of decreasing average particle size as BzA loading increased was observed (Table 3-11). This was expected because the ratio of PDMS-MA to the initial charge of MMA changes. During the first stage of the reaction the particles nucleate and are stabilised by the surfactant, the concentration of surfactant in this stage will dictate the size of the particles produced. As the BzA content increases, the initial charge of MMA decreases but the amount of PDMS-MA remains the same. For the 9 wt% BzA loading, the initial charge of MMA was 9 mL, at a 36 wt% BzA loading this reduced to 6.34 mL, while the PDMS-MA loading remained at 5 wt% (wrt

the total amount of monomer (MMA + BzA)). It has been shown in the literature that increasing the concentration of surfactant in dispersion polymerisation in scCO_2 results in smaller particles being produced.⁷⁸

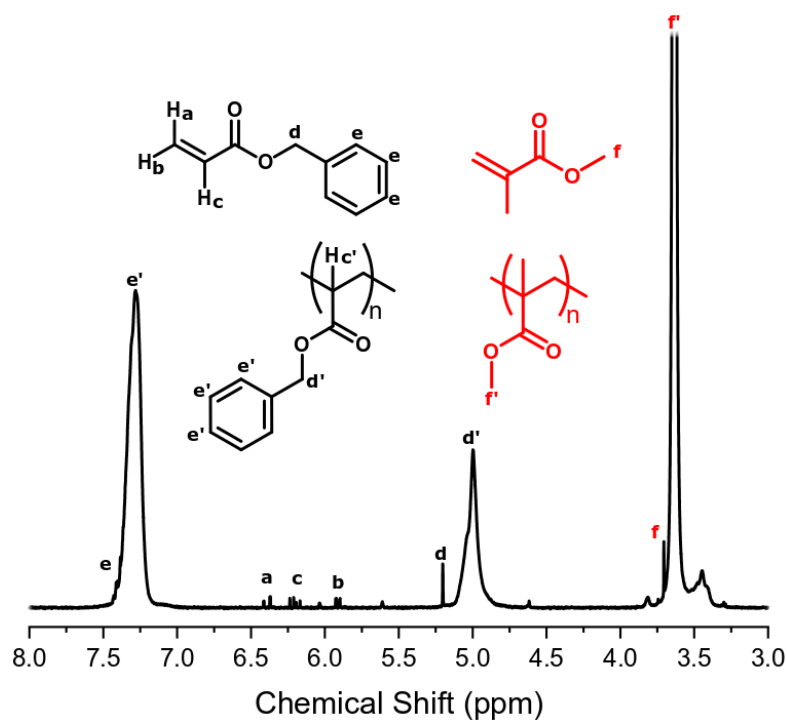


Figure 3-28: NMR trace for a PMMA particle with a feed of BzA (50 wt%) used to calculate the PBzA content. Spectrum was recorded in acetone and reference against the acetone signal peak at 2.05 ppm.

SEM analysis showed that the particle structure was well maintained as the BzA loading increased up to a 36 wt%, with uniform monodisperse particles being formed (Figure 3-29).

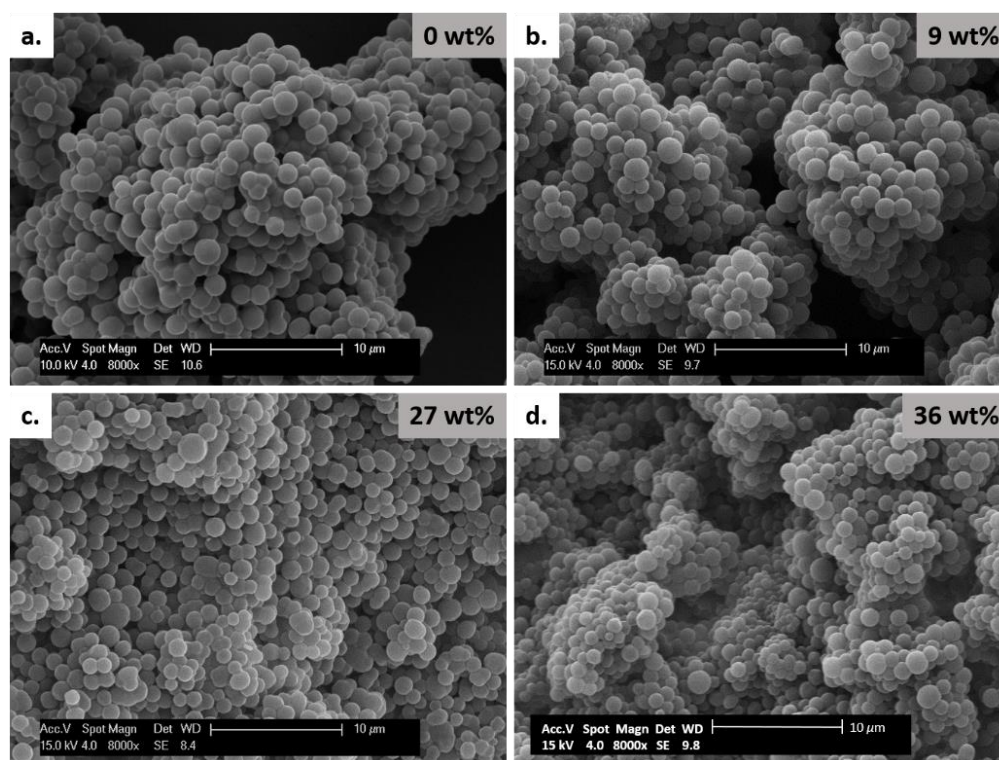


Figure 3-29: SEM images of PMMA particles produced with addition of varying loading of BzA in one-stage; 0 wt% (a), 9 wt% (b), 27 wt% (c), 36 wt% (d). Particle structure was maintained as BzA loading increased All scale bars are 10 µm.

As the BzA loading was increased to 50 wt% the sample produced was no longer homogeneous in composition; a highly agglomerated powder was removed from the autoclave. SEM analysis revealed that, although particles were still produced, high levels of aggregation and fusing of the particles had occurred in comparison to the other loadings (Figure 3-30).

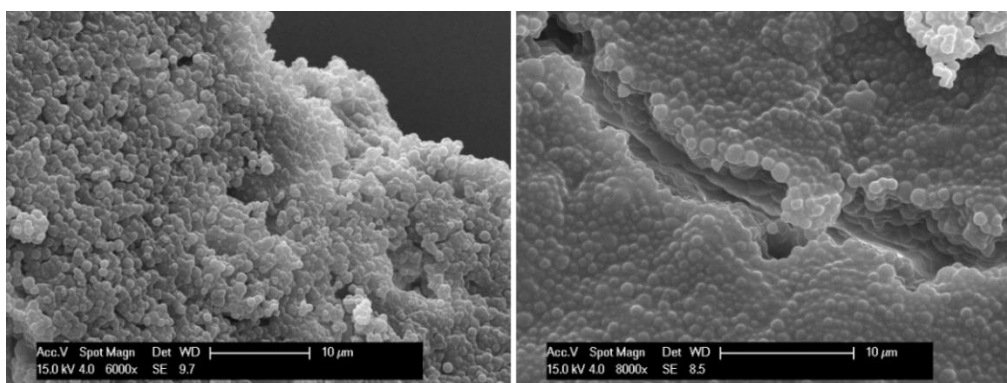


Figure 3-30: SEM images of the sample produced with addition of BzA 50 wt% to PMMA particles in one-stage. High aggregation was observed. Scale bars are 10 µm.

This aggregation is attributed to the injection causing an unstable dispersion because of a sustained change in the reaction medium during injection of the BzA.

Previous work in the group has shown that introducing the monomer in smaller aliquots improved overall particle quality.^{57, 79} This was attributed to there being more control over the reaction. Addition of a second monomer causes a change in the reaction medium as well as leading to particle softening which causes aggregation. Addition over multiple stages would limit the change and minimise particle softening.⁷⁹ The reaction was repeated with the addition of BzA split over two charges. The total monomer content of the reaction was increased to 12 mL compared to the original 10 mL. It is thought that this increase in volume should have minimal effect upon the particles produced. Addition of extra AIBN in the second charge of BzA was necessary as at the time of the injection the reaction had run for longer than the half-life of AIBN under the conditions used, which is 24 hours.⁸⁰ As before, the reactions were performed in a duplicate to test reproducibility (Table 3-12).

Table 3-12: Summary of 60 mL reactions where the BzA monomer was added over two-stages. All reactions were repeated check batch-to-batch variability.

Entry	BzA Loading (wt%)	PBzA Content ^a (%)	BzA Conversion ^a (%)	Particle Size ^b (nm)
1	50	35	99	850 ± 141
2	50	33	99	1040 ± 317
3	50	36	99	990 ± 202
4	60	49	99	<i>Highly aggregated</i>
5	60	50	99	<i>Highly aggregated</i>

^a- measured by ¹H NMR, ^b - measured from SEM images (including standard deviation).

Once again, the PBzA content was lower in the final product than in the feed even though the conversion of BzA was high (> 99%). This was attributed to the removal of unreacted BzA monomer during venting. The average particle diameter is similar to the particles synthesised with a 36 wt% loading (1125 ± 222 nm, average of the two repeat reactions), this is not surprising as the total amount of monomer had

been increased (12 mL). As the BzA loading was increased further to 60 wt% the sample produced was visually clumped when removed from the autoclave, instead of the expected free-flowing powder. It was hypothesised that further increases of BzA would require addition in more than two aliquots. The PMMA particles are soluble in the BzA, as a result the addition of BzA to the reaction would cause softening of the particles. Addition of the BzA over multiple aliquots would allow for a more controlled reaction and would permit formation of high molecular weight chains at high conversion before additions of further aliquots.

SEM analysis showed that addition of the BzA over two-stages had improved the particle structure produced in the sample with a BzA loading of 50 wt% (Figure 3-31, image a). However, SEM images of the particles produced with a BzA loading of 60 wt% showed the particle to be less well-defined and more aggregated, even though the BzA had been added over two-stages. (Figure 3-31, image b). The most likely cause of this that the soft polymer limit has been reached and the low T_g of the particles makes them more prone to aggregation.^{57, 58} The internal morphology of the particles could not be determined by SEM, hence further analysis was required.

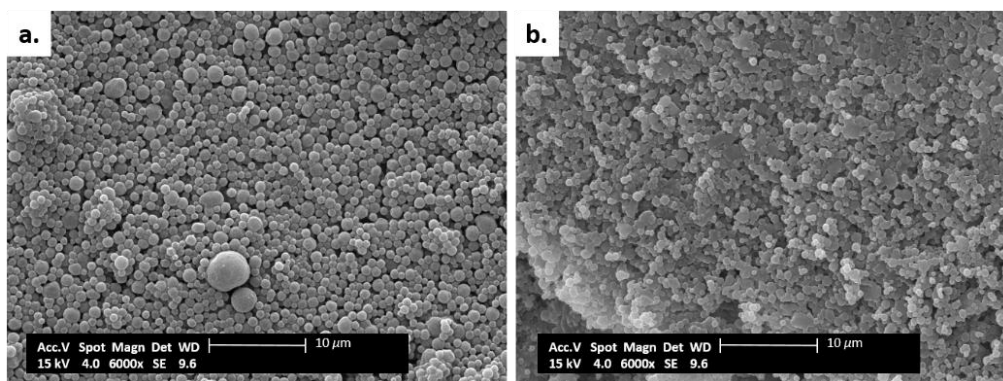


Figure 3-31: SEM images of PMMA particle produced with addition of varying loading of BzA over two-stages; 50 wt% (a) and 60 wt% (b). Well-defined particles were produced for a loading of 50 wt%, whereas for 60 wt% particle structure has deteriorated slightly. Scale bars are 10 µm.

The DMA traces showed two T_g peaks indicating the presence of two different phases for all loadings above 9 wt% (Figure 3-32). For comparison DMA data recorded for pure PMMA and pure PBzA are shown in black and grey respectively. The 9 wt% BzA

sample tested only showed one transition, similar to the peak observed for pure PMMA, suggesting phase separation did not occur. As the loading of BzA increases, a second, lower T_g peak, becomes visible. The lower T_g peak was attributed to a PBzA rich phase, whereas the high T_g peak was attributed to a PMMA rich phase. A shift in T_g away from the pure polymers was observed, suggesting that the phases present are not 100% phase separated but a partial blend. McAllister *et al.* observed similar trends in DMA data using an alternative two monomer system that produced an internal core-shell like morphology.^{57, 66}

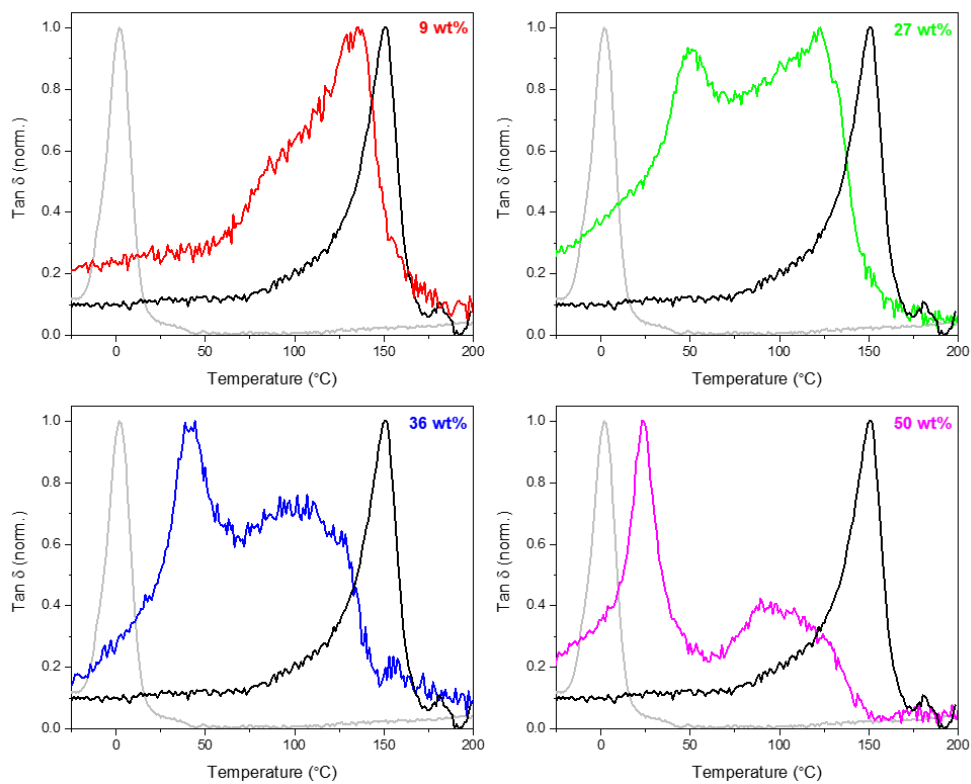


Figure 3-32: DMA traces obtained for various loading of BzA; 9 wt% (top left, red), 27 wt% (top right, green), 36 wt% (bottom left, blue) and 50 wt% (bottom right, pink). A trace for pure PMMA (black) and pure PBzA (grey) is included for comparison. All data has been normalised. Loadings of > 27 wt% exhibit two peaks indicating the presence of two phases.

DSC analysis of the samples agreed with the DMA data; the number of peaks/transitions for the samples were consistent across both techniques (Figure 3-33). For samples synthesised with loadings above 9 wt%, two transitions were present, a lower T_g transition similar to BzA and a higher T_g transition similar to PMMA. This again suggests that two phases were present.

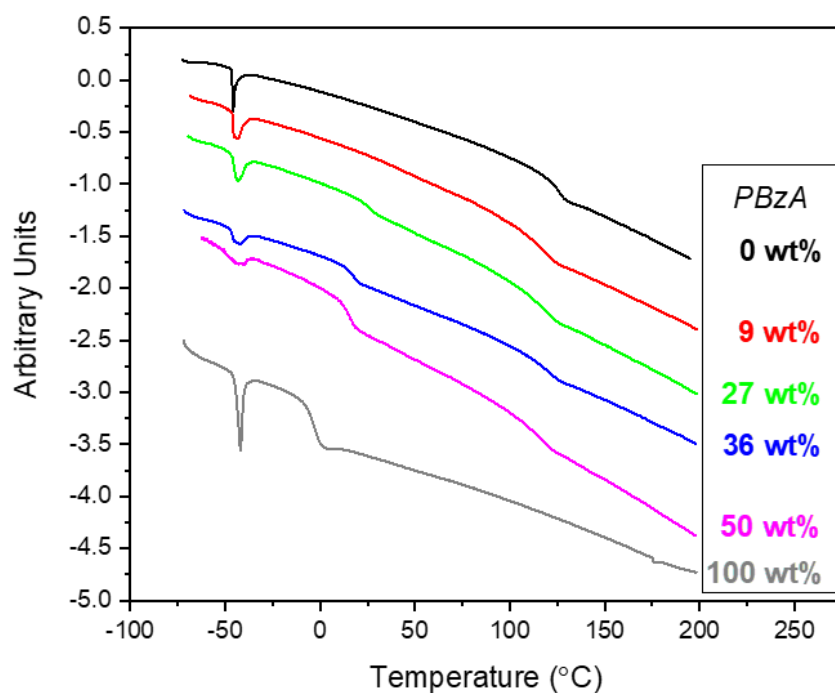


Figure 3-33: DSC traces obtained for various loading of BzA; 0 wt% (black) 9 wt% (red), 27 wt% (green), 36 wt% (blue), 50 wt% (pink) and 100 wt% (grey). Ordered from top to bottom. Loadings of > 27 wt% exhibit two peaks indicating the presence of two phases. Exo up.

PMMA type transitions occurred at similar temperatures across all samples, as did the PBzA transitions (Table 3-13). The transition present at approximately -50 °C is due to the T_m of the stabiliser, PDMS-MA.

Table 3-13: Summary of T_g data recorded by DSC for repeat reactions of varying loading of BzA.

Entry	BzA Loading (wt%)	PBzA T_g (°C)	PMMA T_g (°C)
1	0	-	128
2	9	-	118
3	27	27	117
4	36	25	120
5	50	16	122
6	100	-3	-

Two peaks were detected in GPC analysis for all loadings of PBzA, suggesting the presence of two different molecular weight species (Figure 3-34). Particles with

higher loadings of BzA (> 36 wt%) became difficult to push through the filter during preparation. Reasons for this are discussed further later in the chapter.

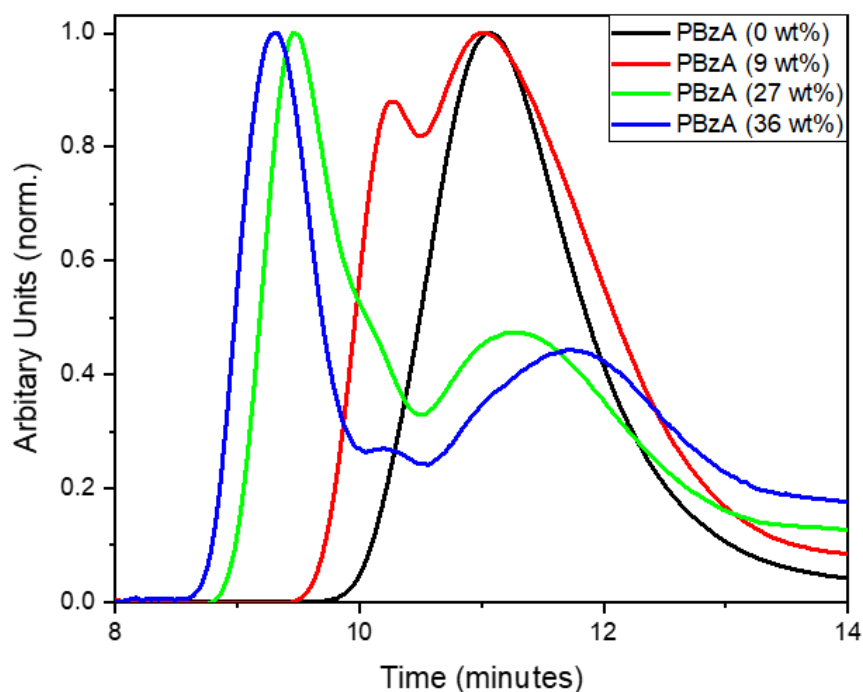


Figure 3-34: GPC trace obtained for the particles produced with varying loadings of BzA; 0 wt% (black), 9 wt% (red), 27 wt% (green) and 36 wt% (blue). Data was collected using GPC system A and has been normalised. All samples containing BzA indicate the presence of more than one species.

Solutions of PBzA and PMMA were analysed using UV spectroscopy and showed that PBzA is UV active at a wavelength of approximately 260 nm, whereas PMMA is not (Figure 3-35). These samples were analysed via a GPC equipped with a UV detector, in order to discover which of the peaks present was due to the PBzA phase.

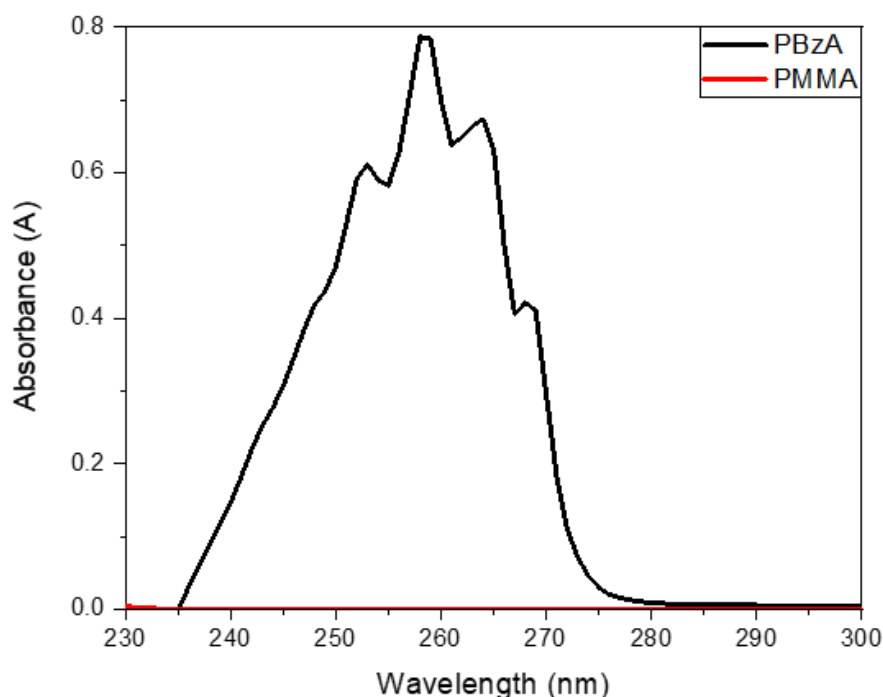


Figure 3-35: UV absorbance traces for PBzA (black) and PMMA (red). PBzA has a UV absorbance at wavelengths at which PMMA does not.

Overlays of the UV and DRI signals, from the GPC, for all loadings of BzA indicated the presence of a UV active species (Figure 3-36), which in all cases is the high molecular weight (lower retention time) species. Addition of monomer part way through a reaction can result in two outcomes; chain extension or formation of a new chain. At this point in the reaction the MMA conversion is high (> 95%), hence it is more likely that any new polymer chains formed at this point would be PBzA homopolymer. As the concentration of AIBN is low, it is expected that this new polymer formed would have a higher molecular weight. A further possible explanation for the PBzA being higher molecular weight could be the presence of branching, which will be discussed in further detail later in the chapter.

Concentrating on the traces obtained from the 9 wt% loading sample (Figure 3-36, red trace), as with the other samples there are two peaks in the DRI. One of the peaks overlaps with the UV signal, whereas the other largely does not. This indicates the presence of a PMMA and PBzA phase. However, there is also a small shoulder peak present in the UV signal which partially aligns with the lower molecular weight peak

present in the DRI. This indicates that there may be a mixed phase of PMMA and PBzA present. This could be used to explain why thermal analysis shows a shift in T_g , indicating that a blend of PMMA and PBzA is being formed as opposed to two pure phases. Upon an increase in BzA loading, the UV signal does not overlap with the PMMA peak observed in the DRI, which further corroborated the data observed from the DMA, that the PBzA and PMMA are phase separated.

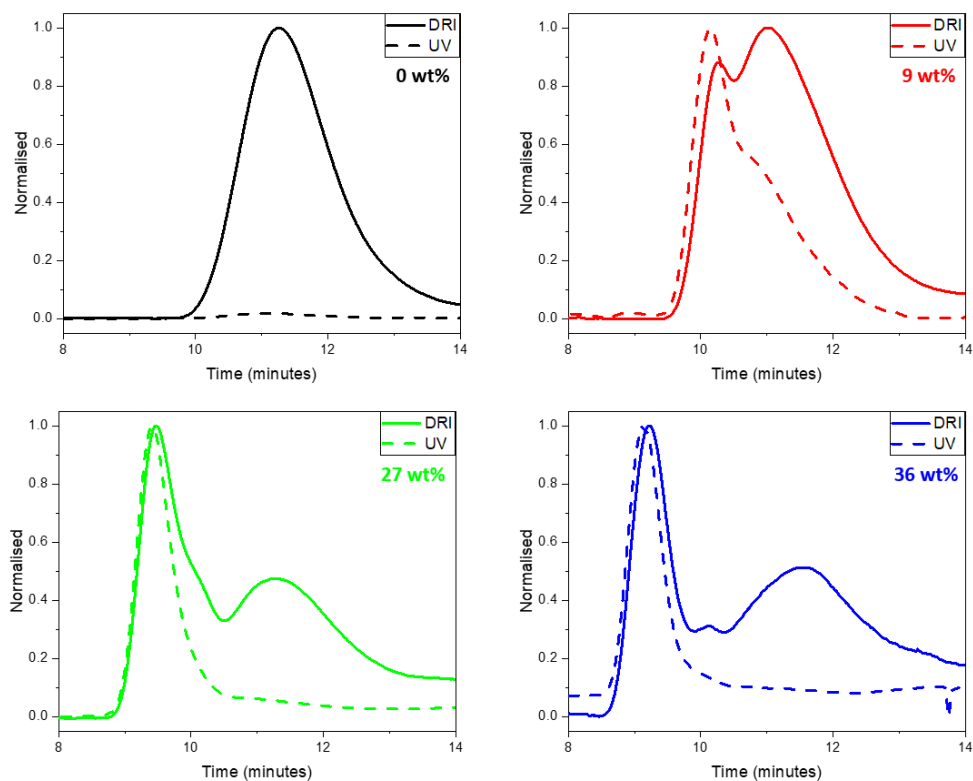


Figure 3-36: GPC traces of PMMA samples containing; 0 wt% (top left, black), 9 wt% (top right, red), 27 wt% (bottom left, green) and 36 wt% (bottom right, blue) loadings of BzA. DRI traces are shown as a solid line and the UV traces as dashed lines. Data was collected using system A and has been normalised. All samples containing BzA exhibited a UV signal that overlapped with one of the peaks in the DRI signal.

In order to investigate the internal morphology of these particles, TEM analysis was performed. The presence of the benzene ring in the PBzA phase should allow preferential staining of this phase.⁷⁷ The particles were set in resin before being microtomed to give thin slices, allowing the internal morphology of the particles to be imaged. The sections of resin were stained using ruthenium tetroxide (RuO_4). The

RuO_4 interacts with the electron density of the benzene ring and causes areas where it is present to appear darker. Contrast in TEM arises from the diffraction of the electron beam. Elements that scatter the electron beam more will appear darker, thus areas of higher electron density, such as Ru stained regions, are darker.³⁶ PDMS-MA contains silicone which has a very high electron density, so also appears dark in the image. Although the Ru is higher in electron density than the Si the PDMS-MA appears as darker patches as it will be in high concentration at the surface of the particles. In contrast, in the stained areas of polymer the Ru is less concentrated, so these areas do not appear as dark.

Pure PMMA particles appear homogeneous and no visible structure was observed. This is as expected as only a PMMA phase should be present (Figure 3-37). DMA, DSC analysis support this observation as they also imply the presence of only one phase.

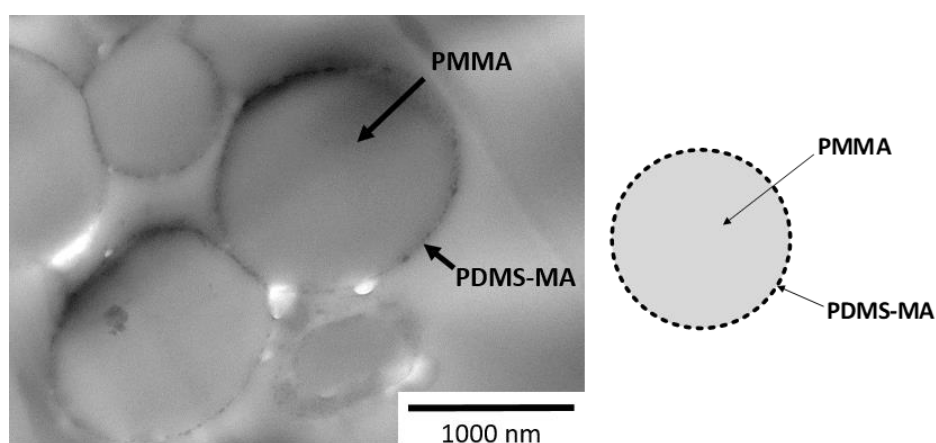


Figure 3-37: TEM image of a sample containing PMMA particles with 0 wt% loading of BzA. Schematic (right) represents the internal morphology present, here no structure is present. Samples were stained with RuO_2 for 4.5 hours prior to imaging.

With a BzA loading of 9 wt%, particles also appeared homogeneous with no visible structure observed (Figure 3-38). This agrees with the thermal analysis, as both DSC and DMA indicated one T_g , shifted in comparison to PMMA, suggesting that, at this concentration, phase separation has not occurred, but blending may be present. GPC analysis also indicated only one phase with one peak present in the trace.

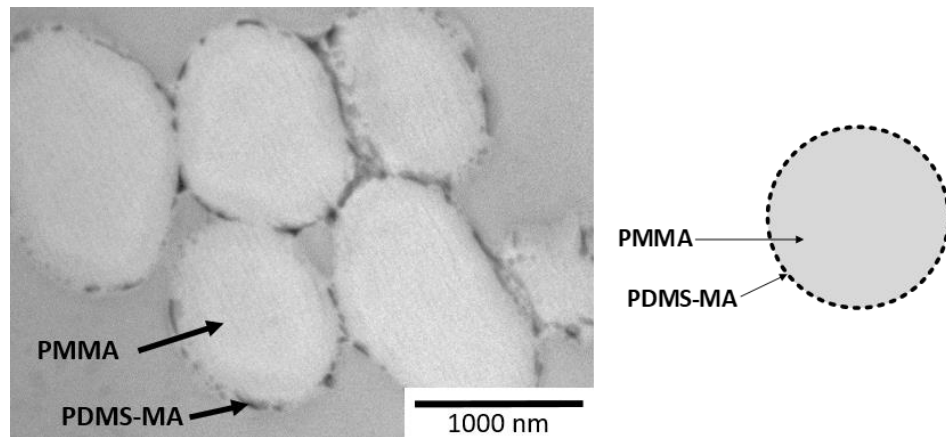


Figure 3-38: TEM image of a sample containing PMMA particles with 9 wt% loading of BzA. Schematic (right) represents the internal morphology present, here no structure is present. Samples were stained with RuO₂ for 4.5 hours prior to imaging.

The presence of an internal morphology was visible in particles synthesised with a BzA loading of 27 wt%. An inverse core-shell (PMMA core, PBzA shell) structure was observed (Figure 3-39).

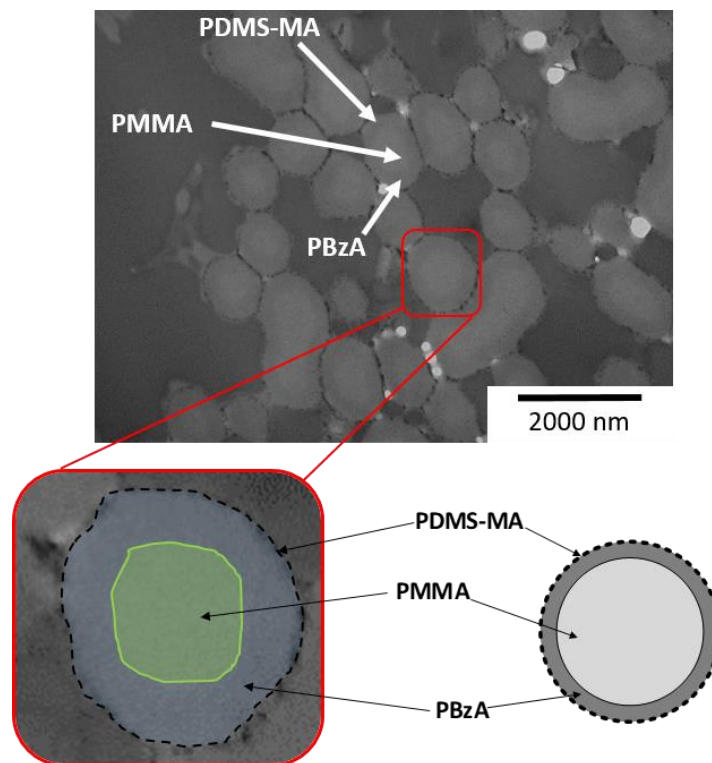


Figure 3-39: TEM images of a sample containing PMMA particles with 27 wt% loading of BzA (top) including a magnified image highlighting the inverse core-shell morphology present (bottom). The sample was stained with RuO₂ for 4.5 hours prior to imaging.

This is supported by the observation that some of the particles appear to be coalescing; if soft material is present on the surface this would be more likely to occur. This is the opposite of what is desired and suggests that the PBzA has not migrated to the interior of the particle. This is a common structure formed by two-stage emulsion polymerisation of PBA/shell core-shell particles. Cook *et al.* reported the “phase-inversion” of these particles, wherein the polystyrene synthesised in the second stage of the reaction migrates to the centre of the particle displacing the first synthesised PBA. The authors attribute this observation to the minimisation of surface energy.⁴² This inverse structure for the synthesised PBzA/PMMA particles was not expected, as from the SEM images the particles look well-defined. If the PBzA (“softer material”) was present on the surface a decline in particle quality, visible via SEM, would be predicted. The dark ring present could also be caused during the preparation of the sample before imaging. Slices of the resin containing particles are weak, which is evident by the holes present (white areas of the image). This may cause the cutting of the sample to yield slices that are not uniform in thickness. A key cause of contrast in TEM is sample thickness, with thicker areas of the sample appearing darker, this is known as mass thickness contrast.⁸¹ This was supported by the fact that this inverse core-shell structure was not as visible in other areas of the sample (Figure 3-40).

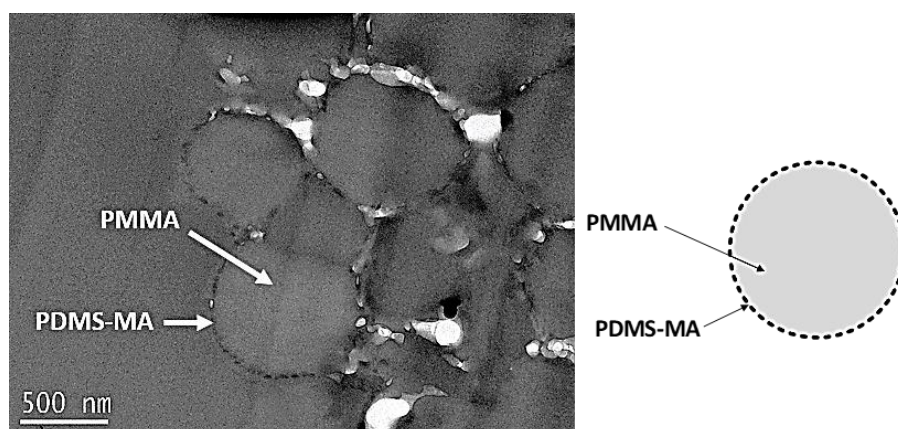


Figure 3-40: TEM images of a sample containing PMMA particles with 27 wt% loading of BzA (left) and schematic of the internal morphology present (right), here no internal morphology is present. The sample was stained with RuO₂ for 4.5 hours prior to imaging.

Upon an increase of the BzA loading to 36 wt% the particles formed showed an internal morphology with smaller domains of PBzA surrounded by PMMA (Figure 3-41). Observation of two phases in the TEM analysis is supported by the thermal and GPC analysis with both showing two transition indicative of phase separation. Phase separation in particles made from block copolymers is a well-studied area.^{12, 82, 83} The internal morphology formed is dependent on the ratio of the blocks. Immiscibility of the two blocks is a crucial factor needed for micro phase separation to occur, forming separate domains. Manipulation of the internal morphology is achieved by varying the block lengths.⁸⁴ This phenomenon could also be occurring in the presented two-phase system. If PBzA is immiscible and at a high enough concentration, internal morphology would be observed.

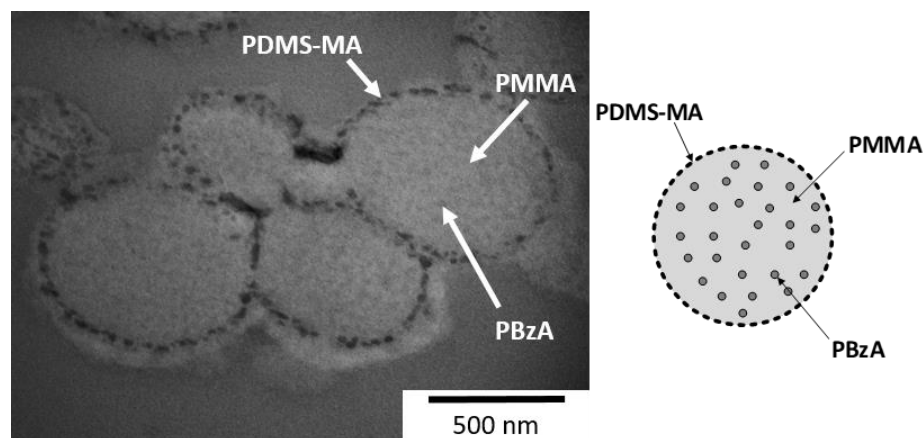


Figure 3-41: TEM image of a sample containing PMMA particles with 36 wt% loading of BzA. Schematic (right) represents the internal morphology present, here domains of PBzA surrounded by PMMA are present. Samples were stained with RuO₂ for 4.5 hours prior to imaging.

Also present in the sample were a small number of particles that showed core-shell structure (Figure 3-42). A structure similar to this had previously been observed in the group with a different monomer system of PMMA/DMAEMA.⁵⁷

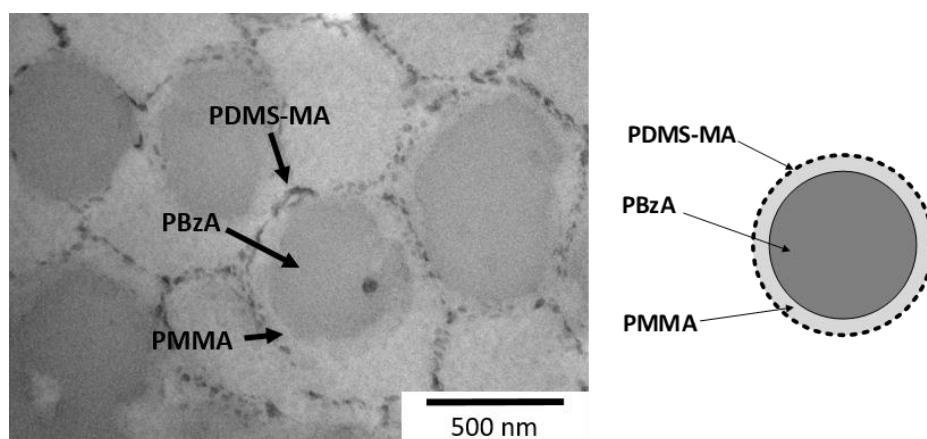


Figure 3-42: TEM image of a sample containing PMMA particles with 36 wt% loading of BzA. Schematic (right) represent the internal morphology present, here a core-shell morphology is present. Samples were stained with RuO₂ for 4.5 hours prior to imaging.

Particles formed at the highest loading of BzA (50 wt%) synthesised using the 3-stage reaction showed a structure similar to that observed with a loading of 36 wt%, small internal domains of PBzA surrounded by PMMA (Figure 3-43), as opposed to the predicted core-shell internal morphology. DMA, DSC and GPC analysis implied the presence of two polymer phases, which is supported by the indication of two separate phase in the TEM analysis.

These particles were less stable in the resin as they contained a high soft component. This results in the resin slice being fragile and under electron beam the sample is prone to exhibit beam damage in the form of holes (Figure 3-43). This often makes the samples difficult to image using this technique.

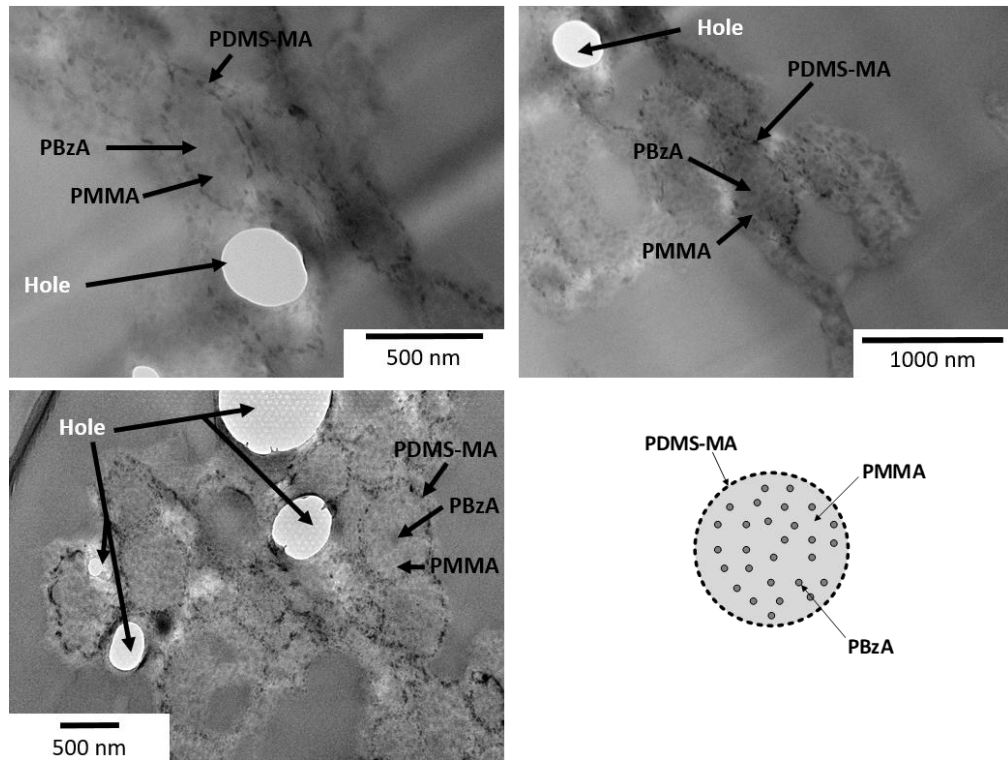


Figure 3-43: TEM images of a sample containing PMMA particles with 50 wt% loading of BzA. Schematic (right) represent the internal morphology present, here domains of PBzA surrounded by PMMA are present. Samples were stained with RuO₂ for 4.5 hours prior to imaging.

Although, in other areas of the sample the structure of the particle was no longer clearly present, but the proposed internal morphology was visible in the TEM images (Figure 3-44, image a). Furthermore, in some areas particle structure was visible but no internal morphology was observed (Figure 3-44, image b and c). This was not as expected as this lack of particle structure was not observed in SEM analysis.

It was originally thought that the lack of particle structure could be caused by the resin setting process. During this procedure the particles are exposed to 40 °C, a temperature well above the T_g of the PBzA phase (2 °C), in a vacuum oven for 48 hours.

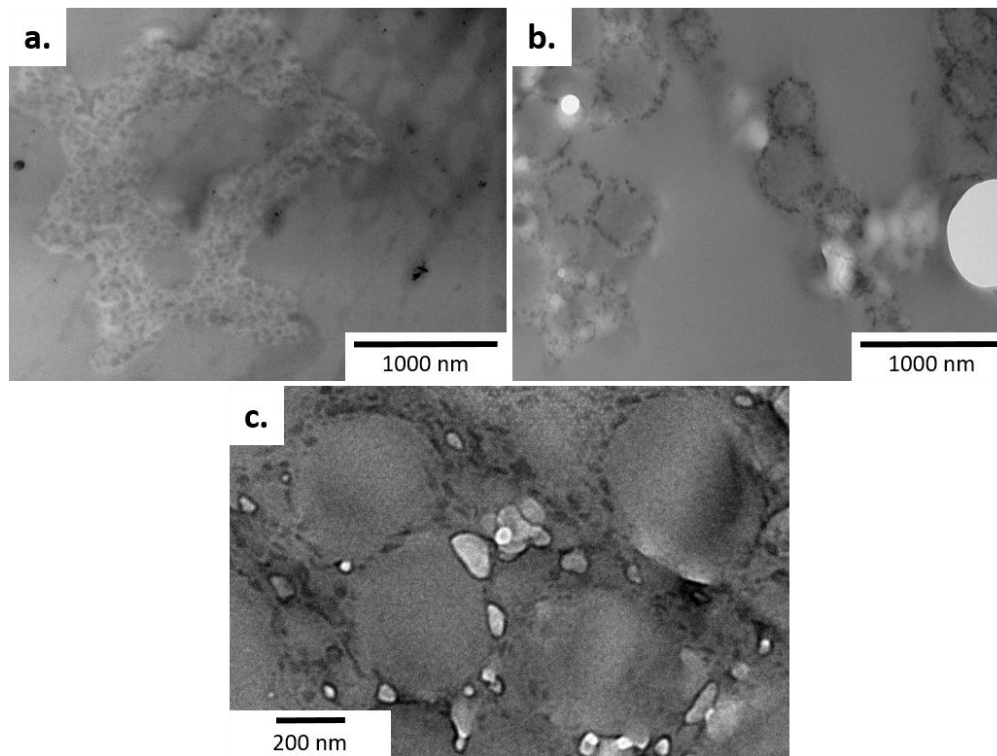


Figure 3-44: TEM image of a sample containing PMMA particles with 50 wt% loading of BzA. (a) Internal morphology present but no particle structure, (b) particle structure present but no/weak internal morphology and (c) no particle structure or internal morphology present. Samples were stained with RuO₂ for 4.5 hours prior to imaging.

To check this, a sample synthesised using a BzA feed of 50 wt% was exposed to these conditions without being set in resin. The samples were imaged via SEM before and after. Some areas of the sample showed fusing and loss of structure. However, most of the sample still showed particle structure even after being exposed to the same conditions used in the resin setting process (Figure 3-45).

Further investigations are needed to probe this loss of structure. One suggestion is the use of a different resin, which may prevent damage caused in sample preparation.

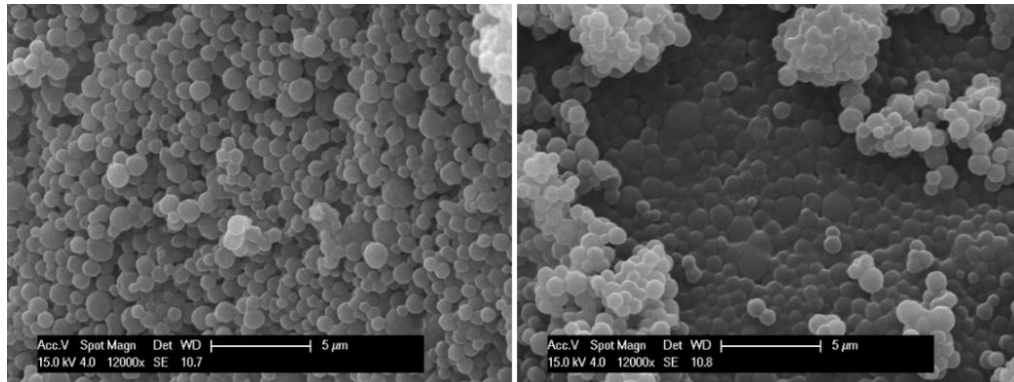


Figure 3-45: SEM images of a sample of PMMA particles containing PBzA (50 wt%) that had been exposed to the resin setting conditions (40 °C, 48 hours, vacuum) without being in resin. Scale bars are 5 µm.

The analytical techniques used to characterise the PMMA/PBzA particles have unanimously demonstrated that phase separation of the two polymers within the particles has taken place. The DMA and DSC show low and high T_g phases, similar to what would be expected with core-shell particles. Although the internal morphology for each loading was not obviously well defined, TEM analysis strongly implies the presence of phase separation and suggests that at higher PBzA contents small internal domains of PBzA are being formed surrounded by PMMA. Testing of the particles, in their desired application of impact modification, is needed to investigate whether the structure present (smaller internal domains of the soft phase) behaves as well as a completely phase separated particle. Initial testing is briefly summarised in the appendix.

To establish the effect the synthesis method had upon the resultant particle structure and internal morphology, the synthesis method was attempted in reverse. The BzA was polymerised first to form the seed particle, followed by addition of MMA in the hope this would form a PMMA shell. This resulted in a white tacky polymer, as opposed to white powder (Figure 3-46). This is almost certainly a result of the low T_g of the PBzA and hence the dispersion did not form stable particles under the conditions used.^{58, 59}



Figure 3-46: Images of sample produced from synthesising PBzA followed by addition of MMA. The soft nature of PBzA means that the particles are prone to aggregation, preventing formation of stable particles in the first stage of the reaction.

3.5.3. Crosslinked Particle Synthesis in 60 mL Autoclave

Crosslinking is an important component to consider for particles being used as impact modifiers. It helps the particle to maintain its structure during processing, which is often at temperatures above the T_g 's of the individual components, as it increases the stability of the particles. To assess the feasibility of adding crosslinking to the dispersion polymerisations in $scCO_2$, reactions were carried out in which a crosslinking species was added. Ethylene glycol dimethacrylate (EGDMA) was chosen as the crosslinker, as it has successfully been used in dispersion polymerisation in $scCO_2$ and is relatively inexpensive (Figure 3-47).⁹

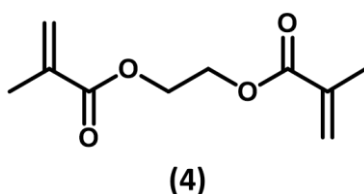


Figure 3-47: Chemical structure of EGDMA (4).

Initial reactions used the one-stage batch reaction technique where all reagents, including the crosslinker were added to the autoclave at the beginning of the reaction (experimental section 3.4.4.1), in an attempt to create fully crosslinked particles.

The loading of EGDMA was varied from 1 to 2 wt %, with SEM analysis showing that even at these low loadings of EGDMA, discrete particles were not formed (Figure 3-48). This suggests that the presence of the EGDMA was disrupting the initial nucleation phase of the reaction.

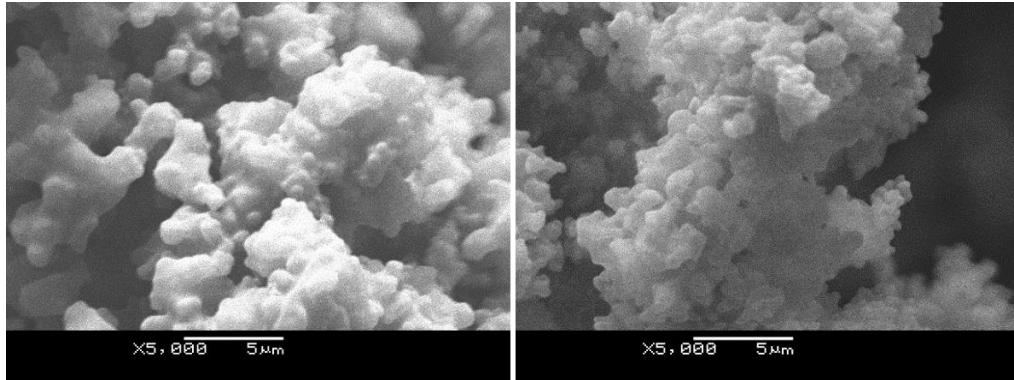


Figure 3-48: SEM images of products from one-stage batch reactions using 1 wt% (left) and 2 wt% (right) loadings of EGDMA. No particles were formed. The scale bars are 5 μm .

Shin *et al.* reported a similar observation, showing that incorporation of as little as 0.4 wt% of various crosslinkers in the dispersion polymerisation of MMA in scCO_2 disrupted the formation of well-defined particles.⁹ Song *et al.* suggested that addition of a crosslinking reagent affects the growth of particles in two ways.⁸⁵ Firstly, the crosslinker interrupts the sensitive particle nucleation stage of the reaction. Secondly, the crosslinked networks formed reduce the ability of the particles to swell (Figure 3-49).

Normally in dispersion polymerisation, the growing particle is swollen, allowing incorporation of new propagating polymer whilst maintaining a spherical shape. As a result of the reduction in the swelling ability of the particle, propagating polymer chains deposit on the surface and have difficulty diffusing into the interior of the growing particles. This causes the development of patches on the particle, producing a rough surface. This is compounded by insufficient stabiliser on the surface of the particle to cover the patches formed and these areas provide sites for aggregation. For this reason, a two-stage reaction method was developed in which the crosslinker

was introduced after particle nucleation. This method was used to produce higher quality, discrete particles.⁸⁵

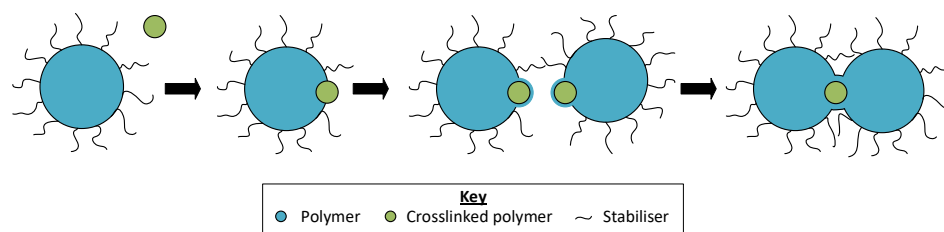


Figure 3-49: Schematic representing the agglomeration of particles caused by crosslinking proposed by Song and Winnik.^{9, 57}

For the reasons discussed, further reactions used a two-stage method as detailed in the experimental section 3.4.4.2. This allowed for particle nucleation to take place before the introduction of EGDMA. Initially, MMA was polymerised under batch conditions. This was followed by the injection of further MMA combined with EGDMA. It was predicted that this technique would produce a PMMA core surrounded by a crosslinked shell (Figure 3-50).

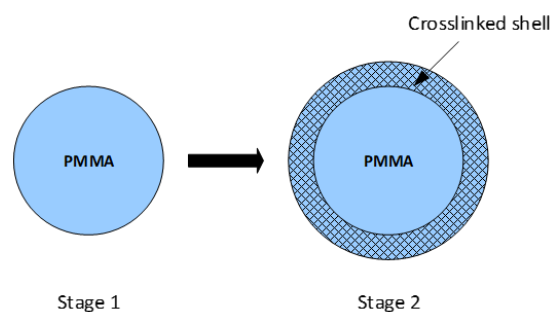


Figure 3-50: Schematic representation of the particles produced from using a two-stage reaction technique showing formation of a PMMA particle followed by formation of a crosslinked shell.

Crosslinked polymers have reduced flexibility and, as such, it was expected that the polymer formed in stage two would be unable to diffuse into the already formed PMMA particle, creating a shell.⁸⁵ The effect of varying the crosslinker loading was investigated and it was hypothesised that as crosslinker content increased, the T_g of

the particle would increase.^{86, 87} EGDMA loadings of 1, 5, 9, 33 and 50 wt% (wrt the second injection of MMA) were studied. As a control, particles were synthesised without EGDMA in the injection of MMA. The structure of the particles produced was analysed by SEM, with discrete, well-defined particles (similar structure to the pure PMMA particles) being observed for all loadings of EGDMA (Figure 3-51).

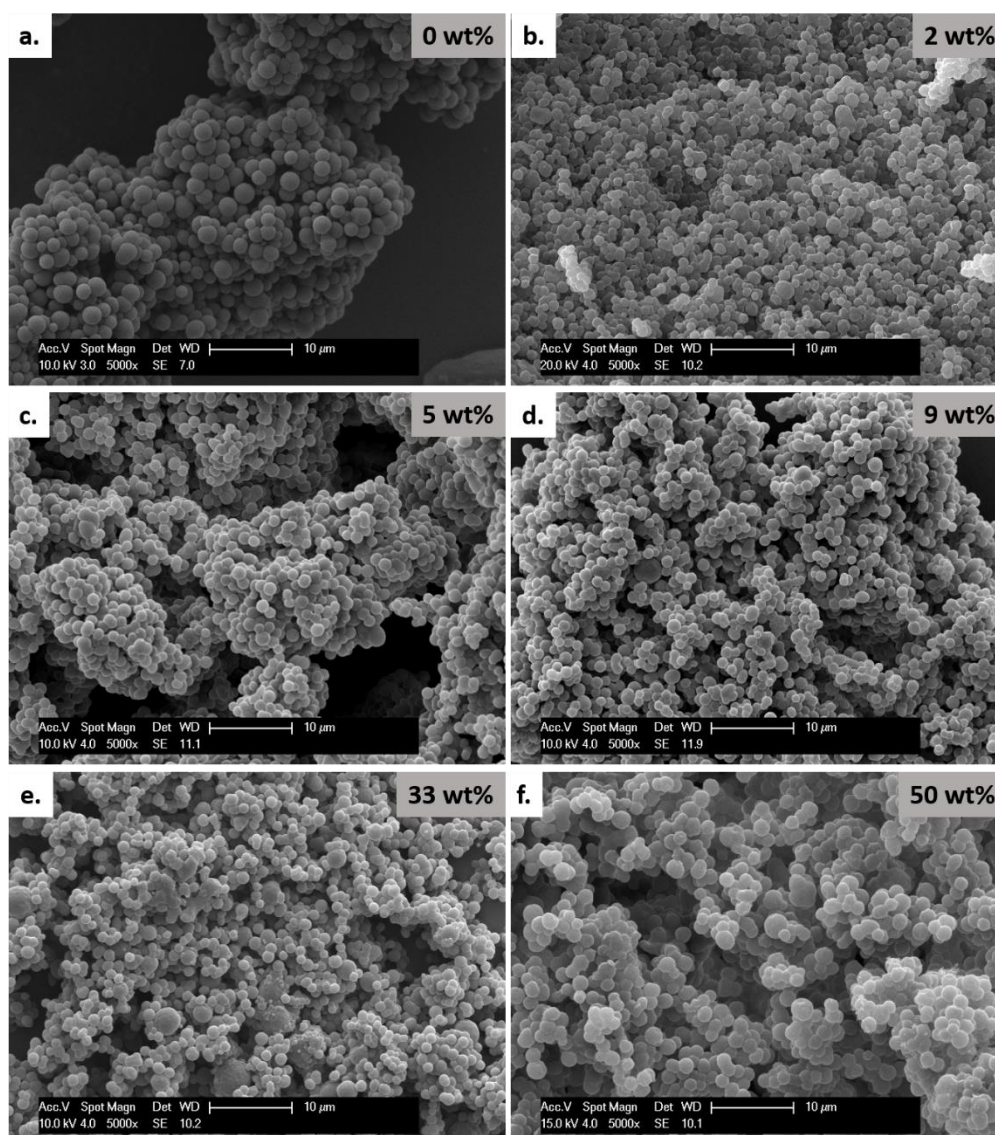


Figure 3-51: SEM images of particles synthesised using a two-stage reaction incorporating: 0 wt% (a), 1 wt% (b), 5 wt% (c), 9 wt% (d), 33 wt% (e) and 50 wt% (f) EGDMA. Particles were imaged straight from the autoclave. Particles maintained their structure as the EGDMA content of the shell was increased. All scale bars are 10 µm.

Particles synthesised using loadings of 1, 5 and 9 wt% EGDMA were solubilised in both THF and acetone when left overnight, whereas the particles with loadings of 33 and 55 wt% did not dissolve. This suggested that at lower EGDMA loading a shell of lightly branched polymer was formed which was soluble. By contrast, at higher loadings a fully crosslinked shell, which would be completely insoluble, was formed.

The T_g s of the particles were determined using DMA (Figure 3-52). As the EGDMA content increases so does the T_g , suggesting an increase in crosslinking density. However, at loadings less than 33 wt%, a reduction in T_g was observed in relation to pure PMMA.

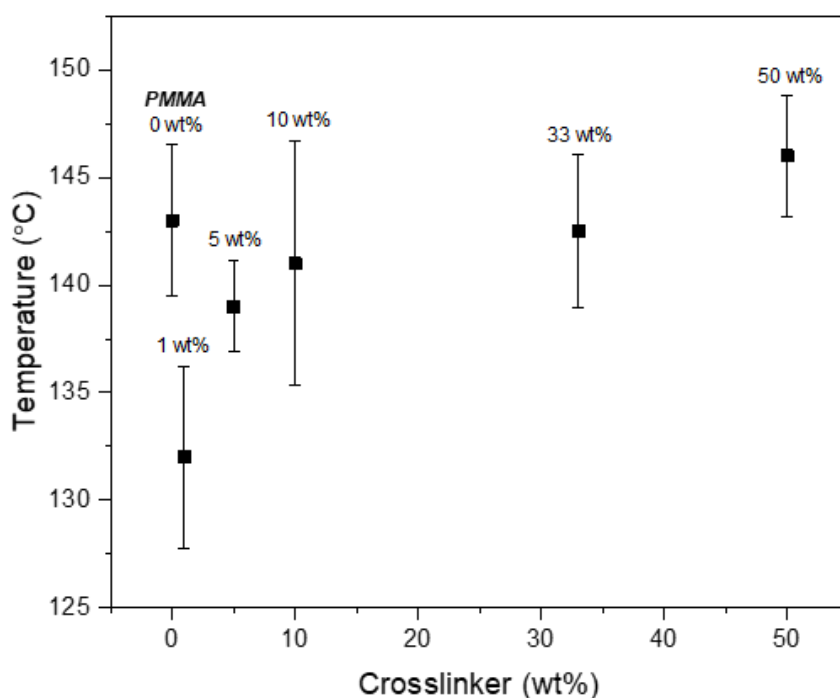


Figure 3-52: Glass transition temperatures of the core-shell crosslinked particles initially decreases in comparison to pure PMMA. However, as the wt% of EGDMA in the shell is increased, a trend of increasing T_g is observed.

This reduction supports the theory that the shells being formed were branched as opposed to crosslinked. Branched polymers generally exhibit lower T_g 's in comparison to linear polymers.⁹ At 33 and 50 wt% the shell was most likely fully crosslinked and hence the T_g increased in comparison to pure PMMA. The DMA

measurements show a trend of increasing T_g with increasing EGDMA content. However, taking repeat measurements of each loading gave an overlap in the error bars, suggesting that the difference in T_g was not significant (Figure 3-52). Therefore, further analysis needs to be recorded to understand the system, including synthesising a greater range of crosslinker wt%. Full crosslinking may not be necessary in particles, to allow them to undergo the craze and cavitation mechanism required to absorb the energy from an impact as described in the introduction.⁵⁴

TEM analysis could be useful to provide confirmation of where the crosslinking was occurring and if a shell was being formed. However, as with the PMMA/BA system, the chemical structures of MMA and EGDMA are too similar, thus preferential staining is not possible. This could be overcome by using a crosslinker such as DVB that contains a benzene ring, which should be susceptible to staining due to its saturated nature.³⁶

3.5.4. Combination of Crosslinking and PBzA

The ideal structure for the application of impact modification would contain a slightly crosslinked soft phase and an uncrosslinked shell that is compatible with the matrix to which the particles are being added, in this case PVC (Figure 3-53).

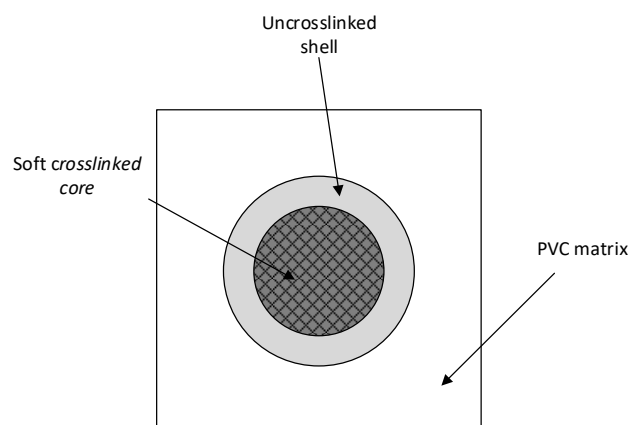


Figure 3-53: Schematic representation of the desired core-shell structure mixed into a PVC matrix.

The crosslinking of the core helps maintain its shape during processing. Having an uncrosslinked shell allows for entanglement with the matrix, resulting in better compatibilisation.⁵⁰ The work previously presented showed that addition of a crosslinking species after the nucleation period of the reaction ensured particle structure was maintained. Thus, to achieve the ideal material synthesis of PMMA, particles with a loading of 50 wt% BzA and incorporation of crosslinking needed to be combined.

Initial experiments investigated the incorporation of a crosslinker with the second charge of BzA in the multi-stage synthesis of the PMMA/PBzA (50 wt%) core-shell particles (Figure 3-54) previously discussed in section 3.5.2.

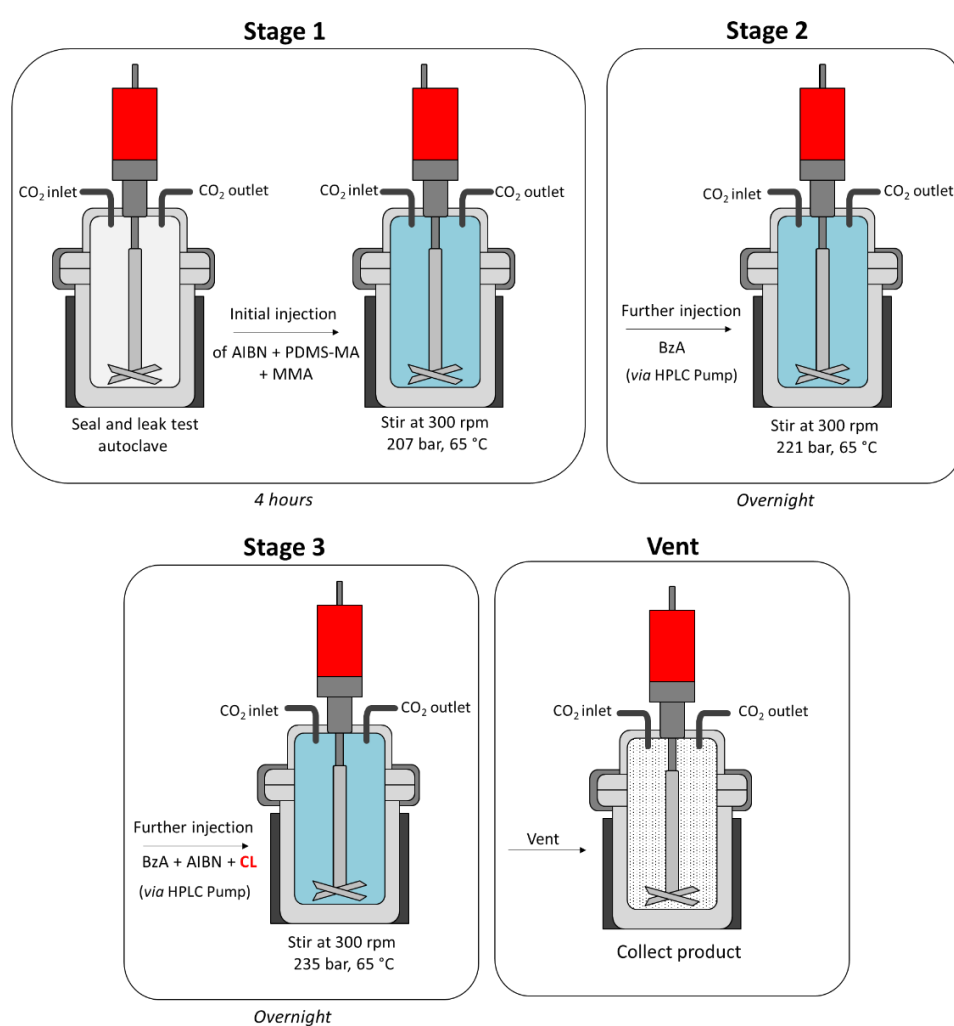


Figure 3-54: Schematic showing the synthesis of PMMA particles following by the addition of BzA over two-stages. The second addition of BzA contained crosslinker (CL).

Although it was previously hypothesised that crosslinked polymer would have reduced flexibility and hence would be unable to migrate to within the particle, it was hoped that the reduction in T_g of the PBzA in comparison to the previously used PMMA would counteract this. Experiments were initially performed using EGDMA as the crosslinker. This was later replaced with divinyl benzene (DVB), due to the presence of the benzene ring. As previously mentioned, if successful particle synthesis was achieved this would allow for preferential staining of the phase containing DVB when analysing via TEM. The samples produced were insoluble in a range of solvents indicating that crosslinking had occurred (Table 3-14).

Table 3-14: Summary of solubility data for sample incorporating crosslinker (1 wt%) with the second charge of BzA.

Entry	Crosslinker	THF	Chloroform
1	DVB	Swells	Swells
2	EGDMA	Swells	Swells

However, SEM analysis of the samples confirmed particle formation in some areas of the sample alongside agglomerated non-structured material. This was the case for each sample synthesised with either crosslinker (Figure 3-55).

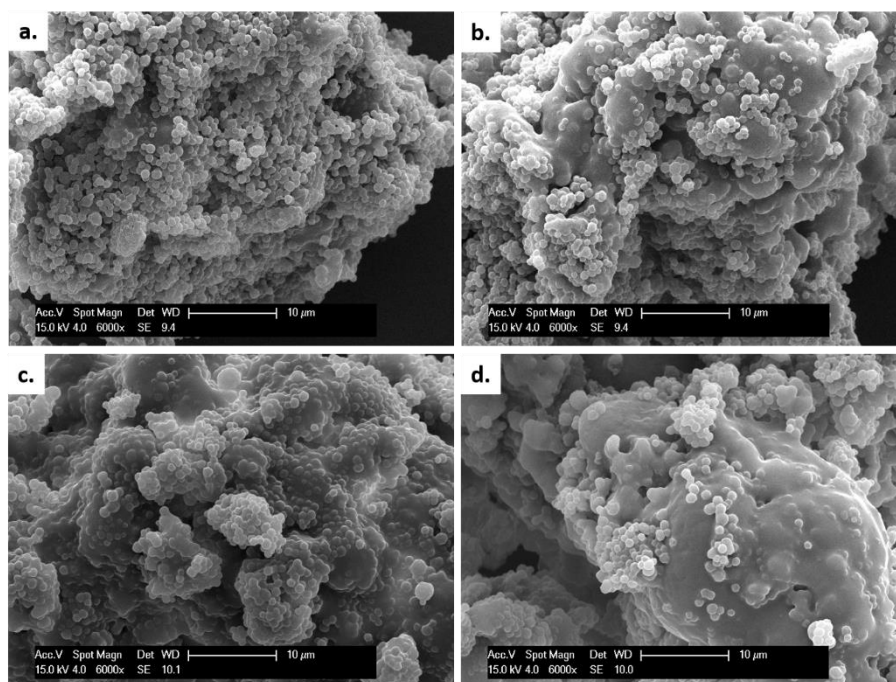


Figure 3-55: SEM images of PMMA particles synthesised with PBzA (50 wt%) added over two-stages. The second charge of BzA contained (1 wt%); DVB (a,b) and EGDMA (c,d). All scale bars are 10 μm . A combination of discrete particles and agglomerated bulk is observed.

This disruption of particle formation upon addition of a crosslinker was also observed for the polymerisation of PMMA particles under the previously discussed batch conditions. It is believed that the first two-stages of the reaction proceed as normal, forming PMMA particles containing PBzA (25 wt%). Addition of crosslinker in stage 3, with the second charge of BzA, disrupts the polymerisation mechanism. Hence, the polymerisation is no longer proceeding via dispersion, causing agglomerated crosslinked material to be formed with the remaining 25 wt% BzA. This material is unable to migrate to the core of the particle. A theoretical structure of what may be being formed is shown in Figure 3-56.

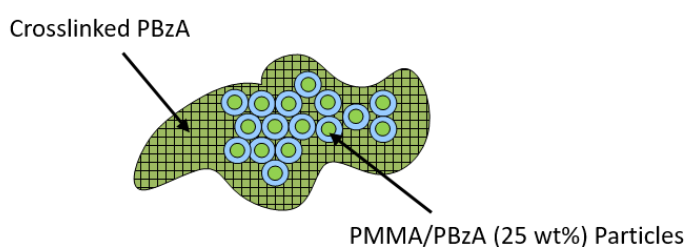


Figure 3-56: Schematic representation of the product formed with addition of 1 wt% crosslinking in the second charge of PBzA. Particles formed contain 25 wt% PBzA and the remaining 25 wt% crosslinked around the particles.

For these reasons a new proposed structure was investigated. The successful incorporation of a crosslinker into the shell of a PMMA particle has already been established in section 3.5.3. The new proposed structure would combine this PMMA crosslinked shell with a PBzA (50 wt%) as the core (Figure 3-57).

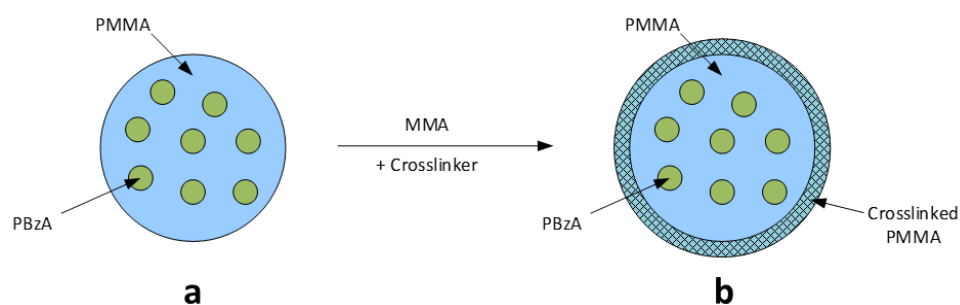


Figure 3-57: Schematic showing the proposed structure combining synthesis of the PBzA (50 wt%) particles (a) and addition of a crosslinked MMA shell (b).

Both these elements have been shown to work separately, so the challenge was getting them to form stable particles when combined. Both EGDMA and DVB were used as crosslinkers for the same reason as mentioned previously.

Once again, the products formed were not soluble in a range of solvents suggesting that crosslinking had occurred, also preventing further analysis by GPC or ^1H NMR (Table 3-15).

Table 3-15: Summary of solubility data for sample incorporating a crosslinked (1 wt%) MMA shell on the PBzA (50 wt%) particles.

Entry	Conditions	THF	Chloroform
1	[MMA/DVB] shell	Swells	Swells
2	[MMA/EGDMA] shell	Swells	Swells

However, the samples formed using this method were not homogeneous and SEM analysis showed poor sample quality (Figure 3-58). Agglomeration was high and

although some particles were present, large areas of the sample showed no particle structure.

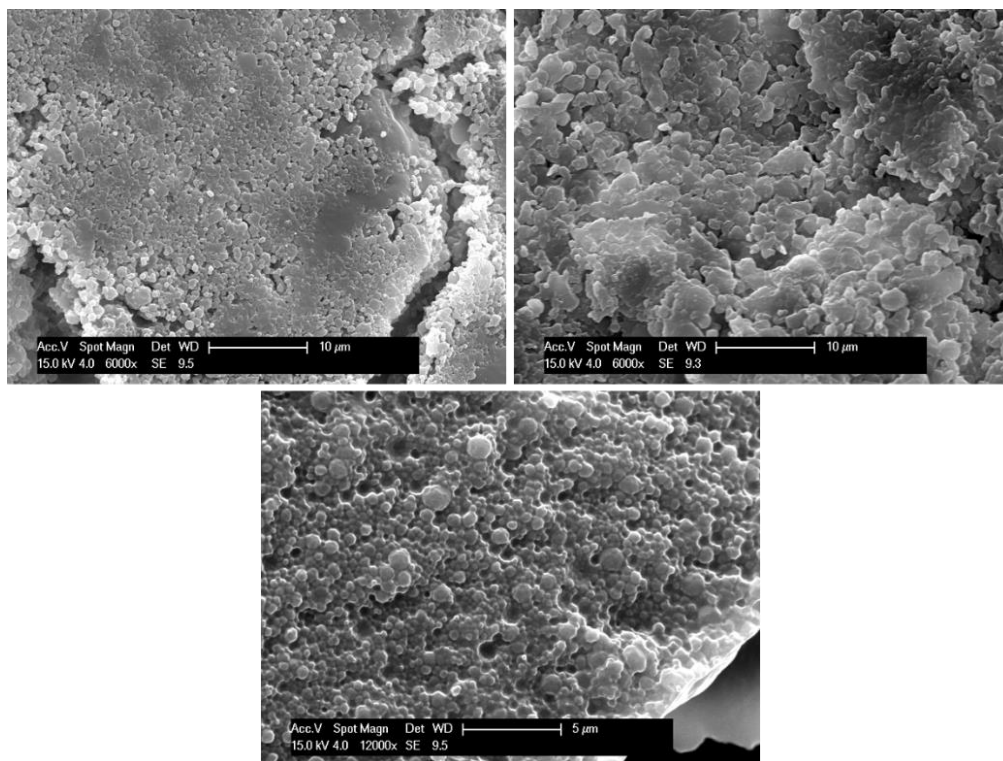


Figure 3-58: SEM images of PMMA particles synthesised with a 50 wt% loading of PBzA and addition of a crosslinked MMA shell. Particle structure is lost and high agglomeration is observed.

To examine the system further, a reaction was carried out using the same steps as above, minus the crosslinker. This was to investigate whether it was the addition of crosslinker that was disrupting the system, or if the total amount of monomer was too high (now 15 mL). Monomer loading has previously been reported as an important factor in dispersion polymerisation in scCO_2 . McAllister *et al.* showed that particle formation was disrupted if the monomer content was too high.⁷⁸

As before, the sample formed was not homogeneous and SEM analysis showed poor particle quality (Figure 3-59). In some areas particles were observed, however, in other areas agglomeration was high and no structure was observed. Surprisingly, despite the absence of a crosslinker, the product was insoluble in a variety of solvents, with swelling observed, suggesting that the sample was crosslinking.

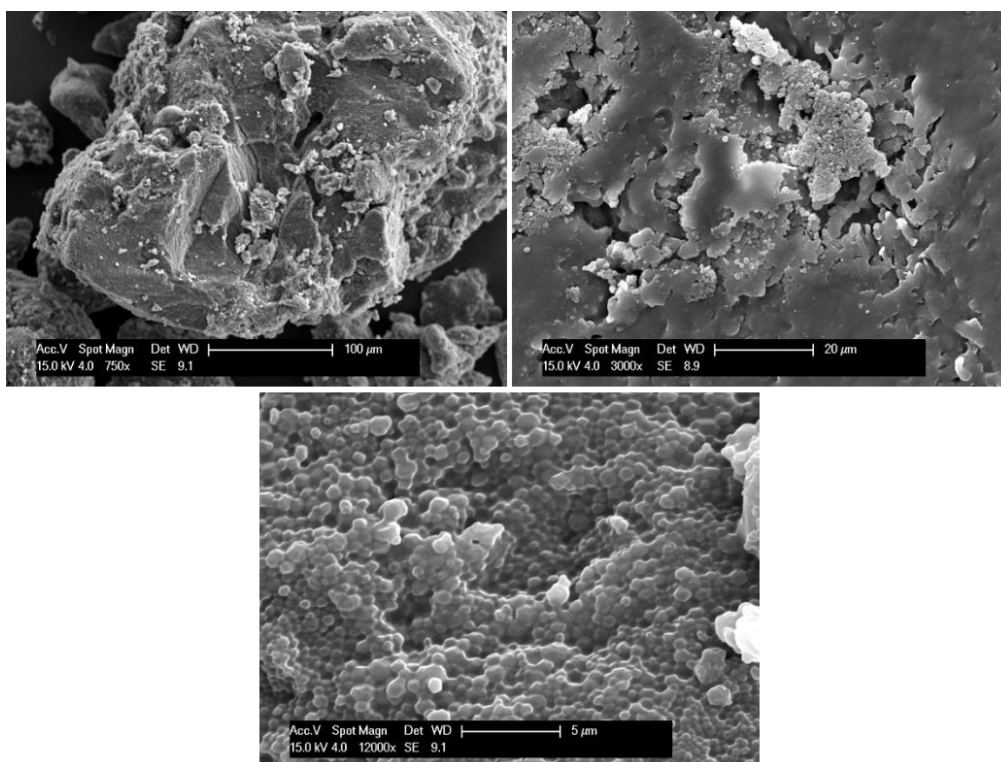


Figure 3-59: SEM images of PBzA synthesis with attempted addition of MMA shell without crosslinker. Loss of particle structure was observed and high levels of agglomeration.

It was thought that the source of the crosslinking could be intermolecular or intramolecular chain transfer. This mechanism occurs via the abstraction of a hydrogen from a tertiary carbon atom within the polymer backbone, forming a midchain radical (MCR) (Figure 3-60). This occurs either by back-biting via a five membered transition state (intramolecular) or through intermolecular abstraction.⁸⁸ This leads to the propagating polymer chain being transferred to this newly formed radical centre, forming a branch. As the reaction proceeds the polymer eventually becomes fully crosslinked. MCRs are more likely to be formed in reactions containing acrylates than in reactions containing methacrylates. This is because abstraction of a hydrogen from an acrylate induces transfer from a secondary propagating radical (SPR) to a tertiary propagating radical (TPR), which is favourable. Whereas, the hydrogen susceptible to extraction in a methacrylate would involve the transfer from a TPR to another TPR and hence is unfavourable as no stability is gained.⁸⁹

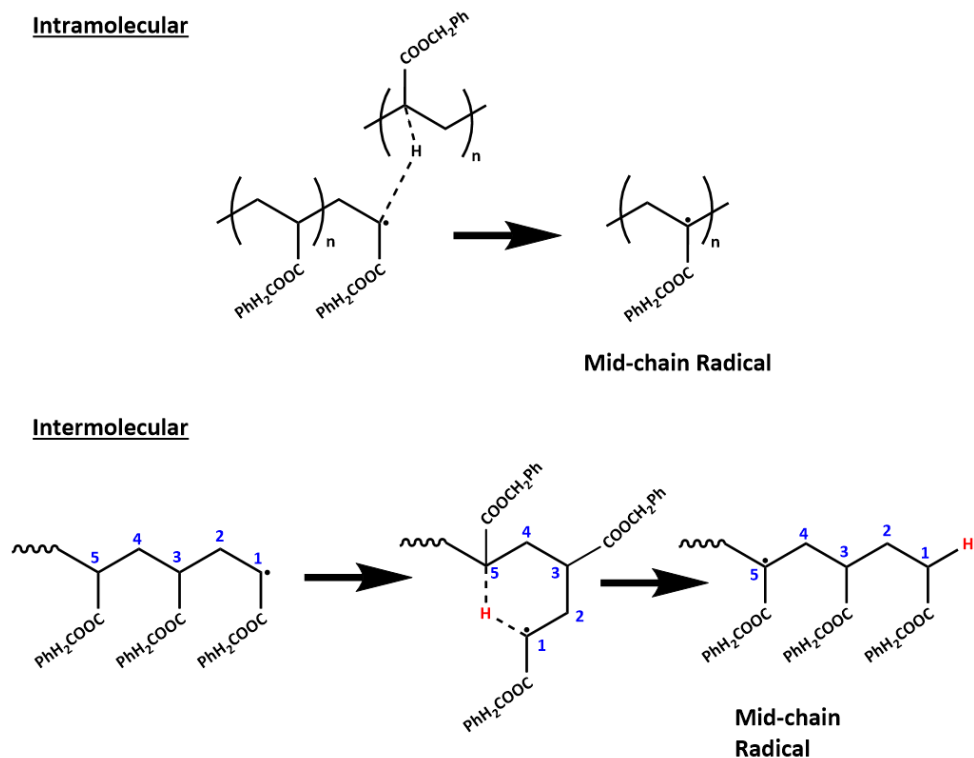


Figure 3-60: Scheme for process of chain transfer forming mid-chain radicals via intramolecular and intermolecular hydrogen abstraction.

Branching and crosslinking of acrylates at high conversion is common.^{90, 91} Hydrogen abstraction in PBzA would lead to chain transfer of the radical as described and branching, which eventually could lead to crosslinking. In the case of PBzA, the tertiary radical is stable and once formed is further stabilised by the presence of the carbonyl group.

Thus, we hypothesised that the PBzA phase of the particle could crosslink if left for long enough and under the right conditions. To test this theory the length of the second addition of PBzA (stage 3) was varied from 24 to 72 hours (Table 3-16). The sample obtained after 72 hours was not homogeneous and high levels of aggregation were observed. By contrast, when the time was reduced to 36 hours a free-flowing powder was obtained.

Table 3-16: Summary of reaction in which the length of the second addition of BzA was varied.

Entry	Time (hours)	Sample Appearance
1	24	Free-flowing powder
2	36	Free-flowing powder
3	72	Agglomerated mass

SEM analysis showed poor particle quality for both the 36 and 72 hour samples. Particle structure could be seen but, as before, there was a large amount of bulk material present (Figure 3-61).

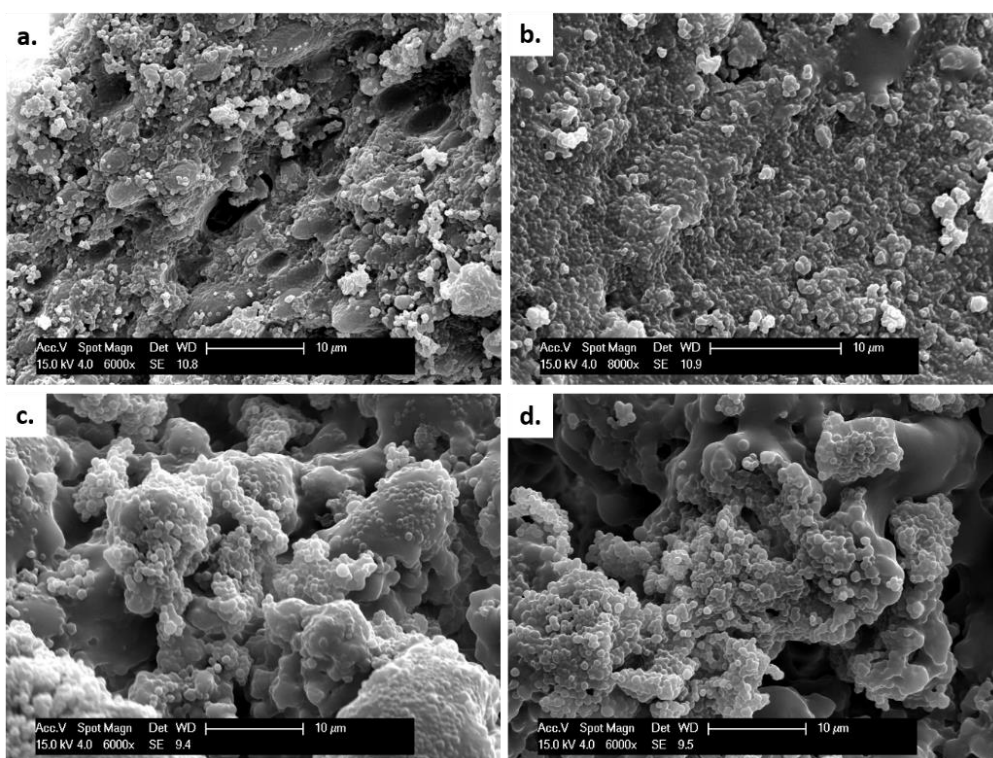


Figure 3-61: SEM images of particles formed when the second charge of BzA was left for; 72 hours (a,b) and 36 hours (c,d). Scale bars are 10 μm. A combination of discrete particles and agglomerated bulk is observed.

The reaction appears to have been left for too long and a high level of crosslinking has caused the particles to aggregate.

Homopolymer PBzA readily dissolves in all the solvents tested. In all cases, the samples initially swelled in a range of solvents suggesting the presence of crosslinking (Table 3-17). The sample with a reaction time of 24 hours appeared to dissolve after 12 hours suggesting that it had lower crosslinking density (Table 3-17, entry 1). This was as expected as the crosslinking density should increase with time. This was confirmed by the samples with a reaction time of 36 and 72 hours remaining insoluble (Table 3-17, entries 2 & 3 respectively).

Table 3-17: Summary of solubility data for PMMA sample incorporating BzA (50 wt%) with varying length of the second charge of BzA.

Entry	Conditions	Time (hours)	THF	Chloroform
1	BzA (50 wt%)	24	Dissolves*	Dissolves
2	BzA (50 wt%)	36	Swells	Swells
3	BzA (50 wt%)	72	Swells	Swells

* - sample was hard to push through the GPC filter.

The GPC traces obtained for the samples gave broad signals suggesting the presence of branching.⁹² The Mark-Houwink equation (*Equation 3-5*) relates the molecular weight of a polymer to its intrinsic viscosity in a given solvent, where η is the intrinsic viscosity, M is the molecular weight and K and α are the Mark-Houwink parameters.⁹³

$$[\eta] = KM^\alpha \quad \text{Equation 3-5}$$

Further analysis of the Mark-Houwink plots confirmed this hypothesis that the BzA is branching. The Mark-Houwink plots (Figure 3-62), exhibit a decrease in intrinsic viscosity upon increase in BzA wt%. This is indicative of increased branching within the same polymer system.⁹²

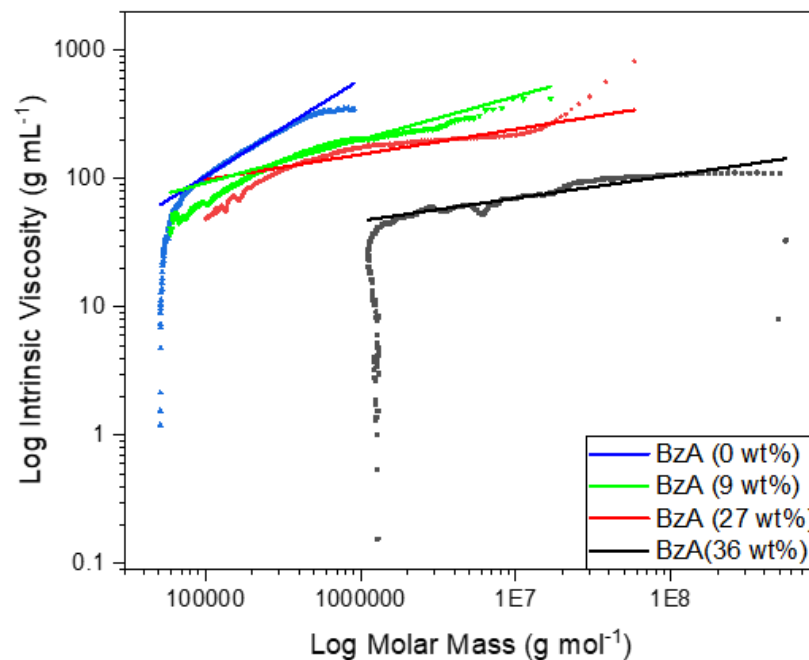


Figure 3-62: Mark-Houwink plot for particles synthesised with various BzA feeds; 0 wt% (green), 9 wt% (blue), 27 wt% (red) and 36 wt% (black). A decrease in intrinsic viscosity was observed with increasing BzA indicating an increase in branching density.

Alpha values can be obtained from the gradient of the line made by plotting log of the intrinsic viscosity vs. log of the molecular weight (Table 3-18). An alpha value around 0.7 indicates a linear polymer, whereas a value around 0.5 or less indicates a branched polymer.⁹³ Samples synthesised without BzA (Table 3-18, entry 1) gave an alpha value indicative of a linear polymer. This is as expected as no crosslinking would be present with pure PMMA. As the BzA feed concentration is increased, a reduction in the alpha value is observed, suggesting an increase in branching. This increase in branching is expected with higher monomer concentration increasing the likelihood of intermolecular chain transfer giving long chain branching. At lower monomer concentrations, intramolecular chain transfer is favoured, with short chain branching observed.^{89, 90, 94} When the monomer concentration is increased further to 50 wt%, this branching becomes crosslinking and the polymer becomes insoluble.

Table 3-18: Alpha values obtained from the Mark-Houwink plots for samples containing increasing concentration of PBzA.

Entry	BzA Feed (wt%)	α
1	0	0.76
2	9	0.34
3	27	0.20
4	36	0.17

To gain more information, pure PBzA was synthesised via free radical dispersion polymerisation in scCO₂. The reaction was left for 48 and 72 hours. After 48 hours a solid, white, tacky lump was produced. The product initially swelled before dissolving in chloroform and THF (Table 3-19, entry 1). The reaction was repeated and left for 72 hours. The product obtained was similar in appearance to the product from the 48 hour reaction. However, the sample swelled in both solvents, suggesting a higher crosslinking density (Table 3-19, entry 2).

Table 3-19: Summary of solubility data for samples of pure BzA synthesis in the autoclave for varying lengths of time.

Entry	Conditions	Time (hours)	Conversion ^a (%)	THF	Chloroform
1	Pure BzA	48	97	Dissolves	Dissolves
2	Pure BzA	72	-	Swells	Swells

^a – obtained from ¹H NMR.

In an attempt to crosslink a PMMA/PBzA sample produced with a lower BzA feed (36 wt%), the addition of BzA was left for 36 hours compared to the previous 24 hours. The product had poor morphology and was clumped at the base of the autoclave. Swelling in THF and chloroform was observed, suggesting that crosslinking was present. SEM analysis showed high levels of aggregation and almost no areas of particle structure (Figure 3-63). It is thought that the higher level of crosslinking that would occur at longer reaction times caused the reaction to no longer proceed via dispersion, forming unstructured material. This has been previously seen in other

sample and has been reported in the literature and is discussed further in section 3.5.3.⁹

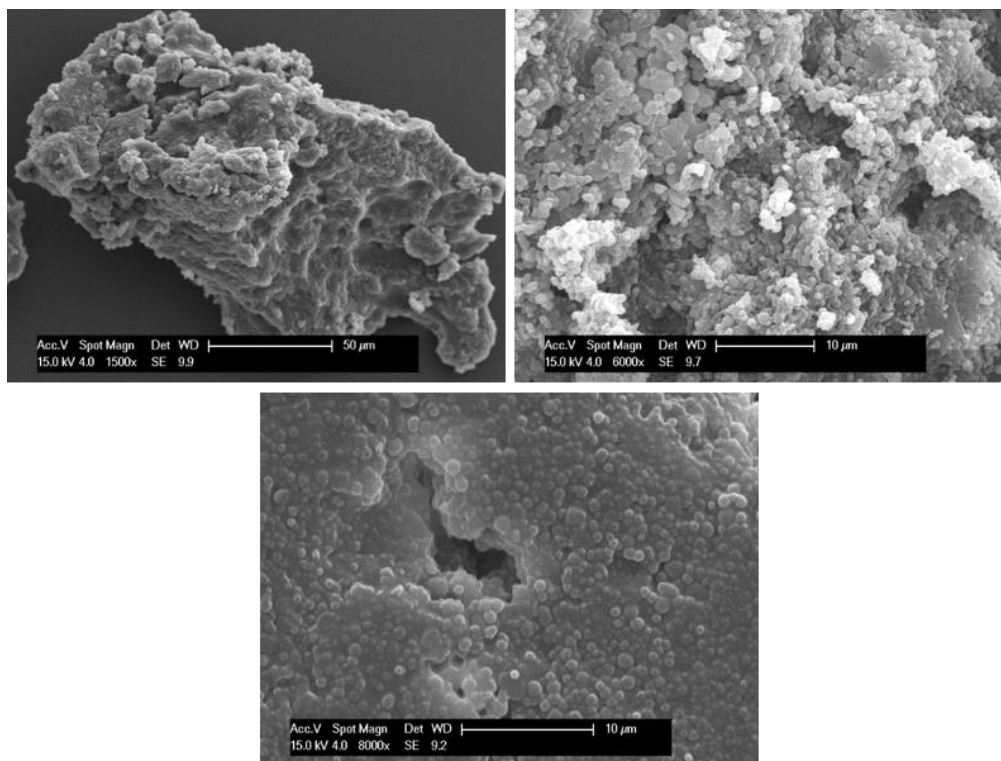


Figure 3-63: SEM images of the sample produced using a BzA feed of 36 wt%, leaving the addition for 36 hours in an attempt to retain particle structure whilst crosslinking the sample. High levels of aggregation were observed.

3.6. Conclusions

Particles containing PBA were synthesised using a two-stage reaction technique with various loadings of BA. SEM analysis indicated that the structure of the particles did not deteriorate as the BA content was increased. At low loadings of BA, DMA analysis suggested that the particles produced were homogeneous containing one phase as opposed to the desired core-shell structure, containing two phases. Nevertheless, it is difficult to say for certain as the T_g of the PBA phase and the PDMS-MA occur at very similar temperatures. At high loading of BA, changes in the DMA trace around -45 °C, along with multimodal peaks in the GPC traces suggested that multiple phases may be present in the particles. Further analytical techniques such as TEM could not help since the two monomers are similar in structure and preferential staining of one phase cannot be used to determine the internal morphology.

For these reasons, the monomer used in the synthesis of the core was changed to BzA. The two-stage reaction technique was used to synthesise PMMA particles containing a feed of up to 36 wt% BzA. For a loading of 50 wt% BzA the addition of BzA was split into two charges in order to maintain particle quality. SEM analysis showed that particle structure did not deteriorate significantly as the PBzA content was increased up to 50 wt%. Increasing the BzA loading to 60 wt% caused high particle aggregation, even when the BzA was added in two steps. ^1H NMR analysis showed high conversion of BzA at all loadings. However, this may be artificially high due to the loss of monomer during venting, which is supported by the PBzA content being slightly lower than the feed. DMA analysis indicated two separate T_g s, signifying the presence of two phases. GPC analysis suggested the presence of two different species; a PMMA and a PBzA phase, confirmed by UV analysis. TEM analysis was promising and suggests that there was internal morphology present. At 36 and 50 wt%, small internal domains of PBzA surrounded by PMMA were observed. Synthesising PBzA first followed by PMMA did not produce particles because the soft seed particles readily agglomerated in the scCO_2 .

Incorporation of crosslinking was essential for the end application of impact modification. Successful synthesis of particles incorporating a crosslinker component

was achieved using a two-stage reaction method. SEM analysis indicated that the structure of the particles did not deteriorate as EGDMA content in the shell was increased. After an initial reduction in T_g , a general trend of increasing T_g with increasing EGDMA content in the particle shell was observed. However, the overlap of error bars from repeat measurements and samples suggests that the change is not significant. Once again analytical techniques such as TEM would be useful to check exactly where the crosslinker is polymerising. However, due to the similarities in the structure of MMA and EGDMA preferential staining of one phase is not possible.

Initial attempts to combine formation of internal structure with crosslinking proved difficult. Incorporation of crosslinker as low as 1 wt% caused a significant reduction in particle quality. High levels of aggregation and loss of particle structure were observed. Similar results were obtained with attempts to incorporate a crosslinked MMA shell.

Additional experiments and reanalysis of the solubility studies suggested the presence of crosslinking in the PMMA samples synthesised with a loading of 50 wt% BzA, even without incorporation of a crosslinking component in the reaction. Further investigation suggested that at high loadings and high conversion of BzA, self-crosslinking of the PBzA was occurring due to chain transfer. SEM analysis confirmed that particles structure was maintained even in the presence of this crosslinking.

Synthesis of particles containing both a soft PBzA phase and crosslinking was successful, hence providing a sample suitable for material testing. Initial testing of the samples is briefly summarised in the appendix. Ideal tests require a large amount of sample (> 100 g). Particle synthesis discussed in this chapter has been completed on the 60 mL scale with yields of < 10 g being achieved. Chapter 4 investigates the feasibility of scale up of high-pressure reaction to the 1 L scale in the hope that similar quality particle can be produced to the 60 mL scale. Yields from reactions at this scale would be great than 100 g, thus eliminating the need for several reaction repeats needed to be completed to provide enough sample for testing.

3.7. References

1. J. M. DeSimone, Z. Guan and C. Elsbernd, *Science*, 1992, **257**, 945-947.
2. J. M. DeSimone, E. E. Maury, Y. Z. Menceloglu, J. B. McClain, T. J. Romack and J. R. Combes, *Science*, 1994, **265**, 356-359.
3. A. M. Gregory, K. J. Thurecht and S. M. Howdle, *Macromolecules*, 2008, **41**, 1215-1222.
4. B. Grignard, C. Jérôme, C. Calberg, R. Jérôme, W. Wang, S. M. Howdle and C. Detrembleur, *Macromolecules*, 2008, **41**, 8575-8583.
5. G. Hawkins, P. B. Zetterlund and F. Aldabbagh, *Journal of Polymer Science Part A: Polymer Chemistry*, 2015.
6. K. J. Thurecht and S. M. Howdle, *Australian Journal of Chemistry*, 2009, **62**, 786-789.
7. P. B. Zetterlund, F. Aldabbagh and M. Okubo, *Journal of Polymer Science Part A: Polymer Chemistry*, 2009, **47**, 3711-3728.
8. T. Casimiro, A. M. Banet-Osuna, A. M. Ramos, M. N. da Ponte and A. Aguiar-Ricardo, *European Polymer Journal*, 2005, **41**, 1947-1953.
9. J. Shin, W. Bae and H. Kim, *Colloid and Polymer Science*, 2010, **288**, 271-282.
10. T. Hasell, K. J. Thurecht, R. D. W. Jones, P. D. Brown and S. M. Howdle, *Chemical Communications*, 2007, 3933-3935.
11. J. Jennings, M. Beija, J. T. Kennon, H. Willcock, R. K. O'Reilly, S. Rimmer and S. M. Howdle, *Macromolecules*, 2013, **46**, 6843-6851.
12. J. Jennings, M. Beija, A. P. Richez, S. D. Cooper, P. E. Mignot, K. J. Thurecht, K. S. Jack and S. M. Howdle, *Journal of the American Chemical Society*, 2012, **134**, 4772-4781.
13. E. C. Achilleos, G. Georgiou and S. G. Hatzikiriakos, *Journal of Vinyl and Additive Technology*, 2002, **8**, 7-24.
14. J. S. Lee and F. C. Chang, *Polymer Engineering and Science*, 2004, **44**, 1885-1889.
15. R. P. Petrich, *Polymer Engineering and Science*, 1973, **13**, 248-254.
16. J. Markarian, *Plastics Additives and Compounding*, 2004, **6**, 46-49.
17. L. M. Robeson, *Polymer Engineering and Science*, 2013, **53**, 453-467.
18. G. Liu and G. Qiu, *Polymer Bulletin*, 2013, **70**, 849-857.
19. I. S. Rabinovic, *Journal of Vinyl Technology*, 1983, **5**, 179-182.
20. J. C. Stevenson, *Journal of Vinyl and Additive Technology*, 1995, **1**, 41-45.
21. K. A. Afrifah and L. M. Matuana, *Macromolecular Materials and Engineering*, 2010, **295**, 802-811.

22. A. K. Banerjee, *United States Pat.*, 5,030,662, 1991.
23. J. T. Lutz, *Journal of Vinyl Technology*, 1993, **15**, 82-99.
24. D. Braun, *Journal of Polymer Science Part A: Polymer Chemistry*, 2004, **42**, 578-586.
25. G. F. Wu, J. F. Zhao, H. T. Shi and H. X. Zhang, *European Polymer Journal*, 2004, **40**, 2451-2456.
26. R. Geyer, J. R. Jambeck and K. L. Law, *Science Advances*, 2017, **3**, e1700782.
27. S. N. Maiti, U. K. Saroop and A. Misra, *Polymer Engineering and Science*, 1992, **32**, 27-35.
28. L. J. Effler and M. T. Berard, *Journal of Vinyl and Additive Technology*, 2003, **9**, 19-25.
29. A. Siegmann and A. Hiltner, *Polymer Engineering and Science*, 1984, **24**, 869-876.
30. Z. Liu, X. Zhu, L. Wu, Y. Li, Z. Qi, C. Choy and F. Wang, *Polymer*, 2001, **42**, 737-746.
31. Z. Zhang, S. Chen and J. Zhang, *Polymer Testing*, 2011, **30**, 534-542.
32. R. D. Deanin and W. Z. L. Chuang, *Journal of Vinyl Technology*, 1987, **9**, 60-62.
33. M. Chen, C. Zhou, Z. Liu, C. Cao, Z. Liu, H. Yang and H. Zhang, *Polymer International*, 2010, **59**, 980-985.
34. S. Wu, M. Chen, G. Wu and C. Zhou, *Journal of Polymer Research*, 2015, **22**.
35. T. I. Min, A. Klein, M. S. El-Aasser and J. W. Vanderhoff, *Journal of Polymer Science: Polymer Chemistry Edition*, 1983, **21**, 2845-2861.
36. M. Gosecka and M. Gosecki, *Colloid and Polymer Science*, 2015, **293**, 2719-2740.
37. Q. B. Si, C. Zhou, H. D. Yang and H. X. Zhang, *European Polymer Journal*, 2007, **43**, 3060-3067.
38. W. J. Ferry, D. H. Jones and R. K. Graham, *United States Pat.*, 3,985,703, 1976.
39. B. E. Larsson, C. F. Ryan and L. C. Souder, *United States Pat.*, 3,655,825, 1972.
40. L. Zhou, X. Wang, Y. Lin, J. Yang and Q. Wu, *Journal of Applied Polymer Science*, 2003, **90**, 916-924.
41. A. Aguiar, S. Gonzalez-Villegas, M. Rabelero, E. Mendizabal, J. Puig, J. Dominguez and I. Katime, *Macromolecules*, 1999, **32**, 6767-6771.
42. D. G. Cook, A. Rudin and A. Plumtree, *Journal of Applied Polymer Science*, 1992, **46**, 1387-1393.
43. D. Huo, D. Liu and P. Sun, *Polymer International*, 2002, **51**, 1417-1421.
44. S. H. Kim, W. K. Son, Y. J. Kim, E. G. Kang, D. W. Kim, C. W. Park, W. G. Kim and H. J. Kim, *Journal of Applied Polymer Science*, 2003, **88**, 595-601.
45. D. J. Walsh and J. G. McKeown, *Polymer*, 1980, **21**, 1330-1334.

46. L. A. Pérez-Carrillo, M. Puca, M. Rabelero, K. E. Meza, J. E. Puig, E. Mendizábal, F. López-Serrano and R. G. López, *Polymer*, 2007, **48**, 1212-1218.
47. K. Cho, J. Yang, S. Yoon, M. Hwang and S. V. Nair, *Journal of Applied Polymer Science*, 2005, **95**, 748-755.
48. D. Dompas and G. Groeninckx, *Polymer*, 1994, **35**, 4743-4749.
49. Y. Zhu, X. Gao and Y. W. Luo, *Journal of Applied Polymer Science*, 2016, **133**.
50. A. Gharieh, A. R. Mahdavian and H. Salehi-Mobarakeh, *Iranian Polymer Journal*, 2014, **23**, 27-35.
51. H. Breuer, F. Haaf and J. Stabenow, *Journal of Macromolecular Science, Part B: Physics*, 1977, **14**, 387-417.
52. A. Tse, E. Shin, A. Hiltner, E. Baer and R. Laakso, *Journal of Materials Science*, 1991, **26**, 2823-2832.
53. Y. Fu, H. Song, C. Zhou, S. Sun and H. Zhang, *Polymer Composites*, 2013, **34**, 15-21.
54. A. Takaki, H. Yasui and I. Narisawa, *Polymer Engineering and Science*, 1997, **37**, 105-119.
55. C. Zhou, M. Chen, Z. Y. Tan, S. L. Sun, Y. H. Ao, M. Y. Zhang, H. D. Yang and H. X. Zhang, *European Polymer Journal*, 2006, **42**, 1811-1818.
56. L. Cao, L. Chen, X. Chen, L. Zuo and Z. Li, *Polymer*, 2006, **47**, 4588-4595.
57. T. D. McAllister, Expanding the Scope of Free-Radical Dispersion Polymerisation in Supercritical Carbon Dioxide, Doctor of Philosophy, The University of Nottingham, 2017, (*PhD Thesis*).
58. W. Wang, M. R. Giles, D. Bratton, D. J. Irvine, S. P. Armes, J. V. Weaver and S. M. Howdle, *Polymer*, 2003, **44**, 3803-3809.
59. M. R. Giles, J. N. Hay and S. M. Howdle, *Macromolecular Rapid Communications*, 2000, **21**, 1019-1023.
60. P. A. Mueller, G. Storti and M. Morbidelli, *Chemical Engineering Science*, 2005, **60**, 1911-1925.
61. P. A. Mueller, G. Storti and M. Morbidelli, *Chemical Engineering Science*, 2005, **60**, 377-397.
62. A. Rosell, G. Storti, M. Morbidelli, D. Bratton and S. M. Howdle, *Macromolecules*, 2004, **37**, 2996-3004.
63. M. A. Winnik, C. L. Zhao, O. Shaffer and R. R. Shivers, *Langmuir*, 1993, **9**, 2053-2065.
64. H.-S. Byun and D.-H. Lee, *Industrial & Engineering Chemistry Research*, 2006, **45**, 3354-3365.

65. V. A. Bhanu and K. Kishore, *Chemical Reviews*, 1991, **91**, 99-117.
66. T. D. McAllister, T. M. Bennett, C. Petrillo, C. Topping, L. Farrand, N. Smith and S. M. Howdle, *Journal of Materials Chemistry C*, 2019, **7**, 12194-12203.
67. M. R. Giles, J. N. Hay, S. M. Howdle and R. J. Winder, *Polymer*, 2000, **41**, 6715-6721.
68. A. M. Aerdt, A. L. German and G. P. M. van der Velden, *Magnetic Resonance in Chemistry*, 1994, **32**, 80-88.
69. M. G. Abiad, O. H. Campanella and M. T. Carvajal, *Pharmaceutics*, 2010, **2**, 78-90.
70. D. Mahlin, J. Wood, N. Hawkins, J. Mahey and P. G. Royall, *International Journal of Pharmaceutics*, 2009, **371**, 120-125.
71. H. Elisa, *An Introduction to Polymer Science* VCH, Weinheim. New York, 1997.
72. W.-G. Yao, L.-Q. Wang, D.-Y. He, S.-C. Jiang, L.-J. An and H.-X. Zhang, *Chinese Journal of Polymer Science*, 2005, **23**, 337-340.
73. K. A. Shaffer, T. A. Jones, D. A. Canelas, J. M. DeSimone and S. P. Wilkinson, *Macromolecules*, 1996, **29**, 2704-2706.
74. S. Kirsch, K. Landfester, O. Shaffer and M. S. El-Aasser, *Acta Polymerica*, 1999, **50**, 347-362.
75. F. Sommer, T. M. Duc, R. Pirri, G. Meunier and C. Quet, *Langmuir*, 1995, **11**, 440-448.
76. S. Jiang, E. D. Sudol, V. L. Dimonie and M. S. El-Aasser, *Journal of Polymer Science Part A: Polymer Chemistry*, 2007, **45**, 2105-2112.
77. J. S. Trent, J. I. Scheinbeim and P. R. Couchman, *Macromolecules*, 1983, **16**, 589-598.
78. T. D. McAllister, L. D. Farrand and S. M. Howdle, *Macromolecular Chemistry and Physics*, 2016, **217**, 2294-2301.
79. M. Alauhdin, PhD., University of Nottingham 2017, (*PhD Thesis*).
80. Z. Guan, J. R. Combes, Y. Z. Menciloglu and J. M. DeSimone, *Macromolecules*, 1993, **26**, 2663-2669.
81. E. J. Roche and E. L. Thomas, *Polymer*, 1981, **22**, 333-341.
82. S. J. Jeon, G. R. Yi and S. M. Yang, *Advanced Materials*, 2008, **20**, 4103-4108.
83. S. J. Jeon, G. R. Yi, C. M. Koo and S. M. Yang, *Macromolecules*, 2007, **40**, 8430-8439.
84. J. K. Kim, S. Y. Yang, Y. Lee and Y. Kim, *Progress in Polymer Science*, 2010, **35**, 1325-1349.
85. J.-S. Song and M. A. Winnik, *Macromolecules*, 2005, **38**, 8300-8307.
86. I. M. Barszczewska-Rybarek, A. Korytkowska-Wałach, M. Kurcok, G. Chladek and J. Kasperski, *Acta of Bioengineering and Biomechanics*, 2017, **19**.
87. K. Tamareselvy and F. A. Rueggeberg, *Dental Materials*, 1994, **10**, 290-297.

88. G. Odian, *Principles of Polymerisation*, John Wiley & Sons, Inc., 4th edn., 2004.
89. C. Barner-Kowollik, S. Beuermann, M. Buback, P. Castignolles, B. Charleux, M. L. Coote, R. A. Hutchinson, T. Junkers, I. Lacík and G. T. Russell, *Polymer Chemistry*, 2014, **5**, 204-212.
90. N. M. Ahmad, F. Heatley and P. A. Lovell, *Macromolecules*, 1998, **31**, 2822-2827.
91. S. K. Patra and D. Mangaraj, *Die Makromolekulare Chemie: Macromolecular Chemistry and Physics*, 1968, **111**, 168-171.
92. E. E. Drott and R. A. Mendelson, *Journal of Polymer Science Part A-2: Polymer Physics*, 1970, **8**, 1361-1371.
93. Agilent, *A Guide to Multi-detector Gel Permeation Chromatography*, 2012.
94. E. Sato, T. Emoto, P. B. Zetterlund and B. Yamada, *Macromolecular Chemistry and Physics*, 2004, **205**, 1829-1839.

Chapter 4: Scale up and Particle Size

Control

4.1. Overview

Supercritical carbon dioxide (scCO₂) is a promising green solvent for several different polymerisation techniques. It is an environmentally viable alternative for organic solvents and water as it is currently an abundant waste stream. Polymerisation using conventional solvents often requires several energy and time intensive work up steps, whereas scCO₂ enables facile access to dry, powdered, polymer particles upon the release of pressure. One challenge associated with this technique is the transition from laboratory to large industrial scale due to the high pressures involved. This chapter aims to assess the feasibility of using scCO₂ as a medium for the production of polymer particles on an industrial scale. Specifically, the first steps towards the scaling up of the free radical dispersion polymerisation of poly(methyl methacrylate) (PMMA), from the millilitre to the litre scale, are described. A reproducible and controlled reaction is desired, which produces well defined polymer particles with a narrow size distribution. A two-stage method was used along with variations of surfactant concentration, to consistently achieve different particle sizes. Comparison of scanning electron microscopy (SEM) images from the 60 mL and 1 L vessel showed similar particle sizes and morphologies were obtained.

Once a reproducible synthesis method was established utilising PMMA, scale up of core-shell particle synthesis was attempted. More specifically, PMMA particles were synthesised before the addition of BA (27 wt%). SEM analysis showed that particles synthesised on the 1 L scale were similar in morphology to the particles produced using analogous conditions on the 60 mL scale.

4.2. Introduction

Polymeric particles have many applications, for example, as additives in paint or to help influence properties of materials such as impact modifiers, which require a range of particle sizes and compositions depending upon the application.¹⁻⁴ The most common methods of synthesising this type of particle are through emulsion, mini-emulsion, dispersion and suspension polymerisation.⁵ An important property to consider is particle size, which is dictated by the end application.⁶ Different polymerisation techniques typically produce specific particle sizes; emulsion 0.06-0.7 μm , dispersion 0.1-10 μm and suspension 50-1000 μm .⁷

4.2.1. Particle Size Control

There are several ways to influence particle size other than changing the polymerisation technique. For example, varying reaction parameters such as temperature, concentration and decomposition rate of the initiator and solvency of the dispersion medium. Through careful control of these parameters, monodisperse particles with varying size can be produced.⁷ A well-studied system is the dispersion polymerisation of MMA to afford PMMA particles. Shen *et al.* investigated the effects of the above parameters on the particle size of PMMA from dispersion polymerisation.⁸ The authors found that monodisperse PMMA particles with diameters ranging between 0.6 to 10 μm could be prepared in a methanol or water/methanol mixture. An increase in particle size was observed with an increase in polymerisation temperature or initiator concentration or decomposition rate (Figure 4-1). These parameters were changed individually as well as in combination, showing the ability to tune the condition dependent on the target particle size desired. Increasing the polymerisation temperature leads to an increase the polymerisation rate. This has an impact on several factors including decreasing the solvency of the surfactant species, polyvinylpyrrolidone (PVP) and decreasing the viscosity of the continuous phase, both of which can contribute to an increase in particle size. The rate of absorption of the PVP stabiliser and the viscosity of the

continuous phase were both increased as the concentration of PVP was increased, resulting in smaller particles being formed. The viscosity of the system also increases significantly with increasing the molecular weight of the PVP stabiliser, again leading to smaller particles being formed. An increase in monomer concentration from 5 to 10 wt% caused a decrease in particle size to a minimum, which subsequently increased with further increases in monomer concentration to 20 wt%. Both the polymerisation rate along with the solvency of the reaction medium would increase with an increase in monomer concentration, leading to the formation of large particles. However, the length of the PMMA segments in a PVP-*g*-PMMA graft copolymer produced *in situ* during the reaction would increase with increasing monomer concentration. This would increase the absorption rate of the stabiliser, favouring the formation of smaller particles. The nonlinear change in particle size with respect to monomer concentration is attributed to the trade-off between these two factors.⁸

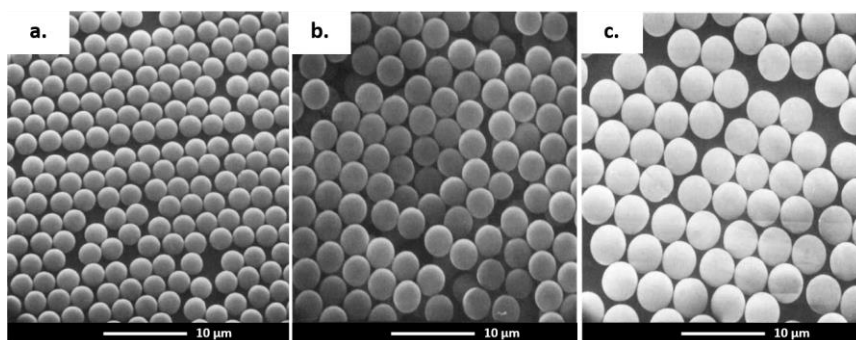


Figure 4-1: SEM images of PMMA particles prepared by dispersion polymerisation in methanol at different reaction temperatures; 50 °C (a), 55 °C (b) and 60 °C (c). An increase in particle size was observed as temperature increased; 2.8 μm (50 °C), 3.2 μm (55 °C) and 4.0 μm (60 °C).⁸

Hu *et al.* reported the first simple and fast one-step method for synthesising monodisperse, micron sized, PMMA particles in organic medium through dispersion polymerisation. By optimisation of the solvent composition, a mixture of dodecane and hexane, particles up to 10 μm were produced. Control of the nucleation time of the particles gave low poly dispersity in particle size of around 1%.⁹

The examples discussed produced latexes; particles suspended in solvent. Many applications require a dry polymer powder and hence several energy intensive steps are needed to remove the solvent post polymerisation. A potential solution to this is to use scCO_2 as the reaction medium. Releasing the pressure post polymerisation affords a dry, solvent free powder. scCO_2 is also considered a more environmentally friendly alternative to the volatile organic compounds (VOCs) traditionally used in dispersion polymerisation.¹⁰

In 1994 DeSimone reported the first example of free radical dispersion polymerisation in scCO_2 .¹¹ Low molecular weight PMMA ($77\text{-}149\text{ kg mol}^{-1}$) and low monomer conversion (10-40%) was achieved by dispersion polymerisation in the absence of any stabiliser, with no particles being formed. Addition of poly(1,1-dihydroperfluorooctylacrylate) (poly(FOA)), a CO_2 soluble stabiliser (Figure 4-2), aided high conversion (> 90%) and high molecular weight ($190\text{-}325\text{ kg mol}^{-1}$) PMMA particles to be formed under mild conditions (65 °C, 204 bar).

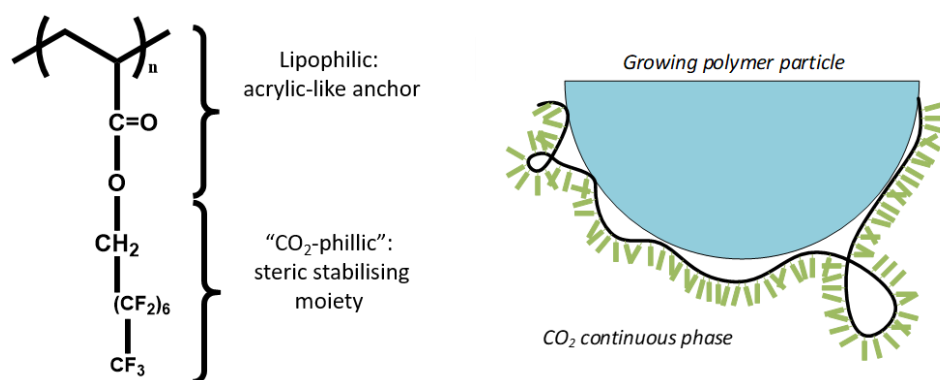


Figure 4-2: The structure of poly(FOA) stabiliser used in the dispersion polymerisation of PMMA (left) and an illustration of the PMMA particle (shown in blue) stabilised by poly(FOA) (right); the lipophilic back bone (shown in black) acts as an anchor for the CO_2 -philic fluorocarbon steric stabilising moiety (shown in green).¹¹

Uniform spherical particles with an average diameter in the range 1.2-2.5 μm , were confirmed via SEM analysis (Figure 4-3).

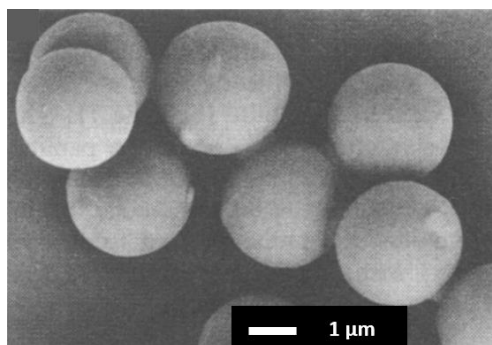


Figure 4-3: SEM image of PMMA particles synthesis by dispersion polymerisation in CO₂. The scale bar is 1 μm.¹¹

4.2.2. Stabiliser

One of the most common ways to influence particle size in dispersion polymerisation is to vary the type and concentration of stabiliser.^{8, 12} The polymerisation process begins with nucleation. During this period of the reaction, new polymer chains propagate. Once the growing polymer chains reach a critical molecular weight, they precipitate to form particles. Upon precipitation, these polymer particles are unstable and prone to coagulation. To prevent this a polymeric stabiliser species (often also referred to as a surfactant) is included in the reaction and as they precipitate the growing particles are stabilised by this species. Two stabilisation mechanisms have been recognised, the species either chemically attaches or adsorbs on to the surface of the growing particle, forming a steric barrier between the growing particles. The stabiliser can be formed *in situ*. Typically, the stabilising species is a block copolymer that contains a block that has a high affinity for the reaction medium and a block that has a high affinity for the growing polymer. The stabiliser plays a vital part in the polymerisation process by forming a “hairy” layer around the growing particles that promotes the formation of individual particles and ultimately dictates the size of the particle formed (Figure 4-4).^{7, 13}

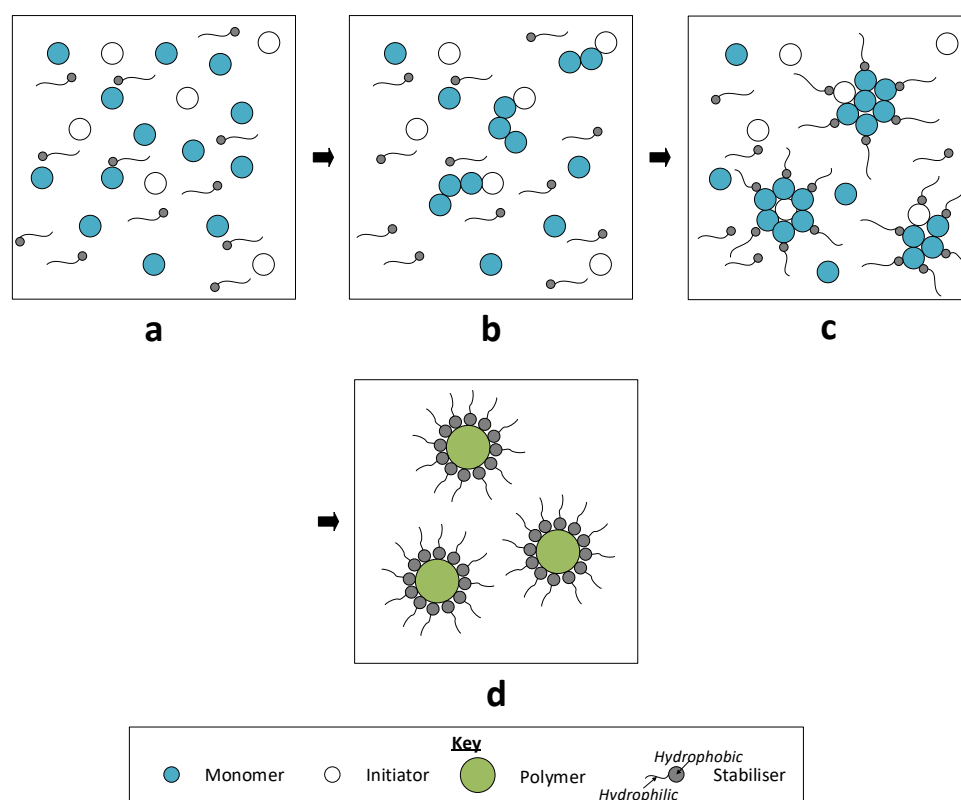


Figure 4-4: Schematic representation of steric stabilisation in dispersion polymerisation. Polymerisation begins (a), polymer chains begin to propagate (b), polymer chains reach critical molecular weight and precipitate before being stabilised (c), particles with a “hairy” layer of stabiliser are formed (d).

To obtain efficient steric stabilisation the following factors are essential; high surface coverage, strong adsorption and a good solvent for the stabilising chains. A higher concentration of stabiliser allows for coverage of a higher surface area, thus smaller particles are produced. If insufficient stabiliser is present, the particles will become unstable and agglomerate.⁷ Choice of stabiliser is key and is directed by the reaction system. For dispersion polymerisation an important property to consider is solubility. The stabiliser must be at least partially soluble in the reaction medium.⁷

Richez *et al.* investigated the synthesis of PMMA particles using a methacrylate terminated poly(dimethylsiloxane) (PDMS-MA) macromolecule as a stabiliser in dodecane. The authors varied not only the concentration (2.5-20 wt%) of the PDMS-MA but also the molecular weight (5,000 and 10,000 g mol⁻¹). Using high molecular weight stabiliser gave hexagonally close packed, typically monodisperse samples (Figure 4-5).

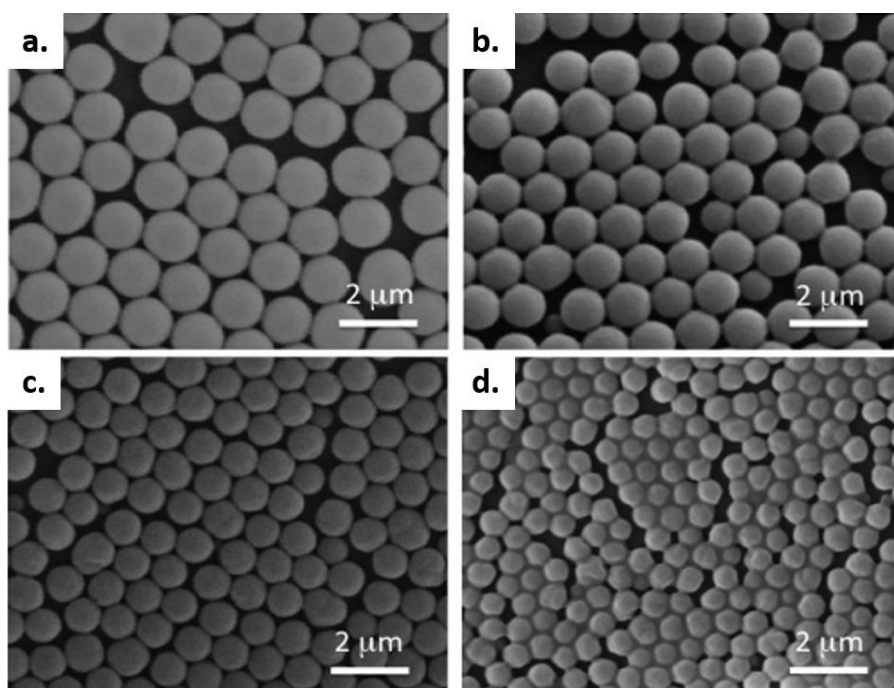


Figure 4-5: Scanning electron micrographs of PMMA particles polymerised with PDMS-MA ($10,000 \text{ g mol}^{-1}$) and different stabiliser concentrations; 2.5 wt% (a), 5 wt% (b), 10 wt% (c) and 20 wt% (d). A reduction of particle size with increasing stabiliser concentration was observed. All scale bars are $2 \mu\text{m}$.⁸

The lower molecular weight stabiliser produced less well-defined particles, attributed to poor stabilisation of particle seeds at the start of the reaction. For both molecular weights, a reduction in average particle size as stabiliser concentration increased was observed.¹⁴

Stabiliser concentration and type can also be used to control particle size in dispersion polymerisation utilising scCO_2 . Many polymeric substances are insoluble in scCO_2 and hence the choice of potential stabilisers is more limited than in traditional solvents.¹⁵ Early dispersion polymerisations using scCO_2 as the reaction medium employed fluorinated polymer as stabilisers.^{11, 12, 16-18} However, with environmental impact in mind, research into polymerisations using non-toxic more environmentally friendly siloxane based surfactants such as poly(dimethyl siloxane) (PDMS) has increased.¹⁹ Silicone based stabilisers are generally cheaper than fluorinated based stabilisers. In 1996 Shaffer *et al.* reported synthesis of high molecular weight PMMA particles via dispersion polymerisation in scCO_2 using PDMS-MA and AIBN ($65 \text{ }^\circ\text{C}$, 340 bar, 4 hours).²⁰

O'Neill *et al.* similarly investigated the dispersion polymerisation of MMA in scCO₂ using a PDMS macromonomer which reacted to form stabilisers *in situ*. Polymerisations were carried out in both liquid and supercritical conditions, giving particles ranging from 1.1-5.8 µm. *In situ* turbidimetry was also used to study particle formation and growth.^{21, 22}

Previously in the Howdle group, Christian *et al.* reported the use of the same type of PDMS macromolecular stabilisers for dispersion polymerisation in scCO₂. The authors found that both polymer yield and molecular weight were strongly influenced by mixing phenomena, particularly when higher concentrations of the AIBN were used.²³ More recently, McAllister *et al.* reported the synthesis of PMMA particles ranging from 0.3 to 5.3 µm using a commercially available PDMS-MA stabiliser. This was achieved by combining control of both the initial monomer and stabiliser loading. Increasing the stabiliser concentration allowed for a larger surface area of the polymer to be stabilised, subsequently favouring synthesis of a larger number of smaller particles. Employing a higher concentration of MMA during the nucleation phase of the reaction favoured formation of bigger particles. This was attributed to higher monomer concentrations delaying the precipitation of propagating polymer chains allowing them to grow longer, causing formation of fewer particle nuclei and consequently the formation of larger particles. This was combined with addition of a second charge of monomer which allowed high molecular weights and yields to be reached. This delayed addition of monomer also reduced batch-to-batch variability and aggregation of the particles.²⁴

As discussed, polymerisation of MMA in scCO₂ has been heavily studied, making it an ideal model system to scale up.²⁴⁻³²

4.2.3. Scale Up

Despite numerous advances of using scCO₂, scale remains a fundamental hurdle which has thus far limited the applicability of dispersion polymerisation in scCO₂ for the production of polymer particles on the commercial scale. Specifically, the typical

vessels used for their synthesis are 150 mL or below, producing ≈ 10 g per batch.^{30, 31,}
³³ Initial research utilising scCO_2 on a large scale focused largely on extraction and polymer processing.³⁴⁻³⁶ An example of the use of scCO_2 at scale is work published by Kasteren *et al.* in which the authors described the design of a production process in which waste cooking oil was converted via supercritical transesterification with methanol to methyl ester, otherwise known as biodiesel. Three plant capacities (125,000: 80,000 and 8,000 tonnes biodiesel/year) were studied concluding that the scale up was successful resulting in high purity of methyl esters and almost pure glycerol obtained as by-products.³⁷

Lebedev *et al.* scaled up the supercritical drying of aerogels. A mathematical model was developed for the hydrodynamics of a supercritical fluid flow, heat and mass transfer in a reactor during the drying process of aerogel. The model was used to scale up the supercritical drying process from 250 to 5000 mL; reactor geometry and process parameters were optimised in order to optimise the production process whilst still achieving desired properties of aerogels.³⁸

The main issue for industrial scale use of SCFs is the absence of economic studies.³⁹ However, more recently this has been addressed with papers being published dealing with the economic feasibility of some developed process, such as extraction of essential oil from rosemary, fennel and anise,⁴⁰ along with brewery grain management.⁴¹

Although extraction vessels designed for high pressure can have very large volumes (450 L) and are capable of reaching pressures of 300 bar at 40 °C, those developed to date are unsuitable for batch reactions as their tubular dimensions are better designed for flow systems.⁴² There are several examples of PMMA synthesis scale up using conventional solvents, however examples using scCO_2 as the reaction medium have not yet been reported.^{43, 44}

4.3. Aims and Objectives

The focus of this chapter is the investigation into the viability of scCO₂ as a solvent for dispersion polymerisation on the industrial scale. Current industrial polymerisations are performed using emulsion methods. This is carried out with water as the solvent, which requires very energy intensive drying steps to yield a powder. Therefore, alternative greener synthesis routes are of interest to many industrial companies. Several types of polymers have been successfully synthesised in the Howdle group on the 60 and 20 mL scale, including PMMA, poly(lactic acid) (PLA), poly(4-vinyl pyridine) (PVP), polycaprolactone (PCL) and poly(2-hydroxyethyl methacrylate) (poly(HEMA)), using various polymerisation techniques.⁴⁵⁻⁵⁰ This chapter investigates the scale up of the well-understood 60 mL scale reactions to the 1 L scale and assesses whether comparable polymers can be synthesised. Initial experiments use a one-step method before implication of a two-stage method to improve batch-to-batch variability. This two-stage method is then coupled with variation of the stabiliser concentration to manipulate the size of the particles produced. Once a reproducible method has been established to produce PMMA particles the synthesis of core-shell particles was scaled up. More specifically, the method to produce PMMA particles containing BA (27 wt%), as this had proved to be consistent on the 60 mL scale.

4.4. Experimental

4.4.1. Materials

Polymerisations were carried out using methyl methacrylate (MMA, ProSciTech, 99%) as a monomer along with 2,2'-Azobis(isobutyronitrile) (AIBN, Sigma Aldrich, 98%) initiator and methacrylate terminated polydimethylsiloxane (PDMS-MA, $M_n \sim 10$ KDa) (ABCR GmbH & Co.) as the stabiliser. All reactions were carried out in SFC grade 4.0 CO₂ ($\geq 99.99\%$), BOC special gases). To simulate industrial processes, all chemicals were used as received.

4.4.2. PMMA Particle Synthesis in 60 mL Autoclave

4.4.2.1. One-stage Reaction

MMA (10 mL, 93.0 mmol) and a mixture of AIBN (1 wt% wrt MMA, 0.094 g, 0.57 mmol) and PDMS-MA (1 wt% wrt MMA, 0.47 g, 0.047 mmol) were separately flushed with argon for 30 minutes to remove oxygen. The autoclave was purged with approximately 2 bar of CO₂ via the key hole for 30 minutes. Following deoxygenation, the MMA and AIBN/PDMS-MA mixture were combined and left to stir until homogeneous. The resulting mixture was injected into the autoclave via a syringe under a positive pressure of CO₂ (1-2 bar). The autoclave was sealed, pressurised to 48 bar, and heated to 65 °C before being pressurised to reaction conditions (207 bar). The reaction was left stirring (300 rpm) for 4 hours. After this time the heat was removed, and the autoclave left to cool naturally to room temperature before being depressurised (Figure 4-6). The resulting product was collected for analysis, typically a free-flowing powder.

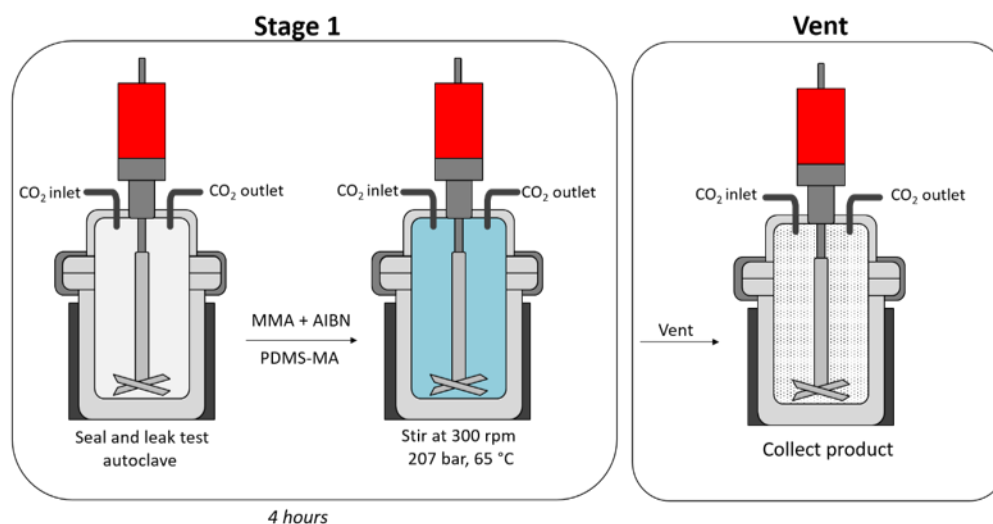


Figure 4-6: Schematic showing the batch synthesis of PMMA in a 60 mL autoclave.

4.4.2.2. Two-stage Reaction

To gain more control over particle size distribution, experiments were performed in which a second charge of monomer was added to the system part way through the reaction (Figure 4-7).

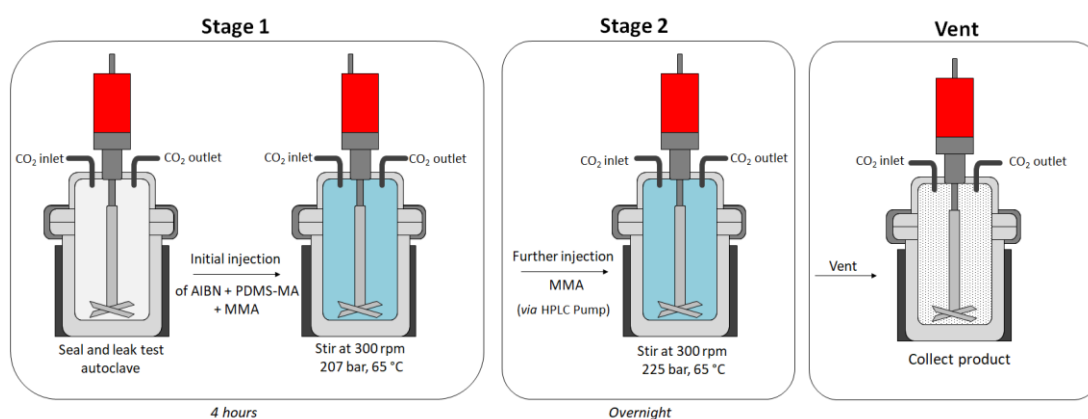


Figure 4-7: Schematic showing a multi-stage synthesis of PMMA in a 60 mL autoclave; stage 1 - particle nucleation and stage 2 - particle growth

MMA (5 mL, 46.48 mmol) and a mixture of AIBN (1 wt% wrt total MMA (7.5 mL), 0.0705 g, 0.43 mmol) and PDMS-MA (amounts shown in Table 4-1) were separately

deoxygenated. This initial charge was added via a syringe, against a positive pressure of CO₂ (1-2 bar), to a purged autoclave. After 1 hour a second charge of MMA (2.5 mL, 23.24 mmol) was pumped into the system via an HPLC pump at a rate of 0.2 mL min⁻¹.

Table 4-1: Amount of PDMS-MA used for different loadings in the two-stage reactions. Loading wt% wrt total MMA (7.5 mL).

Entry	PDMS-MA Loading (wt%)	PDMS-MA (g)	PDMS-MA (mmol)
1	5	0.35	0.035
2	10	0.71	0.071
3	20	1.41	0.141

This process resulted in an increase in the pressure of the system by approximately 7 bar per millilitre of monomer being injected. The reaction was left to stir at 300 rpm for 4 hours, before the heating was removed and allowed to cool naturally to room temperature. The autoclave was depressurised, and the resulting product was collected for analysis, typically a free-flowing powder.

4.4.2.3. Initiator Injection Reactions

MMA (5 mL, 46.47 mmol) and PDMS-MA (5 wt% wrt total MMA, 0.375 g, 0.038 mmol) were flushed separately with argon for 30 minutes. Both were combined and added to the autoclave via a syringe under a positive pressure of CO₂ (1-2 bar) before being sealed and pressurised to 48 bar and heated to 65 °C. Further CO₂ was added until a pressure of 207 bar was reached. Post flushing with argon for 30 minutes, AIBN (1 wt% wrt total MMA, 0.2808 g, 1.71 mmol) was combined with MMA (2.5 mL, 23.23 mmol). The resulting mixture was added to the autoclave via an HPLC pump at a rate of 1 mL min⁻¹. The autoclave was left stirring (300 rpm) for 4 hours. The heating was switched off and the vessel left to cool. The autoclave was vented at room temperature and the resulting product was collected for analysis.

4.4.3. PMMA Particle Synthesis in 1 L Autoclave

4.4.3.1. One-stage Reaction

MMA (150 mL, 1.41 mol) was flushed with argon for 30 minutes. A mixture of AIBN (1 wt% wrt MMA, 1.404 g, 0.0086 mol) and PDMS-MA (5 wt% wrt MMA, 7.02 g, 0.0007 mol) was separately flushed with argon. The components were then combined and stirred until homogeneous. The autoclave was charged with the mixture via a syringe under a positive pressure of CO₂ (1-2 bar) before being pressurised to 48 bar and heated to 65 °C. Further CO₂ was added until a pressure of 207 bar was reached. The autoclave was left stirring for 4 hours, then the heating was switched off and the vessel left to cool overnight. The autoclave was vented via an actuated ball valve at room temperature to ambient pressure and the resulting product was collected for analysis.

4.4.3.2. Two-stage Reaction

The process discussed in section 4.4.2.2 was repeated on the 1 L scale using the following quantities; an initial charge of MMA (100 mL, 0.93 mol), AIBN (1 wt% wrt total MMA, 1.404 g, 0.0086 mol) and PDMS-MA (for amounts see Table 4-2). A second charge of MMA (50 mL, 0.46 mol) was added via a HPLC pump at 4 mL min⁻¹ (keeping the total injection time consistent with the 60 mL scale) after 1 hour. The injection induced a pressure increase approximately 20 bar.

Table 4-2: Amount of PDMS-MA used for different loadings of the two-stage synthesis method. Loading wt% wrt total MMA (150 mL).

Entry	PDMS-MA Loading (wt%)	PDMS-MA (g)	PDMS-MA (mmol)
1	5	7.02	0.702
2	10	14.04	1.404
3	20	28.08	2.808

4.4.3.3. Initiator Injection Reactions

MMA (100 mL, 0.93 mol) and PDMS-MA (5 wt% wrt total MMA, 7.02 g, 0.0007 mol) were flushed separately with argon for 30 minutes. Both were combined and added to the autoclave via a syringe under a positive pressure of CO₂ (1-2 bar) before being pressurised to 48 bar and heated to 65 °C. Further CO₂ was added until a pressure of 138 bar was reached. This was lower than the standard reaction conditions of 207 bar to allow for pressure increases during injection. AIBN (1 wt% wrt total MMA, 1.404 g, 0.0086 mol) and MMA (50 mL, 0.46 mol) were deoxygenated before being combined. The resulting mixture was added to the autoclave via an HPLC pump at a rate of 5 mL min⁻¹. This only slightly increased the pressure and hence the pressure was increased to 179 bar by addition of CO₂. Again, this was lower than standard reaction conditions to allow for any delayed pressure increase. The autoclave was left stirring for 4 hours, after which the pressure had increased to 200 bar. The heating was switched off and the vessel left to cool overnight. The autoclave was vented via an actuated ball valve at room temperature to ambient pressure and the resulting product was collected for analysis.

4.4.4. Core-shell Particles Synthesis in 1 L Autoclave

To further test the system synthesis of core-shell particle was attempted. Due to cost, reaction simplicity and availability of monomer, the BA/PMMA core-shell synthesis was scaled up, using a BA loading of 27 wt%.

4.4.4.1. BA/PMMA Particle Synthesis

MMA (117 mL, 1.09 moles) was deoxygenated under argon for 30 minutes. A mixture of AIBN (1 wt% wrt total monomer, 1.5 g, 9.13 mmol) and PDMS-MA (5 wt% wrt total monomer, 7.65 g, 0.75 mmol) was separately flushed with argon for 30 minutes. The autoclave was deoxygenated by purging with N₂ for 30 minutes at 1-2 bar. The MMA was combined with the AIBN/PDMS-MA and injected into the autoclave via a syringe

under a positive pressure of N₂. The N₂ cylinder was closed and the autoclave was quickly sealed, pressurised to 48 bar, and heated to 65 °C before the addition of further CO₂ to reach reaction pressure (207 bar). The beginning of the reaction was recorded as the moment at which the temperature reached 65 °C, after which the reaction was left stirring (300 rpm) for 4 hour. A charge of BA (27 wt%, 46 mL, 0.32 mol) was added via a HPLC pump at 2.9 mL min⁻¹. The injection induced a pressure increase. The reaction was left overnight (18 hours). After this time the heating was removed, and the autoclave was allowed to naturally cool to room temperature before being depressurised. The resulting product was collected as a free-flowing white powder (Figure 4-8).

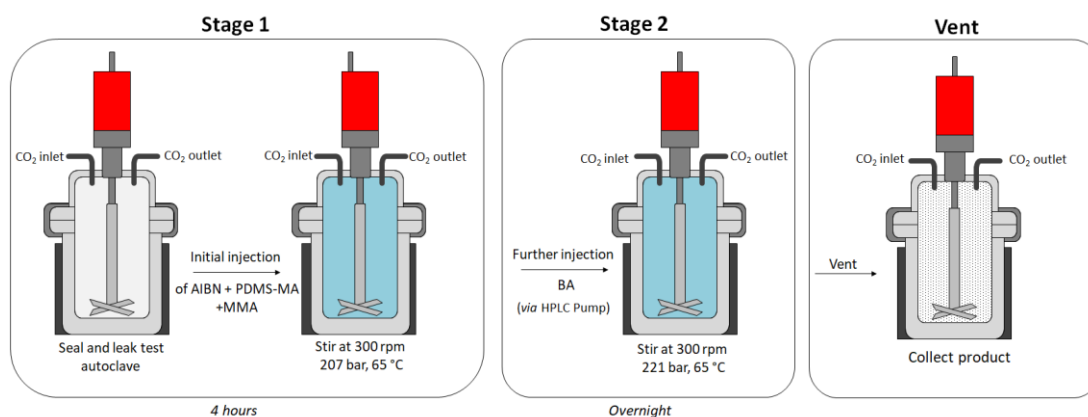


Figure 4-8: Schematic showing the scaled-up multi-stage reaction where PMMA particles were synthesis first followed by addition of BA in the 1 L autoclave.

4.5. Results and Discussion

4.5.1. PMMA Particle Synthesis in 60 mL Autoclave

4.5.1.1. One-stage Reactions

Initial experiments on the 60 mL scale consisted of demonstrating a reproducible PMMA synthesis method. Several repeats of the one-stage PMMA particle synthesis technique described in section 4.4.2.1 were recorded. The product of each experiment was analysed by GPC to determine the molecular weight, ^1H NMR to check the conversion, DSC to investigate the T_g and SEM to look at the morphology of the particles formed (Table 4-3). The results from each of the repeats are compared and discussed in the following section.

Table 4-3: Data collected for three one-stage PMMA particle synthesis repeats in the 60 mL autoclave.

Entry	Yield ^a (g)	Yield (%)	Conversion ^b (%)	M_n^c (g mol ⁻¹)	M_w^c (g mol ⁻¹)	\mathcal{D}^c	T_g^d (°C)	Particle Size ^e (nm)
1	7.58	76	89	169000	263000	1.56	130	2700 ± 306
2	9.01	90	87	145000	222000	1.54	130	3000 ± 382
3	9.00	90	96	227000	401000	1.77	127	2227 ± 340

^a – obtained gravimetrically, ^b – obtained from ^1H NMR, ^c – obtained from GPC system A, ^d - obtained from DSC and ^e – obtained from SEM (including standard deviation). All reactions were carried out using MMA (10 mL), AIBN (1 wt%) and PDMS-MA (5 wt%).

All reactions showed high conversion (> 85%) and similar T_g values (130 °C) comparable to literature results.⁵¹ Conversion was calculated from the ^1H NMR trace, by comparison of the unreacted monomer peak (Figure 4-9, 3.60 ppm, c) with the corresponding protons on the polymer (Figure 4-9, 3.75 ppm, c'). GPC analysis showed similar molecular weights along with dispersity values, which were comparable to what is expected from free radical polymerisation (1.5-2).⁵²

SEM images show successful particle synthesis (Figure 4-10). A comparison of the reaction repeats show that the particles have similar morphology and are uniform in both shape and size. The average particle size was comparable across the three repeats.

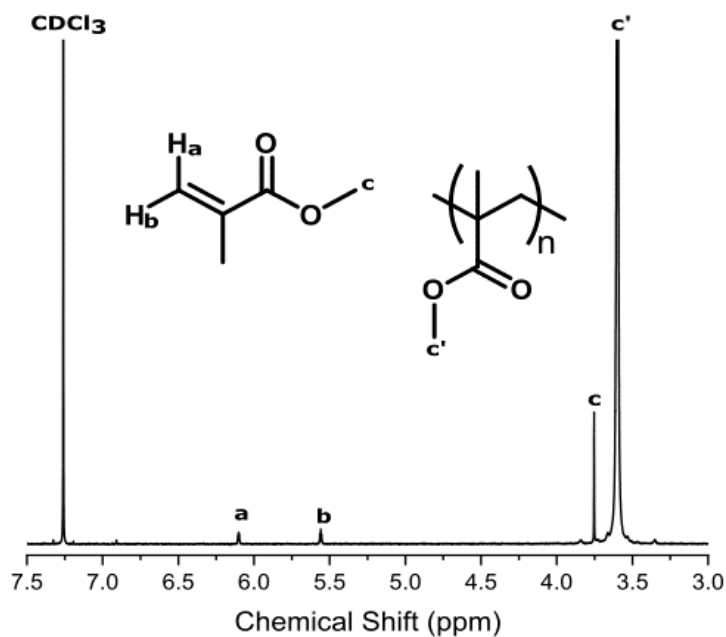


Figure 4-9: ^1H NMR trace for a PMMA dispersion reaction. Conversion was calculated by comparison of the unreacted monomer peak (3.60 ppm, c) with the corresponding protons on the polymer (3.75 ppm, c').

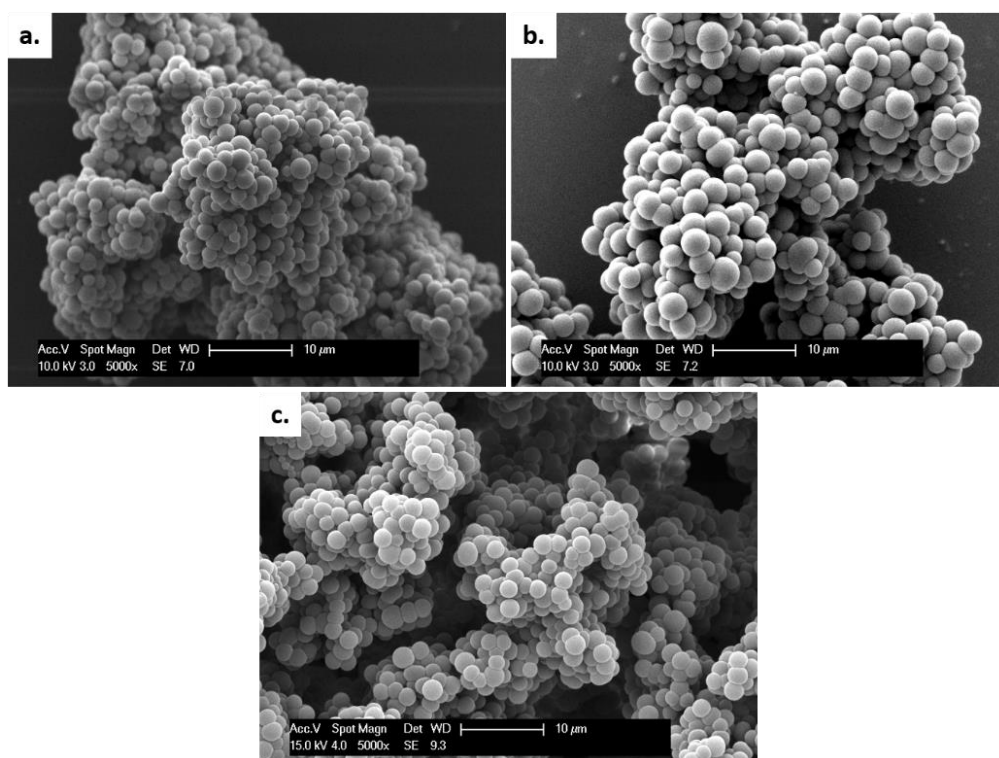


Figure 4-10: SEM images of PMMA particles synthesised from one-stage dispersion polymerisation in a 60 mL autoclave (1 wt% AIBN, 5 wt% PDMS-MA); Table 4-3 entry 1 (a), Table 4-3 entry 2 (b), Table 4-3 entry 3 (c). Comparable particles (morphology and size) were obtained from the reaction repeats. The scale bars are 10 μm .

The aggregation of the particles observed was caused by residual PDMS-MA left in the sample which, if necessary, could be removed by washing with dodecane or extraction with CO₂ at conditions above the solubility of PDMS-MA. This could be confirmed by ¹H NMR.^{24, 26} The removal of the residual PDMS-MA by washing with dodecane often improved the quality of the SEM images obtained (Figure 4-11).

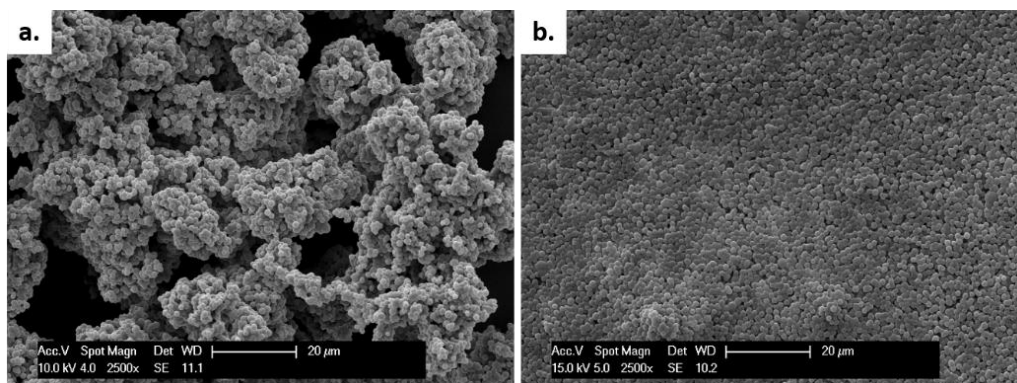


Figure 4-11: SEM images showing; a non-washed PMMA sample (a) and a washed PMMA sample (b). Aggregation was removed through washing with dodecane. Scale bars are 20 µm.

4.5.1.2. Two-stage Reactions

Previous work in the group had shown that batch-to-batch variability in particle size average could be reduced with the use of a multi-stage reaction technique.²⁴ Conditions optimised by McAllister *et al.* showed using an initial loading of MMA (5 mL) allowed ideal conditions for nucleation, and creation of seed particles.²⁴ The addition of a second charge of monomer increased the rate of polymerisation and growth from these seed particles occurred. This two-stage reaction technique (described in 4.4.2) was coupled with increasing stabiliser concentration in an attempt to decrease the average size of the particles produced.

High conversion for all reaction conditions was achieved (> 90%) and similar molecular weights were observed between repeat reactions, along with comparable dispersities. The exception to this was the reaction with no stabiliser (entry 1, Table 4-4), where only low conversion was reached, and no particles were observed. In the absence of stabiliser, the dispersion reaction is unstable and hence only low

conversion is attained. Under these conditions, propagating polymer would precipitate out at low molecular weight but in the absence of a stabilising species the oligomers would agglomerate as opposed to forming particles.^{11, 24}

Table 4-4: Data collected for two-stage PMMA particle synthesis reactions with varying PDMS-MA concentration on the 60 mL scale.

Entry	PDMS-MA (wt%)	Yield ^a (g)	Yield (%)	Conversion ^b (%)	M _n ^c (g mol ⁻¹)	M _w ^c (g mol ⁻¹)	Đ ^c	Particle Size ^d (nm)
1	0	-	-	20	-	-	-	-
2	5	6.37	85	93	173000	304000	1.76	1300 ± 220
3	10	7.12	91	91	195000	362000	1.86	790 ± 106
4	20	6.14	72	92	251000	484000	1.93	690 ± 117

^a – obtained gravimetrically, ^b – obtained from ¹H NMR, ^c – obtained from GPC system A and ^d – obtained from SEM (including standard deviation). Results are an average of three repeats for each set loading of PDMS-MA. All reactions were carried out using MMA (7.5 mL), AIBN (1 wt%) and PDMS-MA (amount stated in the table).

SEM analysis showed well-defined particles were produced for all reaction conditions (Figure 4-12). As expected, a reduction in the average particle size was observed as stabiliser concentration was increased (Table 4-4).^{8, 53} The particles obtained from the two-stage reaction using a PDMS-MA loading of 5 wt% are smaller than the one-stage reaction using the same loading (1300 ± 220 vs. 2640 ± 343 respectively). This is unsurprising due to the fact that the two-stage method uses a lower initial loading of MMA (5 vs. 7.5 mL) but the amount of PDMS-MA is the same and hence the ratio of PDMS-MA to MMA is higher, thus causing smaller particles to be produced. A high level of aggregation was observed with the sample produced using a PDMS-MA concentration of 20 wt% (Figure 4-12, image d). It is believed that this is due to a higher level of PDMS-MA covalently bound to the particle that would be present even post washing.

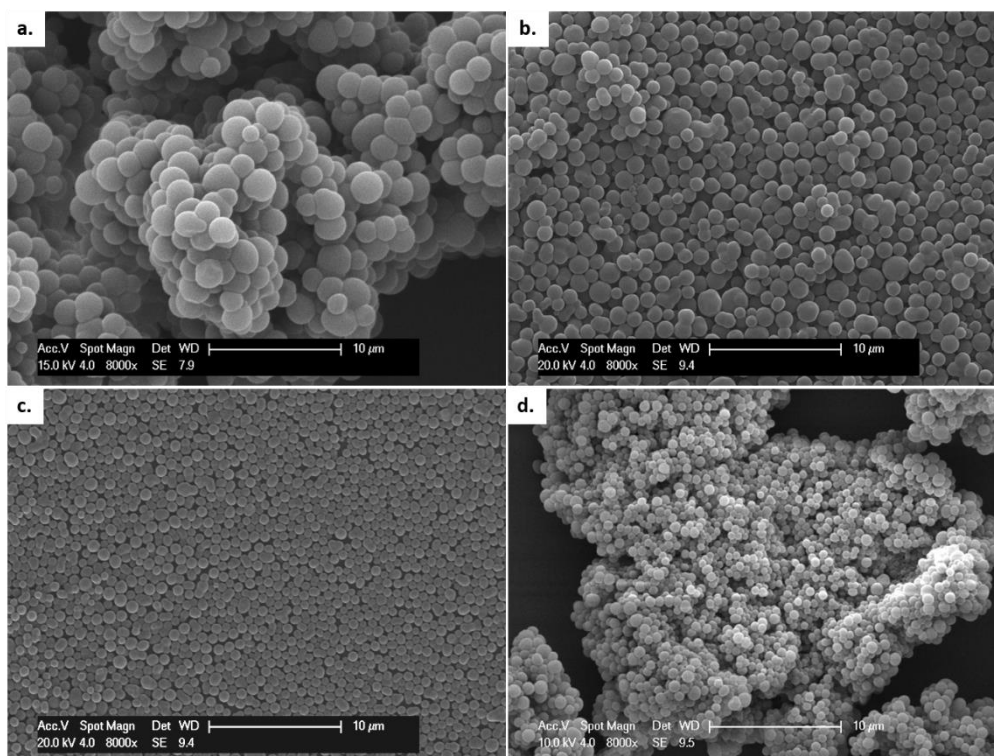


Figure 4-12: SEM images showing PMMA particles synthesised using the one-stage (a) and two-stage (b,c,d) reaction technique, along with varying PDMS-MA loading; 5 wt% (a, b), 10 wt% (c) and 20 wt% (d). The scale bars are all 10 μm. Similar particles were achieved using the one and two stage method. A reduction of particle size as stabiliser concentration was observed.

4.5.1.3. Initiator Injection Reactions

A focus of this work is the scale up of the 60 mL synthesis process to the 1 L scale. The wall thickness of the 1 L vessel is considerably larger than the equivalent 60 mL vessel (25 mm vs. 12 mm), therefore heating to reaction conditions takes longer (30 minutes vs. 10 minutes). The reaction studied uses an initiator that is decomposed thermally to start the polymerisation, therefore the time taken for the autoclave to reach reaction temperature is an important factor to consider. Decomposition over a wide temperature range can lead to an increase in molecular weight dispersities.^{52, 54} With this in mind, a series of experiments were carried out in which the autoclave, containing the majority of the monomer and the PDMS-MA, was brought to reaction conditions before the initiator, dissolved in the remainder of the monomer, was injected into the autoclave via a HPLC pump. The resulting products were collected from the initiator injection reactions, analysed and compared to the products produced using the standard reaction method, where all

the components were added at the start of the reaction (Table 4-5). The initiator injection reaction was repeated to check reproducibility.

Table 4-5: Data collected from PMMA particles produced using the one-stage standard reaction (SR) and the initiator injection reactions (II) on the 60 mL scale.

Entry	Method ^a	Yield ^b (g)	Yield (%)	Conversion ^c (%)	M _n ^d (g mol ⁻¹)	M _w ^d (g mol ⁻¹)	Đ ^d	Particle Size ^e (nm)
1	II	6.45	86	91	211000	355000	1.64	2560 ± 379
2	II	6.14	82	94	190000	291000	1.53	2390 ± 332
3	SR	9.01	90	87	145000	222000	1.54	3000 ± 382

^a – corresponds to the reaction method; initiator injector (II) and standard reaction (SR), ^b – obtained gravimetrically, ^c - from ¹H NMR, ^d - obtained from GPC system A, and ^e – obtained from SEM (including standard deviation). All reactions were carried out using MMA (10 mL), AIBN (1 wt%) and PDMS-MA (5 wt%).

Conversion was high for all reactions (> 85%). The GPC traces obtained from reaction repeats indicated comparable molecular weight distributions to the standard reaction technique. This suggests that the injection of the initiator had little to no effect on the particles formed, in terms of dispersity and molecular weight.

SEM images of the products from both reaction methods showed well defined particles. A comparison of particles produced from a standard one-stage reaction were slightly larger (3000 nm, Figure 4-13, image a) than those produced via an initiator injection reaction (2475 nm, Figure 4-13, image b).

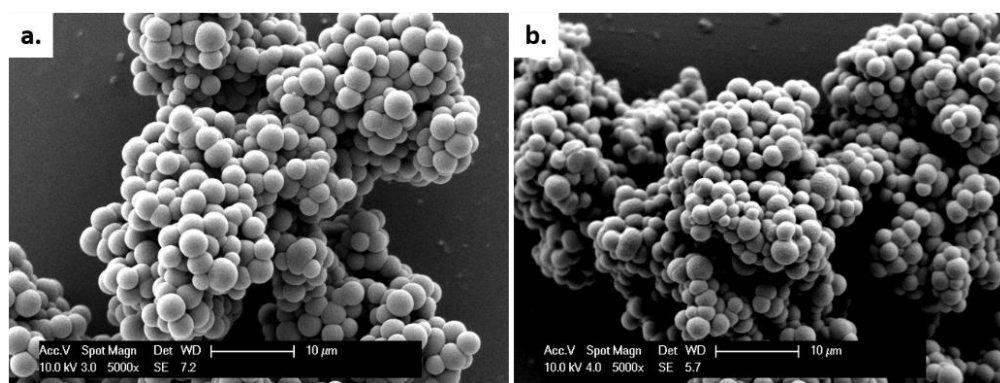


Figure 4-13: SEM images of PMMA particles using the (a) standard one-stage reaction and (b) initiator injection reaction, similar particle morphology was observed. The scale bars are 10 μm.

Morphology was also similar across both experimental methods. This suggests that perhaps the fact that the AIBN decomposes over a wider temperature range in the standard reactions has little effect on the particle formation. For future work, due to simplicity, the standard reaction technique will be used.

4.5.2. PMMA Particle Synthesis in 1 L Autoclave

4.5.2.1. Equipment Test

As this was the first time the equipment had been set up for synthesis, the 1 L autoclave needed to be leak tested to ensure that it operated safely and as expected. The system was designed to allow for control of both the temperature and pressure of the autoclave without the need to enter the room it which it was housed. The set-up is described in more detail in Chapter 2.

Leak Test 1

For the first leak test, the autoclave was pressurised with CO₂ to 41 bar before being heated to 65 °C. After heating, the autoclave had reach 65 bar. Upon attempting to increase the pressure the internal temperature of the autoclave dropped. This was due to fact that the CO₂ being pumped in was cold. Whilst pressurising the autoclave care was taken to avoid the internal temperature dropping below 50 °C and to keep any temperature fluctuations to a minimum. Due to the size of the 1 L vessel, these temperature fluctuation was more extreme than had previously been observed on the 60 mL scale. This caused the pressurising process to take time, approximately 40 minutes, which was much longer than the 15 minutes required for the 60 mL autoclave. For safety reasons, the autoclave was only pressurised to 138 bar before being left for approximately 4 hours. The data collected for the temperature and pressure is shown in Figure 4-14.

The traces show six different stages corresponding to the following periods during the process; initial pressurisation of vessel to approximately 40 bar at room

temperature (Figure 4-14, b, stage 1). This was followed by heating to 65 °C causing a gradual increase in pressure to approximately 65 bar (Figure 4-14, b, stage 2). A second pressurisation stage was required to reach test conditions of approximately 138 bar and 65 °C (Figure 4-14, b, stage 3). The autoclave was left at test conditions (138 bar, 65 °C) for 4 hours (Figure 4-14, stage 4) before the heating was switched off causing a steady drop in pressure and temperature over 4 hours (Figure 4-14, stage 5). The autoclave was vented to atmospheric pressure causing a sharp decline in the temperature (Figure 4-14, stage 6).

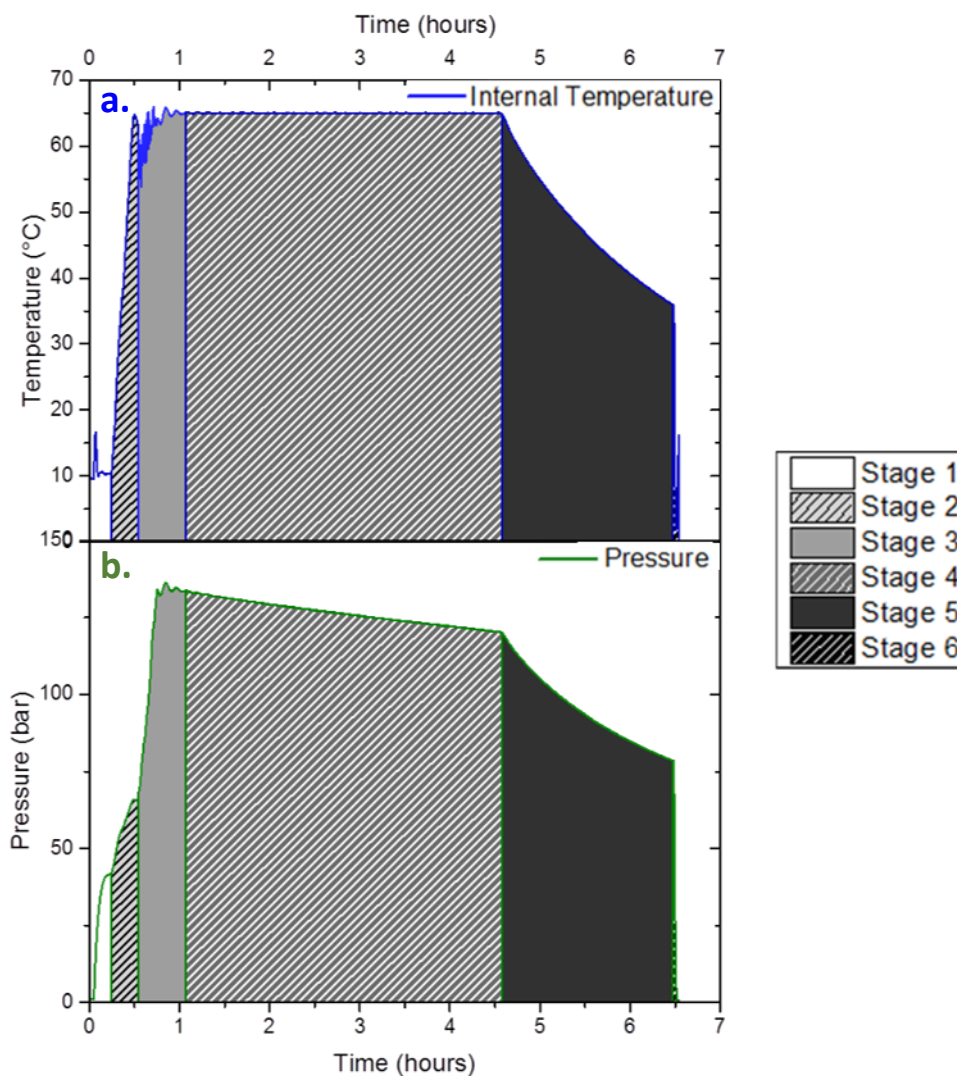


Figure 4-14: Temperature (a, blue) and pressure (b, green) data collected from the first CO₂ leak test. The vessel was pressurised and heated before being left to stabilise. The different stages of the leak test are highlighted (1-6); initial pressurisation and heating (1), heating to 65 °C (2), second pressurisation stage (3), leak test (4), cooling (5) and venting (6).

The pressure of the autoclave gradually decreased throughout the test time (Figure 4-14, b, stage 4), by approximately 10 bar in total, suggesting there may have been a small leak. However, the pressure loss was deemed insignificant over the time period and could have been due to stabilisation of the system.

As the pressurisation step took a significant amount of time, longer than the 60 mL scale (approximately 40 minutes compared to 15 minutes), the process was repeated to assess if the time could be reduced.

Leak Test 2

For the second pressure test the autoclave was initially pressurised to 48 bar, which was slightly higher than the 40 bar used for the first test (Figure 4-15, b, stage 1). It was subsequently heated to 50 °C where it was stabilised before heating to 65 °C (Figure 4-15, a, stage 2). After heating, the autoclave had reached 125 bar. Due to the increased starting pressure the subsequent pressurisation step (Figure 4-15, b, stage 2 and 3) was quicker than for test one (approximately 20 minutes) with fewer fluctuation in the internal temperature observed. Therefore, with this approach it is possible to reach reaction condition in a comparable time to the 60 mL scale.

Due to time constraints the system was left at these conditions (65 °C, 207 bar) for 30 minutes. The results suggested that the conditions were stable with only a slight fluctuation in the temperature (± 1 °C) and a small decrease in pressure (Figure 4-15, b, stage 4). Cooling the system to less than 35 °C took over 2 hours (Figure 4-15, a, stage 5), much longer than the 1 hour needed on the 60 mL scale.

During leak testing of the autoclave it was found that it was essential to start with a higher pressure of CO₂ prior to heating and that the autoclave would need to be left overnight to cool. Both of these observations were factored into the following polymerisation reactions.

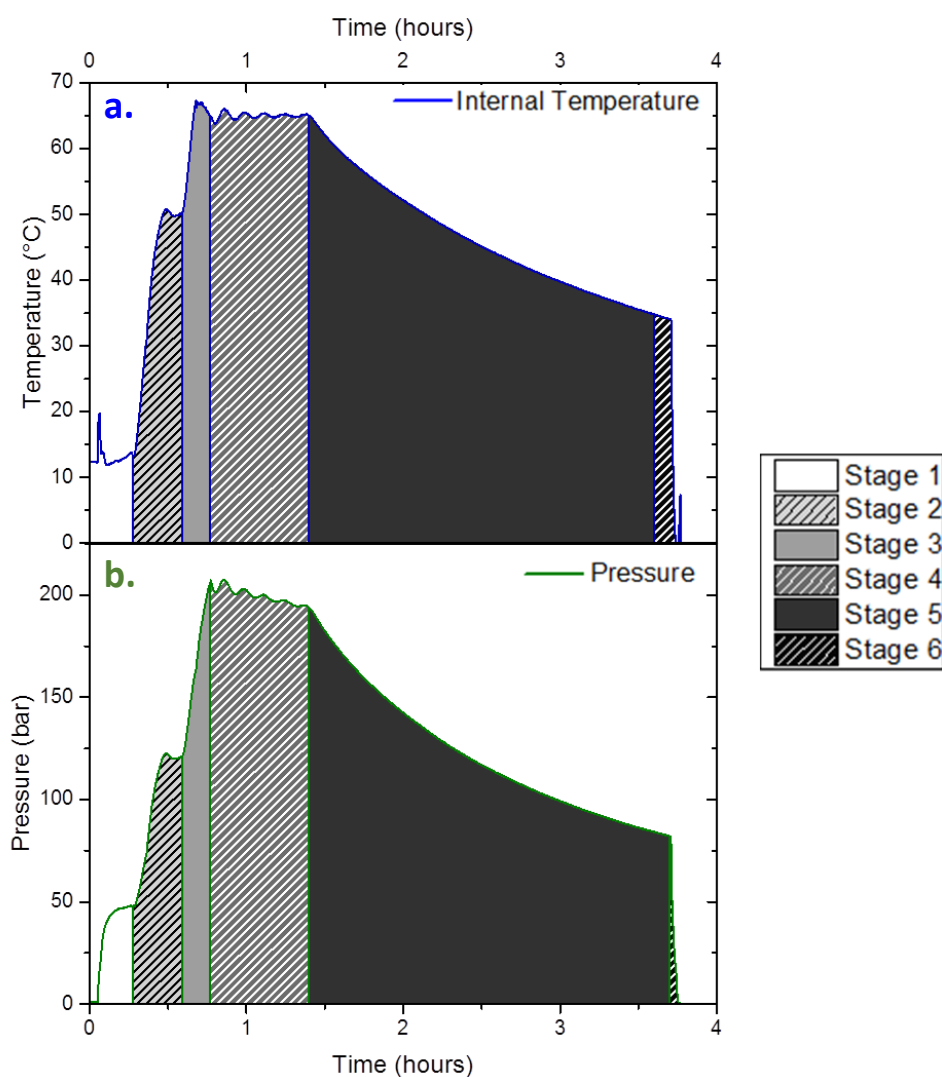


Figure 4-15: Temperature (a, blue) and pressure (b, green) data collected from the second CO₂ test. Vessel was pressurised and heated before being left to stabilise. The different stages of the leak test are highlighted (1-6); initial pressurisation and heating (1), heating to 65 °C (2), second pressurisation stage (3), leak test (4), cooling (5) and venting (6).

4.5.2.2. One-stage Reactions

The first polymerisations carried out in the 1 L autoclave were a direct scale up of the one-stage 60 mL autoclave reactions. The reagents were added to the 1 L autoclave via a syringe, as with the 60 mL reactions. The system was initially pressurised to approximately 48 bar (Figure 4-16, b, stage 1) before the temperature controller was set to 55 °C.

The pressure of the system increased rapidly (> 138 bar) with a less than 10 °C increase in temperature (Figure 4-16, stage 2). This was not in agreement with the findings from the leak tests and so at this point the temperature was set to 45 °C and heating continued 1 °C at a time, allowing for more control over the process.

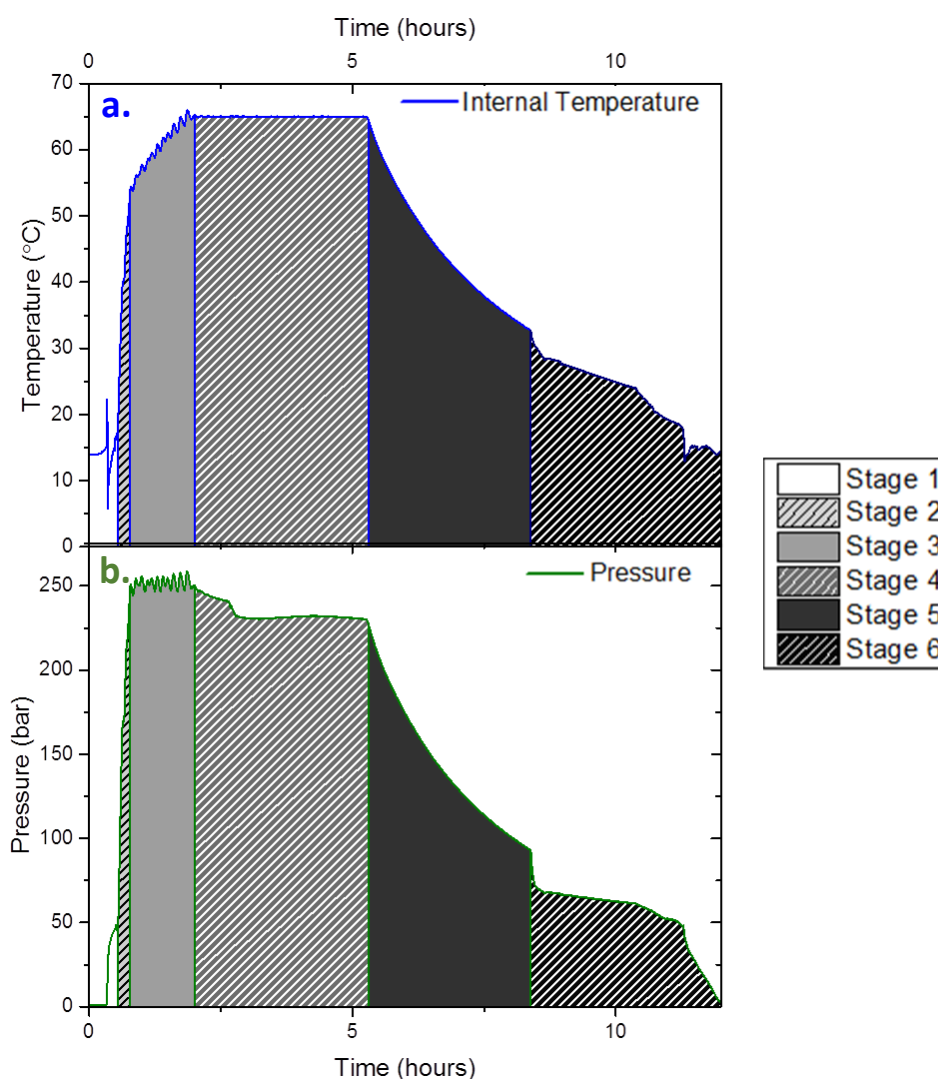


Figure 4-16: Temperature (a, blue) and pressure (b, green) data collected from the first MMA polymerisation in the 1 L autoclave. Different stages of the reaction are highlighted by the shaded areas (1-6); initial pressurisation and heating (1), heating to 65 °C (2), second pressurisation stage (3), reaction period (4), cooling (5) and venting (6).

However, this approach was very slow, taking 1.5 hours to reach 65 °C (Figure 4-16, a, stage 3), compared to the 20 minutes observed during the leak test. The reaction

was left at 204 bar and 65 °C for 4 hours (Figure 4-16, stage 4) before the heating was switched off. The vessel was then left to cool overnight (Figure 4-16, a, stage 5). Venting of the autoclave began rapidly, at the expected rate, causing a decrease in temperature. Over time the rate of pressure reduction slowed, potentially due to a blockage, caused by the formed polymer in the CO₂ outlet (Figure 4-16, b, stage 6). After a period of time the venting speed increased again suggesting the blockage had potentially become dislodged with the release of pressure. Despite the challenges experienced during the reaction set-up and venting, the temperature remained constant throughout the reaction and the change in pressure was not significant.

Once the system was vented and the temperature and pressure had returned to ambient conditions, the white powder product was collected for analysis, showing successful polymerisation had occurred (Figure 4-17). The results from analysis are discussed later in the chapter.



Figure 4-17: Images showing the product collected from the first MMA polymerisation in the 1 L autoclave. 150 g of free flowing PMMA was produced.

In order to confirm that the scale up was reproducible the reaction was repeated. For the second reaction the heating process was smoother and more comparable to that observed with the 60 mL autoclave (Figure 4-18, a). It is unknown what caused the rapid increase in pressure observed in the first polymerisation reaction. Once again, the reaction data showed six clear transitions relating to the different stages of the reaction (Figure 4-18). However, the connection with the control box was lost during the cooling stage, hence the absence of the venting stage. Throughout the

reaction the temperature remained constant; while the pressure increased gradually (Figure 4-18, stage 4). This observation has previously been reported in the literature. Wang *et al.* reported similar trends in pressure and temperature during synthesis of PMMA by dispersion polymerisation in $scCO_2$, using calorimeter to monitor the reaction.⁵⁵ Similar trends were observed, where the temperature of the reaction remained constant and the pressure steadily increased. The rise in pressure was accredited to successful polymerisation, with the rate of the pressure increase being related to the rate of polymerisation.

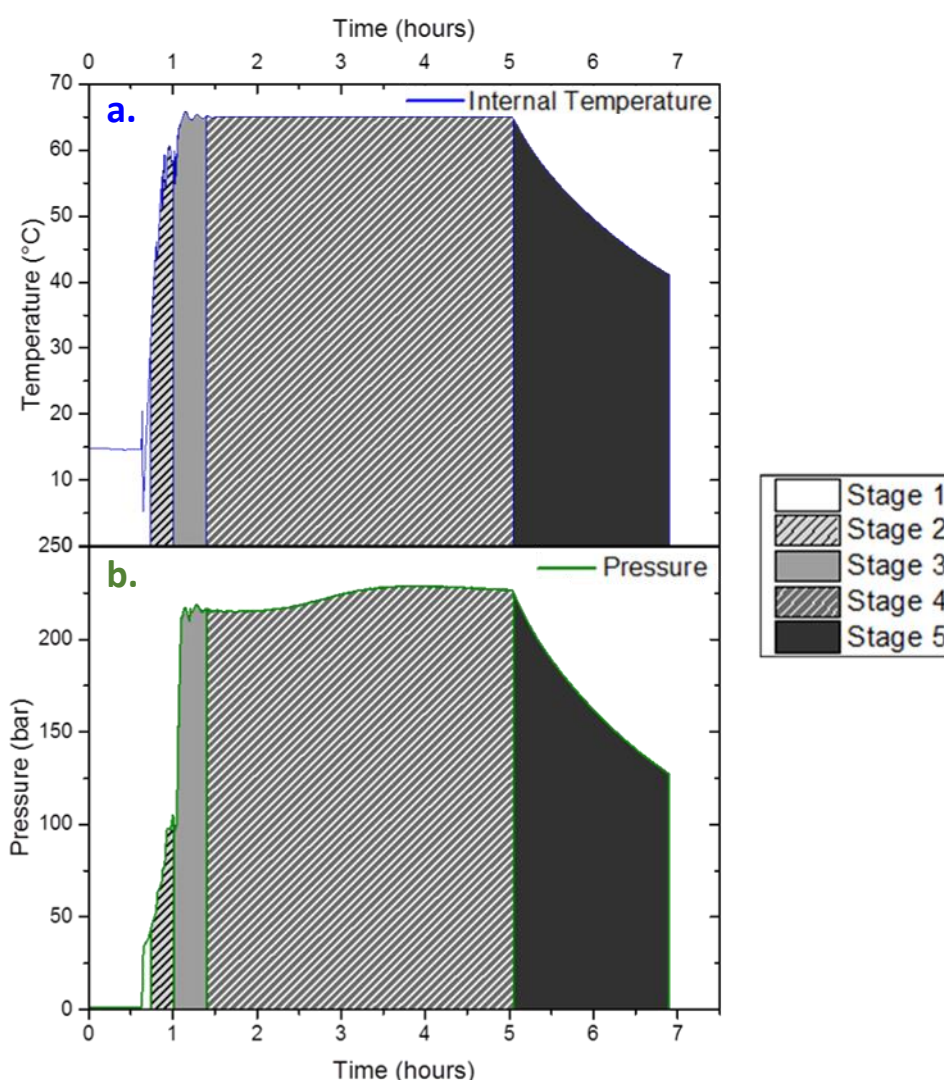


Figure 4-18: Temperature (a, blue) and pressure (b, green) data collected from the second MMA polymerisation in the 1 L autoclave. Different stages of the reaction are highlighted by the shaded areas (1-5); initial pressurisation and heating (1), heating to 65 °C (2), second pressurisation stage (3), reaction period (4) and cooling (5).

Similar trends were also observed in the polymerisation of glycidyl methacrylate in scCO_2 .⁵⁶ Lepilleur *et al.* discussed the theory behind this observed pressure increase and concluded that in a sealed reactor, changes in volume upon polymerisation will induce a pressure change. Considering the molar volume of most vinyl monomers is higher than the subsequent polymer, a reduction in pressure is expected as the reaction proceeds. However, throughout the reaction as the composition of the system changes, the volume change on mixing for each phase in the system can also change. Using extensive mathematical modelling, Lepilleur *et al.* showed how a pressure increase throughout the reaction could be observed.³⁰

During the cleaning of the autoclave after both polymerisations it was discovered that several of the pipes were blocked (Figure 4-19). This made the cleaning process time consuming and led to the need to replace many of the pipes. As this was not an ideal situation measures needed to be taken to prevent the blockage of the pipes.



Figure 4-19: Images of PMMA pellets discovered when cleaning the 1 L autoclave. Left hand image is a face on image of a blocked pipe (CO₂ outlet), right hand image shows PMMA pellets removed from several pipe joints.

A potential solution to this problem was to place filters over the end of the pipes, this would still allow CO₂ to pass through but prevent the particles from passing through, hence reducing the risk of a blockage (Figure 4-20).

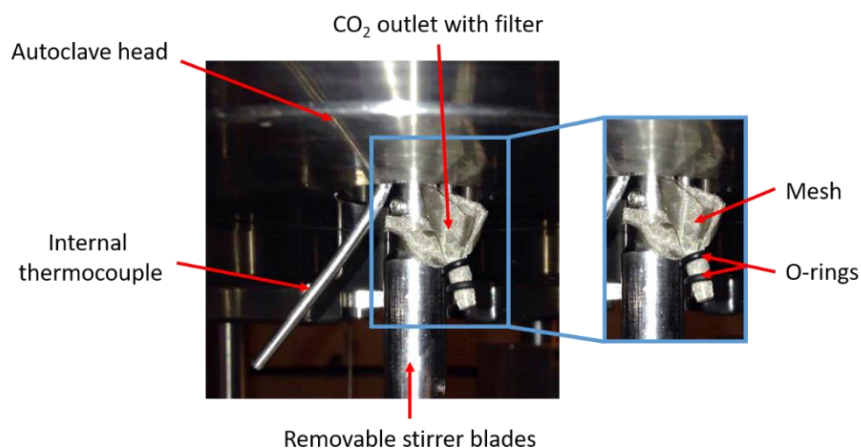


Figure 4-20: Filter system implemented on the CO₂ outlet pipe, consisting of mesh held in place by O-rings.

For the following experiment this system was implemented, and a mesh filter was placed over the CO₂ outlet pipe inside the reactor, as this was found to be the pipe that was the most susceptible to blocking. In order for this system to work, the mesh size had to be smaller than the particle size (100 μm mesh size vs. 2-3 μm particle diameter).

Upon attempting to vent the system, once again the pipes became blocked, even though the mesh filter had been placed on the CO₂ outlet pipe. It is thought that the filter had successfully prevented PMMA particles from traveling through the pipe however, MMA dissolved in scCO₂ would be able to pass through the filter and theoretically polymerise directly in the pipe. The next proposed solution was to increase the size of the outlet pipe from a $\frac{1}{8}$ " to a $\frac{1}{4}$ " pipe; the increase in pipe diameter should reduce the likelihood of blockage. Products produced during the 1 L one stage reactions were analysed as discussed in the following section (Table 4-6).

Particle Analysis

All reactions achieved high conversion (> 90%) and produced high yields of product (> 85%). DSC analysis gave similar T_g values (129 °C), that were comparable to the 60 mL products. The difference in yield and conversion is attributed to the fact that not all the product could be collected from the vessel post polymerisation as some

of it was stuck to the walls of the autoclave resulting in a lower yield. Different levels of residual monomer may have been removed during the venting processes causing the measured conversion to be higher.

Table 4-6: Data collected from PMMA particles produced using the one-stage standard reactions in the 1 L autoclave.

Entry	Yield ^a (g)	Yield (%)	Conversion ^b (%)	M _n ^c (g mol ⁻¹)	M _w ^c (g mol ⁻¹)	Đ ^c	T _g ^d (°C)	Particle Size ^e (nm)
1	127	85	93	219000	378000	1.72	127	2600 ± 1369
2	143	95	98	219000	396000	1.81	129	3660 ± 1153

^a – obtained gravimetrically, ^b – obtained from ¹H NMR, ^c – obtained from GPC system A, ^d – obtained from DSC and ^e – obtained from (SEM including standard deviation). Both reactions used MMA (150 mL), AIBN (1 wt%) and PDMS-MA (5 wt%).

The GPC traces obtained from both of the one-stage 1 L PMMA polymerisations were very similar, giving a comparable distribution of molecular weights and dispersities typical of free radical polymerisations.⁵²

Particles produced were similar in morphology to those produced using comparable conditions on the 60 mL scale (Figure 4-21).

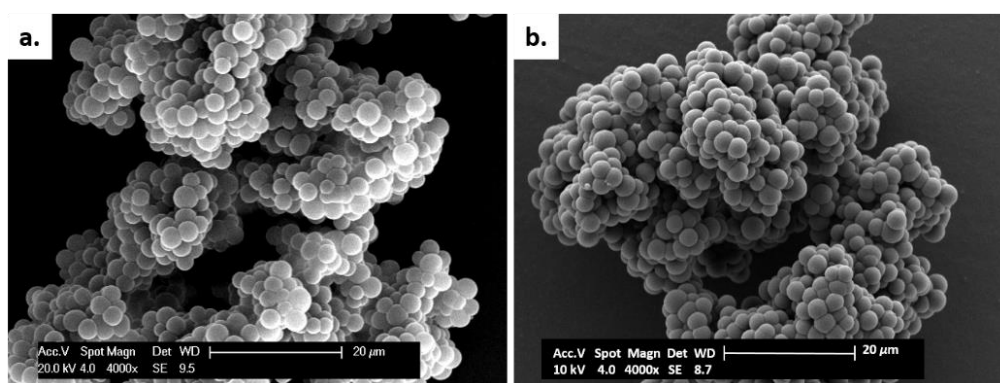


Figure 4-21: SEM comparison of particles synthesis using the standard batch reaction on the 60 mL scale (a) and 1 L scale (b), similar morphology and particle size was observed. The scale bars are 20 µm.

However, SEM images of repeat reaction show a varying degree of uniformity in particle size (Figure 4-22). All particles formed were spherical in morphology suggesting successful stabilisation was achieved. Though, reaction 2 (Table 4-6, entry 2) produced many particles of similar size but also a few much larger particles (Figure 4-22, image b).

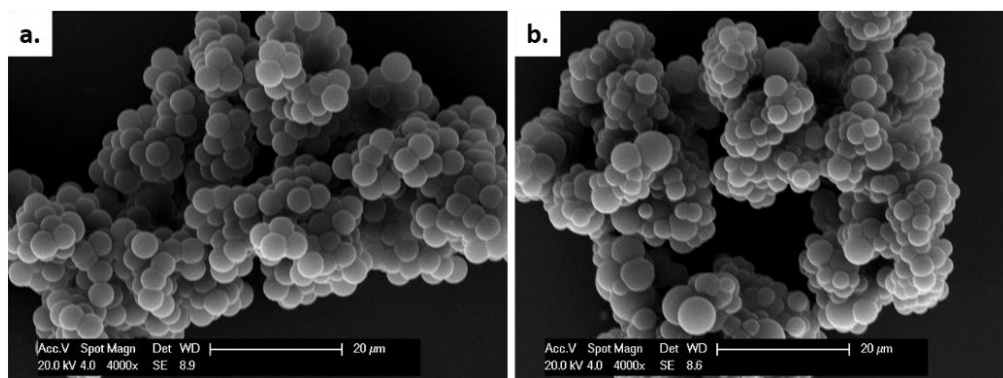


Figure 4-22: SEM comparison of particles synthesised in 1 L batch reactions (MMA 150 mL, AIBN 1 wt%, PDMS-MA 1 wt%, 65 °C, 248 bar, 4 hours); Table 4-6, entry 1 (a) and Table 4-6, entry 2 (b). A larger particle size distribution was observed for sample b. The scale bars are 20 µm.

This caused the average particle size from the reaction to be larger than the other 1 L reaction and the corresponding 60 mL reaction (3600 vs. 2500 nm). Arguably, reaction 1 (Table 4-6, entry 1) visually produced the most uniform particles (Figure 4-22, image a), with the only experimental difference being the heating, suggesting that a slower, more controlled heating may form better particles.

With particle quality in mind the next experiment used the initiator injection technique previously employed at the 60 mL scale. It was thought that the injection would allow for more control over the AIBN decomposition and give more control over molecular weight and particle structure.

4.5.2.3. Initiator Injection Reactions

The autoclave, containing the majority of the monomer and all the stabiliser, was heated to 65 °C and pressurised to 138 bar (Figure 4-23, stage 1). The vessel was

allowed to equilibrate at 138 bar, below the normal reaction pressure of 207 bar (Figure 4-23, stage 2). This allowed for any fluctuations in pressure during the injection of the initiator (Figure 4-23, stage 3).

The period of injection, highlighted in purple, caused a slight increase followed by a decrease in pressure. Generally, after the injection the pressure would be increased to 207 bar. However, because of the uncertainty in what would happen after injection, in this instance the pressure was only increased to approximately 178 bar (Figure 4-23, stage 4). This allowed for a delayed pressure increase from injecting. As the reaction proceeded post injection, the pressure steadily increased as seen before in the one stage batch reactions, indicating successful polymerisation. The reaction was left to cool overnight and vented the following day (Figure 4-23, stage 5).

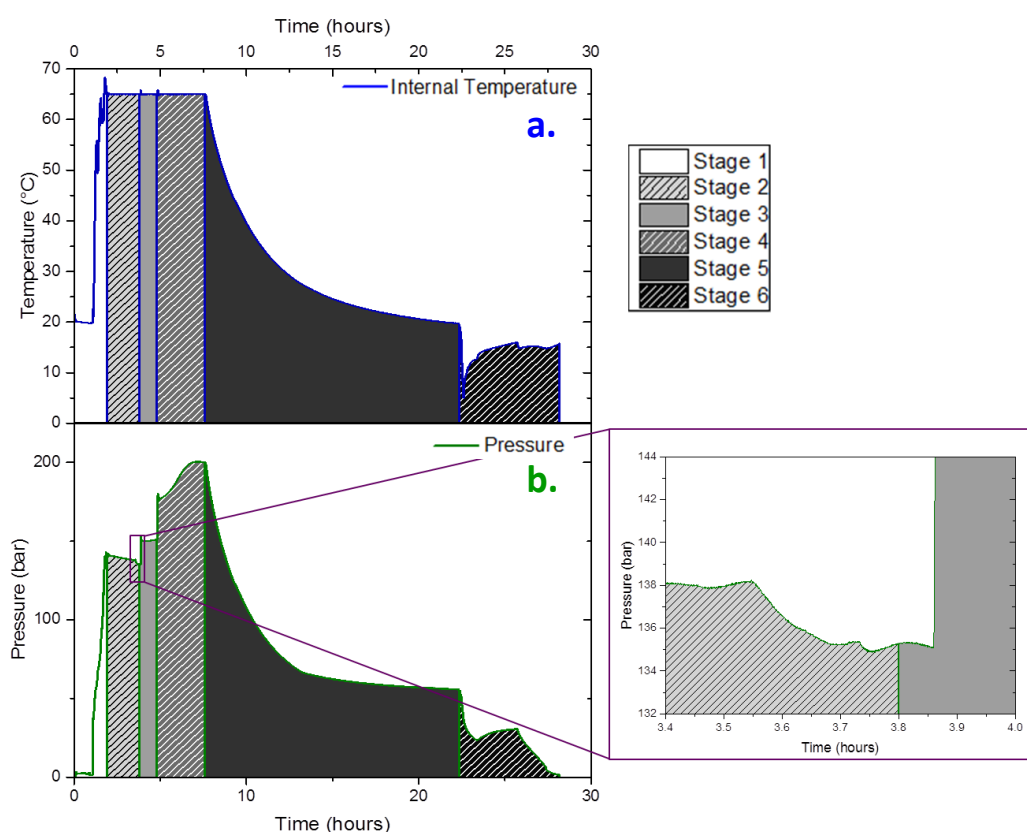


Figure 4-23: Temperature (a, blue) and pressure (b, green) data collected from the initiator injection reaction. The purple highlighted region indicates the drop in pressure induced by the injection. The different stages of the reaction are highlighted by the shaded areas (1-6); initial pressurisation and heating (1), heating to 65 °C (2), second pressurisation stage (3), reaction period (4), cooling (5) and venting (6).

For the first time the autoclave successfully vented very slowly via the actuated ball valve, suggesting that increasing the outlet pipe to a ¼" had prevented a blockage being formed (Figure 4-23, stage 6). The product was collected as a free-flowing white powder and compared to the products produced from the previous batch reactions (Table 4-7).

Table 4-7: Data collected from PMMA particles produced using the one-stage standard reaction (SR) and the initiator injection reactions (II) on the 1 L scale.

Entry	Method ^a	Yield ^b (g)	Yield (%)	Conversion ^c (%)	M _n ^d (g mol ⁻¹)	M _w ^d (g mol ⁻¹)	Đ ^d	Particle Size ^e (nm)
1	SR	127	85	93	219000	378000	1.72	2600 ± 1369
2	II	131	87	94	249000	411000	1.65	2750 ± 396

^a – corresponds to the reaction method; initiator injector (II) and standard reaction (SR), ^b – obtained gravimetrically, ^c – obtained from ¹H NMR, ^d – obtained from GPC system A and ^e – obtained from SEM (including standard deviation). Both reactions used MMA (10 mL total), AIBN (1 wt%) and PDMS-MA (5 wt%).

The GPC trace obtained for the initiator injection product was similar to that of a standard batch reaction product. Comparable dispersity and molecular weight were achieved suggesting that injection of AIBN under reaction conditions had no impact on these properties.

Comparison of SEM images showed both techniques produced uniform particles of similar size and morphology, suggesting that the AIBN injection method does not improve particle quality (Figure 4-24).

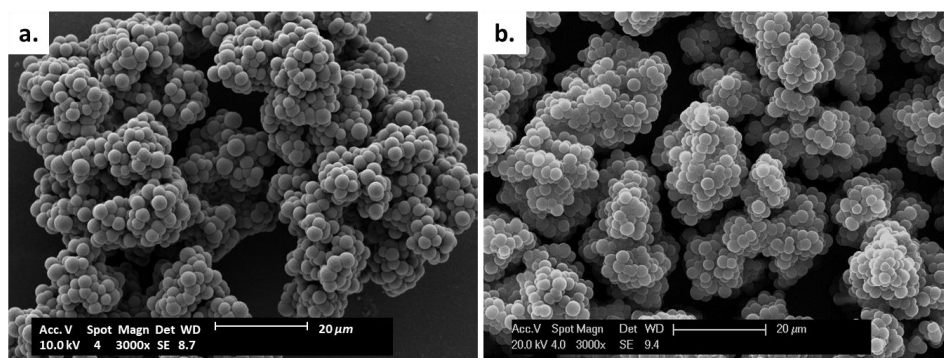


Figure 4-24: SEM comparison of particles produced from a standard one-stage reaction (a) and an initiator injection reaction (b), similar particle size and morphology was observed between the two synthesis methods. The scale bars are 20 µm.

Analysis of the SEM images gave an average particle size of 2750 nm which is similar to the standard 1 L one-stage reaction (2600 nm) but slightly higher than the comparable 60 mL initiator injection reactions (2480 nm). Since there was no obvious improvement in the particle structure with the initiator injection method all future reactions were performed using the one-stage synthesis method.

4.5.2.4. Two-stage Reactions

In line with the 60 mL scale reactions, a series of experiments were performed using the two-stage reaction method (described in section 4.4.3.2). The effect of stabiliser concentration on particle size was again studied. As with the 60 mL, three different concentrations of PDMS-MA were investigated (20 wt%, 10 wt% and 5 wt%).

At a PDMS-MA loading of 20 wt% high conversion (98%) and high yield (> 95%) were achieved for both reaction repeats on the 1 L scale. This was comparable to reaction using the same conditions on the 60 mL scale (Table 4-8). Similar molecular weights were also observed.

Table 4-8: Data collected from PMMA particles produced using a two-stage reaction with a PDMS-MA loading of 20 wt%.

Entry	Scale (mL)	Yield ^a (g)	Yield (%)	Conversion ^b (%)	M _n ^c (g mol ⁻¹)	M _w ^c (g mol ⁻¹)	Đ ^c	Particle Size ^d (nm)
1	1000	142	99	98	160000	312000	1.99	455 ± 109
2	1000	168	95	98	185000	281000	1.52	401 ± 50
3	60	7.14	84	94	254000	381000	1.50	680 ± 107
4	60	5.13	60	90	276000	383000	1.39	678 ± 127

^a – obtained gravimetrically, ^b – obtained from ¹H NMR, ^c – obtained from GPC system A, ^d – obtained from SEM (including standard deviation). The 60 mL and 1 L reactions used MMA (10 and 150 mL respectively) along with AIBN (1 wt% wrt to MMA) and PDMS-MA (20 wt% wrt MMA).

SEM analysis showed that monodisperse discrete particles had been produced at both reaction scales (Figure 4-25). A slightly smaller average particle size was

measured for the particles produced on the large scale compare to the smaller scale (455 vs. 680 nm). This difference is discussed further later in the chapter.

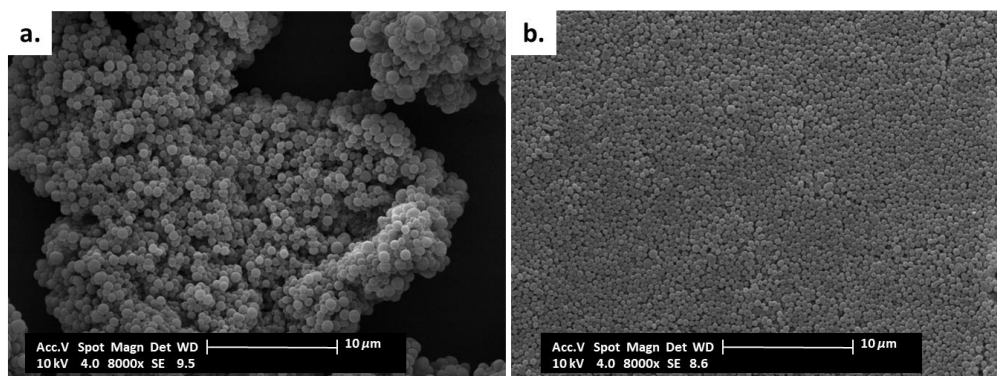


Figure 4-25: SEM images of particles produced using a PDMS-MA loading of 20 wt% in the 60 mL (a) and 1 L (b) autoclaves. Similar particle sizes were observed. The scale bars are 10 μm .

Next, in an attempt to produce larger particles the PDMS-MA loading was reduced to 10 wt%. Once again, high conversions (> 97%) and high yields (97%) were achieved at the 1 L scale and found to be comparable to that achieved at the 60 mL scale (Table 4-9). Comparable molecular weights were also observed.

Table 4-9: Data collected from PMMA particles produced using a two-stage reaction with a PDMS-MA loading of 10 wt%.

Entry	Scale (mL)	Yield ^a (g)	Yield (%)	Conversion ^b (%)	M_n^c (g mol ⁻¹)	M_w^c (g mol ⁻¹)	\bar{D}^c	Particle Size ^d (nm)
1	1000	156	97	98	200800	375300	1.87	455 \pm 109
2	1000	146	97	97	290800	467900	1.61	Bimodal
3	60	6.97	89	94	160000	299000	1.87	805 \pm 89
4	60	7.27	93	88	173600	260700	1.50	775 \pm 122

^a – obtained gravimetrically, ^b – obtained from ¹H NMR, ^c – obtained from GPC system A, ^d – obtained from SEM (including standard deviation). The 60 mL and 1 L reactions used MMA (10 and 150 mL respectively) along with AIBN (1 wt% wrt to MMA) and PDMS-MA (10 wt% wrt MMA).

SEM analysis for the first repeat of the reaction on the 1 L scale showed that monodisperse discrete particles had been produced (Figure 4-26, image b). The same could be seen for both the 60 mL scale reactions. A slightly smaller average particle

size was measured for the particles produced on the 1 L scale compare to the 60 mL scale (455 vs. 805 nm). As expected, the particles produced in the 60 mL autoclave were larger in comparison to the particles produced with a PDMS-MA loading of 20 wt% (680 nm). This trend was not observed with the particles produced on the 1 L scale, both 5 and 10 wt% loadings produced particles of 455 nm, reason for this will be explored later in the chapter.

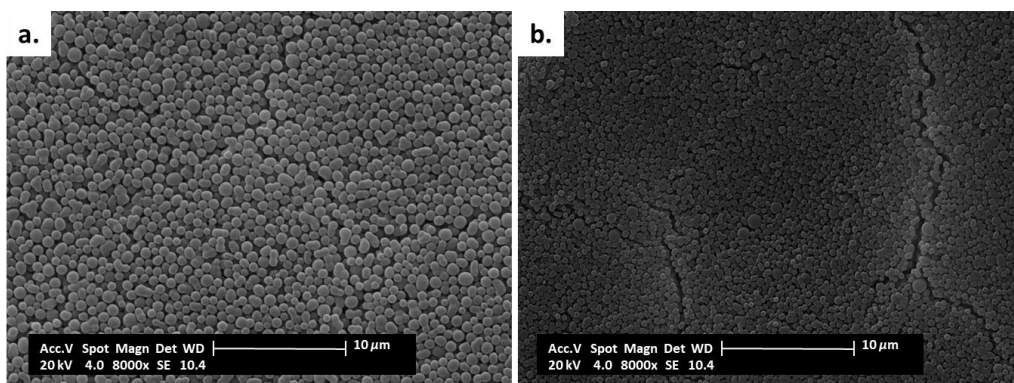


Figure 4-26: SEM images of particles produced using a PDMS-MA loading of 10 wt% in the 60 mL (a) and 1 L (b) autoclaves. Smaller particles were produced on the 1 L scale. The scale bars are 10 µm.

SEM analysis of the second 1 L reaction showed a bimodal particle size distribution with some much smaller particles being formed (Figure 4-27). This made particle size analysis difficult.

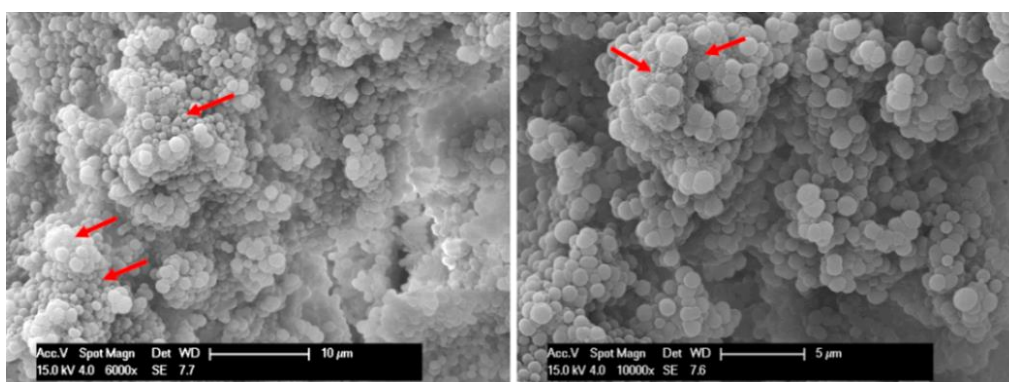


Figure 4-27: SEM images of particles produced in the second reaction repeat of PMMA synthesis using a PDMS-MA loading of 10 wt% on the 1 L scale. The arrows indicate the smaller particles being formed.

The only notable difference between the two reactions was that the stirring stopped part way through the second reaction. Upon opening the vessel at the end of the second reaction the product had formed a chunk around the stirrer and prevented it from turning. Several more repeats using these conditions were recorded, however results remained inconsistent.

To investigate whether the limit of the PDMS-MA content had been reached the stabilised loading was reduced further to 5 wt%. Both reaction repeats gave high conversion (> 95%) and high yield (> 92%), as well as similar molecular weights. All of which were comparable to the particles produced using analogous conditions on the 60 mL scale (Table 4-10).

Table 4-10: Data collected from PMMA particles produced using a two-stage reaction with a PDMS-MA loading of 5 wt%. The size of the autoclave used is indicated.

Entry	Scale (mL)	Yield ^a (g)	Yield (%)	Conversion ^b (%)	M _n ^c (g mol ⁻¹)	M _w ^c (g mol ⁻¹)	Đ ^c	Particle Size ^d (nm)
1	1000	146	98	99	296000	401000	1.56	<i>Bimodal</i>
2	1000	139	93	96	258000	379000	1.47	<i>Bimodal</i>
3	60	6.67	89	93	133000	250000	1.88	1400 ± 205
4	60	6.07	81	93	145000	222000	1.54	1192 ± 235

^a – obtained gravimetrically, ^b – obtained from ¹H NMR, ^c – obtained from GPC system A and ^d - obtained from SEM (including standard deviation). The 60 mL and 1 L reactions used MMA (10 and 150 mL respectively) along with AIBN (1 wt% wrt to MMA) and PDMS-MA (5 wt% wrt MMA).

SEM analysis of the products formed on the 1 L scale showed high levels of aggregation and a bimodal particle (Figure 4-28, image b). This was in contrast to the monodispersed particles produced on the 60 mL scale using a PDMS-MA loading of 10 wt% (Figure 4-28, image a).

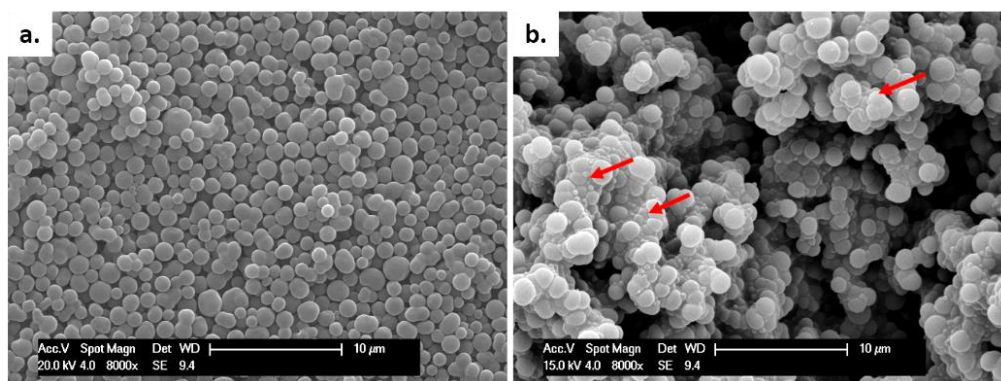


Figure 4-28: SEM images of particles produced using a PDMS-MA loading of 5 wt% in the 60 mL (a) and 1 L (b) autoclaves. The arrows indicate areas where smaller particles produced are causing aggregation. The scale bars are 10 µm.

As with the previous reactions the stirrer locked up part way through the reactions. The samples produced were more granular and less free flowing than previous samples (Figure 4-29).

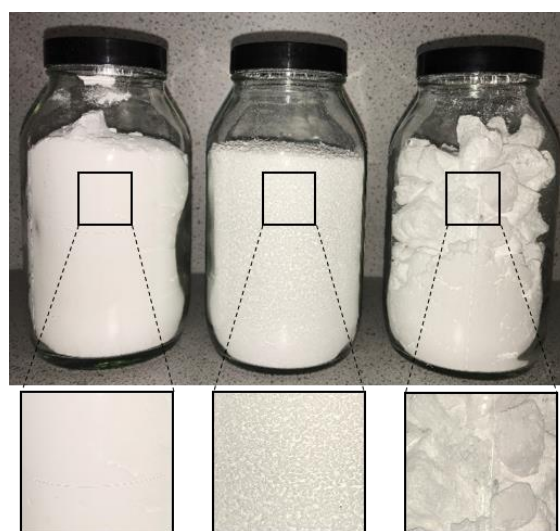


Figure 4-29: Images of samples prepared in the 1 L autoclave using the two-stage reaction technique with PDMS-MA loadings of 20 wt% (left), 10 wt% (middle) and 5 wt% (right). At lower loadings of PDMS-MA the product was more granular.

McAllister *et al.* had previously observed a broad particle size distribution of PMMA particles synthesised in sCO_2 on the 60 mL scale when the injection speed of monomer was too fast.²⁴ In this case lowering the injection speed gave a better distribution (Figure 4-30). The injection process induced changes in polymer

solubility and as well as created inhomogeneous monomer concentrations in the continuous phase. These factors were exacerbated at higher injection speeds resulting in a loss of particle control and high agglomeration.

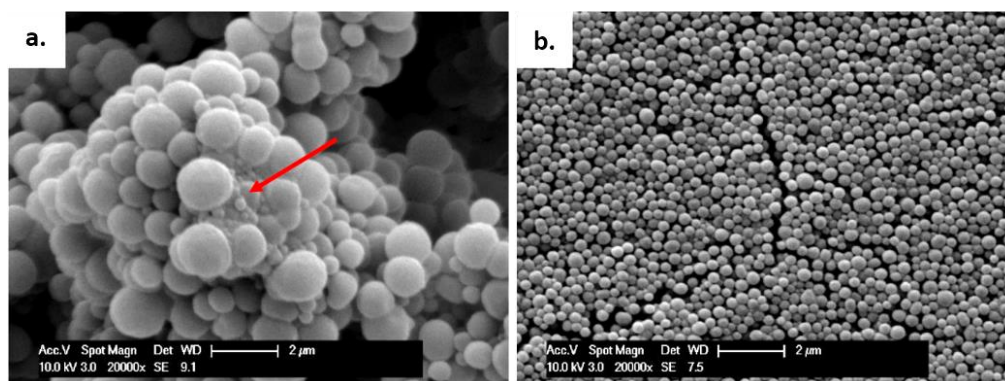


Figure 4-30: PMMA particles synthesised using a two-stage method. The injection rate was reduced from 1 mL min^{-1} (a) to 0.2 mL min^{-1} (b) with a marked improvement to particle quality.²⁴ The arrow indicates smaller particles. The scale bars are $2 \mu\text{m}$.

This was investigated on the 1 L scale by reducing the injection speed from 4 mL min^{-1} to 2 mL min^{-1} . This increased the injection time from 12.5 minutes, which had been consistent with the 60 mL scale reaction to 25 minutes. The reaction using a PDMS-MA loading of 5 wt% was used as this had been the most unreliable and therefore most likely to be affected.

The sample produced using the slower injection speed showed a bimodal distribution for particles size (Figure 4-31). Unfortunately, the bimodal distribution was more pronounced than at the faster injection speed. This effect is attributed to the change in composition of the reaction mixture during in injection and secondary nucleation.²⁴

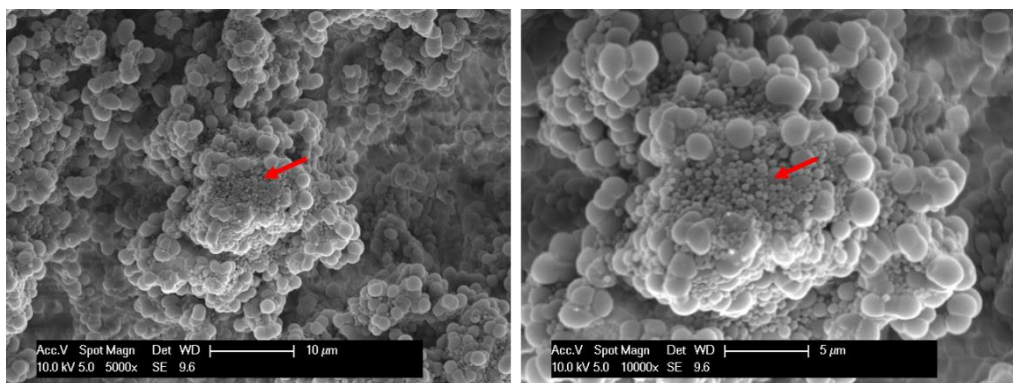


Figure 4-31: SEM images of particles produced using a PDMS-MA loading of 5 wt% in the 1 L autoclave using a slower injection speed of 2 mL min⁻¹ for the addition of MMA. The arrow indicated the smaller particles produced.

It had been noted that, in almost all the reactions in which a bimodal type particle size distribution was observed the stirrer had become locked and stopped stirring. Therefore, it was possible that this loss of stirring could be impacting the reaction and causing the bimodal distribution. To investigate this further a reaction was performed using a slower stirring speed of 100 rpm as opposed to 300 rpm. The standard one-stage PMMA synthesis was chosen as this had been the most reproducible.

SEM analysis indicated the presence of an even broader particle size distribution at 100 rpm (Figure 4-32). High levels of aggregation were also observed, making quantitative particle size analysis difficult. However, it was evident that both the stirring speed and injection speed of the monomer was affecting the quality of the particles produced.

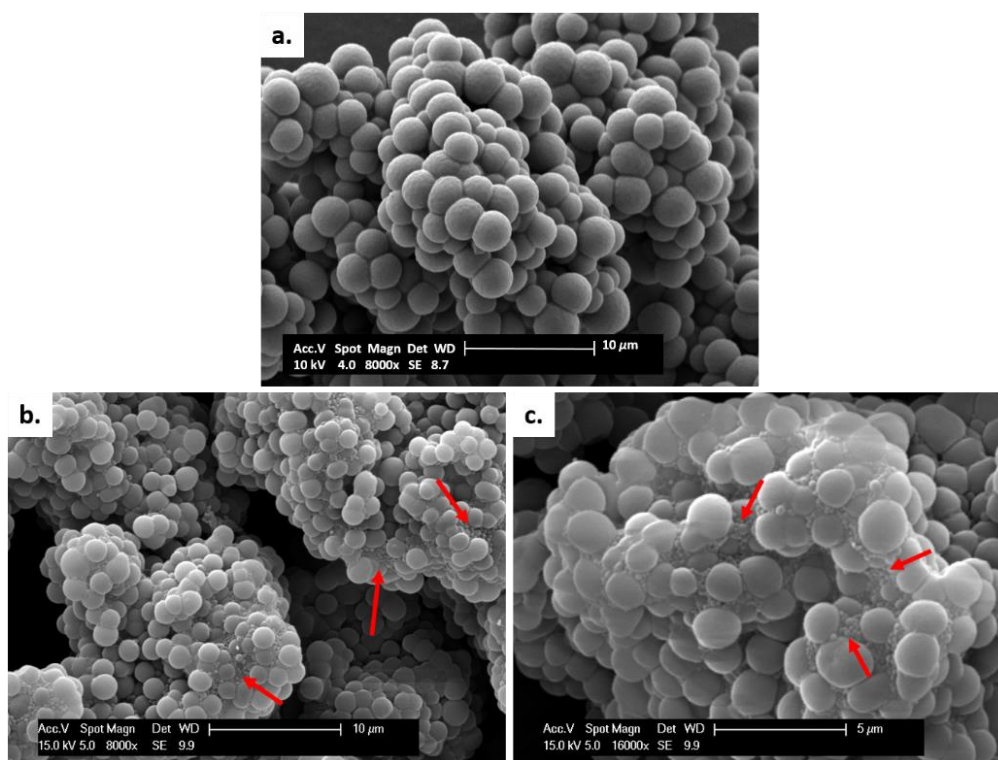


Figure 4-32: SEM images of a sample produced using standard one-stage batch PMMA synthesis with a stirring speed of 300 rpm (a) and 100 rpm (b and c). The arrows indicated the smaller particles being produced that cause aggregation.

It was noted that the stirrer used in the 1 L system contained a two-stage paddle in comparison the one-stage paddle used in the 60 mL autoclave (Figure 4-33). To investigate this further, calculations were performed by the supporting company using mixing simulation software VisiMix to assess the stirring efficiency of the 1 L autoclave. With this information a stirrer that could provide optimal mixing could be designed. There are several parameters to consider; including but not limited to speed of rotation, stirrer height, diameter of stirrer blades, clearance from the bottom of the autoclave, pitch of the blades and density of the mixing medium. Ideally laminar flow would be created by efficient stirring.⁵⁷

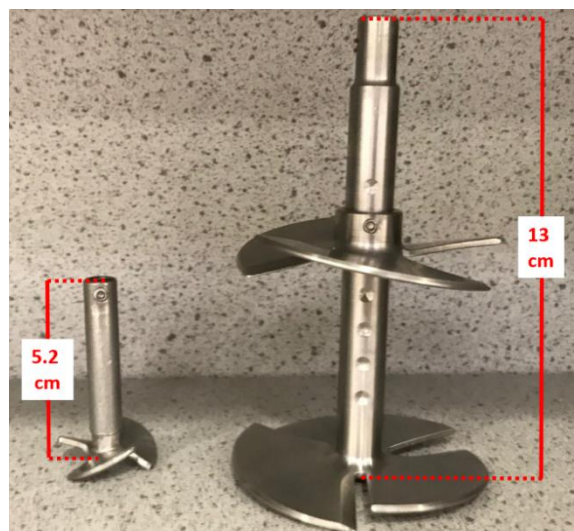


Figure 4-33: Image showing the stirrers used for the 60 mL (left) and 1 L (right) autoclaves. The 60 mL Autoclave used a one-stage paddled stirrer, whereas the 1 L autoclaves used a two-staged paddled stirrer.

The calculation for the two paddled stirrer used in the 1 L autoclave showed that inefficient turbulent flow was being created during the reaction. This was mainly because there was minimal clearance between the bottom blade and the base of the autoclave and hence there was no space to create a flow pattern below the blades (Figure 4-34, image a). Coupled with this, the pitch of the blades was too shallow, further preventing an inefficient flow pattern. The stirrer also contained two sets of blades, which were close together. Each blade set creates separate flow patterns that would induce a turbulent flow as opposed to a laminar flow (Figure 4-34, image b). All these factors would result in a non-homogeneous flow in the autoclave.

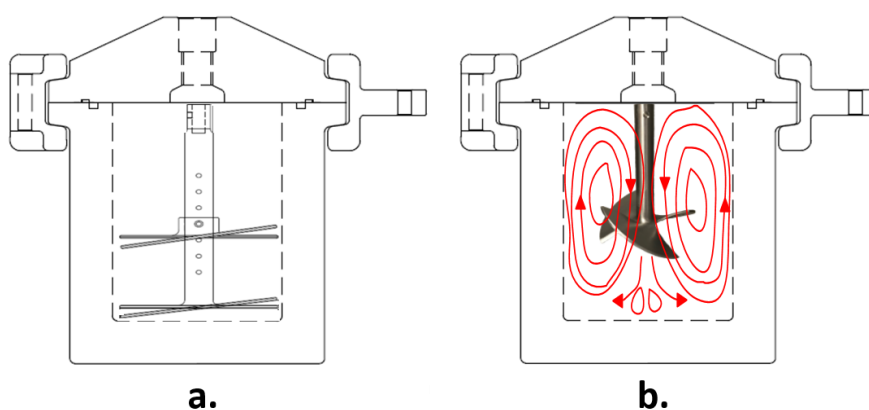


Figure 4-34: Schematic showing the stirring of the 1 L autoclave. The two paddled stirrer (a) is too close to the base and side of the autoclave, hence preventing the ideal laminar flow patten (b).

For optimal stirring to be achieved i.e. laminar flow, it was calculated that the pitch of the blade needed to be 45 °C, with a clearance from the bottom of the autoclave of $\frac{1}{6}$ to $\frac{1}{2}$ of the vessel diameter. The ratio between the diameter of the blades and the diameter of vessel needed to be between 0.7 and 1. Based on this calculation a new stirrer was fabricated (Figure 4-35).

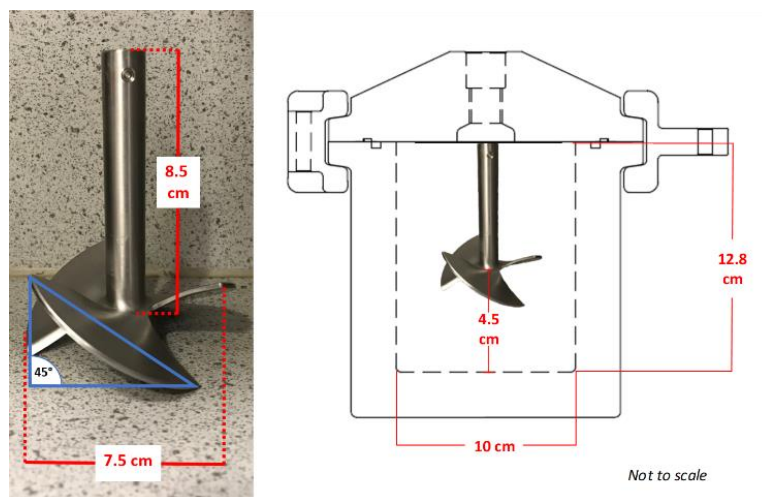


Figure 4-35: Image showing optimised stirrer fabricated using the dimensions from VisiMix calculations. Stirrer height is 8.5 cm, blade diameter is 7.5 cm, clearance from the bottom of the autoclave is 4.5 cm and blade pitch was 45 °. Images are not to scale.

All reaction conditions with the various loadings of PDMS-MA were repeated in duplicate using the new one-stage stirrer (Table 4-11). Changing the stirrer in the 1 L autoclave gave more reproducible products, which were more comparable to those seen on the 60 mL scale. A trend of increasing molecular weight as the stabiliser concentration increased was observed on both scales. In many cases this trend is not observed, as the reaction kinetics for dispersion polymerisation are typically independent of stabiliser concentration. However, this trend has previously been observed for the same stabiliser in scCO_2 .^{24, 26} McAllister *et al.* suggest the cause could be because under the conditions used the polymer phase is significantly plasticised which would allow for greater diffusion of radicals and an increased propagation time. In contrast, solvent based dispersions have conditions similar to bulk polymerisation and the viscosity of the polymer phase is high enough to prevent efficient diffusion of radicals and so termination is limited as in the Trommsdorf

effect. At a higher loading of stabiliser there would be a greater number of particles for the radicals to be divided into and hence the rate of termination would be reduced causing the chains to grow for longer. This effect is well documented for conventional emulsion polymerisation.²⁴

The 1 L scale produced particles with higher molecular weights than at comparable conditions on the 60 mL scale. This could also be due to a reduced rate of termination, which would be explained by a decrease in diffusion of polymer. In polymer kinetics, propagation is first order in polymer radical and monomer concentration and is diffusion controlled as the small monomer can diffuse rapidly. Termination is a bimolecular reaction between two large polymer radicals and hence is very susceptible to changes in viscosity as seen in the extreme case by the Trommsdorf effect.⁵⁸ The measured molecular weight will thus be very dependent on viscosity, stirring speed, reactor size, etc.⁵² To reduce the molecular weight in the 1 L reactor one approach would be to increase the number of radicals by either increasing the initiator concentration or raising the temperature.

Table 4-11: Summary of 60 mL and 1L reactions varying concentration of PDMS-MA. 1 L reactions used the new one-stage stirrer.

Entry	Scale (mL)	Method ^a	PDMS-MA (wt%)	Yield ^b (g)	Yield (%)	Conversion ^c (%)	M _n ^d (g mol ⁻¹)	M _w ^d (g mol ⁻¹)	Đ ^d	Particle Size ^e (nm)
1	60	One	5	8.3	83	88	202000	367000	1.80	2850 ± 344
2	1000	One	5	146	97	99	279000	61000	2.19	2910 ± 336
3	60	Two	0	-	-	20	-	-	-	-
4	1000	Two	0	-	-	-	-	-	-	-
5	60	Two	5	6.37	85	93	173000	304000	1.76	1300 ± 220
6	1000	Two	5	144	96	99	251000	512000	2.04	1980 ± 391
7	60	Two	10	7.12	91	91	195000	362000	1.86	790 ± 106
8	1000	Two	10	156	94	99	260000	540000	2.08	1290 ± 391
9	60	Two	20	6.14	72	92	251000	484000	1.93	690 ± 117
10	1000	Two	20	168	97	98	269300	585100	2.18	660 ± 129

^a - corresponds to the reaction technique used; one-stage or two-stage, ^b - obtained gravimetrically, ^c - obtained from ¹H NMR, ^d - from GPC system A and ^e - obtained from SEM (including standard deviation).

SEM analysis showed that discrete, well-defined particles were produced for all loadings of PDMS-MA on both scales (Figure 4-36).

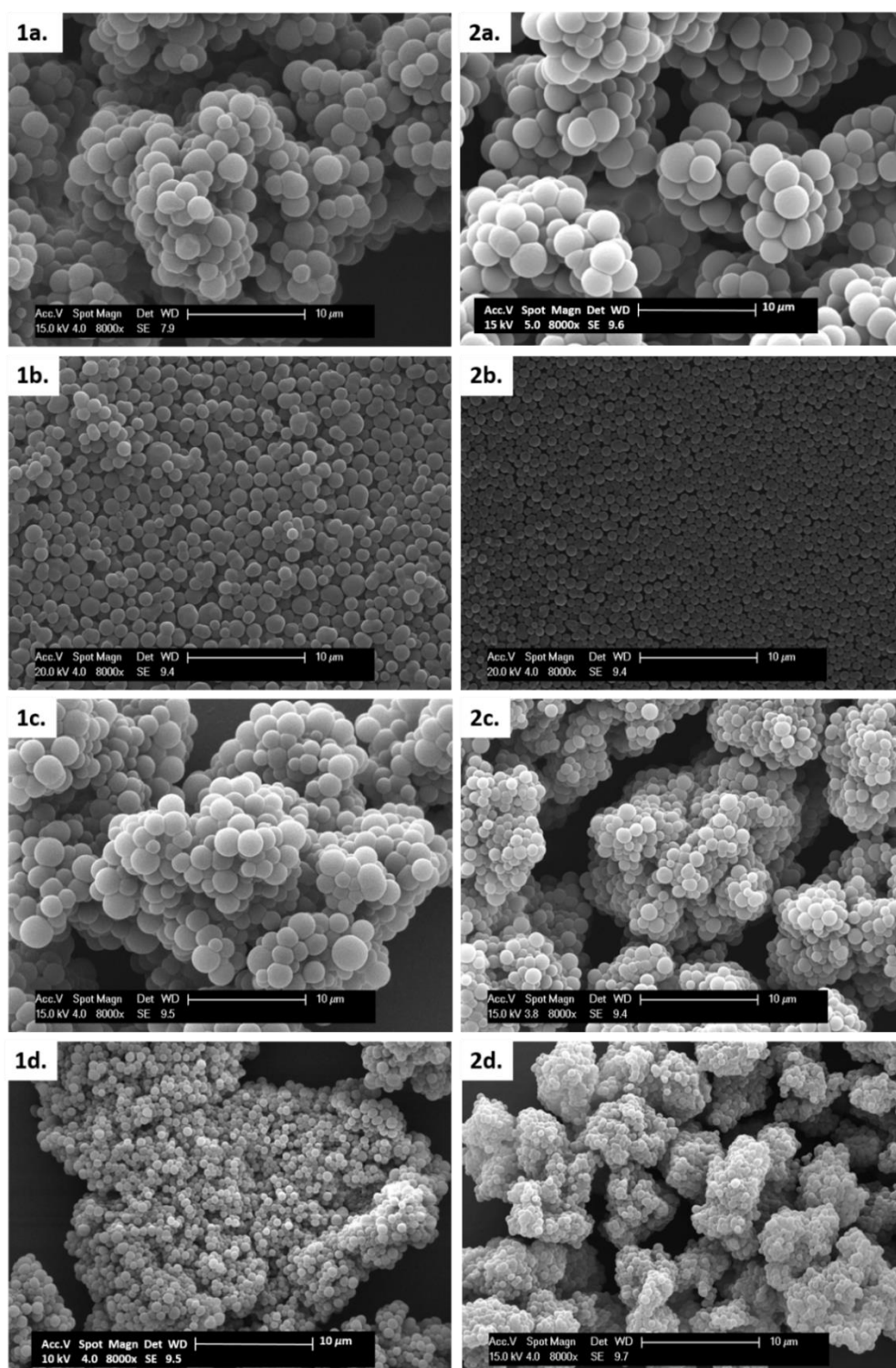


Figure 4-36: SEM images showing particles produced on the 60 mL (1) and 1 L (2) scale using one-stage batch reaction conditions (a) and the two-stage reaction technique with 5 wt% (b), 10 wt% (c) and 20 wt% (d) loadings of PDMS-MA. Comparable particles were achieved for all conditions. Particle size decreased as stabiliser concentration increased. All scale bars are 10 µm.

As expected, a trend of increasing particle size with decreasing stabiliser loading was also observed. Comparing between the two scales, the size of the particles produced on the 1 L scale were slightly larger for all loadings of PDMSMA with the exception of the 20 wt% loading. A possible explanation for this is that the time needed to take the 1 L autoclave to reaction conditions was considerably longer than the 60 mL autoclave (30 minutes vs. 10 minutes respectively). The particles nucleate in the initial period of the reaction and this difference in time could be causing bigger particles to be produced.

Alternatively, in dispersion polymerisation an increase in solvent absorption leads to an increase in particle size of the dispersed phase. MMA can act as a cosolvent for PMMA in dense phase CO₂.^{8, 24} On the 1 L scale the initial filling degree of the autoclave for the two-stage reactions is higher than the corresponding 60 mL reactions, hence the ratio of MMA:CO₂ is higher (Table 4-12). Therefore, on the 1 L scale the PMMA particles could precipitate at a higher molecular weight due to the difference in the liquid phase solubilising properties and, as a result are larger.^{8, 24}

Table 4-12: Summary of filling degree data and particle size for all condition on the 60 mL and 1 L scale.

Entry	Method ^a	PDMS-MA (wt%)	Initial Filling Degree ^b (v/v%)		Difference (%)	Particle Size (nm)	
			60 mL	1 L		60 mL	1 L
1	One	5	17.60	15.90	1.70	2850 ± 344	2910 ± 336
2	Two	5	10.83	12.99	2.16	1300 ± 220	1980 ± 391
3	Two	10	9.62	11.54	1.92	790 ± 106	1290 ± 391
4	Two	20	9.01	10.81	1.80	690 ± 117	660 ± 129

^a - corresponds to the reaction technique used; one-stage or two-stage, ^b - initial filling of autoclave with monomer surfactant and initiator and ^c - from SEM images (including standard deviation).

4.5.3. BA/PMMA Particle Synthesis in 1 L Autoclave

Due to cost, simplicity of reaction and availability of monomer the BA/PMMA core-shell particle synthesis was scaled up, using a BA loading of 27 wt%. The results of the scaled-up reaction will be compared to those seen with the analogous reaction

on the 60 mL scale (Table 4-13). BA conversion was lower on the 1 L scale (54% vs. 68%), reasons for this are unknown.

Table 4-13: Comparison of PMMA particles synthesised with an addition of BA (27 wt%) on the 60 mL and 1 L scale.

Entry	Scale (mL)	Yield ^a (g)	Yield (%)	BA Conversion ^b (%)	PBA Content ^b (%)	Particle Size ^c (nm)
1	60	7.3	75	68	22	900 ± 150
2	1000	142	89	54	19	1970 ± 311

^a – obtained gravimetrically, ^b – obtained from ¹H NMR and ^c – obtained from SEM (including standard deviation).

The product for the 1 L reaction was collected as a free-flowing white powder (Figure 4-37), similar to what was observed on the 60 mL scale. As expected, a larger amount of product was collected from the 1 L scale reaction (142 vs. 7.3 g).



Figure 4-37: Images showing the free-flowing powder produced in the 1 L autoclave from a reaction where PMMA particles were synthesised before the addition of BA (27 wt%). A yield of 142 g of free flowing white powder was obtained.

SEM analysis show that well-defined, discrete, monodisperse particles similar to those produced on the 60 mL scale were synthesised on the 1 L scale (Figure 4-38). A slightly large particle size was observed in the 1 L scale (1970 vs. 900 nm). This trend was also observed when comparing PMMA particles synthesis on the 60 mL scale and the 1 L scale using analogous conditions. This difference is attributed to the variation in initial filling degree between the 60 mL and 1 L autoclave.

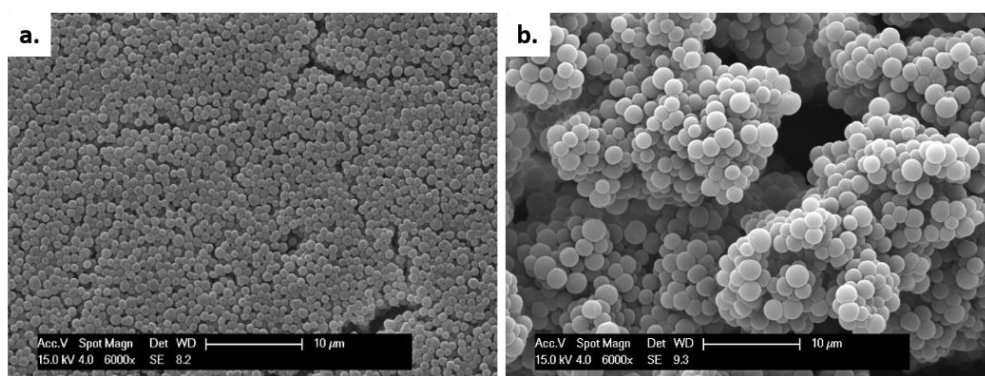


Figure 4-38: SEM images of PMMA particles synthesised with an addition of BA (27 wt%) on the 60 mL (a) and 1 L (b) scale. Similar particle morphology was observed, however smaller particles were produced on the 1 L scale. Both scale bars are 10 µm.

DMA was recorded to investigate the T_g of the sample produced and for comparison to the particles produced on the 60 mL scale (Figure 4-39).

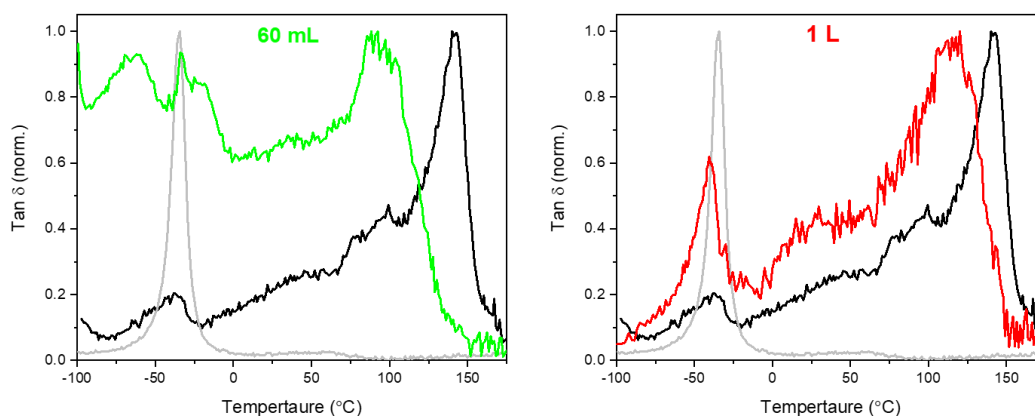


Figure 4-39: DMA of PMMA particle synthesised with an addition of BA (27 wt%) on the 60 mL (left, green) and 1 L (right, red) scale. Traced for PMMA particles (including PDMS-MA, black) and PBA homopolymer (grey) are given for comparison.

A greater shift in the “PMMA type” peak is not unexpected with the particles synthesised on the 60 mL scale (Table 4-14). This is because the conversion of BA was higher and thus the PBA content was higher which, if blended with the PMMA phase would cause a larger shift according to the Flory-Fox equation as discussed in Chapter 3, section 3.8.1. The shapes of DMA traces obtained from the samples of both are similar. As with the particles synthesised on the 60 mL scale, the shift in the “PMMA type” peak observed with the particles synthesised on the 1 L suggested that blending was occurring. However, it is difficult to tell if full phase separation is

occurring due to the overlapping T_g of the PDMS-MA present in the sample. Further insight into the internal structure present is needed, however as previously mentioned in Chapter 3, this is difficult due to the two monomers being chemically similar.

Table 4-14: Table summarising T_g s, measured by DMA, of PMMA particle synthesised with an addition of BA (27 wt%) on the 60 mL and 1 L scale.

Entry	Scale (mL)	PMMA Type T_g ($^{\circ}$ C)	PBA Type T_g ($^{\circ}$ C)
1	60	83	-32
2	1000	117	-40

GPC analysis of products synthesised on both scales showed the presence of several species, evident by the multimodal peak present in the DRI traces (Figure 4-40). The trace obtained for the 60 mL scale product suggests the presence of three species, whereas the 1 L traces suggest only the presence of two species. These species in both samples could be a number of things including: a more PBA rich species, a more PMMA rich species and a copolymer of PMMA and PBA. Both traces show the presence of PDMS-MA, indicated by the low molecular weight shoulder peak seen before in Chapter 3.

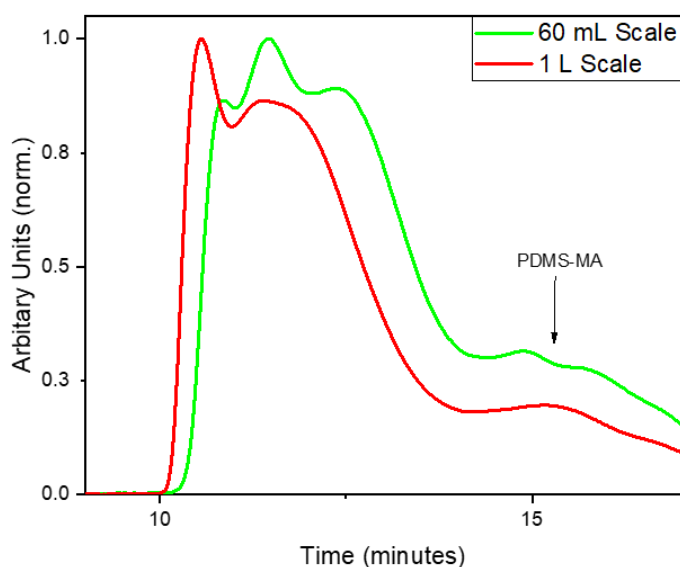


Figure 4-40: GPC traces (DRI) of PMMA particles synthesised with an addition of BA (27 wt%) on the 60 mL (green) and 1 L (red) scale. Data was collected using GPC system B.

4.6. Conclusions

PMMA particles were successfully synthesised by dispersion polymerisation using a one-stage reaction technique on the 60 mL scale. Based on previous work, this method was expanded to include a second stage, implementing the addition of a second charge of monomer after one hour. The ability to control particle size was demonstrated by varying the concentration of stabiliser, where an increase in PDMS-MA resulted in a decrease in particle size. Comparison of SEM images showed similar, uniform morphologies were obtained with average particle size ranging from 2900 nm for 5 wt% PDMS-MA to 700 nm for 20 wt% PDMS-MA. Injecting the initiator at reaction conditions gave no improvement in particle quality.

The design and implementation of a 1 L autoclave was successful and showed promise for scaling to the industrial scale. Remote monitoring and control of the system from outside the room it was housed in allowed for safe operation. The set-up was used to synthesise PMMA via free radical dispersion polymerisation. Initial experiments were inconsistent yielding unreproducible products. Increasing the diameter CO₂ outlet from 1/8" to 1/4" prevented blockages during venting of the reactor. Increasing the speed of injection of the second charge of monomer in the two-stage reaction method gave a reduction in particle quality. An investigation into stirring speed showed that reducing the stirring speed also led to a decrease in the particle quality and broad particle size distributions. Simulations showed that the mixing regime created by the two-paddle stirrer used was inefficient and following this a new stirrer was manufactured to produce optimal laminar mixing. Repeat reactions implementing the optimised stirrer gave similar molecular weights, dispersity values and particle morphologies, not only between reactions on the 1 L scale but also to the particles synthesised on 60 mL scale using comparable reaction conditions. As with the 60 mL autoclave, the size of the particles produced was manipulated by varying the amount of stabiliser. Particles ranging from 2900 nm (5 wt% PDMS-MA) to 660 nm (20 wt% PDMS-MA) were achieved. SEM analysis confirmed uniform, monodisperse particles were produced.

Following successful synthesis of PMMA particles of comparable quality between the 60 mL and the 1 L scale, scale-up of the synthesis process for particles containing a feed of BA (27 wt%) was demonstrated. DMA analysis showed similar thermal transitions were present on particles produced on the large scale compared to the small scale. Definitive confirmation of separation of the two phases (PMMA and PBA) was not possible due to the similarities in T_g s of the PBA phase and the PDMS-MA stabiliser used. Further analysis by TEM was also not possible, owing to the chemical similarity between the two phases. SEM analysis indicated particles with a slightly larger diameter were produced in the 1 L reactor. This was similar to what was seen with the PMMA particles, however reason for this observation are currently not clear.

The results presented are encouraging that further scale-up of a dispersion polymerisation reaction utilising $scCO_2$ should be possible.

4.7. References

1. C. K. Ober and K. P. Lok, *United States*, 4,617,249 Pat., 1986.
2. Q. B. Si, C. Zhou, H. D. Yang and H. X. Zhang, *European Polymer Journal*, 2007, **43**, 3060-3067.
3. F. Sommer, T. M. Duc, R. Pirri, G. Meunier and C. Quet, *Langmuir*, 1995, **11**, 440-448.
4. G. F. Wu, J. F. Zhao, H. T. Shi and H. X. Zhang, *European Polymer Journal*, 2004, **40**, 2451-2456.
5. M. Gosecka and M. Gosecki, *Colloid and Polymer Science*, 2015, **293**, 2719-2740.
6. B. Y. Shekunov, P. Chattopadhyay, H. H. Y. Tong and A. H. L. Chow, *Pharmaceutical Research*, 2007, **24**, 203-227.
7. S. Kawaguchi and K. Ito, in *Polymer Particles*, Springer, 2005, pp. 299-328.
8. S. Shen, E. D. Sudol and M. S. El-Aasser, *Journal of Polymer Science Part A: Polymer Chemistry*, 1993, **31**, 1393-1402.
9. H. Hu and R. G. Larson, *Journal of the American Chemical Society*, 2004, **126**, 13894-13895.
10. C. Boyère, C. Jérôme and A. Debuigne, *European Polymer Journal*, 2014, **61**, 45-63.
11. J. M. DeSimone, E. E. Maury, Y. Z. Menceloglu, J. B. McClain, T. J. Romack and J. R. Combes, *Science*, 1994, **265**, 356-359.
12. Y.-L. Hsiao, E. E. Maury, J. M. DeSimone, S. Mawson and K. P. Johnston, *Macromolecules*, 1995, **28**, 8159-8166.
13. A. P. Richez, H. N. Yow, S. Biggs and O. J. Cayre, *Progress in Polymer Science*, 2013, **38**, 897-931.
14. A. P. Richez, L. Farrand, M. Goulding, J. H. Wilson, S. Lawson, S. Biggs and O. J. Cayre, *Langmuir*, 2014, **30**, 1220-1228.
15. N. A. Birkin, N. J. Arrowsmith, E. J. Park, A. P. Richez and S. M. Howdle, *Polymer Chemistry*, 2011, **2**, 1293-1299.
16. D. A. Canelas and J. M. DeSimone, *Metal Complex Catalysts Supercritical Fluid Polymerization Supramolecular Architecture*, 1997, **133**, 103-140.

17. H. Shiho and J. M. DeSimone, *Journal of Polymer Science Part A: Polymer Chemistry*, 2000, **38**, 1146-1153.
18. Y. L. Hsiao and J. M. DeSimone, *Journal of Polymer Science Part A: Polymer Chemistry*, 1997, **35**, 2009-2013.
19. H. Moretto, M. Schulze and G. Wadner, in *Ullmann's Encyclopedia of Industrial Chemistry*, VCH Weinheim, 2012, vol. 32, pp. 675-712.
20. K. A. Shaffer, T. A. Jones, D. A. Canelas, J. M. DeSimone and S. P. Wilkinson, *Macromolecules*, 1996, **29**, 2704-2706.
21. M. L. O'Neill, M. Z. Yates, K. P. Johnston, C. D. Smith and S. P. Wilkinson, *Macromolecules*, 1998, **31**, 2838-2847.
22. M. L. O'Neill, M. Z. Yates, K. P. Johnston, C. D. Smith and S. P. Wilkinson, *Macromolecules*, 1998, **31**, 2848-2856.
23. P. Christian, M. R. Giles, S. M. Howdle, R. C. Major and J. N. Hay, *Polymer*, 2000, **41**, 1251-1256.
24. T. D. McAllister, L. D. Farrand and S. M. Howdle, *Macromolecular Chemistry and Physics*, 2016, **217**, 2294-2301.
25. P. Christian, M. R. Giles, R. M. T. Griffiths, D. J. Irvine, R. C. Major and S. M. Howdle, *Macromolecules*, 2000, **33**, 9222-9227.
26. M. R. Giles, J. N. Hay, S. M. Howdle and R. J. Winder, *Polymer*, 2000, **41**, 6715-6721.
27. M. R. Giles and S. M. Howdle, *European Polymer Journal*, 2001, **37**, 1347-1351.
28. M. Haruki, Y. Kodama, K. Tachimori, S. I. Kihara and S. Takishima, *Journal of Applied Polymer Science*, 2016.
29. H. S. Hwang, W.-K. Lee, S.-S. Hong, S.-H. Jin and K. T. Lim, *The Journal of Supercritical Fluids*, 2007, **39**, 409-415.
30. C. Lepilleur and E. J. Beckman, *Macromolecules*, 1997, **30**, 745-756.
31. P. F. Oliveira, R. A. F. Machado, D. Barth and E. D. Acosta, *Chemical Engineering and Processing: Process Intensification*, 2016, **103**, 46-52.
32. H. Yuvaraj, H. S. Hwang, W. S. Kim, H. G. Kim, E. D. Jeong and K. T. Lim, *European Polymer Journal*, 2008, **44**, 2253-2261.

33. F. Stassin, O. Halleux and R. Jérôme, *Macromolecules*, 2001, **34**, 775-781.
34. F. Cansell, B. Chevalier, A. Demourgues, J. Etourneau, C. Even, V. Pessey, S. Petit, A. Tressaud and F. Weill, *Journal of Materials Chemistry*, 1999, **9**, 67-75.
35. M. Perrut and J.-Y. Clavier, *Industrial & Engineering Chemistry Research*, 2003, **42**, 6375-6383.
36. S.-D. Yeo and E. Kiran, *The Journal of Supercritical Fluids*, 2005, **34**, 287-308.
37. J. M. N. Van Kasteren and A. P. Nisworo, *Resources, Conservation and Recycling*, 2007, **50**, 442-458.
38. A. E. Lebedev, A. M. Katalevich and N. V. Menshutina, *The Journal of Supercritical Fluids*, 2015, **106**, 122-132.
39. M. Herrero, J. A. Mendiola, A. Cifuentes and E. Ibáñez, *Journal of Chromatography A*, 2010, **1217**, 2495-2511.
40. C. G. Pereira and M. A. A. Meireles, *Flavour and Fragrance Journal*, 2007, **22**, 407-413.
41. M. P. Fernández, J. F. Rodriguez, M. T. Garcia, A. De Lucas and I. Gracia, *Industrial & Engineering Chemistry Research*, 2008, **47**, 1614-1619.
42. P. Manninen, J. Pakarinen and H. Kallio, *Journal of Agricultural and Food Chemistry*, 1997, **45**, 2533-2538.
43. P. A. Fleury, Charlotte, NC, 2006.
44. T. Meyer, *Organic Process Research & Development*, 2003, **7**, 297-302.
45. P. Baheti, O. Gimello, C. Bouilhac, P. Lacroix-Desmazes and S. M. Howdle, *Polymer Chemistry*, 2018, **9**, 5594-5607.
46. P. Christian, S. M. Howdle and D. J. Irvine, *Macromolecules*, 2000, **33**, 237-239.
47. A. R. Goddard, S. Pérez-Nieto, T. M. Passos, B. Quilty, K. Carmichael, D. J. Irvine and S. M. Howdle, *Green Chemistry*, 2016, **18**, 4772-4786.
48. B. Grignard, C. Jérôme, C. Calberg, R. Jérôme, W. Wang, S. M. Howdle and C. Detrembleur, *Macromolecules*, 2008, **41**, 8575-8583.
49. R. Parilti, D. Alaimo, B. Grignard, F. Boury, S. M. Howdle and C. Jérôme, *Journal of Materials Chemistry B*, 2017, **5**, 5806-5815.

50. W. Wang, M. R. Giles, D. Bratton, D. J. Irvine, S. P. Armes, J. V. Weaver and S. M. Howdle, *Polymer*, 2003, **44**, 3803-3809.
51. U. Ali, K. J. B. A. Karim and N. A. Buang, *Polymer Reviews*, 2015, **55**, 678-705.
52. G. Odian, *Principles of Polymerisation*, John Wiley & Sons, Inc., 4th edn., 2004.
53. K. P. Lok and C. K. Ober, *Canadian Journal of Chemistry*, 1985, **63**, 209-216.
54. G. Moad and D. H. Solomon, *The chemistry of radical polymerization*, Elsevier, 2006.
55. W. Wang, R. M. T. Griffiths, M. R. Giles, P. Williams and S. M. Howdle, *European Polymer Journal*, 2003, **39**, 423-428.
56. W. Wang, R. M. T. Griffiths, A. Naylor, M. R. Giles, D. J. Irvine and S. M. Howdle, *Polymer*, 2002, **43**, 6653-6659.
57. R. E. Hayes, A. Afacan, B. Boulanger and P. A. Tanguy, *Chemical Engineering Research and Design*, 1998, **76**, 73-81.
58. J. W. Nicholson, *The Chemistry of Polymers*, The Royal Society of Chemistry, 2006.

Chapter 5: Conclusions and Future Work

5.1. Overview

This chapter summarises the key findings of this work regarding the synthesis of novel core-shell particles in scCO₂. The scale-up of reactions utilising scCO₂ as the reaction medium as a step towards using this green solvent on an industrial level is also discussed. Potential areas of interest that could be expanded on in the future are outlined including analysis methods that could further probe the internal morphology present and different particle compositions that could be synthesised.

5.2. Conclusions

The synthesis of core-shell particles by dispersion polymerisation in scCO₂ has been explored and described in detail in Chapter 3, including the synthesis of particles containing either a “soft” polymer phase or crosslinking, along with a combination of both. Use in impact modification has been the focus for the application of these particles. Initial work targeted the production of particles containing a “soft” poly(butyl acrylate) (PBA) core encased in a “hard” poly(methyl methacrylate) (PMMA) shell.

Whilst SEM analysis confirmed well-defined particles had been formed with loadings of butyl acrylate (BA) up to 27 wt%, probing of the internal morphology and determining whether phase separation had occurred proved difficult. This was as a result of both the chemical similarities between the PBA and PMMA, along with the closeness in T_g of PBA (-45 °C) and the PDMS-MA (-50 °C) stabiliser used in the synthesis. To overcome this drawback, the core material (PBA) was substituted for poly(benzyl acrylate) (PBzA) to increase the contrast by the introduction of the aromatic groups. SEM analysis confirmed the formation of well-defined particles up to a loading of 36 wt% benzyl acrylate (BzA). Increasing the loading further to 50 wt%

required the addition of BzA to be carried out over two stages in order to maintain good particle morphology. Both thermal analysis, including DMA, and GPC analysis supported the conclusion that phase separation had occurred, indicating both a PBzA and PMMA phase. The presence of the aromatic ring gave the ability to probe the internal morphology formed by preferential staining of the PBzA phase of the particle before visualisation under TEM. TEM analysis of particles synthesised using both 36 and 50 wt% BzA showed formation of small domains of PBzA surrounded by PMMA. Lower loadings of BzA showed no clear internal morphology, suggesting that they would not be efficient in the application of impact modification.

Crosslinking is a key property required for particles to be used as impact modifiers. The ability to produce crosslinked PMMA particles has been demonstrated. However, synthesis of particles incorporating both a crosslinking species and PBzA (50 wt%) proved unsuccessful. SEM analysis showed loss of particle structure and high levels of agglomeration. Nevertheless, it was found that under the right conditions (time and conversion) self-crosslinking of the PBzA phase occurred. It was hypothesised that this was via intermolecular hydrogen abstraction. Initial testing of the synthesised materials is briefly summarised in the appendix.

A key area of investigation was the feasibility to increase the scale of the high-pressure reactions for potential future applications in industry. Chapter 4 focused on whether similar quality particles could be produced on a 1 L scale in comparison to the 60 mL scale. The well-studied synthesis of PMMA was used as a proof of concept reaction. A key parameter that was analysed was the particle size. Initial reactions highlighted that differences in the mixing regime of the reactors caused inconsistencies in the particles produced in the 1 L reactor. High aggregation and bimodal particle size distribution were observed with the particles synthesised in the 1 L autoclave, in contrast to well-defined particles synthesised used analogous conditions on the 60 mL scale. Calculations performed by the supporting company showed that the original two paddled stirrer used in the 1 L autoclave created an inhomogeneous flow pattern. Based on these calculations, a new stirrer was fabricated which contained only one paddle and the diameter and pitch of the blades

was altered to achieve homogeneous, lamellar flow. Previous reactions were repeated utilising this new stirrer and afforded well-defined spherical particles at all conditions tested. Ability to control the particle size through variation of the surfactant concentration was also demonstrated on both scales. Particles ranging from 690 to 2850 nm and 660 to 2910 nm were produced on the 60 mL and 1 L scales respectively.

Following successful synthesis of PMMA particles on the 1 L scale of comparable quality to the 60 mL scale, a scale up of the two-stage synthesis process for particles containing a feed of BA (27 wt%) was demonstrated. Comparable thermal and molecular weight data were observed, however SEM analysis showed that particles with a larger diameter were produced on the 1 L scale compared to the 60 mL (2000 and 900 nm respectively). Similar observations were made for PMMA particles and further experiments are needed to fully understand why particle size changes. It is hypothesised that the cause is related to the initially filling degree of the reactor being greater for the 1 L autoclave.

The work presented in this thesis has demonstrated the ability to produce novel polymer particles incorporating various components, such as a “soft” polymer phase, or a crosslinking component as well as a combination of both. Scale-up of reactions utilising scCO₂ as the reaction medium were also demonstrated, providing the ability to produce these polymer particles in a larger yield. Opportunities to further expand on this work and potentially improve the particles ability in the desired application of impact modification are detailed in section 5.3.

5.3. Future Work

Synthesis of the core-shell particles initially focused on producing particles containing a PBA core and a PMMA shell. This is the traditional composition present in particles used as impact modifiers, which are usually synthesised by conventional methods. The chemical similarities of PMMA and PBA, and the closeness of T_g 's of PBA (-45 °C) and the PDMS-MA (-50 °C) stabiliser made confirmation of phase

separation and characterisation of the internal morphology difficult. A potential solution to overcome this would be the use of AFM analysis in tapping mode. Combined with microtoming of the particles prior to analysis, similar to the sample preparation required in TEM, this technique would utilise differences in T_g s and provide a map of the internal morphology. Although this technique would still encounter the same issue of the similar T_g 's of PBA and PMMA, it is hoped that as a result of the location of the PDMS-MA (on the surface of the particle) it would still be able to provide a better understanding as to whether or not a "soft" low T_g phase was present inside the particles. This type of analysis has been demonstrated by others to characterise core-shell particles.^{1, 2} A further analytical technique that could give insight into the composition of the particles is time-of-flight secondary ion mass spectrometry (TOF-SIMS).³ This is a surface sensitive technique that uses a pulsed ion beam to remove molecules from the outer most surface of a sample. The material that is removed can be detected by a mass spectrometer enabling identification of what is present. This technique could be used to gradually remove material from the particle surface to see if the composition changes. If the particles are formed from a blend of PMMA and PBA the composition would not change. In contrast, if different phases of polymer are present the composition and hence the depth profile measured would change as more sample was removed.³

Focusing on the particles containing PBzA, further investigation into increasing the PBzA content would be of interest to see if this might improve the impact modification properties of the particles. It was shown in this work that particle quality was improved by addition of the BzA over multiple steps. However, with a loading of 60 wt%, addition of the BzA over just two-steps afforded heavy agglomeration. It could be possible to reach higher loadings of BzA by lowering the amount of BzA added in each step and increase the number of additions. This would minimise the change in composition during the injection and hopefully lead to the production of well-defined particles with no agglomeration.

Further investigations are required to better understand the crosslinking of the PBzA phase, more specifically where the crosslinking is occurring and how this could be

controlled. This could be probed by solid state, or gel phase, NMR. Both techniques have previously been reported in the analysis of crosslinked polymers.⁴⁻⁶ Electron paramagnetic resonance (EPR) could be used to investigate where the hydrogen abstraction is occurring, again this is a common technique used in polymer chemistry.⁷

Synthesis of core-shell particles in $scCO_2$ has previously been demonstrated.⁸ Therefore, another area of investigation is what other monomer systems can be used to give the core-shell morphology. A very desirable morphology suggested by the supporting company would contain a PBA core encased in a polystyrene (PSt) shell (Figure 5-1). Particles with this morphology would also have applications in impact modification. For products requiring a strong material whilst maintaining transparency, PSt is preferable over PMMA because of its higher refractive index.

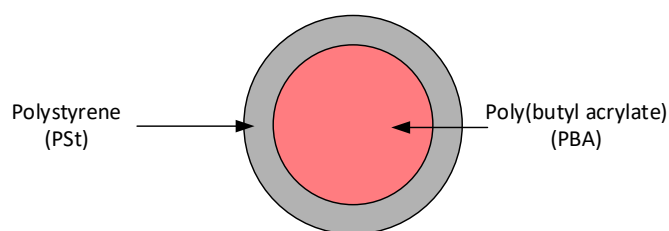


Figure 5-1: Schematic representation of a further core-shell structure of interest; PBA core encased in a PSt shell.

PSt has a T_g of 110 °C, measure by DMA. This is different to both PMMA (141 °C, measured by DMA) and PDMS-MA (-44 °C, measured by DMA), meaning that DMA analysis could be used to confirm of the presences of separate phases. The aromatic ring would also allow for preferential staining of the PSt phase prior to TEM analysis, which has previously been reported in the literature.⁹ The synthesis of PSt has already been reported in $scCO_2$,¹⁰ hence use of St as the second monomer in the two-stage synthesis outlined in this thesis should be feasible.

The work presented using the synthesis of PMMA has shown that scale-up of reactions utilising $scCO_2$ as the reaction medium are possible. Incorporation of a

HPLC pump allowed for the addition of reagents part way through the reaction whilst the reactor is under pressure. This introduces the possibility to scale-up more complex reactions. An example of this was demonstrated with the synthesis of the PMMA/PBA core-shell synthesis. The scale-up is not limited to reactions presented in this work and could be expanded further to synthesis of block copolymers via RAFT polymerisation that have already been demonstrated on the 60 mL scale.^{11, 12}

5.4. References

1. S. H. Kim, W. K. Son, Y. J. Kim, E. G. Kang, D. W. Kim, C. W. Park, W. G. Kim and H. J. Kim, *Journal of Applied Polymer Science*, 2003, **88**, 595-601.
2. F. Sommer, T. M. Duc, R. Pirri, G. Meunier and C. Quet, *Langmuir*, 1995, **11**, 440-448.
3. M. C. Davies, R. A. P. Lynn, J. Hearn, A. J. Paul, J. C. Vickerman and J. F. Watts, *Langmuir*, 1996, **12**, 3866-3875.
4. M. Andreis and J. L. Koenig, in *Advances in Polymer Science*, Springer, 1989, pp. 69-160.
5. N. M. Ahmad, F. Heatley and P. A. Lovell, *Macromolecules*, 1998, **31**, 2822-2827.
6. C. Braunschier and C. Hametner, *QSAR & Combinatorial Science*, 2007, **26**, 908-918.
7. J. Barth, M. Buback, P. Hesse and T. Sergeeva, *Macromolecular Rapid Communications*, 2009, **30**, 1969-1974.
8. T. D. McAllister, Expanding the Scope of Free-Radical Dispersion Polymerisation in Supercritical Carbon Dioxide, Doctor of Philosophy, The University of Nottingham, 2017, (*PhD Thesis*).
9. D. G. Cook, A. Rudin and A. Plumtree, *Journal of Applied Polymer Science*, 1992, **46**, 1387-1393.
10. S. Beuermann, M. Buback, C. Isemer and A. Wahl, *Macromolecular Rapid Communications*, 1999, **20**, 26-32.

11. J. Jennings, M. Beija, J. T. Kennon, H. Willcock, R. K. O'Reilly, S. Rimmer and S. M. Howdle, *Macromolecules*, 2013, **46**, 6843-6851.
12. J. Jennings, M. Beija, A. P. Richez, S. D. Cooper, P. E. Mignot, K. J. Thurecht, K. S. Jack and S. M. Howdle, *Journal of the American Chemical Society*, 2012, **134**, 4772-4781.

Appendix

Analysis and Testing of Core-shell Particles

Overview

Chapter 3 discussed the development of a novel method for synthesising two phase core-shell particles using scCO₂ as the reaction medium. Excellent control over the particle size and loading of various components was demonstrated. In this final phase of the thesis, the next key step was to record very early stage measurements of the potential of these particles for use in impact modification applications. The successful synthesis of particles containing a soft component (PBzA) within the hard PMMA and the introduction of crosslinking provided the opportunity to test the materials against commercial samples once incorporated in a PVC formulation. Three particle structures were tested; PMMA particles with a crosslinked shell and the PMMA particles obtained with addition of 36 and 50 wt% BzA. All of the particles that had been synthesised using scCO₂ as the reaction medium, were compared to commercially available particles synthesised by the supporting company. A range of standard industrial tests were used. Properties including gelation, matting ability and transparency were measured along with impact resistance. Tests were carried out at the supporting company and allowed key information to be gained about the structure of the particles synthesised that supported the data obtained in Nottingham. Testing of the materials at the supporting company gave access to industrial standard test methods and equipment not available at Nottingham.

Background

Testing of new materials prior to use in a specific application is very important. It ensures the integrity of the material under extreme conditions, such as temperature and force that it may experience during its use. Areas of weakness can be highlighted

during testing that can be improved upon through modification. Depending on the use of the material, there are a wide range of tests that can be performed such as; rheology, tensile testing, thermal shock testing, pressure testing and mechanical shock testing, to name a few.¹ It is intended that the materials synthesised in this thesis will be used for impact modification. Hence, testing will mainly focus on the tensile properties observed when the synthesised particles are blended with PVC, however other tests were also performed. The properties that will be tested are discussed in the following sections.

Brabender Gelation

An important property to consider when processing polymers is viscosity. Viscosity is the measure of a fluid's resistance to deformation at a given rate.² This can be investigated using rheology; the study of deformation and flow of matter under an applied stress.

Prior to shaping into a specific thermoplastic part, formulations of PVC including any additives such as impact modifiers or processing aids, must undergo mixing. It is well known that the properties of the part produced depend on the composition of the PVC formulation, as well as on the conditions at which it was processed.^{3, 4} During processing, the PVC formulation undergoes a process called gelation (Figure A-1), which affects its viscosity. Gelation is the transition from the PVC grain structure to a melted form and can also be known as fusion.^{5, 6} PVC grain is made up of an agglomerate of smaller primary particles of PVC.

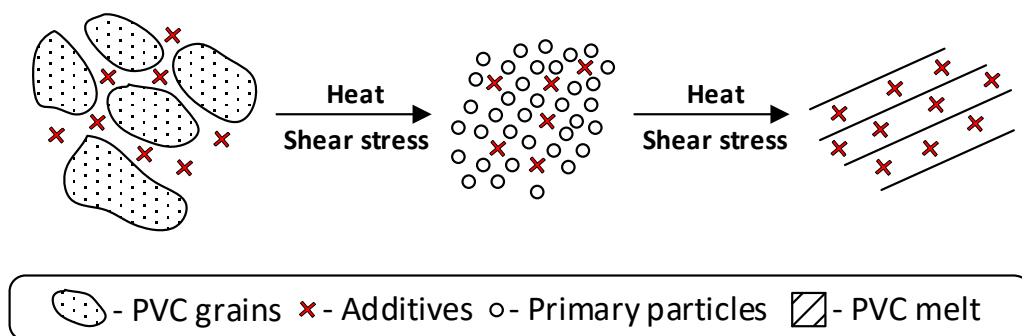


Figure A-1: Schematic representing gelation in PVC caused by torque rheometry; grains are mixed with additives before being broken down into their primary particles followed by formation of a PVC melt. Image adapted from Marques et al.⁷

This process requires shear (force) along with heat and consists of four phases; compaction of the PVC powder, breakdown of the grain into primary particles, fusion of the crystallites in the primary particles and recrystallisation.⁸ The gelation of a mixture is accompanied by a sudden increase in viscosity.⁹ Poor gelation can lead to the formation of brittle areas within the material.¹⁰

The progression of gelation of a formulation can be measured using a torque rheometer, also known as a Brabender mixing measurer. This consists of a heated mixing chamber containing two counter-rotating blades which can be rotated at various speeds (Figure A-2).^{10, 11} The mixer can be used to simulate flow conditions experienced by a melted polymer during its time in a processing machine. PVC gelation is induced by rotation of these blades, which causes heating of the polymer, and its intensive mixing by shearing.¹⁰ This allows for recording of the time-dependent changes of the torque, necessary for the characterisation of the progress in the gelation of the PVC formulation. Measurements of the melt temperature throughout the process allow for continuous observation of torque in the shearing of a polymer with a range of temperatures and shear rates.¹⁰

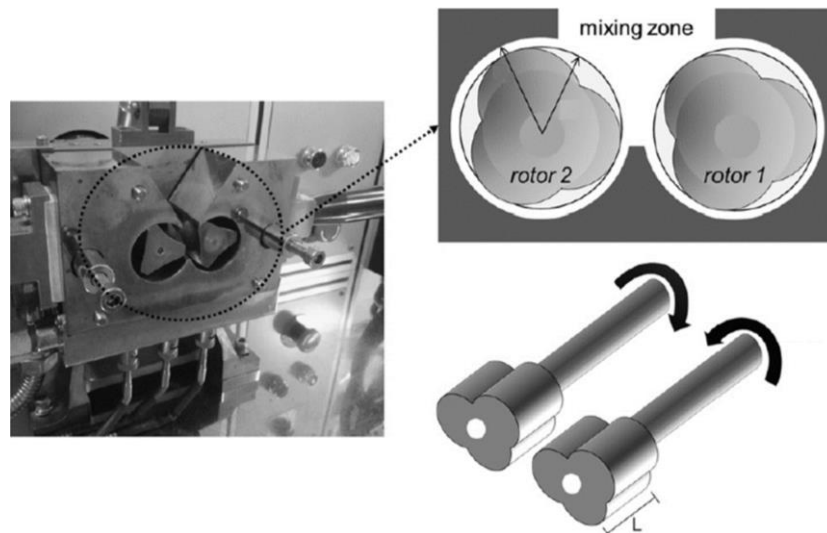


Figure A-2: Images showing the inside of a Brabender torque rheometer including the heated mixing chamber and blades used to induce shear and in turn gelation. Image adapted from Choi *et al.*¹¹

Gelation can be measured by two parameters; degree of gelation and speed of gelation. The degree of gelation is measured visually during processing and can also be measured post gelation by DSC. The speed of gelation can be calculated from the Brabender plastograph (plot of torque vs. time), using the gradient of the trace (Figure A-3).^{10, 12} There are several points of interest on the curve; loading of the sample into the mixing chamber which causes a significant increase in torque (Figure A-3, A), the minimum torque which is commonly noted as the beginning of gelation (Figure A-3, B), a curve maximum indicating the highest torque (Figure A-3, X) and the end of the measurement often known as the equilibrium (Figure A-3, E).¹⁰ All these points provide useful information about the processing of the polymer tested under defined conditions.

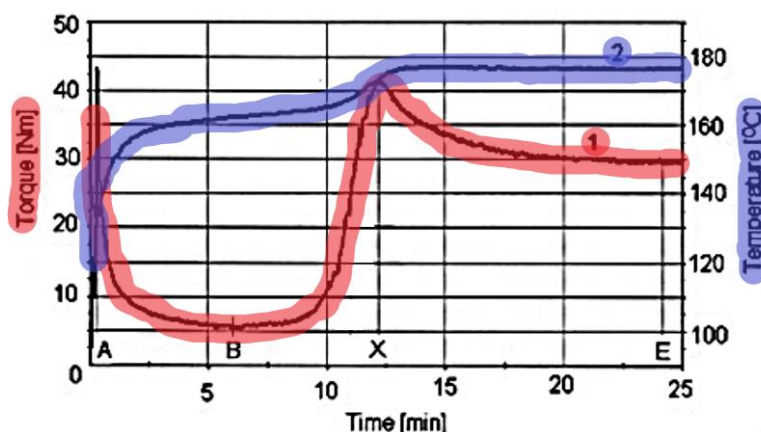


Figure A-3: Typical torque rheometer process curve for rigid PVC; curve 1 (highlighted red) shows the loading of the sample (A), minimum torque (B), maximum torque (X) and the end of the test, often known as the equilibrium (E). Curve 2 (highlighted blue) shows the temperature throughout the process.¹⁰

Transparency

Another important material property to consider is optical transparency. For some applications, a transparent or semi-transparent material is required. Incorporation of polymer particle additives can alter the transparency of a material if the particles are bigger than the wavelength of light.¹³ Transparency refers to the optical distinctness with which an object can be seen when viewed through a film or sheet of a material such as glass or plastic and is measured using a spectrophotometer.¹⁴ The transparency of a material is measured by its total transmittance (T_r), which is the ratio of transmitted light (I) to the incident light (I_0) (Equation A-1).¹³ This is influenced by two factors; reflection and absorption.

$$T_r = \frac{I}{I_0} \quad \text{Equation A-1}$$

A further parameter associated with transparency is haze.¹⁴ When light hits a surface three things can occur; the light is reflected, refracted or it passes straight through the material. Light passing through the sample is important when considering transparency and it can be affected by irregularities in the material, such as poorly

dispersed particles, contaminants (e.g. dust) or air spaces. These all result in the light passing through to be scattered in different directions. The extent to which this occurs depends on the size of the irregularities present. Small irregularities cause the light to scatter or diffuse in all directions, resulting in a loss in clarity. This can be thought of as “see through quality” and is also known as narrow angle scattering. Large irregularities cause the light to be scattered forward in a narrow cone, causing haze as a result of the loss of transmission contrast.^{14, 15} This is known as wide angle scattering.¹⁶ There are two types of haze that can occur in a material; reflective haze which occurs when the light is reflected from the surface of the material and transmission haze which occurs when light passes through a material.¹³ In this thesis only transmission haze was considered. Haze is calculated using Equation A-2, where T is transmission (%).

$$\%Haze = \frac{T_{Diffuse}}{T_{Total}} \times 100 \quad \text{Equation A-2}$$

Along with haze, a closely linked property to transparency is matting. The phenomenon of matting is commonly used to decrease the gloss of a surface and is related to the scattering of light, often as a result of the surface roughness. The occurrence of matting is an important property to consider when incorporating particulate additives into a material, as it is not always desirable. However, additives known as matting agents can be incorporated into a material to deliberately form a ‘matt’ surface finish.

Particulate additives can also affect the colour of a material. An additional parameter that can be measured using a spectrophotometer is the yellowness index (Y_i). This describes the change in colour of a test sample from white to yellow and is measured relative to white magnesium oxide. It is often used to evaluate colour changes in a material caused by real or simulated outdoor exposure.¹⁷ It is calculated from Equation A-3, where X_{CIE} , Y_{CIE} and Z_{CIE} are the tristimulus values obtained from the spectrophoto-measurement.¹⁸

$$Y_i = \frac{[100(1.28X_{CIE} - 1.06Z_{CIE})]}{Y_{CIE}} \quad \text{Equation A-3}$$

A positive value indicates the presence and magnitude of yellowness, whereas samples with a negative value would appear bluish.¹⁸

Tensile Strength and Impact Testing

There are several tests that can be used to investigate the strength of a material, such as the Izod, Charpy and tensile tests. Properties including ultimate tensile strength, breaking strength and maximum elongation can be measured by tensile strength tests. Specimens used for this type of testing take a “dog bone” shape (Figure A-4). These specimens are clamped at either end (usually vertically) and stretched.¹⁹

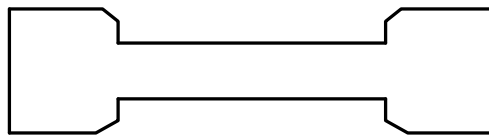


Figure A-4: Schematic of a specimen used for tensile strength tests, usually called a “dog bone”.

The Izod and Charpy test are used to measure the impact resistance of a material. For these tests, samples are made into a bar containing either one or two notches, which helps concentrate the stress and encourage fracture (Figure A-5). Both methods use a three-point bend configuration and the main difference between the two is how the test specimen is clamped. For the Izod test the bar is vertical, whereas for the Charpy test the bar is horizontal. The energy needed to break the sample under specific conditions such as specimen mounting, notching and pendulum velocity at impact is measured in both tests.^{20, 21}

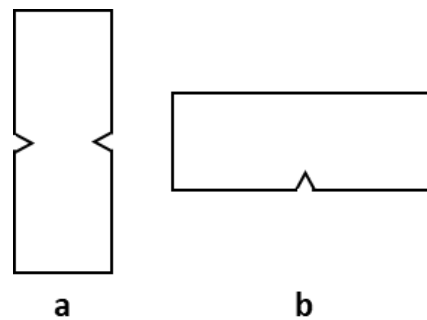


Figure A-5: Images showing specimens used for testing by the Izod or Charpy impact test. The bar sample contains a notch which helps concentrate the stress and encourage fracture: double notched (a) or single notched (b).

The apparatus used to test the specimen consists of a weighted pendulum, which is dropped from a specific height to make contact with the bar. The energy transferred to the material can be calculated by comparing the difference in height at which the pendulum starts and the swing height after fracture. Testing can be performed at both ambient and reduced temperature. For the Izod test, the notch is located on the same side as the impact (Figure A-6), in contrast in the Charpy test the notch is located on the opposite side to the impact. For this reason, Charpy values have a significantly higher impact strength than Izod values.^{20, 21} Several factors can influence tensile strength such as formulation, incorporation of additives, temperature, compounding and moulding conditions. PVC bar specimens containing the particles synthesised in this thesis as additives were tested using the Izod impact test.

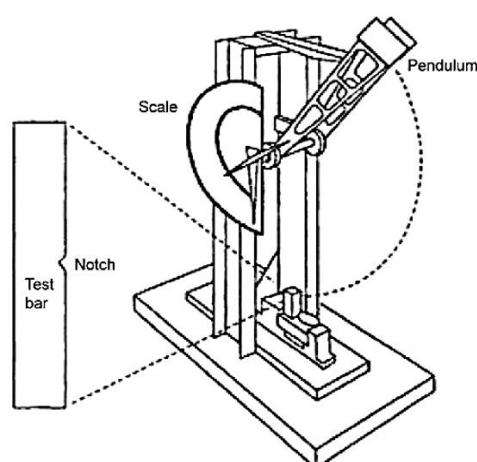


Figure A-6: Image showing the equipment used for an Izod impact test along with the test specimen.²⁰

Aims and Objectives

The aim of this work was to take promising core-shell materials synthesised in $scCO_2$ and perform material tests on the resulting PVC-particle formulation. Various tests were recorded on the formulations produced including; Brabender gelation, transparency and the Izod impact test. Particles synthesised in $scCO_2$ (Figure A-7 images a and b), were tested and compared to a particle structure synthesised by the supporting company (Figure A-7, image c).

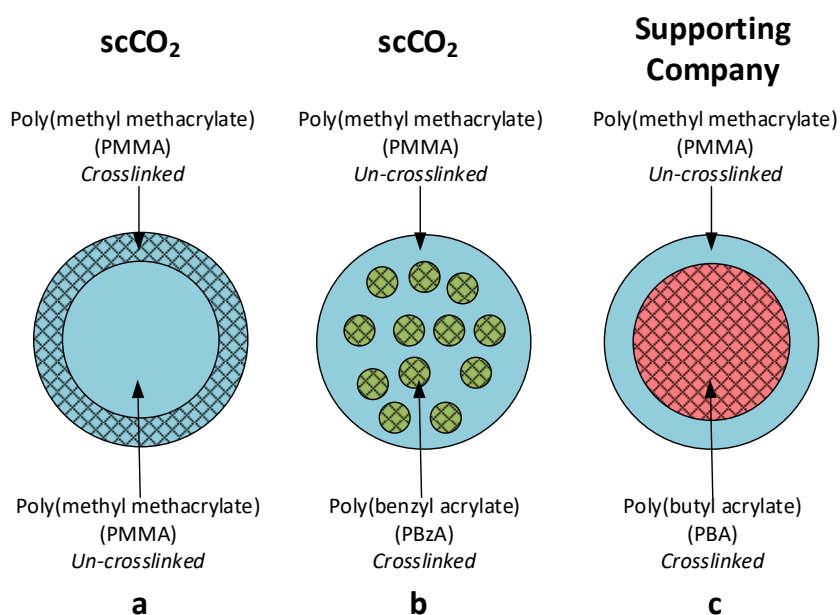


Figure A-7: Schematic showing the structure of the particles tested. Particles synthesised in $scCO_2$ (a and b) and in traditional solvents by the supporting company (c).

Tests were carried out at the supporting company where stated. Conclusions were drawn from the data about the structure of the particles, to complement the experimental information collected in Nottingham.

Experimental

Testing Methods

Testing of the samples was carried out at the supporting company using typical test methods. Test specimens were made following standard procedures. In the following sections, descriptions of the production of the test specimens and the parameters used for each test are given. The PVC formulation into which the synthesised particles were mixed was dependent on the application, for example, different grades of PVC were used for the test corresponding to matting efficiency in comparison to the Izod impact test. This was because of the fact that transparency is important for matting, but not necessarily for thermoplastics designed to withstand impact. Parts per hundred rubber (phr) is used by the supporting company to represent the amount of ingredients used. The base PVC matrix is always 100 phr and the amount of each component that is added is calculated in relation to this. For confidentially reasons, specific chemical structures for the individual components are not given, instead the purpose of the component is given (e.g. stabiliser).

Brabender Gelation

For the Brabender gelation measurements the synthesised particles were added to PVC matrix formulation (Table A-1) before being mixed using the Brabender torque rheometer (described in the introduction).

Table A-1: Summary of the formulation used in the Brabender gelation measurements.

Component	Amount (phr)
Base Resin (PVC)	100
Stabiliser 1	1.5
Stabiliser 2	1.5
Lubricant 1	1.0
Lubricant 2	0.5
Processing aid	2.5

The parameters that were applied during the test are summarised in Table A-2.

Table A-2: Summary of parameters applied during the Brabender gelation measurements.

Parameter	Conditions
Temperature ($^{\circ}\text{C}$)	160
Rotation Speed (<i>rpm</i>)	30
Additive Amount (<i>phr</i>)	2.5
Chamber Filling (<i>g</i>)	52

Matting Properties

A further property that can be adjusted by using additives is matting. An important characteristic to consider with matting is transparency. In order to measure the transparency properties, sheets and press plates were made from the PVC formulation containing the particles (Table A-3).

Table A-3: Summary of the formulation used to make the test specimens for transparency measurements.

Component	Amount (<i>phr</i>)
Base Resin (PVC)	100
Stabiliser 1	1.5
Stabiliser 2	1.5
Lubricant 1	1.0
Lubricant 2	0.5
Processing aid	2.5

This formulation was rolled into sheets using a roll mill (Collin Lab & Pilot Solutions). Five of these sheets were stacked before being placed in a press to make the final press plate. The parameters used to make the sheets and plates are summarised in Table A-4.

Table A-4: Summary of parameters applied to make the sheets and press plates used for the transparency measurements.

Parameter	Conditions
Roll Temperature (°C)	180
Roll Time (min)	5
Additive Amount (phr)	1,2,4
Press Temperature (°C)	180
Press Time (min)	15

Transparency measurements and yellowness indices were recorded with a Colourquest XE spectrophotometer (Hunterslab).

Izod Impact Test

To test the impact modification ability of the particles, Izod impact tests were recorded. For this the PVC matrix formulation containing the synthesised particles was rolled into sheets using a roll mill (Collin Lab & Pilot Solutions) (Table A-5).

Table A-5: Summary of the formulation used in the synthesis of the bars used for the Izod impact tests.

Component	Amount (phr)
Base Resin (PVC)	100
Stabiliser	3
Lubricant	0.5
Pigment	4

Five of the sheets were stacked before being placed in a press to make the final plate. The parameters used to make the sheets and plates are summarised in Table A-6. An opaque single notched bar was used with dimensions 63.5 x 12.5 x 6.0 mm. The test specimens were equilibrated at 25 °C and 50% humidity overnight before testing.

Table A-6: Summary of the parameters used to produce the sheets and plates used to make the test specimens for the Izod impact tests.

Parameter	Conditions
Roll Temperature ($^{\circ}\text{C}$)	180
Roll Time (<i>min</i>)	10
Additive Amount (<i>phr</i>)	10
Press Temperature ($^{\circ}\text{C}$)	180
Press Time (<i>min</i>)	15

Results and Discussion

Testing of PMMA Particles Containing a Crosslinked Shell

The matting properties and gelation behaviour of the PMMA particles containing a crosslinked (CL) MMA shell from Chapter 3 section 3.5.3., produced via dispersion polymerisation in scCO_2 were tested and compared to particles produced at the supporting company, (Table A-7).

Table A-7: Summary of crosslinked particles used for testing. Entries 1-2 were samples prepared by the supporting company and entries 3-6 were synthesised in Nottingham.

Entry	Sample	Particle Size (<i>nm</i>)	Composition BA/MMA/CL (<i>phr</i>)	Crosslinking Reagent - Location
1	S1	3570 ^a (2000-7000)	-	AMA - core
2	S2	-	-	AMA - core
3	PMMA	3100 ^b (± 480)	0/100/0	-
4	CL_50-S1	1570 ^b (± 180)	0/100/20	EGDMA - shell
5	CL_50-S2	1900 ^b (± 185)	0/100/20	EGDMA - shell
6	CL_50-S3	2170 ^b (± 160)	0/100/20	EGDMA - shell

^a - d-50 based on laser diffraction (including 5 and 95% value), ^b - particle size from SEM (including standard deviation). AMA is allyl methacrylate.

The difference between the two samples from the supporting company tested (S1 and S2) was that S2 contained less emulsifier which gave it improved heat stability. Crosslinked samples produced in scCO_2 were synthesised with an increasing particle size, to determine what effect this had on the parameters measured. The content of the crosslinking component was kept constant (50 wt%).

SEM analysis of all the samples tested prior to processing showed well-defined particles (Figure A-8) with various sizes (Table A-7).

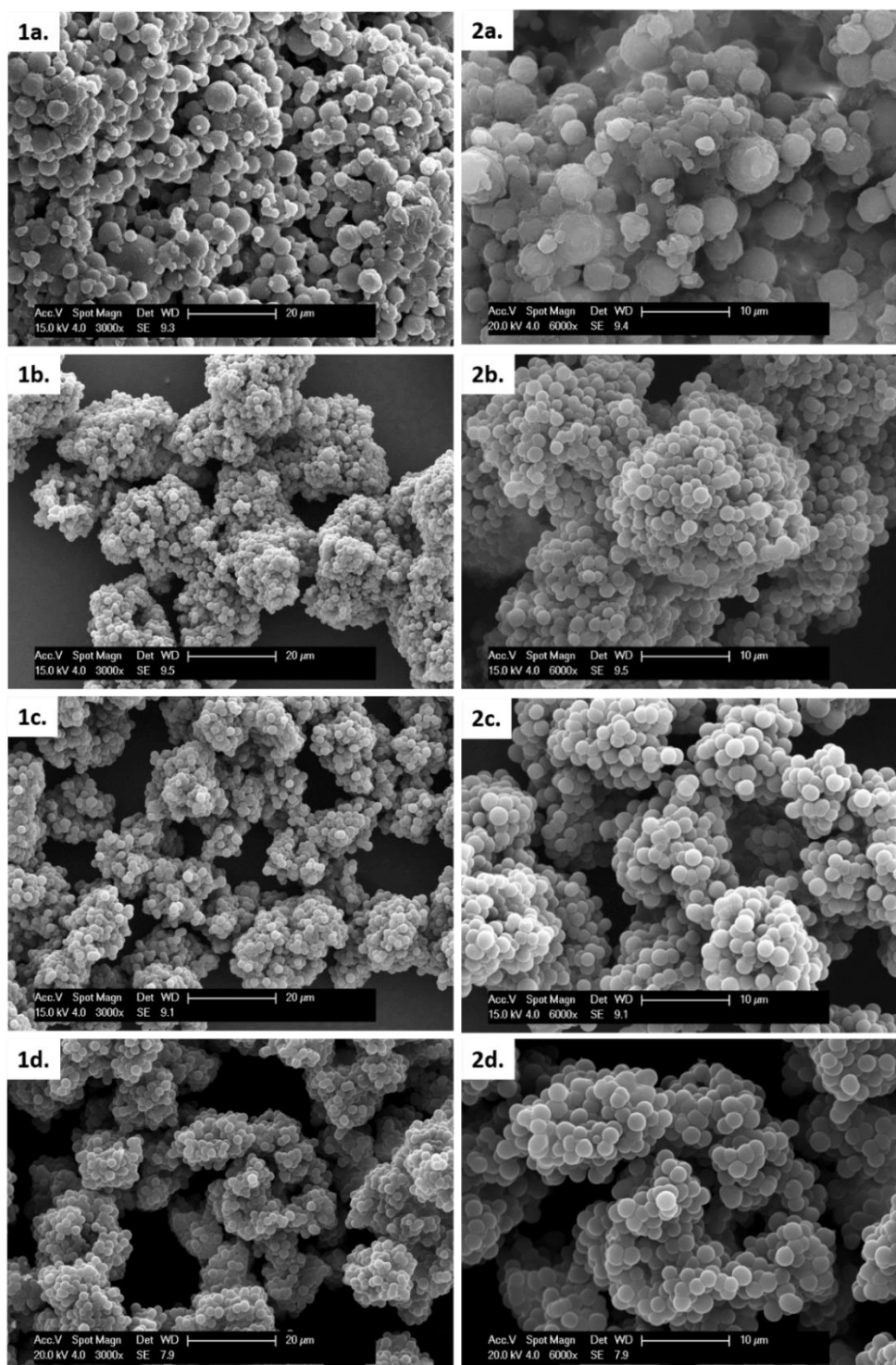


Figure A-8: SEM images of S1 (a), CL_50-S1 (b), CL_50-S2 (c) and CL_50-S3 (d), at various magnification 3000x (1) and 6000x (2). Increasing particle size was observed with the particles produced in scCO₂. In comparison, the particles produced at the supporting company were much larger. Images recorded in Nottingham.

An increasing particle size was observed with the scCO₂ synthesised particles. This was as expected as the amount of MMA used in the polymerisation was increased whilst the concentration of the stabiliser was kept constant.

Brabender Gelation

For successful application as additives, the particles need to be mixed with a PVC matrix formulation. As mentioned, the properties of products depend on the composition of the PVC formulation coupled with the conditions at which it was processed. For example, the degree of gelation of the PVC affects the impact strength of the material.¹⁰ Gelation was measured using a torque rheometer (Brabender mixing measurer), for all samples. A blank sample and a formulation containing pure PMMA particles as an additive were also included as a control experiment. This allowed for comparison and a clear indication of the influence of the addition of the particles with differing parameters, such as particle size and the presence of crosslinking.

A plot of torque against temperature (Figure A-9) provided information about the samples. The trace minimum corresponds to the point at which gelation of the formulation begins. This point is linked to the T_g of the material, with a lower temperature indicating a lower T_g . The curve maximum indicates the temperature and torque at which the mixture is homogeneous. The slope of the trace gives information on the gelation speed, a steeper gradient indicates more flexibility within the polymer and a lower T_g .

Commercial samples produced by the supporting company (S1 and S2) exhibited comparable gelation profiles. In the lower temperature region, a 'hump' was observed in the profile (indicated by the arrow). The source of this is believed to be the broad particle size distribution in these samples, more specifically the presences of some much larger particles.

Similar plots for the scCO₂ synthesised particles are shown in Figure A-10. For the smaller CL_50 particles (sky blue line) the gelation starts at a slightly higher

temperature in comparison to the other CL_50 samples (157 vs. 155 °C), resulting in a lower torque (7.5 vs. 11 Nm).

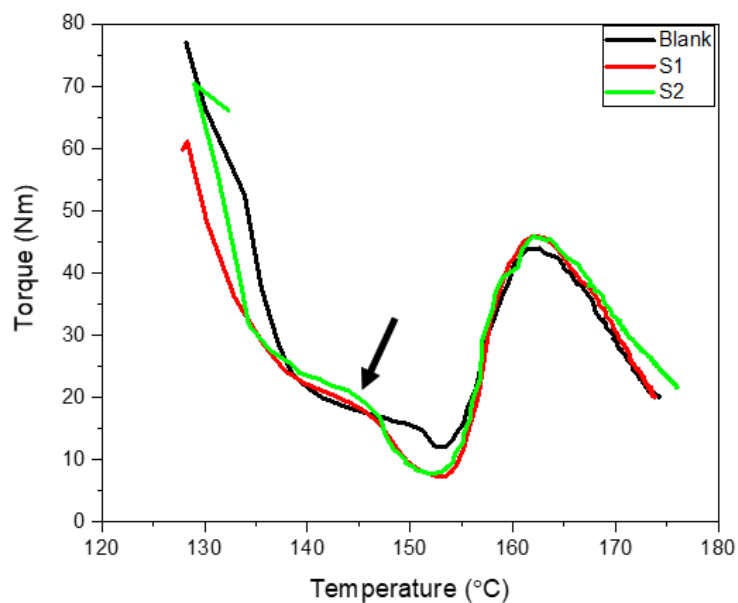


Figure A-9: Brabender gelation data for the particles synthesised by the supporting company once mixed with PVC; blank (black), S1 (red) and S2 (green). The arrow indicates a 'hump' in profile, attributed to both larger and smaller particles being present. Data collected by the supporting company.

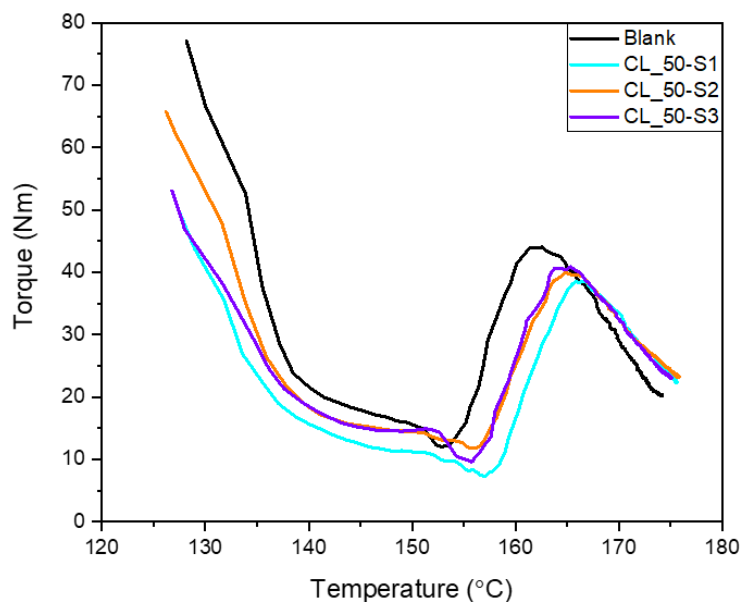


Figure A-10: Brabender gelation data for the particles synthesised in $scCO_2$ once mixed with PVC; blank (black), CL_50-S1 (sky blue), CL_50-S2 (orange) and CL_50-S3 (purple). Data collected by the supporting company.

A comparison of the particles synthesised by the supporting company (S) to the particles synthesised utilising scCO_2 (CL) is shown in Figure A-11. The lower torque before the start of gelation for the Kaneka samples (7 vs. 12 Nm) is related to the BA content and resulting lower T_g . The earlier onset of gelation at a lower temperature for the particles synthesised by the supporting company is attributed to the non-crosslinked nature of the shell, as well as the bigger particle size. The scCO_2 synthesised samples exhibit comparable gelation behaviour to the supporting company's samples with regards to the shape of the traces. However, it can be concluded the start of the gelation process is strongly dependent upon particle morphology, size and size distribution and monomer composition affects the torque before the gelation process starts.

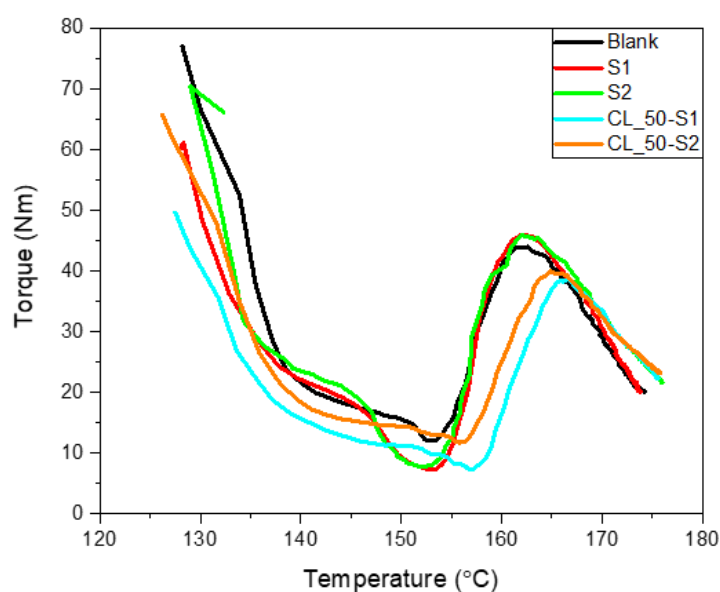


Figure A-11: Brabender gelation data for the various particles when mixed with PVC; blank (black), S1 (red), S2 (green), CL_50-S1 (sky blue) and CL_50-S2 (orange). Data collected by the supporting company.

Transparency and Matting Efficiency

Some applications require a transparent material and hence it is an important parameter to consider. Samples were tested by mixing with PVC before being rolled

into sheets and pressed into plates. Transparency data was recorded for test specimens containing the particle with a crosslinked shell synthesised in scCO₂ and the particle synthesised by the supporting company. Various loadings of additives were tested (1, 2 and 4 phr). A blank control sample containing no particulate additives along with a sample containing pure PMMA particles was used for reference. For these tests, a decrease in transparency indicated a higher matting efficiency.

Matting efficiency can be tested by inspection of the halo produced from shining a light through a sheet containing the particles. The halo around the light shone through the sheets containing particles synthesised by the supporting company (Figure A-12, image a) was “hazy”, indicating a higher matting efficiency. In contrast, the halo around the light shone through the sheets containing the particles synthesised in scCO₂ (Figure A-12, image b) was sharper indicating a lower matting efficiency.

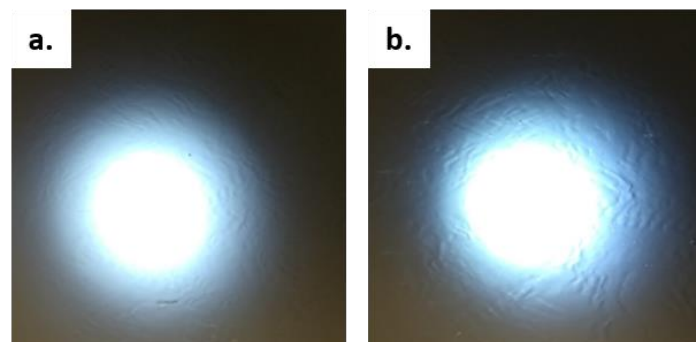


Figure A-12: Images of sheets containing S1 (a) and CL_50-S3 (b) at a loading of 2 phr, evaluated for the matting by a LED flashlight. A sharper halo was observed for the sheets containing the particles synthesised in scCO₂ indicating a lower matting efficiency. Images taken by the supporting company.

For both the scCO₂ and the supporting company's samples, it was also observed that a higher loading (phr) of additive increased the blurriness of the halo, indicating an increase in the matting effect (Figure A-13). This is as expected as there are more particles to scatter the light.

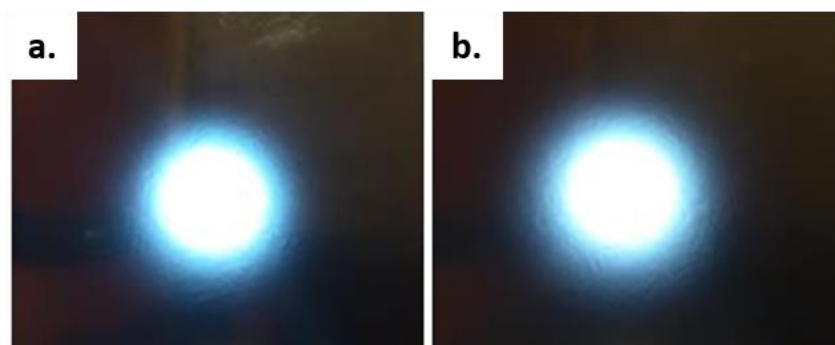


Figure A-13: Images of sheets containing CL_50-S1 at; 1 phr (a) and 2 phr (b). An increase in matting ability is observed with an increase in additive loading, indicated by increased blurriness of the halo. Images taken by the supporting company.

Measurements of the press plates containing the particles confirmed that at higher loading a lower transparency and hence improved matting was observed for all samples (Figure A-14). The specimens containing the supporting company’s samples (SC) have a lower transparency and hence a higher matting efficiency. Thus, as these particles are larger, it can be concluded that the higher matting efficiency can be attributed to particle size. Larger particles scatter light more, therefore producing a greater matting efficiency.¹³ Comparing the CL_50 samples synthesised in sCCO₂, it was seen that the increase in particle size led to a lower transparency and in turn improved matting efficiency.

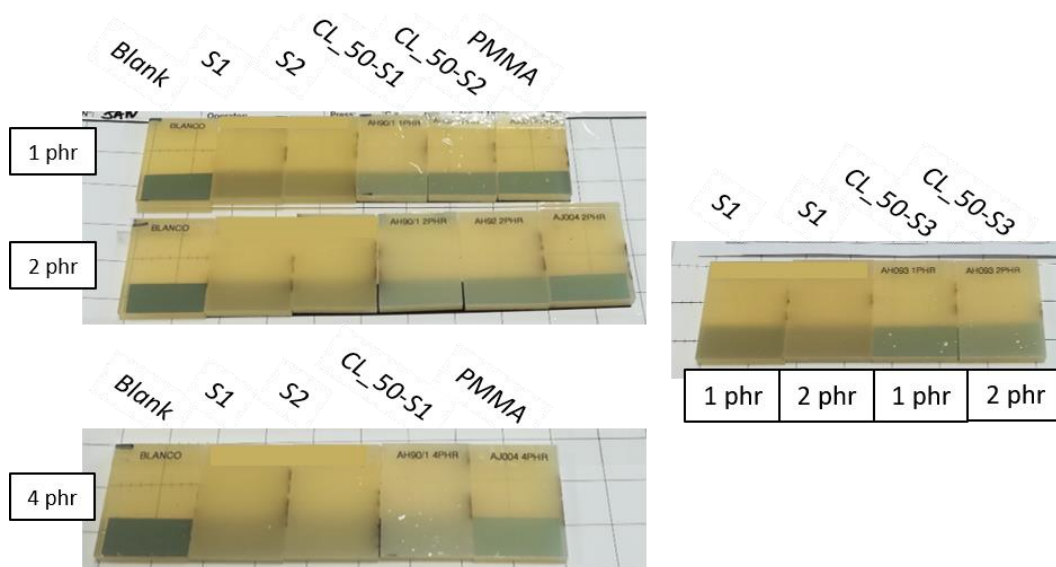


Figure A-14: Press plates used in the transparency test for the different samples and addition levels (phr). Images and data collected by the supporting company.

The spectrophotometer was also used to measure the yellowness index (Y_i) of the press plates. The Y_i of a material can be used to analyse how it changes in yellowness whilst it is processed. Here, it was used as a relative measure of yellowness caused by the incorporation of the different additives. A blank control sample without particulate additives was also measured for comparison. An average of three measurements of the blank sample is shown on the graph as a dashed black line (Figure A-15). Almost all of the samples containing the particles showed higher Y_i values than the blank. It can also be seen that all the particles that had been synthesised in $scCO_2$ showed a higher Y_i than the particles produced by the supporting company. This is perhaps attributable to the presence of very small amounts of impurities, residual monomers or decomposition products. A further cause of yellowness is related to the refractive index (RI) mismatch between the particles and the PVC matrix.¹³

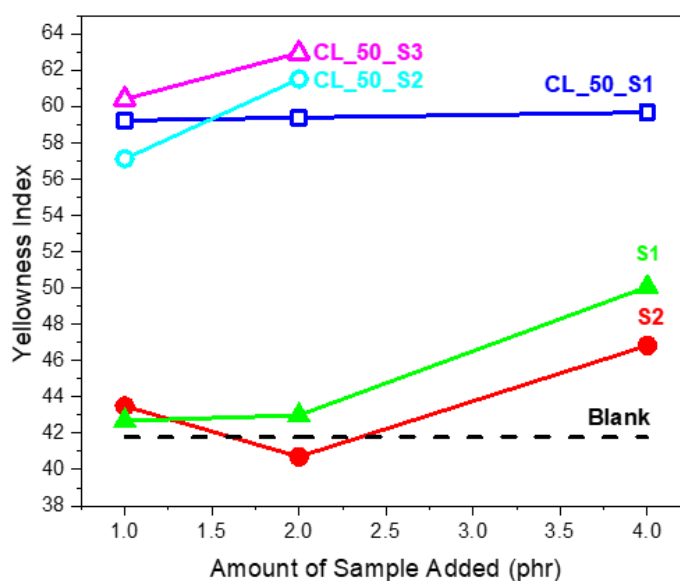


Figure A-15: Yellowness index measurements for PVC formulations to which; no particles (black, ---), S1 (red, ●), S2 (green, ▲), CL_50-S1 (royal blue, □), CL_50-S2 (sky blue, ○) and CL_50-S3 (pink, △) have been added. Data was collected by the supporting company.

The majority of the samples showed a general trend of increasing yellowness as the additive concentration (phr) increased. This is as expected as at higher loadings, the incorporation of trace impurities or unreacted monomer would be exaggerated.

Measurements of plates containing higher loading of CL_50_S2 and CL_50_S3 was not possible as a result of the limited amount of these particles synthesised in Nottingham.

SEM analysis was used to evaluate the dispersion of the particles, via imaging both the cross-section of the sheet and the press plate (Figure A-16). For both the supporting company's and scCO₂ produced samples, a good dispersion of the particles could be observed, in the sheet as well as the press plate. In the cross sections, holes were observed rather than the particles for the scCO₂ synthesised particles. This can be explained by the particle morphology. The particles produced by the supporting company (S1) contained an MMA shell which has no crosslinking and can entangle with the PVC matrix, securing it within the cross-section. In contrast, the particles produced using scCO₂ (CL_50-S1) contained a crosslinked MMA shell, are less likely to become tangled within the PVC matrix, hence making it susceptible to falling out.

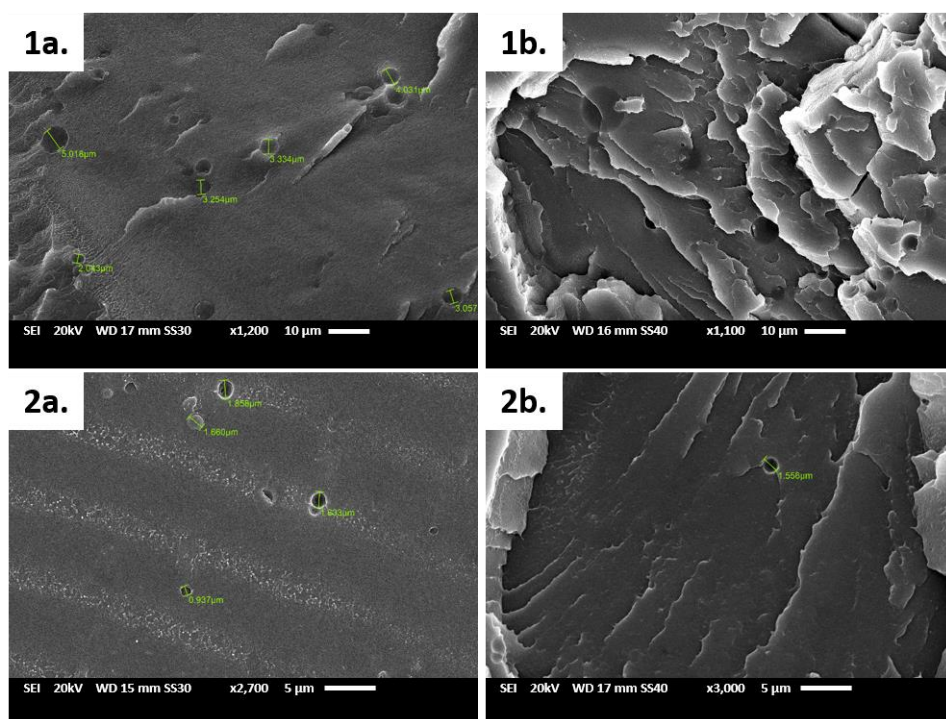


Figure A-16: SEM images of the cross section of the sheet (a) and press plate (b) in which S1 (1) and CL_50-S1 (2) have been added at a loading of 2 phr. Images collected by the supporting company.

To summarise the transparency measurements, the particles synthesised in scCO₂ exhibited a matting effect similar to that observed with the particles produced by the supporting company. The efficiency of the matting effect was affected by the addition level as well as the size of the particles. The difference between the samples containing the particles synthesised in scCO₂ in comparison to the particles produced by the supporting company was attributed to the particle size difference present (3600 vs. 2000 nm respectively). The use of scCO₂ in order to produce particles having a similar matting efficiency compared to the supporting company's existing product portfolio was successful.

Mechanical Testing of PMMA Particles Containing PBzA

The impact modification behaviour of the PMMA particles containing a PBzA phase, produced via dispersion polymerisation in scCO₂, was tested. The results were compared to particles produced at the supporting company, along with PMMA particles containing a crosslinked MMA shell also produced via dispersion polymerisation in scCO₂ (Table A-8). The exact composition of the particles produced at the supporting company was not given, however it was known that they all consisted of a PBA core and a PMMA shell in different ratios. It was also known that the sample labelled S5 contained the lowest ratio of PBA to PMMA.

Table A-8: Summary of PBzA containing and crosslinked particles synthesised in scCO₂ used for testing (entries 1-3). Along with samples produced by the supporting company for comparison (entries 4-6).

Entry	Sample	BzA Content ^a (%)	Particle Size ^b (nm)	Synthesis Solvent
1	BzA_36	27	1125 ± 225	scCO ₂
2	BzA_50	35	990 ± 210	scCO ₂
3	CL_33	0	1440 ± 235	scCO ₂
4	S3	-	-	Water
5	S4	-	-	Water
6	S5	-	-	Water

^a – measure from NMR and ^b – measured from SEM (including standard deviation).

Izod Impact Test

Izod impact tests were recorded on all the particles once they had been incorporated in a PVC formulation matrix (composition detailed above) and pressed into plates (Figure A-17).



Figure A-17: Image showing the single notched test specimens used for the Izod impact testing.

It can be seen that the samples containing the particles synthesised in $scCO_2$ showed similar impact resistance to the blank sample containing no impact modifier additives (Figure A-18).

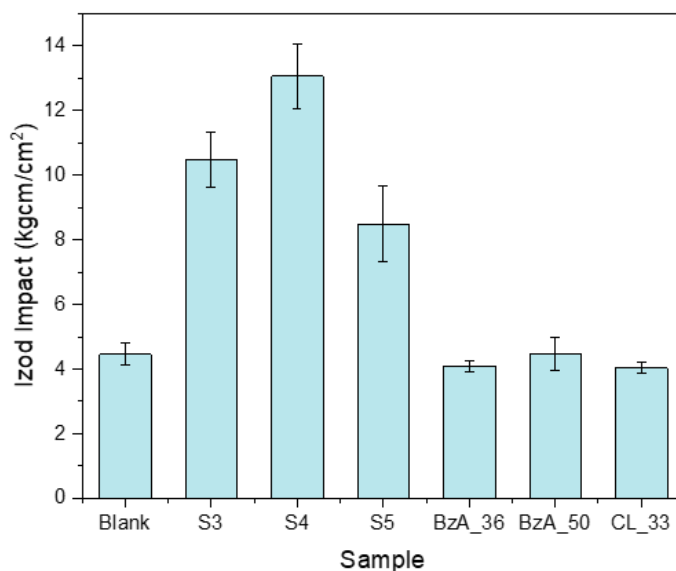


Figure A-18: Data collected from Izod impact tests performed on particles synthesised in $scCO_2$ (BzA/CL) and by the supporting company (S) when incorporated into a PVC matrix. Data collected by the supporting company. Samples synthesised in $scCO_2$ showed no increase in impact strength when compared to a blank sample.

Arguably, there is a slight increase in resistance between the specimens containing samples synthesised with a BzA feed of 36 wt% to 50 wt%. However, this increase is small and within the error of the measurement. Repeat testing of samples synthesised with these feeds is needed to confirm that an actual trend is present. Measurements of samples containing both less and more PBzA would also help with potentially confirming this.

It is believed that the samples containing particles synthesised in scCO₂ showed no significant increase in impact performance as a result of several reasons. Firstly, the particles may not contain sufficient crosslinking. This would cause the particle to lose its morphology during processing, hence causing it to be ineffective in absorbing the energy from impact.²² A second reason could be that the amount of PBzA (core) is too low in comparison to the MMA (shell). Particles used for impact modification typically contain a larger amount of “soft” core material. Li *et al.* investigated the effects of the ratio of core to shell in an acrylic impact modifier (AIM) upon impact resistance properties of PLA.²³ The authors found that the ratio had a significant influence on the toughening of PLA. It was found that an AIM with 79.2 (PBA) to 20.8 (PMMA) gave the greatest impact strength when mixed in a ratio of 80 (PLA) to 20 (AIM). Despite this, it is believed that the low soft material content is not the reason why the scCO₂ particles performed poorly as the sample synthesised by the supporting company, labelled SC5, has a similar ratio of hard to soft material as the particles synthesised in scCO₂. The sample containing the SC5 as an additive exhibited higher impact resistance than the sample containing the particles that were synthesised in scCO₂.

A third possible explanation is related to composition of the particles and the internal structure present. All the particles synthesised by the supporting company contained the traditional core-shell structure used for impact modification, consisting of one continuous phase of soft material encased in a hard shell (Figure A-19, image a).²⁴ By contrast, TEM analysis (shown in Chapter 3, section 3.5.2.) indicated that the particles synthesised in scCO₂ contained small domains of “soft” (PBzA) surrounded by “hard” material (PMMA) (Figure A-19, image b). A further factor that may be

influencing the particles ability to act as an impact modifier is the T_g of the “soft” polymer phase. The particles synthesised in $scCO_2$ contain PBzA as their “soft” phase, which has a T_g of 2 °C, approximately 47 °C higher than the PBA “soft” phase present in the particles synthesised by the supporting company (-45 °C). It is possible that the PBzA does not have a low enough T_g to be efficient at absorbing the energy from impact. This difference in T_g combined with the internal morphology present may be the reason why the particles synthesised in $scCO_2$ are not as effective for impact modification.

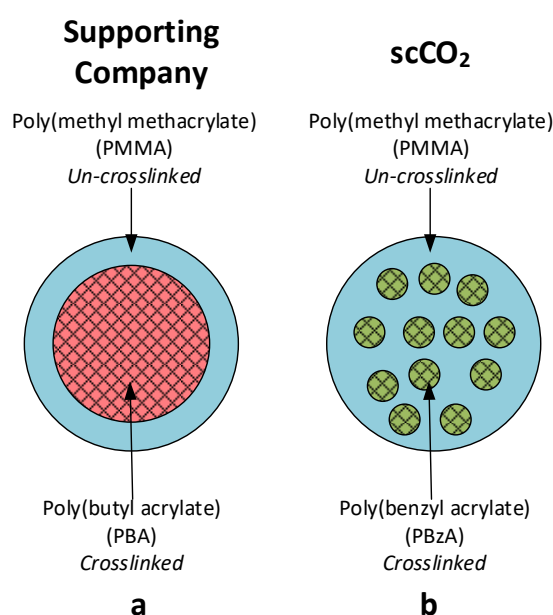


Figure A-19: Schematic representing the internal structure present in the tested particles; synthesised by the supporting company (a) and in $scCO_2$ in Nottingham (b).

Finally, if the particles are poorly dispersed within the PVC matrix they would be ineffective at increasing the impact resistance. Inter particle distance is an important parameter to consider. Michler *et al.* reported the findings of a minimum and a maximum distance to prevent rapid crack propagation which, was related to the diameter of the particle.²⁵ However, it is believed that poor dispersion of the particles synthesised in $scCO_2$ was not the cause of the poor impact resistance. This is because SEM images recorded of similar samples used for other tests (discussed

previously in the appendix) showed good dispersion of the particles in the press plates.

Conclusions

The testing of the samples produced gave a good insight into the particle structure present, as well as the effectiveness of the particles as additives with regards to formulation viscosity, transparency, matting efficiency and impact modification. From the Brabender gelation data it was concluded that the particles synthesised in scCO₂ exhibited similar gelation behaviour to the particles synthesised at the supporting company. It was found that the following parameters influenced the gelation process; the particle composition, size and its distribution affected the start of gelation (trace minimum) and the particle composition affected the torque before gelation started.

Tests of the matting ability of the particles showed that the particles synthesised in scCO₂ displayed a matting effect comparable to that observed with the particles produced by the supporting company. The supporting company's particles exhibited a slightly higher matting efficiency. The efficiency of the matting effect was affected by the addition level as well as particle size for both the scCO₂ and the supporting company synthesised samples. The difference between the two was attributed to the particle size difference present (3600 vs. 2000 nm respectively). It can be concluded that the particles synthesised using scCO₂ as a reaction medium had a similar matting efficiency compared to the supporting company's existing product portfolio.

Izod impact testing of the particles synthesised in Nottingham using scCO₂, once they had been incorporated into a PVC formulation, showed no significant increase in the impact resistance compared to a blank PVC sample containing no particulate additives. It is believed that the main reason for this was because of the internal morphology present in the scCO₂ samples. Smaller domains of PBzA were simple not as efficient as the commercial samples formed with one large soft domain.

Additionally, our use of PBzA for the soft phase may not have been as effective as the soft PBA phase present in the commercial samples. The particles synthesised in Nottingham that contained a PBA phase were not tested because the internal structure was not clear. However, it is hoped that in the future these materials can be tested to see if further information about the structure can be gained. The scale up reaction presented in Chapter 4 section 4.5.3. showed promise that the material containing PBA can be produce in large quantities, which should help facilitate testing.

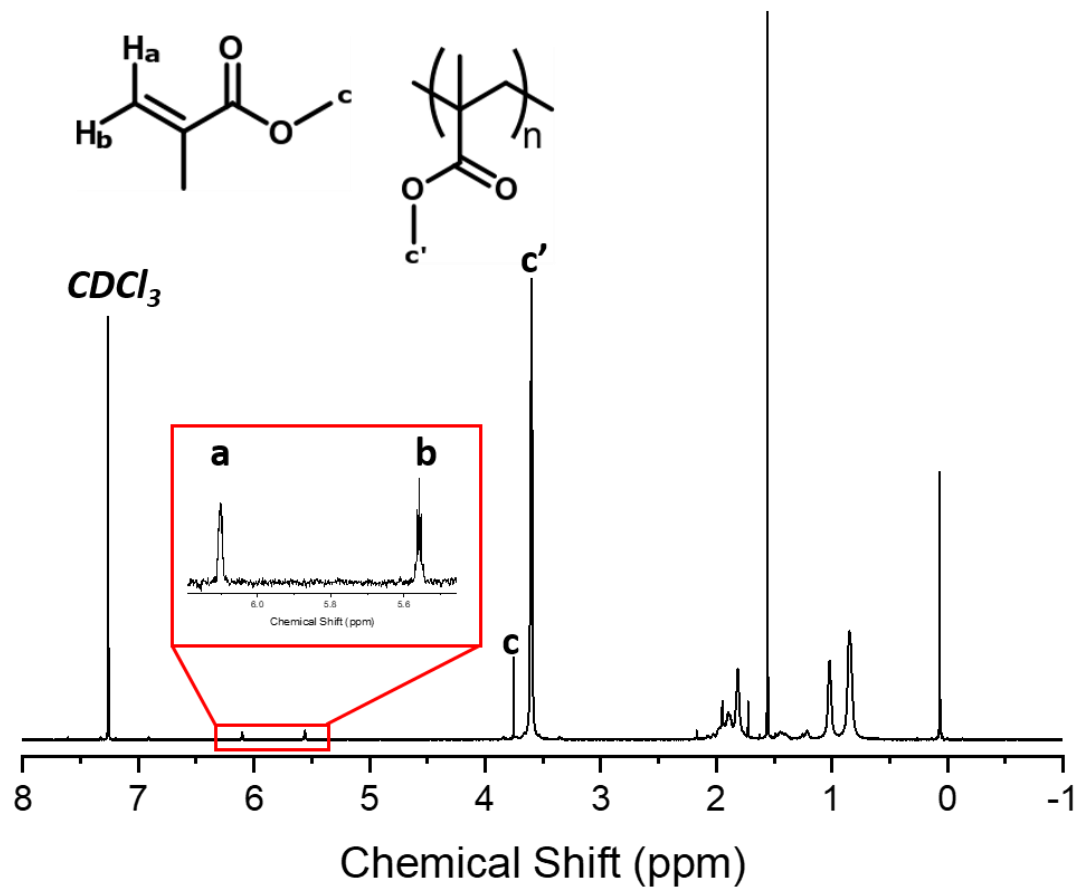
References

1. W. Grellmann and S. Seidler, *Polymer Testing*, Hanser Munich, 2007.
2. H. A. Barnes, J. F. Hutton and K. Walters, *An Introduction to Rheology*, Elsevier, 1989.
3. M. Moghri, H. Garmabi and M. Akbarian, *Journal of Vinyl and Additive Technology*, 2003, **9**, 81-89.
4. M. Moghri, H. Garmabi and M. Akbarian, *Journal of Vinyl and Additive Technology*, 2008, **14**, 73-78.
5. M. W. Allsopp, *Mechanism of gelation of rigid PVC*, CRC Press, Boca Raton, Florida, United States, 1982.
6. M. Gilbert, *Brydson's plastics materials*, William Andrew, 2016.
7. R. P. Marques and J. A. Covas, *Processing characteristics of U-PVC compounds*, 2003.
8. J. Parey and G. Menges, *Journal of Vinyl Technology*, 1981, **3**, 152-156.
9. G. Odian, *Principles of Polymerisation*, John Wiley & Sons, Inc., 4th edn., 2004.
10. J. Tomaszewska, T. Sterzyński and K. Piszczek, *Journal of Applied Polymer Science*, 2004, **93**, 966-971.
11. J.-P. Choi, H.-G. Lyu, W.-S. Lee and J.-S. Lee, *Powder Technology*, 2014, **261**, 201-209.
12. W. Guoquan and C. Yiaoting, *Polymer Testing*, 1991, **10**, 315-324.

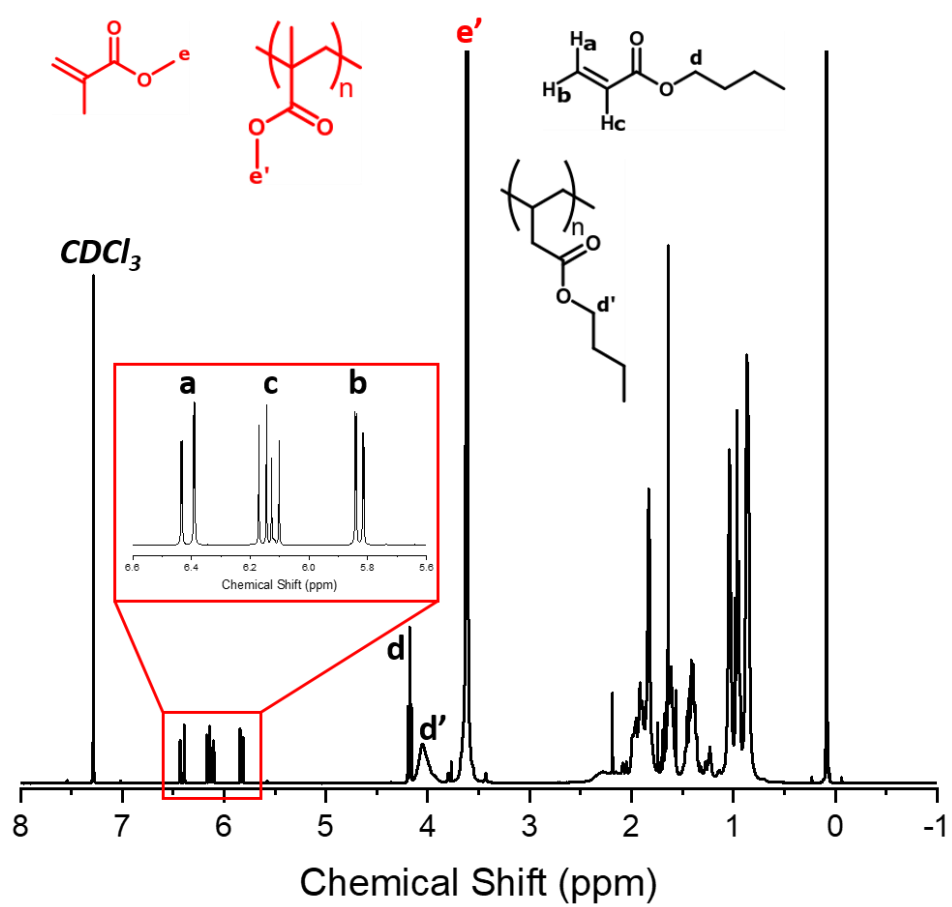
13. L. Wang, M. R. Kamal and A. D. Rey, *Polymer Engineering and Science*, 2001, **41**, 358-372.
14. A. C. Webber, *Journal of the Optical Society of America*, 1957, **47**, 785-789.
15. L. Øgdenal, *Light Scattering: A Brief Introduction*, 2013.
16. Y. Maruhashi and S. Iida, *Polymer Engineering and Science*, 2001, **41**, 1987-1995.
17. L. P. Real, J.-L. Gardette and A. P. Rocha, *Polymer Degradation and Stability*, 2005, **88**, 357-362.
18. D. ASTM, *Annual Book of ASTM Standards*, 1970, 167-169.
19. J. R. Davis, *Tensile Testing*, ASM international, 2004.
20. S. A. Ashter, *Thermoforming of Single and Multilayer Laminates: Plastic Films Technologies, Testing, and Applications*, William Andrew, 2013.
21. T. Kobayashi, *Impact Testing*, Elsevier, Oxford, 2001.
22. C. B. Bucknall, I. K. Partridge and M. V. Ward, *Journal of Materials Science*, 1984, **19**, 2064-2072.
23. W. Li, Y. Zhang, D. Wu, Z. Li, H. Zhang, L. Dong, S. Sun, Y. Deng and H. Zhang, *Advances in Polymer Technology*, 2015, **36**, 21632-21632.
24. L. A. Pérez-Carrillo, M. Puca, M. Rabelero, K. E. Meza, J. E. Puig, E. Mendizábal, F. López-Serrano and R. G. López, *Polymer*, 2007, **48**, 1212-1218.
25. G. H. Michler, *Acta polymerica*, 1993, **44**, 113-124.

^1H NMR Data

PMMA



PMMA/BA



PMMA/BzA

